Novel Proteins Associated with GLUT4 Vesicle Subcellular Traffic

Pereira, Vinit

Award date:
2014

Awarding institution:
University of Bath

Novel Proteins Associated with GLUT4 Vesicle Subcellular Traffic

Vinit Joaquim Pereira

A thesis submitted for the degree of Doctor of Philosophy

University of Bath
Department of Biology and Biochemistry

August 2014

Abstract

GLUT4 mobilisation involves endocytic and exocytic processes that are profoundly enhanced by insulin. Insulin indirectly mediates GLUT4 sorting into storage or recycling pools via endosomal trafficking proteins and phosphoinositides. The Endosomal Sorting Complex Required for Transport (ESCRT) machinery is involved in the endosomal sorting of ubiquitinated and phosphoinositide regulated cargo into subcellular pools. The findings in this thesis implicate the involvement of the ESCRT machinery in sorting ubiquitinated GLUT4 to direct it to its specialised storage compartment. Overexpression of ESCRT-III dominant negative constructs (CHMP3 $^{1-179}$ and Vps4 ^{E235Q}) in rat adipocytes led to accumulation of GLUT4 in enlarged compartments. Consequently, GLUT4 seems to be trapped in the enlarged compartment and prevented from sorting to storage and recycling pools. The enlarged GLUT4 containing compartment was positive for early endosomal and TGN-associated markers, suggesting that it is a hybrid compartment formed during ESCRT-III-dependent sorting of GLUT4 into other subcellular pools.

Once sorted into its specialised storage compartment, GLUT4 movement to the plasma membrane requires exocytic proteins involved in vesicle translocation, tethering, docking and fusion. The study described in this thesis aimed to characterise the involvement of Rab3B as a potential regulator of GLUT4 exocytosis. Rab3B was identified as an insulin-responsive Rab that regulated GLUT4 trafficking. Overexpression of the constitutively active Rab3B construct led to an increase in cell surface GLUT4 in basal rat adipocytes compared to the wild type or dominant negative Rab3B constructs. Noc2 was explored as a potential Rab3B effector due to its known involvement in Rab3-mediated trafficking in other vesicular trafficking processes. Noc2 showed reduced interaction with Rab3B in insulin-treated adipocytes and the overexpression of wild type Noc2 in adipocytes led to a reduction in cell surface GLUT4 upon insulin stimulation. It was concluded that Noc2 has an inhibitory effect on Rab3B action in GLUT4 exocytosis.

The findings in this thesis uncover novel signalling and trafficking pathways that are important in regulating cell surface levels of GLUT4 in response to insulin. The proteins described in this thesis were shown to influence GLUT4 mobilisation making them important regulators of GLUT4 traffic.

Acknowledgements

I would sincerely like to thank my supervisor Professor Geoff Holman for giving me this opportunity to work in his laboratory and guiding me throughout my project. It is due to his patience and perseverance that the work in this thesis has been made possible. I am also grateful to my co-supervisor Dr Françoise Koumanov for patiently teaching me all the laboratory skills necessary to carry out my work and helping me with the data analysis.

It has been an enriching experience working with so many people in the Biology and Biochemistry department. I would like to take this opportunity to thank Dr Paul Whitley for allowing me to use his laboratory instruments and reagents. I would also like to thank staff in Dr Stefan Bagby's lab (namely Dr Abhishek Upadhyay and Dr Mareike Posner) for allowing me to use their laboratory equipment and for their assistance in my protein purification experiments. The past and present members from the Holman lab (namely Judith, Lucy, Samantha and Rich) have also been of great help during my time in the lab. I would also like to thank Dr D. J. Fazakerley for contributing to the work that helped produce Fig. 4.5. The support staff in the teaching labs (Mick and Anna), bio-imaging suite (Dr Adrian Rogers), technical staff (Ewan) and additional support staff (Jane and Louise) have all been of assistance during the course of my research and hence I would like to thank them as well. I am also grateful to the University of Bath for funding my project.

I would finally like to thank my family and friends for being there in good and difficult times. A special thank you goes to Drs Anil and Marie Anne Pinto for their constant support and advice during the course of my studies. My parents, Fremiot and Margaret Pereira have been instrumental in supporting me all along and it goes without saying that I am thankful to them for everything I have achieved so far.

Abbreviations

AAA	ATPases associated with diverse cellular activities
AIP1	Actin interacting protein 1
AMSH	Associated molecule with the SH3 domain of STAM
AP	Adaptor protein
APS	Ammonium persulfate
APS	Adaptor protein with pleckstrin homology and Src homology 2 domains
AS160	Akt substrate of 160 kDa
ATP	Adenosine 5'-triphosphate
BCA	Bicinchoninic acid
Bro1 domain	Baculovirus repeated open reading frames
BSA	Bovine serum albumin
C-terminus	Carboxy-terminal region
cDNA	Complementary DNA
CDR	Complementarity determining region
CHMP	Charged multivesicular body protein
COPI/II	Coat protein I/II
Ct	Threshold cycle
Daxx	Death domain-associated protein
ddH_2O	Double-distilled water
DENN domain	Differentially expressed in neoplastic versus normal cells
DEPC	Diethylpyrocarbonate
DMEM	Dulbeco's modified Eagle's medium
Doa4	Degradation of alpha 4

Doc2b	Double C2-like domain-containing protein beta
DTT	Dithiothreitol
DUB	Deubiquitinase
EAP20	ELL-associated protein of 20 kDa
ECL	Enhanced chemiluminescence
E.coli	*Escherichia coli*
EDL	Extensor digitorum longus
EDTA	Diaminoethanetetraacetic acid disodium salt
EEA1	Early endosome antigen 1
EGFP	Enhanced green fluorescent protein
EM	Electron microscopy
ERK	Extracellular-signal-regulated kinase
ESCRT	Endosomal Sorting Complex Required for Transport
FDB	Flexor digitorum brevis
FDG	Fluorescein di-β-D-galactopyranoside
FYVE	Fab1p, YOTB, Vac1p and EEA1
GAP	GTPase activating protein
GDI	GDP dissociation inhibitor
GDF	GDI-displacement factor
GDP	Guanosine diphosphate
GEF	GDP/GTP exchange factor
GGA	Golgi-localized, gamma adaptin ear-containing, Arf-binding
GGT	Geranylgeranyl transferase
GLUE domain	GRAM-like ubiquitin-binding in EAP45

GLUT	Glucose transporter
GLUT4	Glucose transporter 4
GRP	Glucose-regulated protein
GSV	GLUT4 storage vesicle
GST	Glutatione S-transferase
GTP	Guanosine triphosphate
GTPγS	Guanosine [gamma thio] triphosphate
h	Hours
HA	Haemagglutinin
HEPES	4-(2-hydroxyethyl)-1-piperazineethanesulfonic acid
HES	HEPES/EDTA/sucrose
HG	HA-GLUT4 translocation assay
HRP	Horseradish peroxidise
HRS	Hepatocyte growth factor-regulated tyrosine kinase substrate
Hsp (Hsc)	Heat shock protein or heat shock cognate
IF	Immunofluorescence
IR	Insulin receptor
IRAP	Insulin-responsive aminopeptidase
IRS	Insulin receptor substrate
IPTG	Isopropyl β-D-1-thiogalactopyranoside
KD	Knock down
kDa	Kilo Daltons
KIF	Kinesin superfamily proteins
KRH	Krebs-Ringer-HEPES

LB	Lysogeny broth
LIP5	Lysosomal trafficking regulator-interacting protein 5
LRP1	Lipoprotein receptor-related protein 1
M	Molar
M6PR	Mannose-6-phosphate receptor
MADD	MAP-kinase activating death domain
MAPK	Mitogen-activated protein kinase
MBP	Maltose-binding protein
MIM domain	Missing in metastases
Min	Minutes
MIT domain	Microtubule interacting and trafficking
mRNA	Messenger ribonucleic acid
mTOR	Mammalian target of rapamycin
Munc18	Mammalian uncoordinated-18
N-terminus	Amino-terminal region
Noc2	No C2 domain protein
NSF	N-ethylmaleimide sensitive factor
OCRL-1	Oculocerebrorenal syndrome of Lowe (inositol polyphosphate 5-phosphatase)
O-GlcNAc	O-linked N-acetylglucosamine
PBS	Phosphate-buffered saline
PCR	Polymerase chain reaction
PDK1	3’-Phosphoinositide-dependent kinase-1
PI 3K	Phosphatidylinositol 3-kinase
PH domain	Pleckstrin-homology domain

PKB/Akt	Protein kinase B
PKC	Protein kinase C
PM	Plasma membrane
PtdIns	Phosphatidylinositol
PTP1B	Protein tyrosine phosphatase 1 B
PX domain	Phox homology domain
qPCR	Quantitative PCR or real-time PCR (RT-PCR)
REP	Rab escort protein
RICTOR	Rapamycin-insensitive companion of mTOR
RIM	Rab3-interacting molecule
s	Seconds
SDS	Sodium dodecyl sulphate
SDS-PAGE	Sodium dodecyl sulphate-polyacrylamide gel electrophoresis
SH2	Src homology 2
SHIP	Syntaxin 6-interacting protein
siRNA	Small interfering RNA
SKD1	Suppressor of K^+ transport growth defect 1
Slp4a	Synaptotagmin-like protein 4-a or granuphilin
SNAP	Soluble NSF attachment protein
SNARE	SNAP receptor
SM proteins	Sec/mammalian uncoordinated proteins (Munc)
SOCS	Suppressor of cytokine signalling
STAM	Signal-transducing adaptor molecule
SUMO	Small ubiquitin-like modifier

TA	Tibialis anterior
TBS	Tris-buffered saline
TBS-T	Tris-buffered saline containing Tween-20
TEMED	N,N,N,N'-tetramethylethylenediamine
TFB	Transformation buffer
TfR	Transferrin receptor
TGN	Trans-Golgi network
TIRF	Total internal reflection fluorescence microscopy
Tm	Primer melting temperature
Tris	Tris(hydroxymethyl)methylamine
Tsg-101	Tumour susceptibility gene 101
TUG	Tether containing an UBX domain, for GLUT4
Tween-20	Polyoxyethylene sorbitan monolaureate
U	Unit
Ub	Ubiquitin
UBAP1	Ubiquitin-associated protein 1
Ubc9	Ubiquitin-conjugating enzyme 9
UBPY	Ubiquitin-specific protease Y
UEV	Ubiquitin E2 variant
UIM	Ubiquitin-interacting motif
VAMP	Vesicle-associated membrane protein
VHS domain	Vps-27, Hrs and STAM
Vps	Vacuolar protein sorting
WB	Western blotting
WT	Wild type

Table of Contents

List of figures

List of tables

List of supplementary section information

List of publications arising from this thesis

Koumanov, F., Pereira, V. J., Whitley, P. R. and Holman, G. D. (2012). GLUT4 traffic through an ESCRT-III-dependent sorting compartment in adipocytes. *PLoS ONE* **7**, e4414. *(Attached)*

Koumanov, F., Pereira, V. J., Richardson, J. D., Sargent, S. L., Fazakerley D. J., and Holman, G. D. (2012). Rab3 is activated by insulin action and modulates GLUT4 vesicle translocation through interaction with its negative-effector protein Noc2. *(Manuscript in preparation)*

1 Introduction

Glucose uptake in insulin target tissues involves coordination between insulin signalling and the vesicular movement of the glucose transporter GLUT4. This thesis aims to investigate key proteins that are involved in GLUT4 movement 'to' and 'from' the plasma membrane (PM). A complete investigation of these key proteins will aid in understanding which proteins are crucial for GLUT4 mobilisation. These findings will also help us understand if some proteins can be pharmacologically manipulated at the subcellular level to increase the efficiency of glucose transport in disorders such as type 2 diabetes.

1.1 Glucose homeostasis

Whole body homeostasis or equilibrium is maintained by a number of physiological and biochemical processes. One of the important regulators of physiological homeostasis is control of blood glucose. A postprandial rise in blood glucose is countered by pancreatic insulin secretion. Insulin causes glucose to be assimilated by insulin-responsive tissues. In hypoglycaemic conditions, the pancreas secretes glucagon that causes cells to release glucose into the bloodstream. Both insulin and glucagon participate in normalising blood glucose to a baseline level of ~5.4 mM. In cells, glucose is necessary for the glycolytic pathway and the citric acid cycle, to generate the energy-yielding molecule ATP. Excess glucose may be stored as glycogen in skeletal muscles and hepatocytes or as triglycerides in cells such as adipocytes. Impairment in maintaining blood glucose to baseline levels is a hallmark of diabetes. A complete review of glucose homeostasis is beyond the scope of this thesis but the reader is referred to (Gibbs et al., 1995; Herman and Kahn, 2006; Liu et al., 1993; Wallberg-Henriksson and Zierath, 2001) for consideration of the relationship of regulated glucose transport to whole body glucose utilisation and storage.

1.2 Impairment of glucose uptake in type 2 diabetes

As impaired glucose transport is associated with insulin resistance, it is pertinent here to consider the relationship of insulin-regulated glucose transport to type 2 diabetes. With an ever increasing incidence of obesity and an unbalanced diet or hereditary risks, the odds of developing type 2 diabetes are proportionally increased (Mokdad et al., 2001; Mokdad et al., 2003; Scott et al., 2007; Tuomilehto et al., 2001). The pathophysiology of type 2 diabetes includes reduced pancreatic insulin secretion or insulin resistance as primary causes of this disorder (Buchanan et al., 2002; Reaven, 1988). Some of the changes at the molecular level of insulin-responsive tissues that contribute to type 2 diabetes include desensitisation at the insulin target receptor (abbreviated as IR) (Draznin, 2006; Longo et al., 2002), reduced glucose transporter 4 (GLUT4) expression (Gaster et al., 2001) or genetic mutations in GLUT4 associating proteins (Yoshimura et al., 1997). These abnormalities can result in reduced glucose uptake. Combatting this disease-associated impairment will require a better understanding of the GLUT4 transporter and factors that regulate its expression at the cell surface. This thesis adds information on novel intermediates that can in the future be investigated as disease related factors. These factors could in the future be investigated in patients.

1.3 The GLUT family

The GLUT family is a group of 14 known facilitative glucose transporters. The GLUT transporter comprises 12 trans-membrane spanning α-helices with intracellular N and C termini (depicted in Fig. 1.1). A number of exofacial residues on the GLUT transporter recognise the glucose molecule while helices 5, 7, 10 and 11 of the GLUT transporter are thought to help in glucose permeation (Hruz and Mueckler, 2001). A recent study proposed the involvement of an ICH (intracellular helical bundle) domain in GLUT1 that helps in facilitated glucose transport. This ICH domain allows GLUT1 to maintain an *'outward open'* conformation facilitating glucose binding; upon ligand binding the interactions within the ICH domain weaken leading to an *'inward open'*

conformation thereby allowing glucose release into the intracellular space (Deng et al., 2014). GLUTs 1-4 are the most studied isoforms of this GLUT transporter family and are classified as class I GLUTs. In the class I family, GLUT1 was the first GLUT to be identified and has been well characterised due to its expression in a number of tissues. The brain accounts for most of the body glucose uptake and GLUT1 accounts for most of this glucose supply across the blood brain barrier (where it is extensively expressed) (Redzic, 2011). GLUT2 is localised to the PM of pancreatic β-cells, intestines, kidney and liver cells. GLUT2 is involved in the bidirectional transport of a number of different sugars (Leturque et al., 2005). GLUT3 is restricted to neurons and is involved in cerebral glucose uptake (Vannucci et al., 1997). GLUT4 is the main insulin-responsive glucose transporter in adipose tissue and skeletal muscle. GLUT4 trafficking has been studied in detail in recent years due to its association with insulin resistance and type 2 diabetes (Gaster et al., 2001). Class II- (GLUTs 5, 7, 9, 11) and class III- (GLUTs 6, 8, 10, 12 and HMIT) transporters show structural differences to the class I GLUTs. Little is known about class II and class III GLUTs, though some of them have shown specificity to bind and transport glucose, fructose and inositol (Uldry et al., 2001; Zhao and Keating, 2007). Table 1.1 lists the known GLUT transporters, their tissue expression and function.

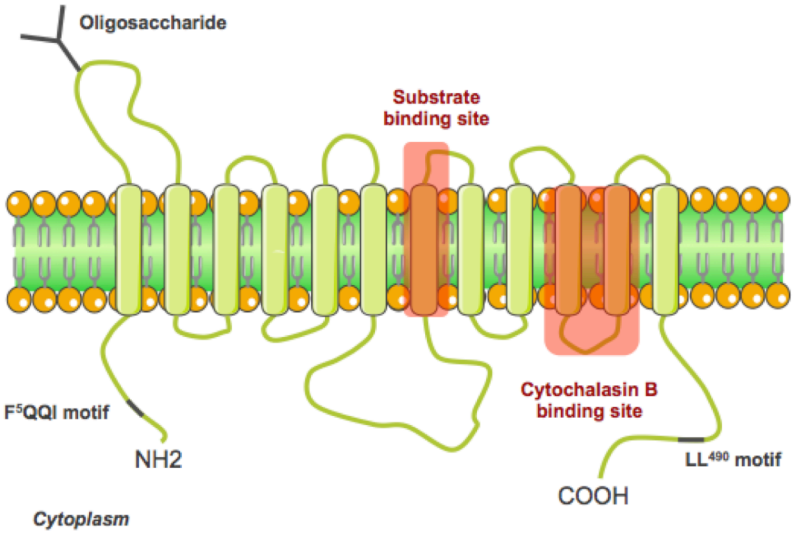

Figure 1.1: Diagram depicting the class I GLUTs. The GLUT transporter consists of 12 predicted transmembrane alpha helices. A glycosylation site is present at the N-terminal exofacial loop. Substrate binding likely occurs via a QLS motif in helix 7 (in GLUTs 1, 3 and 4), an STSIF motif in loop 7 and amino acids (Trp ^{388} and Gln ^{161}) in helix 5. The cytoplasmic F^{5}QQI and LL ^{490} motifs are recognition sites for proteins that facilitate subcellular GLUT4 mobilisation. Figure adapted from Augustin, 2010, Joost and Thorens, 2001.

Class	GLUT	Tissue expression	Function
I	GLUT1	Erythrocytes, blood-brain barrier, adipocytes, muscle	Glucose, galactose and ascorbic acid transport; basal glucose uptake
	GLUT2	Renal, hepatic and pancreatic-β cells and intestinal epithelium	Glucose, fructose and galactose transport
	GLUT3	Brain and neurons. Low expression in hepatocytes, myocardium, testes and placenta	Glucose and galactose transport
	GLUT4	Skeletal muscle, adipocytes and cardiomyocytes	Insulin regulatable glucose transporter
II	GLUT5	Small intestine, sperm, kidney, brain, adipocytes and muscle	Fructose transport
	GLUT7	Small intestine, colon and testes	Glucose and fructose transport
	GLUT9	Hepatocytes and renal cells	Uric acid transport
	GLUT11	Heart and skeletal muscle	Glucose and fructose transport
III	GLUT6	Spleen, brain and leucocytes	--
	GLUT8	High expression in testes and brain; some expression detected in liver, heart and blastocyst	Glucose and fructose transport; insulin-stimulated glucose transport in blastocyst
	GLU10	High expression in liver and pancreas; heart, lung, brain, skeletal muscle, kidney	Glucose and galactose transport
	GLUT12	Highly expressed in heart; some expression detected in prostrate	--
	GLUT13	Brain	H+/myo-inositol co-transport

Table 1.1: Table with a list of GLUT transporters, location and function. Data adapted from Epstein et al., 1999; Joost and Thorens, 2001.

1.3.1 GLUT4: The insulin-responsive glucose transporter

Preliminary studies on cellular glucose transport used an inhibitor of hexose transporters called cytochalasin b to help characterise hexose trafficking mechanisms (Jung and Rampal, 1977). Cytochalasin b studies led to an understanding of subcellular distribution of glucose transporters and their transport to the PM (Cushman and Wardzala, 1980; Delicado et al., 1988). However, use of cytochalasin b was unable to distinguish between different hexose transporters and so it was unable to identify which glucose transporter responded to insulin (Holman et al., 1990; Joost et al., 1988; Shisheva et al., 1999). The GLUT4 transporter was cloned in 1988 and identified as an insulin regulatable transporter that translocates to the PM in response to insulin in adipocytes (James et al., 1988; James et al., 1989). These findings were corroborated by studies on skeletal muscles supporting the translocation mechanism of GLUT4 (Friedman et al., 1991; Fushiki et al., 1989; Marette et al., 1992). A bis-mannose photolabelling technique in combination with GLUT4/GLUT1 immuno-specific antibodies was used in studies to characterise the insulin-responsive GLUT transporter. This technique helped quantify the amount of GLUT4 or GLUT1 at the PM of rat adipocytes treated with insulin (Holman et al., 1990). The photolabelling-immunoprecipitation technique showed a 15-20 fold increase in GLUT4 at the PM upon insulin stimulation and only a 5 fold increase in GLUT1 at the PM, confirming GLUT4 is the predominantly insulin-responsive glucose transporter (Holman et al., 1990).

GLUT4-mediated glucose uptake by insulin-responsive tissues contributes to maintenance of whole body glucose homeostasis (Kotani et al., 2004; Liu et al., 1993; Shepherd et al., 1993; Ziel et al., 1988). GLUT4 heterozygous knockout mice ($GLUT4^{+/-}$) become insulin resistant and are susceptible to diabetes (Stenbit et al., 1997), while mice overexpressing the GLUT4 transporter show improved basal and insulin glucose uptake (Brozinick et al., 2001). Understanding the mechanisms of GLUT4 trafficking is crucial to deciphering the current (incompletely understood) insulin signalling pathway.

1.4 The insulin signalling pathway

Insulin stimulation of cells initiates a number of downstream cellular signals. One of the crucial downstream signals is GLUT4 trafficking and glucose uptake. The first point of contact for insulin is the IR (insulin receptor). The IR is a heterotetrameric protein consisting of two extracellular α subunits linked via disulphide bonds to two transmembrane β subunits (Jacobs et al., 1980), the latter of which possesses catalytic potential (Baltensperger et al., 1992). Insulin binding to the IR causes a conformational change in the α subunits leading to autophosphorylation at intracellular IR residues (Lee et al., 1997). This autophosphorylation event activates IR tyrosine kinases that catalytically phosphorylate the insulin receptor substrate (IRS), adapter proteins with pleckstrin homology and Src homology 2 domains (APS), signal regulatory proteins (SIRPs), Cbl and Gab-1 on specific tyrosine residues (Saltiel and Kahn, 2001). Autophosphorylation of the IR can be negatively regulated by protein tyrosine phosphatase 1 B (PTP1B) that deactivates the IR by dephosphorylation (Goldstein et al., 2000). Other negative regulators include suppressors of cytokine signalling (SOCS1, SOCS3) (Ueki et al., 2004), plasma cell glycoprotein (PC1) (Maddux and Goldfine, 2000) and growth factor receptor-bound protein 10 (Grb10) (Wick et al., 2003) that sterically interfere with the interaction between the IR and IRS. Tyrosine phosphorylated IRS1 and IRS2 provide docking sites to the Src homology 2 (SH2) domain molecules (Lee et al., 1993; White, 1998). Two important SH2 proteins include the Grb2 and class IA phosphatidylinositol-3-kinase (PI 3K). Grb2 is involved in the Ras mitogen-activated protein kinase/extracellular-signal-regulated kinase (MAPK/ERK) pathway regulating nuclear transcription (Myers et al., 1994). PI 3K will be discussed in more detail due to its relevance in the GLUT4 trafficking pathway.

PI 3K is recruited to the IRS at the PM upon insulin stimulation and converts the phosphoinositide PtdIns(4,5)P_2 to PtdIns(3,4,5)P_3 (Whitman et al., 1988). PI 3K is a heterodimer consisting of a regulatory (p85) subunit and a catalytic (p110) subunit (Carpenter et al., 1990). The p85 subunit contains an SH2 domain that is capable of binding the tyrosine phosphorylated IRS. Inactivation of PI 3K by using its inhibitor wortmannin (Clarke et al., 1994) or by overexpression of a dominant negative PI 3K construct leads to an inhibition of many aspects of

cellular insulin signalling and suppressed glucose uptake (Cheatham et al., 1994). However, overexpression of the p85 regulatory subunit in mice has been linked to insulin resistance (Barbour et al., 2004), while mice lacking p85 show increased insulin sensitivity (Terauchi et al., 1999). To understand these effects of p85, we must keep in mind that p85 is generally present as a monomer in excess to the p85-p110 heterodimer (Mauvais-Jarvis et al., 2002; Ueki et al., 2000). The p85 monomer competes for IRS with the p85-p110 heterodimer (Ueki et al., 2000). This competition serves to negatively regulate the IRS signal (Luo et al., 2005). In the insulin-stimulated state, it is likely that phosphorylation of the IRS may far outweigh any cellular monomeric p85, thereby facilitating p85-p110 (PI 3K) binding and PtdIns(3,4,5)P_3 synthesis (Mauvais-Jarvis et al., 2002).

The PI 3K synthesised lipid secondary messenger PtdIns(3,4,5)P_3 interacts with pleckstrin homology (PH) domain proteins such as 3-phosphoinositide protein kinase 1 (PDK1) and protein kinase C (PKC) isozymes ς and λ, thereby activating them. Though PKC activation is reduced in type 2 diabetic individuals (Koya and King, 1998) and disrupting it can lead to defective GLUT4 transport (Bandyopadhyay et al., 1999), its precise role in regulating GLUT4 traffic still needs more investigation. The other PI 3K activated kinase, PDK1, phosphorylates Thr308 of an important signalling intermediate, protein kinase B (PKB/Akt) (Alessi et al., 1997). Akt is one of the most well studied signalling intermediates in the insulin signalling pathway. There are 3 isoforms of Akt: Akt1, Akt2 and Akt3. Akt2 is the functionally important isoform in insulin-responsive tissues and will be explored in this literature review. Akt2, is also phosphorylated on Ser473 (in addition to Thr308) by another protein complex, mammalian target of rapamycin (mTOR) that associates with the regulatory protein (RICTOR) (Vander Haar et al., 2007). A crucial event that follows Akt activation is the phosphorylation and subsequent inactivation of the 160 kDa Rab GTPase activating protein (GAP) AS160/TBC1D4 (Kane et al., 2002). It is believed that insulin-mediated inactivation of AS160 removes a restriction in GLUT4 traffic leading to recruitment of Rab GTPases to facilitate GLUT4 trafficking to the PM.

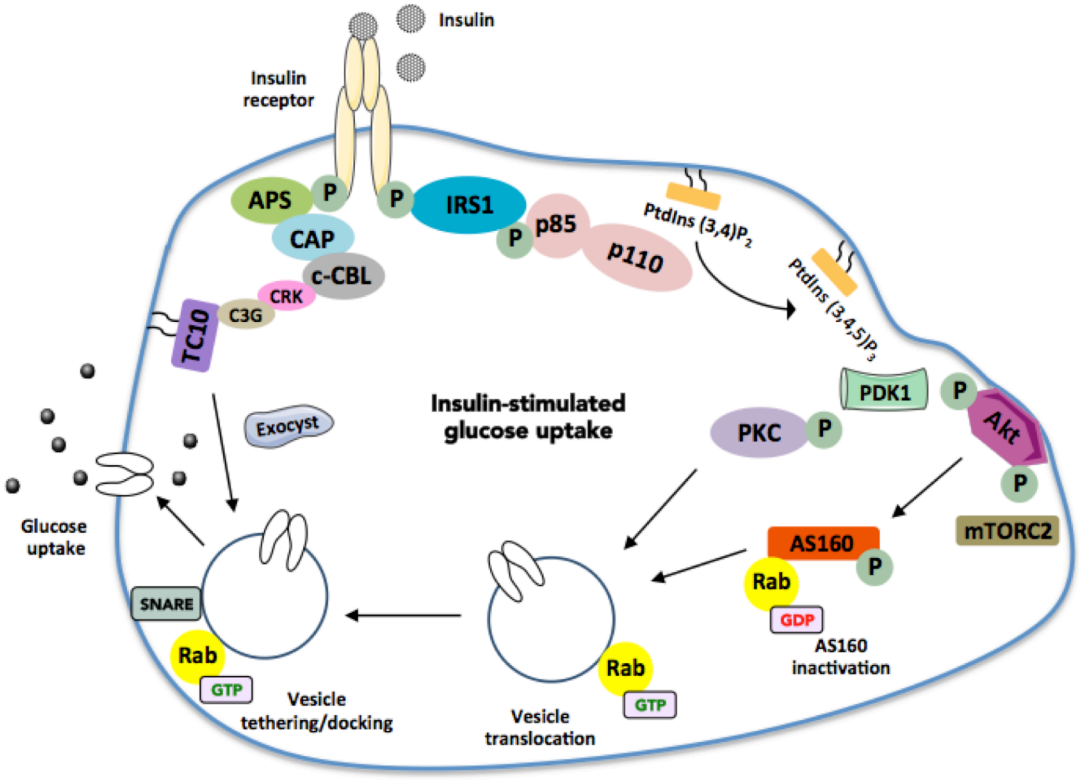

Figure 1.2: Insulin signalling cascade in adipocytes. Insulin binding to its receptor leads to autophosphorylation by the receptor tyrosine kinase in the beta subunit of the insulin receptor (IR). The IR in turn phosphorylates the insulin receptor substrate (IRS1), which binds to the regulatory (p85) subunit of phosphatidylinositol 3-kinase (PI 3K) and phosphorylates p85. PI 3K synthesises PtdIns(3,4,5)P_3 from PtdIns(3,4)P_2. An elevation in PtdIns(3,4,5)P_3 levels leads to recruitment of a phosphoinositide dependent kinase 1 (PDK1), protein kinase B (Akt/PKB) and protein kinase C (PKC) to the plasma membrane (PM). Akt is phosphorylated by PDK1 and mammalian target of rapamycin complex 2 (mTORC2) while PKC is phosphorylated by PDK1. Akt and PKC both regulate downstream effects of insulin signalling. Phosphorylation of Akt is a key event in the insulin signalling cascade as it activates pathways for glucose metabolism, lipid/protein synthesis, cell growth, gene expression and GLUT4 translocation. For activation of GLUT4 translocation, Akt phosphorylates a Rab GAP called AS160 (TBC1D4), which results in AS160 inactivation. Inactivation of AS160 leads to Rabs being GTP bound and this causes Rabs to be activated. Activated Rabs facilitate GLUT4 translocation and glucose uptake. The insulin signalling cascade also involves activation of a PI 3K independent pathway that assists in GLUT4 exocytosis. Tyrosine phosphorylation of the IR activates two adaptor proteins APS and CAP and protooncogene (cCBL). Tyrosine phosphorylation of cCBL leads to recruitment of the CRK adaptor protein and a guanine nucleotide exchange factor C3G. C3G exchanges the TC10 bound GDP for GTP leading to activation of TC10. TC10 is responsible for facilitating the activation of a number of proteins associated with an exocyst complex that helps in GLUT4 vesicle docking to the PM.

1.5 GLUT4 trafficking

Considerations of the GLUT4 trafficking mechanism are assembled from a number of studies that have aimed to characterise either cellular localisation of GLUT4 or signalling intermediates that may directly or indirectly influence GLUT4 movement.

1.5.1 From biogenesis to the plasma membrane

GLUT4 is mainly localised to intracellular stores in the basal state and translocates to the PM rapidly upon insulin activation. Using techniques such as electron microscopy (EM) to scan rat adipocyte cryosections, it was shown that GLUT4 primarily associated with intracellular tubulo-vesicular structures in the basal state (Malide et al., 2000). This EM study demonstrated that about 60% of GLUT4 was sequestered in vesicular structures in the basal state, 35% was not associated with membranous structures and only ~5% was present at the PM. Insulin-stimulated adipocytes however, showed a ~38% increase in GLUT4 at the PM (Malide et al., 2000). This corroborates the 15-20 fold increase in surface GLUT4 upon insulin stimulation that was reported using the bis-mannose photolabelling technique (Holman et al., 1990).

Some translated proteins are transported from the rough endoplasmic reticulum to the Golgi, which serves as a hub for protein sorting. Around 20% of intracellular GLUT4 was shown to be sequestered in the trans-Golgi network (TGN) (Slot et al., 1991). GLUT4 also colocalised with a number of Golgi markers such as TGN38 (Ralston and Ploug, 1996), golgin-130 (Blot and McGraw, 2006; Williams et al., 2006), syntaxin-6 and syntaxin-16 (Shewan et al., 2003). GLUT4 sorting from the TGN to insulin-responsive compartments was shown to require Golgi-localized, γ-ear-containing, Arf-binding (GGA) proteins (Li and Kandror, 2005). Dominant negative GGA constructs inhibited biogenesis of insulin-responsive GLUT4 compartments and led to impaired glucose uptake (Li and Kandror, 2005). The insulin-responsive compartments that originated from the TGN have been characterised as GLUT4 storage vesicles (GSVs) to distinguish them from any GLUT4 ‘containing’ vesicles that do not respond to insulin (Rea and James, 1997). It is worth noting that another marker called

insulin-responsive aminopeptidase (IRAP) is also localised to GLUT4 vesicles and may aid in GSV formation (Yeh et al., 2007). Besides IRAP, vesicle sorting proteins such as sortilin (Shi and Kandror, 2005) and LRP1 (Jedrychowski et al., 2010) also aid in GSV biogenesis. IRAP, LRP1 and sortilin may be considered as markers for identifying and distinguishing GSVs from other GLUT4 containing compartments.

1.5.2 Tethering, docking and fusion

GLUT4 vesicles translocate from a storage pool towards the PM (Martin et al., 2000). A coiled-coil domain on the Exo70 protein was shown to assist GLUT4 vesicle tethering to the PM (Inoue et al., 2003). Exo70 complexes with a multimeric exocyst to assist in tethering GLUT4 to the PM (Inoue et al., 2003). The exocyst interacts with Rho and Ral small GTPases that are regulated in an insulin-dependent manner and recruited to the PM (Chen et al., 2007). It is a combination of the exocyst, GLUT4 vesicle proteins and small GTPases that tether a vesicle to the PM (Novick and Guo, 2002). Docking and fusion to the PM is dependent on soluble N-ethylmaleimide sensitive factor (NSF) acceptor protein receptor (SNARE), which forms a multi-subunit complex with the GLUT4 vesicle (Cheatham et al., 1996). A technique called total internal reflection fluorescence microscopy (TIRFM) was used to monitor GSVs at the periphery of the PM. Studies using TIRFM showed that upon insulin stimulation, a number of GLUT4-containing vesicles accumulated ~200 nm below the PM leading to vesicle tethering and ultimately PM fusion (Lizunov et al., 2005). TIRFM studies by another group revealed that insulin decreased the time needed for GLUT4 vesicles to dock to the PM and increased the number of fusion events (Huang et al., 2007). Shuttling of GLUT4 vesicles to the PM and their subsequent tethering, docking and fusion events are thought to occur with the help of Rabs and the cell cytoskeleton. En-route to the PM, microtubule elements called kinesins have also been reported to associate with the GSVs (Emoto et al., 2001). Two specific kinesins, KIF5B (Semiz et al., 2003) and KIF3A (Guo et al., 2012) escort GLUT4 vesicles along the microtubule towards the PM. Actin binding myosin motors Myosin-2A (Chung et al., 2010), Myosin-5A (Chen et al., 2012) and Myosin-1C

(Bose et al., 2004) further advance GLUT4 vesicle motility along actin filaments. GLUT4 vesicle tethering to the PM occurs prior to the association of the vesicle with the SNARE machinery. Myosin-1C was shown to participate in actin remodelling thereby facilitating GLUT4 vesicle tethering process to the PM (Boguslavsky et al., 2012). Myosin-5A together with Myosin-2A are involved in docking the GSV to the PM (Chen et al., 2012; Chung et al., 2010).

Insulin stimulation rapidly increases the flux of GSV exocytosis and subsequent vesicle docking/fusion with the PM. TIRFM studies show the involvement of a vesicle associated membrane protein 2 (VAMP2) in GLUT4 vesicle fusion (Xu et al., 2011). A distinguishing feature of GSVs is that they do contain VAMP2 (Martin et al., 1998), which makes them competent for PM fusion. VAMP2 however, does not act alone and interacts with syntaxin-4 (Olson et al., 1997) and synaptosomal-associated membrane protein of 23 kDa (SNAP-23) (Kawanishi et al., 2000) to form a ternary fusion 'ready' SNARE complex. This multi-subunit ternary complex allows the GLUT4 vesicle to fuse with the PM, which is facilitated by two additional proteins, Munc18c (Thurmond et al., 2000) and Doc2b (Fukuda et al., 2008).

The IR tyrosine kinase phosphorylates Munc18c (on Tyr521) and activates it (Schmelzle et al., 2006). Activated Munc18c competes with VAMP2 for syntaxin-4 binding (Thurmond et al., 1998). Activation of Munc18c (Bakke et al., 2013) leads to its dissociation from syntaxin-4 thereby allowing syntaxin-4 to interact with the SNARE complex during insulin stimulation and facilitate vesicle fusion (Aran et al., 2011; Jewell et al., 2011). Doc2b is another syntaxin-4 interacting protein (Fukuda et al., 2008) that likely associates with syntaxin-4 following Munc18c dissociation. Doc2b promotes SNARE dependent fusion of GLUT4 vesicles in a calcium dependent manner (Fukuda et al., 2008; Yu et al., 2013). Munc18c has hence been postulated to be a negative regulator of GLUT4 exocytosis whereby it possibly sequesters syntaxin-4, preventing vesicle fusion. A study using Munc18c$^{-/-}$ mice showed enhanced insulin-stimulated GLUT4 externalisation in adipocytes (Kanda et al., 2005). However, further characterisation studies on insulin signalling have shown that Munc18c phosphorylation by the IR was necessary for SNARE dependent vesicle fusion

(Jewell et al., 2011). The phosphorylation of Munc18-c by the IR implies that insulin stimulation not only activates GLUT4 translocation via the PI 3K signalling cascade but also readies the SNARE complex for GLUT4 vesicle fusion to the PM. Thus, the role of IR phosphorylated Munc18c is to regulate SNARE-mediated fusion of docked vesicles mainly by releasing syntaxin-4. However, it is still unclear how exactly Munc18c facilitates vesicle fusion (Jewell et al., 2011). Two possible hypotheses are that the IR may only phosphorylate a Munc18c-syntaxin-4 complex or that phosphorylated Munc18c is required for Doc2b binding and a Doc2b-Munc18c complex positively regulates GLUT4 exocytosis (Jewell et al., 2008; Jewell et al., 2011).

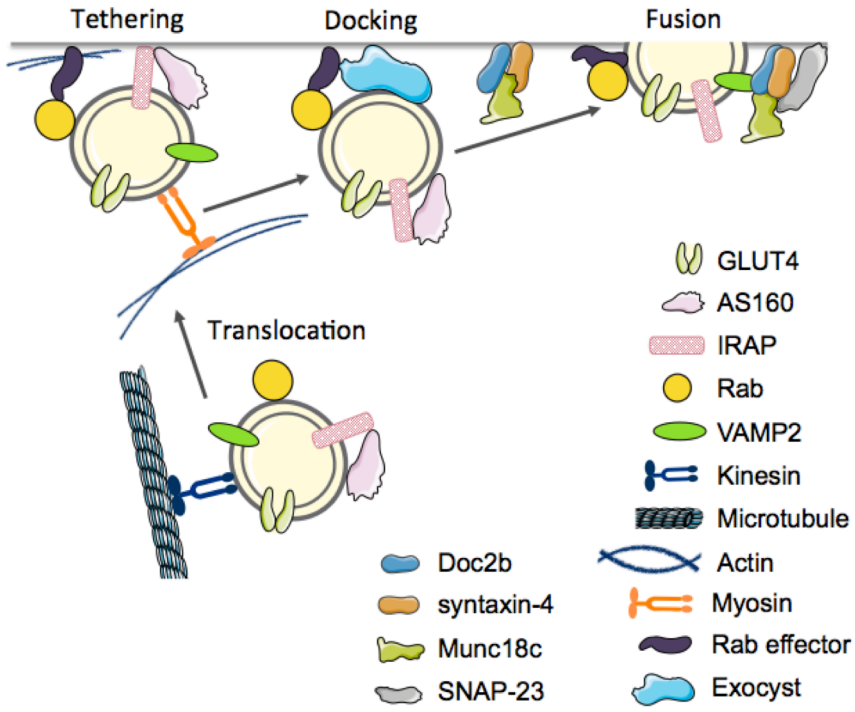

Figure 1.3: Exocytosis of GLUT4 to the plasma membrane. Insulin stimulation enriches GLUT4 storage vesicles (GSVs) with a number of molecules that assist in its delivery to the plasma membrane (PM). Some of the key molecules on GSVs include AS160, activated Rabs (namely Rab8A and Rab10), the SNARE component VAMP2 and the insulin regulatable aminopeptidase (IRAP). GSV movement along microtubules is brought about by kinesins (KIF3 and KIF5B). Myosins motors (Myosin-5A and Myosin-1C) drive GSVs along the actin cytoskeleton towards the PM. Tethering of GSVs to the PM is facilitated by AS160 and actin. Rab effectors possess lipid interacting motifs that may play a role in the tethering process. Tethering and docking of the GSV is stabilised by a multi-subunit exocyst. The exocyst interacts with actin, Rabs and other small molecule GTPases such as Rho, Ral and TC10 to stabilise the GSV at the PM. Following docking of the GSV at the PM, SNARE fusion machinery (syntaxin-4 and SNAP23) are recruited to the GSV. The SNARE machinery interacts with VAMP2 and mediates GLUT4 vesicle fusion with the PM. Doc2b and Munc18c also regulate the fusion process. Figure adapted from Stöckli et al., 2012.

1.5.3 Endocytosis and recycling

GLUT4 is rapidly internalised together with IRAP from the PM. Two possible mechanisms for retrograde traffic from the PM have been reported for GLUT4 in adipocytes. In the basal state, majority of GLUT4 is endocytosed by cholesterol-mediated endocytosis (CME) requiring lipid rafts and caveolin (Ros-Baro et al., 2001). In the insulin-stimulated state however, most GLUT4 is endocytosed via the clathrin adapter AP-2 pathway and formation of clathrin coated pits (Blot and McGraw, 2006; Huang et al., 2007). The N-terminal F^5QQI motif of GLUT4 is crucial for this interaction with AP-2 (Blot and McGraw, 2006). Knockdown of AP2 inhibits internalisation of GLUT4 under insulin conditions while cholesterol inhibition using a nystatin inhibitor reduces basal GLUT4 CME internalisation (Blot and McGraw, 2006).

Rab5 guides endocytic GLUT4 vesicles along microtubules in retrograde transport (Huang et al., 2001). Dynein, a minus end microtubule motor is anchored by Rab5 onto the GLUT4 vesicle (Huang et al., 2001). Early endosomal markers such as EEA1 (Ramm et al., 2000) and TfR (Zeigerer et al., 2002) have also been detected on recently endocytosed GLUT4 vesicles. The fate of endocytic GLUT4 vesicles depends on which signalling molecules are involved. Rab4 and its interacting protein Rabip4 cause GLUT4 to recycle back to the PM from insulin-responsive sequestered vesicle pools (Mari et al., 2006). GLUT4 may also be sorted away from the recycling route and directed towards the TGN via another clathrin adapter AP-1 (Blot and McGraw, 2008; Martin et al., 2000). AP-1 interacts with the LL^{490} motif on GLUT4. Knockdown of the AP-1 complex or mutating the LL^{490} motif increases the basal GLUT4 retention time by 2-fold after withdrawal of insulin (Blot and McGraw, 2008).

One of the hallmarks of endocytosed cargo is ubiquitination. Ubiquitin generally ‘labels’ cargo for endocytosis and degradation. Removal of ubiquitin (deubiquitination) controls cargo degradation, recycling to a storage pool or trafficking towards the plasma membrane. Studies in yeast have indicated that GLUT4 ubiquitination is necessary for trafficking in the endocytic pathway (Shewan et al., 2013). Another set of proteins called the GGA proteins were

described in section *1.5.1* as being responsible for sorting GLUT4 into GSVs. Studies have shown that for GGA-mediated TGN sorting of GLUT4 into GSVs, ubiquitination was necessary (Lamb et al., 2010). These interactions have been investigated in this thesis.

1.5.4 GLUT4: Intracellular sequestration and trafficking routes

In the absence of insulin, intracellular movement of GLUT4 is proposed to occur in two possible ways. GLUT4 may either be present in GSVs in a non-cycling 'static' pool or a continuously cycling 'dynamic' pool. The static pool GSVs do not associate with the GLUT4 in a dynamic pool. Static retention of GLUT4 might occur with the help of proteins such as TUG (tether containing a UBX domain) (Bogan et al., 2003) or p115 (belonging to the PI 3K subunit) (Hosaka et al., 2005) in the basal state (Larance et al., 2007). Dynamic GLUT4 cycles from the cytoplasm to the PM and may undergo endosomal recycling via the TGN (Martin et al., 2006). Insulin stimulation increases the rate of GLUT4 cycling and likely causes the release of GLUT4 from the static pool into a rapidly recycling pool. This phenomenon is best be described by a model proposed by Coster et al., (2004) which suggests that exchange of GLUT4 between endosomes and the static GSV pool occurs in a transient manner in the basal state. However, only in the presence of insulin is there a transient but 'quantal release' of GLUT4 from the static pool into the continuously cycling pool (Coster et al., 2004). This quantal release increases the size of the cycling pool but the release of GSVs by this quantal mechanism is mainly dependent on the rate of GLUT4 endocytosis (Muretta and Mastick, 2009).

Cycling of GLUT4 through pools is regulated by a number of proteins. Figure 1.4 demonstrates the currently known routes of GLUT4 trafficking upon insulin stimulation and likely storage/recycling pools. Fast recycling may occur if GLUT4 enters an endosomal-recycling compartment (ERC). Slow recycling is likely to occur if endocytosed GLUT4 is shunted to the TGN. The TGN acts as a hub where GLUT4 may recycle to the PM in a retrograde fashion or new GLUT4 vesicles may bud and join the current recycling pathway.

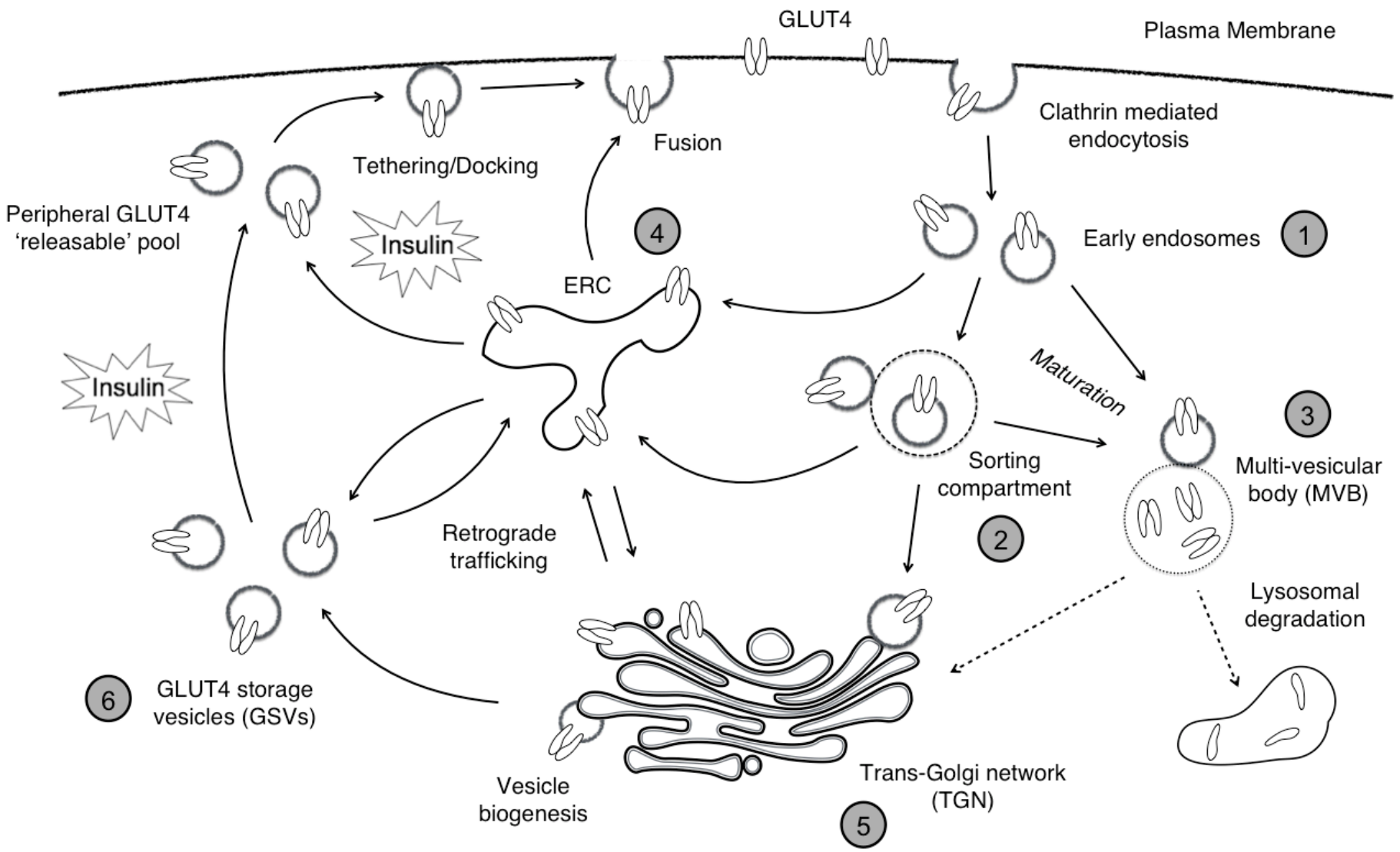

ERC: Endosomal recycling compartment

Figure 1.4: GLUT4 trafficking routes during insulin stimulation. Ubiquitinated GLUT4 undergoes endocytosis together with the transferrin receptor (TfR) via clathrin-coated pits. Newly endocytosed GLUT4 is sorted into early endosomes that contain the early endosomal antigen 1 (EEA1) and Rab5. ***(1)*** From early endosomes, TfR and GLUT4 may independently recycle back to the plasma membrane (PM) via the endosomal-recycling compartment (ERC) (fast recycling). GLUT4 may also traffic into sorting compartments and/or mature into late endosomes leading to formation of a multi-vesicular body (MVB). ***(2)*** GLUT4 from the sorting compartment may recycle to the ERC, undergo retrograde trafficking via the trans-Golgi network (TGN) or mature into late endosomes followed by formation of a MVB. ***(3)*** A small amount of GLUT4 that enters into a MVB is destined for lysosomal degradation. Recent studies suggest that GLUT4 may be rescued from the MVB into sorting/recycling endosomes or to the TGN. ***(4)*** The endosomal recycling compartment (ERC) is insulin-regulated and rapidly traffics GLUT4 to the PM. Insulin also regulates the steps downstream of the ERC that include tethering, docking and fusion of GLUT4 vesicles. Recently, Rab14 positive GLUT4 vesicles were shown to traffic from the ERC to the PM. Alternatively, the ERC may also sort GLUT4 into 'slow cycling' GSV pools or to the TGN. ***(5)*** GLUT4 enters the TGN from compartments associated with retrograde GLUT4 trafficking. TGN-regulated biogenesis involves packaging of GLUT4 into vesicles and delivery to the ERC or GSVs. ***(6)*** GLUT4 storage vesicles (GSVs) are insulin-regulated and exocytose GLUT4 to the PM after recruitment of the necessary trafficking machinery (that include VAMP2, Rab10 and IRAP). Figure adapted from Foley et al., 2011; Muretta and Mastick, 2009. For more detailed information on GLUT4 trafficking models, please refer to a review by Muretta and Mastick (2009).

1.5.5 AS160 as a regulator of GLUT4 traffic

During the insulin signalling cascade, one of the downstream substrates of Akt is AS160. Activation of Akt leads to Ser/Thr phosphorylation of AS160 *(see Figure 1.2)*. Phosphorylation of AS160 renders it inactive and unable to bind Rab GTPases (Bruss et al., 2005; Karlsson et al., 2005). AS160 is a Rab GAP (Mîinea et al., 2005) and GAPs are known to hydrolyse the guanine within a Rab from GTP to GDP. This GTP hydrolysis renders a Rab being GDP-bound, inactive and unable to perform its function. Hence the phosphorylation and inactivation of AS160 by Akt results in active (GTP-bound) Rabs. Active Rabs can hence facilitate GLUT4 vesicle exocytosis.

Studies in humans with type 2 diabetes showed that Akt dependent AS160 phosphorylation was reduced in skeletal muscle in comparison to individuals without type 2 diabetes (Karlsson et al., 2005). Phosphorylation at Thr308 on

AS160 was reduced by 51% in the skeletal muscle of type 2 diabetic individuals (Karlsson et al., 2005). Another study found that in individuals with a rare inherited heterozygous truncation mutant of AS160, there was postprandial hyperinsulinemia that contributed to the development of insulin resistance. Expression of the AS160 truncated mutant in 3T3L1 adipocytes showed a significant reduction in GLUT4 translocation to the PM in insulin-stimulated adipocytes (Dash et al., 2009; Koumanov et al., 2011). The truncated AS160 mutant increased basal GLUT4 translocation but reduced insulin-stimulated GLUT4 translocation in 3T3L1 adipocytes (Dash et al., 2009). These results possibly implicate AS160 and/or Rab GTPases as signalling intermediates that, when functionally impaired, can lead to insulin resistance.

Human AS160 has six potential consensus Akt phosphorylation sites (Ser318, Ser570, Ser588, Ser711, Thr642, Thr751). Mutating four of these phosphorylation sites to alanine generates an AS160-4P mutant. AS160-4P is a phosphorylation deficient mutant that inhibits GLUT4 translocation and causes impaired glucose uptake (Kramer et al., 2006; Sano, 2003). Adipocytes with siRNA knockdown (KD) of AS160 show increased basal GLUT4 translocation and increased basal glucose uptake implying that AS160 is a negative regulator of basal GLUT4 exocytosis (Eguez et al., 2005). However, overexpression of wild type AS160 does not inhibit insulin-regulated glucose uptake in the 3T3-L1 cell system (Kramer et al., 2006). Overexpressing a dominant negative AS160 ^{R973K} GAP mutant also removes the inhibitory potential of the AS160-4P mutant (Eguez et al., 2005). The studies hence suggest that AS160 helps maintain GLUT4 to intracellular stores (in the absence of insulin) and for this it requires a functional GAP domain (Eguez et al., 2005, Larance et al., 2005). However, the key steps in AS160 modulation of GLUT4 exocytosis need more investigation. AS160 has been clearly detected on GLUT4 vesicles and does not dissociate from them following insulin stimulation of adipocytes (Koumanov et al., 2011), though some studies claim that AS160 dissociates from trafficking GLUT4 vesicles following insulin treatment of cells (Stöckli et al., 2008, Larance et al., 2005).

AS160's presence on GLUT4 vesicles likely regulates the activation states of one or more key Rabs upon insulin signalling. The study undertaken in this thesis aims to identify Rabs downstream of Akt/AS160 phosphorylation that may be involved in GLUT4 exocytosis. A number of exocytic Rabs have been identified in vesicle exocytosis in other cell types. A preliminary study in the Holman lab identified Rabs that associated with total membrane preparations in adipocytes upon insulin stimulation of these cells. Among these identified Rabs, the exocytic Rabs will be explored in this thesis to study their role (if any) in GLUT4 translocation. The findings will hopefully bring us closer to identifying Rabs that may be involved in the final stages of GLUT4 translocation to the plasma membrane i.e. vesicle docking and fusion.

1.5.6 Rabs in GLUT4 traffic

The discovery that a GAP played such a crucial role in GLUT4 translocation automatically led to a number of studies to identify Rabs that may be targets downstream of AS160. One of the first studies to identify potential Rabs that could be substrates of AS160 led to the identification of Rab2, Rab8, Rab10 and Rab14 as targets for AS160 GAP activity; these Rabs were also present on GLUT4 vesicles (Mîinea et al., 2005; Sano et al., 2008). Other studies identified Rab4 (Cormont et al., 1996), Rab5 (Huang et al., 2001), Rab11 (Zeigerer et al., 2002), Rab13 (Sun et al., 2010), Rab31 (Lodhi et al., 2007) and Rab35 (Davey et al., 2012) as associating with different compartments (or pools) of GLUT4 vesicles *(see Table 1.1 for functions of these Rabs)*. Out of these Rabs, Rab10 is particularly well characterised as being responsible for delivering GSVs to the plasma membrane. Knockdown of Rab10 inhibited insulin-stimulated GLUT4 translocation in adipocytes making it an important regulator of GLUT4 traffic (Sano et al., 2008). The microtubule motor Myosin-5A was identified as a Rab10 effector, linking Rab10 to the cytoskeletal movement of the GSV to the PM (Chen et al., 2012). At the PM periphery, Rab10 and AS160's involvement was demonstrated at the vesicle-docking step, but it is unclear whether these two proteins regulate vesicle fusion (Chen and Lippincott-Schwartz, 2013; Chen et al., 2012; Jiang et al., 2008).

Rab4	Sorting of GLUT4 from endosomes (Cormont et al., 1996) and possible role in GSV formation (Chen and Lippincott-Schwartz, 2013; Leto and Saltiel, 2012).
Rab5	GLUT4 internalisation from the plasma membrane via the dynein microtubule motor (Huang et al., 2001).
Rab8A	AS160 dependent Rab involved in GLUT4 translocation to the plasma membrane mainly in muscle cells (Ishikura and Klip, 2008; Randhawa et al., 2008; Sun et al., 2010; Sun et al., 2014).
Rab10	AS160-regulated Rab that associates with GSVs and facilitates their translocation and docking to the PM (Chen et al., 2012; Sadacca et al., 2013; Sano et al., 2007; Sano et al., 2008).
Rab11	Endosomal recycling of the GLUT4 transporter and GLUT4 translocation to the plasma membrane (Kessler et al., 2000; Uhlig et al., 2005; Zeigerer et al., 2002).
Rab13	Another possibly AS160-regulated Rab involved in GLUT4 translocation in muscle (Sun et al., 2010).
Rab14	Endosomal GLUT4 trafficking (Chen et al., 2012; Reed et al., 2013).
Rab31	A possible negative regulator of GLUT4 exocytosis. Rab31 is localised to the TGN-endosomal interface (Lodhi et al., 2007).
Rab35	Regulation of GLUT4 translocation (Davey et al., 2012).

Table 1.2: Rab GTPases in GLUT4 traffic. A list of the Rabs identified as playing a part in GLUT4 trafficking together with their proposed function.

The Rabs identified in insulin signalling have been implicated in either endocytic or exocytic stages of GLUT4 trafficking. However, none of these recently identified Rabs have been directly implicated with GLUT4 vesicle fusion to the plasma membrane. In order to implicate Rabs in the PM docking/fusion stages, an association with the SNARE machinery and/or microfilaments would be needed. This opens the possibilities to exocytic Rabs that may be involved in GLUT4 vesicle docking/fusion to the PM that have not yet been characterised in adipocytes. Preliminary studies in the Holman lab used a photolabelling technique to identify Rabs that may be activated upon insulin stimulation in rat adipocytes. Rab3B was identified by this photolabelling technique as being an insulin activated Rab on total membranes. Members of the Rab3 family have

been implicated together with Rab effectors in vesicle docking/fusion in synaptic and endocrine cells (Martelli et al., 2000; van Weering et al., 2007; Wang et al., 1997). The studies described in this thesis investigate the involvement of Rab3B as a regulator of GLUT4 exocytosis and aims to identify its binding partners that may assist in GLUT4 vesicle docking/fusion.

1.5.7 Role of phosphoinositides in GLUT4 traffic

Cargo recognition proteins are fundamental for correctly trafficking vesicles and recruiting necessary machinery to assist vesicle movement. Rabs constitute one such set of proteins, as they are involved in recruiting machinery and facilitating vesicle movement. Phosphoinositides are another class of cellular signalling molecules. Phosphoinositides serve as lipid secondary messengers that orchestrate vesicle identity leading to regulation of vesicle traffic at different stages of a signalling pathway (Behnia and Munro, 2005; Fili et al., 2006). Phosphoinositides are the phosphorylated form of a phosphatidylinositol and contain a glycerol backbone, two non-polar fatty acid tails and a polar inositol head conjugated to one or more phosphate groups. The position and number of the phosphate groups on the inositol head are responsible for the diversity of cargo recognition. Recognition between phosphate groups and cytosolic or membrane cargo proteins occurs via electrostatic interactions between the inositol phosphate head and basic amino acids in the cargo protein. The binding between a phosphoinositide and cargo protein is further strengthened by the interaction between the phosphoinositide and membrane lipids (Lemmon, 2003). It is hence not surprising that a number of phosphoinositides are involved in the different stages of vesicle trafficking. Maintenance of phosphoinositide levels is key for successful GLUT4 trafficking (Shisheva, 2008).

Phosphoinositides were briefly described earlier in section *1.4* in relation to the insulin signalling pathway and with regard to the conversion of PtdIns(4,5)P_2 to PtdIns(3,4,5)P_3 by the insulin activated class IA PI 3K. The class IA PI 3K regulatory subunit (p110) is a Rab5 effector (Christoforidis et al., 1999). Rab5 is also involved in the generation of PtdIns(3)P on early endosomes by recruiting

the phosphoinositide kinases Vps34 and PI 3Kβ and phosphatases PI 4-phosphatase and PI 5-phosphatase (Shin et al., 2005). PtdIns(3)P though comprising a small percentage of the total phosphoinositides in a cell, is postulated to increase at the PM in the insulin activated state (Maffucci et al., 2003). Increase in PtdIns(3)P levels may be attributed to activation of the class III PI 3K (known as Vps34 in yeast) or the class II PI 3K-C2α. In insulin-stimulated cells, the class II PI 3K-C2α is shown to increase PtdIns(3)P levels (Falasca et al., 2007). Inhibition of PtdIns(3)P levels in L6 muscle cells by knocking down its kinase (PI 3K-C2α) has been linked to impaired glucose uptake and reduced GLUT4 translocation (Falasca et al., 2007). Studies on Munc18c$^{-/-}$ mice (that exhibited impaired GLUT4 trafficking) showed that exogenous delivery of PtdIns(3)P to adipocytes induced GLUT4 externalisation to the PM in the absence of insulin stimulation (Kanda et al., 2005). PtdIns(3)P may help in GLUT4 vesicle trafficking by associating with early endosomes via endosomal proteins containing the Fab1p, YOTB, Vac1p and EEA1 (FYVE) or phox homology domain (PX) domain (Cozier et al., 2002; Falasca et al., 2007; Stenmark et al., 1996). PtdIns(3)P may hence function in the insulin-signalling pathway by facilitating early endosomal and plasma membrane recycling.

PtdIns(3,5)P_2 is another predominantly intracellular phosphoinositide that may be synthesised on early endosomes (Cooke, 2002). Disruption of PtdIns(3,5)P_2 can cause mis-sorting of cargo in the endocytic pathway leading to enlarged/swollen endosomes (Dong et al., 2010). PtdIns(3,5)P_2 levels on intracellular membranes increases in response to insulin (Ikonomov et al., 2007). This increase in PtdIns(3,5)P_2 can be attributed to its kinase PIKfyve, which is present on endosomal membranes and phosphorylates PtdIns(3)P to yield PtdIns(3,5)P_2 (Shisheva et al., 1999; Zolov et al., 2012). The essential requirement for PIKfyve was demonstrated by siRNA knockdown of PIKfyve and/or its regulator ArPIKfyve. This knockdown led to a reduction in GLUT4 on the cell surface and which in turn led to impaired glucose uptake in insulin-stimulated 3T3L1 adipocytes (Ikonomov et al., 2007). The impaired glucose uptake has been attributed to a reduction in levels of PtdIns(3,5)P_2 (Shisheva, 2008). Additional studies that disrupted levels of PtdIns(3,5)P_2 by using a PIKfyve inhibitor called

YM201636 also showed reduced glucose uptake and inhibition of insulin-induced GLUT4 translocation (Ikonomov et al., 2009; Jefferies et al., 2008). With the understanding that PtdIns(3)P, PtdIns(3,5)P_2 and the PtdIns(3,5)P_2 synthesising kinase PIKfyve are indispensable in glucose uptake, it is worth studying their interacting partners in relation to GLUT4 trafficking.

One group of PtdIns(3)P and PtdIns(3,5)P_2 interacting proteins are those belonging to the Endosomal Sorting Complex Required for Transport (ESCRT) family. ESCRTs are a group of proteins that interact directly with PtdIns(3)P and PtdIns(3,5)P_2 and have hence been a focus of the studies described in this thesis. ESCRTs recognise both PtdIns(3)P and PtdIns(3,5)P_2 on endocytosed vesicles (Stahelin et al., 2002; Whitley et al., 2003). ESCRT proteins contain FYVE or GLUE domains (within which is embedded a positive zinc finger motif) that interacts with PtdIns(3)P (Kutateladze and Overduin, 2001). The FYVE domain contains histidine residues in a conserved RR/KHHCR motif that links the zinc clusters in the zinc finger motif. It is these histidine residues which when protonated coordinate PtdIns(3)P and ESCRT protein binding (Kutateladze, 2010; Lee et al., 2005). PtdIns(3,5)P_2 is also involved with ESCRT mediated endosomal trafficking and interacts with an ESCRT protein further downstream of PtdIns(3)P interacting proteins. This ESCRT protein is CHMP3 (Muzioł et al., 2006; Whitley et al., 2003). CHMP3 is crucial for mediating ESCRT disassembly. Overexpression of a truncation mutant of CHMP3 leads to vacuolation and a disruption in ESCRT-mediated endosomal trafficking (Teis et al., 2008; Whitley et al., 2003). Phosphoinositides and phosphoinositide interacting ESCRT components are hence crucial for ESCRT-dependent endosomal trafficking.

1.6 Aims and motivation for the work described in this thesis

Studies using insulin-responsive tissues have given us considerable knowledge on glucose flux in maintaining body homeostasis and in understanding GLUT4 trafficking. The overall aims of the study described in this thesis is to identify novel regulators of GLUT4 trafficking at the subcellular level by using primary adipocytes as the test system.

The endocytic route for GLUT4 is incompletely understood. PtdIns(3)P and PtdIns(3,5)P_2 are well characterised as key lipid signalling molecules in endosomal GLUT4 vesicle traffic. PtdIns(3,5)P_2 is synthesised in response to insulin signalling and is required for GLUT4 translocation. PtdIns(3,5)P_2 also forms a part of the endosomal ESCRT signalling pathway where it interacts with the ESCRT component, CHMP3. Is the functional ESCRT machinery required for insulin-stimulated GLUT4 translocation?

The recent evidence showing that postprandial hyperinsulinemia and insulin resistance are caused due to a truncation mutant of a Rab GAP called AS160 opens the possibility to involvement of Rab GTPases as regulators of GLUT4 translocation and glucose uptake in insulin responsive tissues. Akt (which is a key insulin activated kinase) directly regulates AS160 in the insulin signalling cascade, implicating that Rabs may well be insulin-regulated via AS160 or another insulin signalling protein. Preliminary studies in the Holman lab identified the exocytic Rab3B as being insulin responsive whereby it gets GTP-loaded in response to an insulin stimulus. Though a number of Rabs have been identified in GLUT4 trafficking, the Rabs involved in the final stages of GLUT4 vesicle docking and fusion have not been clearly documented. Until recently, only Rab10 was shown to be involved with GLUT4 vesicle docking in adipocytes but not in vesicle fusion. Based on literature from other vesicle trafficking pathways where Rab3 isoforms play a key role in vesicle docking and fusion, I hypothesise that Rab3B may have a similar role in GLUT4 trafficking and possibly vesicle fusion. Work described in this thesis therefore aims to investigate the possible involvement of the exocytic Rab3B and its effectors in the final stages of GLUT4 translocation.

2 Materials and Methods

2.1 Materials

2.1.1 Chemicals, reagents and instrumentation

All laboratory chemicals were of analytical grade and purchased from Sigma-Aldrich Chemical Company (Sigma-Aldrich) or Fisher Scientific UK Ltd. (Fisher Scientific) unless otherwise stated. Double distilled H_2O (ddH_2O) was used in preparation of all buffers and reagents unless otherwise specified.

Company	Address
Ambion	Paisley, RFW, Scotland
Amersham Biosciences	Little Chalfont, BKM, UK
Applied Biosystems	Warrington, CHS, UK
BD Biosciences	Oxford, OXF, UK
Beckman Coulter	Wycombe, BKM, UK
Bethyl Labs.	Montgomery, TX, USA
Bio-rad	Hempstead, HRT, UK
BMG Labtech.	Aylesbury, BKM, UK
Calbiochem	Watford, HRT, UK
Carl Zeiss, Ltd.	Welwyn, HRT, UK
CBS Scientific Systems	Del Mar, CA, USA
Clontech Labs. Inc.	St-Germain-en-Laye, France
Covance Res. Products	Berkeley, CA, USA
Enzo Life Sci.	Exeter, DEV, UK
Eppendorf	Cambridge, CAM, UK
Fisher Scientific UK Ltd.	Loughborough, LEI, UK
Fujifilm	Sheffield, SYK, UK
Greiner	Stonehouse, GLS, UK
Invitrogen	Paisley, RFW, Scotland
Life Technologies	Paisley, RFW, Scotland

Millipore	Watford, HRT, UK
MJ Research	Waltham, MA, USA
Molecular Probes	Paisley, RFW, Scotland
MSE	London, UK
MWG Biotech.	London, UK
New England Biolabs	Hitchin, HRT, UK
Pall Life Sciences	Port Washington, NY, USA
Pierce	Cramlington, NLD, UK
Proteintech Group Inc.	Manchester, GTM, UK
Sarstedt	Leicester, LEI, UK
Sigma-Aldrich Chem. Co.	Gillingham, DOR, UK
Stratagene	La Jolla, CA, USA
Thomas Scientific	Swedesboro, NJ, USA
UVP	Cambridge, CAM, UK
Vector Labs.	Peterborough, CAM, UK
Worthington Biochem.	Lakewood, NJ, USA
Zymed Labs.	San Francisco, CA, USA

Table 2.1: List of suppliers. The table provides the names and addresses of all the suppliers from which laboratory reagents or equipment were purchased/used.

2.1.2 Antibodies

Primary antibodies	Clonality/ purification	Specifications	Source (Cat. No.)
Mouse anti-FLAG	Monoclonal (Clone M2)	1:1000 (WB)	Sigma (F3165)
Goat anti-GST	Polyclonal, affinity purified	1:5000 (WB)	Bethyl Labs. (S190-121)
Mouse anti-HA	Monoclonal (Clone16B12)	1:1000 (WB) 1:500 (IF) 1 μg/ml (HG)	Covance (MMS-101P)
Mouse anti-EEA1	Monoclonal purified	1:250 (IF)	BD Biosciences (610456)
Mouse anti-Ubiquitin (Ub)	Monoclonal (Clone FK2)	1:400 (IF)	Enzo Life Sciences (BML-PW8810-0100)
Mouse anti-syntaxin-6 (Stx6)	Monoclonal purified	1:200 (IF)	BD Biosciences (610635)
Mouse anti-Transferrin receptor (TfR)	Monoclonal purified (Clone H68.4)	1:100 (IF)	Zymed Labs. (136800)
Rabbit anti-GLUT4 C-terminus	Polyclonal, serum purified	1:10,000 (WB) 1:1000 (IF)	In-house
Mouse anti-MBP	Monoclonal (Clone MBP-17)	1:5000 (WB)	Sigma (M6295)
Rabbit anti-Noc2	Polyclonal	1:1000 (WB)	Proteintech (15297-1-AP)

Table 2.2: Sources of primary antibodies with dilutions for usage. The table provides a list of primary antibodies used together with their source and dilution for western blotting (WB), immunofluorescence (IF) and HA-translocation studies (HG). The antibodies for WB were diluted in TBS-T with BSA to a final concentration of 1% BSA and 0.02% NaN_3 and stored at 4°C until use *(as described in section 2.2.5.6)*. The antibodies for IF were prepared in permeabilisation buffer *(as described in section 2.2.4.1)*. The anti-HA antibody for the HG assay was prepared in KRH buffer (as described in section 2.2.3.4).

Secondary antibodies	Clonality/ purification	Specifications	Source (Cat. No.)
AlexaFluor® conjugated	-	1:300 (IF)	Molecular Probes
anti-mouse with HRP	Serum affinity purified	1:5000 (WB)	Thomas Scientific (C986W66)
anti-rabbit with HRP	Serum affinity purified	1:5000 (WB)	Millipore (AP188P)
anti-goat with HRP	Serum affinity purified	1:5000 (WB)	Sigma (I 5256)
anti-mouse with β-galactosidase	Serum affinity purified	1 μg/ml (HG)	Southern Biotech. (1030-06)

Table 2.3: Sources of secondary antibodies with dilutions for usage. The table provides a list of secondary antibodies used together with their source and dilution for western blotting (WB) or immunofluorescence (IF). Secondary antibodies for WB were prepared in 5% milk in TBS-T *(as described in section 2.2.5.6)* and temporarily stored at 4°C until use. The antibodies for IF were prepared in permeabilisation buffer *(as described in section 2.2.4.1).*

2.1.3 Rats

The animals used in the following studies were male Wistar rats that weighed 180-200 g and were 7-8 weeks old. The rats were sacrificed by cervical dislocation and immediately dissected to remove the necessary tissues. For mRNA extraction, tissues were stored in liquid nitrogen. For isolation of adipocytes, tissues were placed in Krebs-Ringer-HEPES-BSA (KRBH) buffer (131 mM NaCl, 4.7 mM KCl, 1.25 mM $MgSO_4.7H_2O$, 2.5 mM $CaCl_2.2H_2O$, 2.5 mM $NaH_2PO_4.2H_2O$, 10 mM HEPES pH 7.4 with 1% BSA (w/v)) and maintained at 37°C until tissue digestion.

2.2 Methods

2.2.1 Preparation of constructs for cloning

2.2.1.1 Primer generation

Rattus norvegicus (TaxID: 10116) cDNA sequences for the gene of interest were obtained from NCBI's nucleotide repository. A restriction enzyme map of the gene's coding sequence was generated with the New England Biolabs cutter (Vincze et al., 2003) to identify potential restriction sites present within a cDNA sequence. Primers (with non-naturally occurring restriction sites) were selected using the OligoCalc engine for determining primer-melting temperature (Tm) (Kibbe, 2007). Primers were selected based on their ability to avoid self-complementarity and hairpins as determined by the OligoCalc engine. Primers were purchased from Invitrogen/MWG Biotech. Primers were reconstituted as 50 μM stock solutions and stored at -20°C until use.

2.2.1.2 General cloning methodology

Total tissue cDNA was prepared as described in section *2.2.4.3*. All the reaction components were made up on ice. The master mix for specific cDNA amplifications were prepared using the *Phusion*® (New England Biolabs) DNA polymerase and its respective buffer *(see description in Table 2.4).* PCR reactions were carried out using a PTC-150 MiniCycler PCR machine (MJ Research). The final volume of the reaction mixture was 50 μl and constituted as described in the Table 2.4 below.

A

Component	Amount/reaction	Concentration/reaction
DNA template*	5 μl	0.05 or 50 ng
10 μM 5'-3' primer	2.5 μl	0.5 μM
10 μM 3'-5' primer	2.5 μl	0.5 μM
10 mM dNTP	1 μl	200 μM
5X buffer	10 μl	1X
DNA polymerase	0.5 μl	1 U
ddH_2O	make upto 50 μl	-

B

Stage	Temp.	Cycles	Time
Initial denaturation	95°C	1	2 min
Denaturation	95°C	35 cycles	2 min
Annealing	*Tm* minus 5°C		30 s
Extension	72°C		1 min/kb
Final extension	72°C	1	10 min
Storage	4°C	-	∞

C

Stage	Temp.	Cycles	Time
Initial denaturation	95°C	1	1 min
Denaturation	95°C	30 cycles	2 min
Annealing	*Tm* minus 5°C		30 s
Extension	68°C		2.5 min/kb
Final extension	68°C	1	10 min
Storage	4°C	-	∞

Table 2.4: Cloning conditions for PCR. The table 'A' provides the components required for setting up a PCR to clone the Noc2 and Rab3 cDNA. The table 'B' lists the cycling conditions for cloning. The table 'C' lists the conditions for generating site-directed mutants for Rab3B and Noc2 constructs.
** 0.05 ng was used when a plasmid was used as the DNA template and 50 ng was used when a cDNA library was the template DNA.*

2.2.1.3 Preparation of XL-1-Blue competent cells

On day 1, an inoculation loop was used to streak a glycerol stock of XL1-Blue cells (Stratagene) on a sterile lysogeny broth (LB; commonly referred to as Luria broth (Bertani, 2004)) agar plate (1% (w/v) Bacto^{TM} tryptone (BD Biosciences), 0.5% (w/v) Bacto^{TM} yeast extract (BD Biosciences), 0.5% NaCl pH 7.5, 1.5% (w/v) agar, autoclaved). The plate was incubated at 37°C for 16 h. On day 2, a single colony was picked from the LB agar plate, inoculated into 2.5 ml of LB broth (1% (w/v) Bacto^{TM} tryptone, 0.5% (w/v) Bacto^{TM} yeast extract, 0.5% NaCl pH 7.5, autoclaved) and incubated overnight at 37°C at 250 x *g* on a shaking incubator. On day 3, the entire overnight culture was diluted 1:100 by inoculating the culture into 250 ml of LB broth containing 20 mM $MgSO_4$ in a 1 l flask. The 1 l flask containing this culture was incubated at 37°C on a shaking incubator at 250 x *g*. The density of the culture measured from absorption at 600 nm ($A_{600\ nm}$) was checked at regular 1 h intervals using a spectrophotometer. Once the $A_{600\ nm}$ reached 0.6, the incubation was stopped and the cells were pelleted by centrifuging the culture at 4500 *x g* for 5 min at 4°C. The cell pellet was gently re-suspended (using chilled pipettes and pipette tips) in ice-cold transformation buffer I (30 mM CH_3COOK, 10 mM $CaCl_2$, 50 mM $MnCl_2$, 100 mM RbCl, 15% glycerol (v/v)**.** The pH was adjusted to 5.8 with 1 M CH_3COOH. The buffer was filter sterilised using a 0.2 µm filter (Millipore) and stored at room temperature). The cell suspension was incubated on ice for 5 min followed by centrifugation at 4500 x *g* for 5 min at 4°C. The cell pellet was gently re-suspended in 10 ml of ice-cold transformation buffer II (10 mM PIPES, 75 mM $CaCl_2$, 10 mM $RbCl_2$, 15% glycerol (v/v). pH was adjusted to 6.5 with 1 M KOH. The buffer was filter sterilised using a 0.2 µm filter and stored at room temperature). The cell suspension was incubated on ice for 60 min and then aliquots of 200 µl were transferred into 0.5 ml microfuge tubes (Eppendorf). Microfuge tubes were frozen in dry ice and isopropanol bath and stored at -70°C.

2.2.2 Quantitative PCR (qPCR)

2.2.2.1 Primer generation for qPCR

Primers to the concerned cDNA were generated using NCBI's primer BLAST software (Ye et al., 2012) and the Primer3 software (Untergasser et al., 2007). The newly obtained primers were checked for self-complementarity using the OligoCalc software (Kibbe, 2007). Primers were also checked for 40-70% GC content, a Tm difference of 0.5°C between primers and no more than two G/C in the last 5 nucleotides at the 3' end (if possible). A folding map of the cDNA of interest was generated to identify folding patterns in the DNA such as hairpins that could form at the primer annealing temperature of 60°C (Zuker, 2003). On analysis of the folding map, primers were selected that did not bind to the hairpin regions of the folded DNA template. Finally, another filter was used to select the optimal primers. Only those primers that spanned an intron were selected to avoid amplification of any contaminating genomic DNA that may have been retained in the final cDNA preparation by unavoidable experimental error. Exon-intron boundaries for the respective gene were identified using a BLAST-like alignment tool (BLAT) (Kent, 2002). Two sets of primers were selected for each cDNA and validated as per the procedure in section *2.2.2.5* to select the best primer based on the qPCR readout.

2.2.2.2 RNA isolation

Prior to isolating tissues, all the dissecting equipment was cleaned with 99.9% ethanol followed by RNase AWAY® (Sigma-Aldrich). Tissues were isolated from rats as described in *2.1.3*, wrapped in clean aluminium foil squares and immediately frozen in liquid nitrogen. The tissue sample was weighed to contain 1 g of tissue material and any additional tissue was cut off using a clean scalpel/blade. A mortar and pestle (precooled to -80°C) was used to grind the tissue to a fine powder. The mortar was kept in an ice bucket and liquid nitrogen was slowly added during the grinding process. The powdered tissue was transferred to a 55 ml Potter-Elvehjem glass pestle tissue grinder and mixed with 10 ml of TRIzol® (Life Technologies) RNA isolation reagent. The mixture was

homogenised with 20 strokes at 1600 rpm using a Rexon DP-200 AS bench top drill. The homogenised mixture was clarified by centrifugation at 12,000 x *g* for 5 min at 4°C. The supernatant was transferred to a fresh 30 ml aluminosilicate glass tube (Corex No. 8445) and allowed to stand at room temperature for 5 min. 2 ml chloroform was added to the sample, the mouth of the glass tube was sealed in Parafilm® (Sigma-Aldrich) and the tube was vortexed for 15 s. The mixture was allowed to stand at room temperature for 10 min. The tubes were then centrifuged at 12,000 x *g* for 15 min to separate the contents into three phases. The upper colourless phase contained RNA, the interphase contained DNA and the bottom red organic phase contained protein. The upper colourless phase was transferred into a new 30 ml glass tube, mixed with 5 ml of isopropanol, sealed with Parafilm® and inverted several times to mix. The mixture was incubated for 10 min at room temperature to facilitate RNA precipitation. The mixture was then centrifuged at 12,000 x *g* for 5 min at 4°C to pellet the RNA. The supernatant was discarded and RNA pellet was re-suspended in chilled 75% ethanol. The RNA was pelleted again by centrifugation at 7,500 x *g* for 5 min at 4°C. The ethanol supernatant was discarded and RNA was dissolved in 500 µl of diethylpyrocarbonate (DEPC)-treated water (0.1% (v/v) DEPC in Milli-Q® H_2O incubated at 37°C for 12 h and autoclaved). The dissolved RNA was transferred to 1.5 ml RNase free microfuge tubes (Eppendorf). The microfuge tubes containing RNA solution were incubated at 55°C for 15 min to completely dissolve the RNA. Freshly prepared RNA was quantified using a Bio Photometer UV spectrophotometer (Eppendorf) and stored at -80°C until cDNA preparation.

2.2.2.3 cDNA preparation

The following procedure was performed in a laminar airflow hood to avoid contamination. 5 µg of the RNA solution that was prepared as described in section *2.2.2.2* was pipetted into a 0.2 ml DNase/RNase free PCR tube and made up to 20 µl together with the addition of 1 µl of DNase I (Ambion) and 1 µl of DNase I buffer (Ambion). The DNA digestion reaction was carried out for 1 h at 37°C in a PCR machine. DNase I was inactivated by heating the reaction at 75°C

for 15 min. RNA concentration was quantified using a spectrophotometer. 1 μg of RNA was used for generating the cDNA using the SuperScript® III First-Strand Synthesis SuperMix kit (Invitrogen). The following components were made up in an ice bucket. 10 μl RT reaction mix, 2 μl RT enzyme mix and 1 μg RNA were made up to 20 μl using DEPC-treated RNase free water. The contents were gently mixed and incubated at 25°C for 10 min followed by incubation at 50°C for 30 min. Heating the tube at 85°C for 5 min terminated the reaction. The mixture was allowed to cool to room temperature. 1 μl (2 U) of RNase H was added to the mixture and it was incubated at 37°C for 20 min to dissolve any remaining RNA. The cDNA solution was diluted in a 1.5 ml DNase/RNase free microfuge tube (Eppendorf) with DEPC-treated RNase free water to get approximately 1 ng/μl and stored at -80°C until use.

2.2.2.4 qPCR assay setup and data analysis

All procedures for setting up the qPCR assay plate were done in a laminar airflow cabinet and made use of DNase/RNase free filter tips. A 96-well MicroAmp® (Applied Biosystems) plate was used to set up the qPCR reaction in a small ice bucket. Each well contained 5 ng of cDNA, 7.5 μl of iTaq SYBR Green Supermix with ROX (Biorad), 7.5 pmoles each of forward and reverse primers and DEPC-treated RNase free water made up to a final volume of 15 μl. A control was used for each sample tested. This control contained only DEPC-treated RNase free water, primers, supermix and it was devoid of any cDNA sample. The qPCR plate was read on a qPCR machine (Applied Biosystems). The program that was set up included initial denaturation at 95°C for 2 min. Cycling was performed at 95°C for 15 s followed by 60°C for 1 min. The cycling step was repeated 40 times. For the melt curve, the samples were heated up to 95°C for 15 s and then cooled down to 60°C for 1 min. The temperature was then increased by 0.7°C increments until 95°C following which the reaction was stopped.

The qPCR data was analysed to check for optimal amplification efficiency (slope close to -3.3), optimal correlation coefficient (R^2 value >0.99) and threshold cycle

(Ct) values. The Ct value is the number of cycles needed to surpass the background/threshold fluorescence signal. The lower the Ct value, the greater the amount of target in the sample. Hence, the Ct value is inversely proportional to the target oligo in the cDNA sample. The melt curve was also analysed for primer efficiency. The presence of one single peak on a melt-curve graph indicated primer specificity to the target oligo sequence and a good melt curve. If more than one peak was observed, the primer(s) were not used as it indicated primer self-complementarity or more than one annealing site in the cDNA sample. Ct values were calculated as follows:

Step1:
Normalise sample to the housekeeping gene,
ΔCt = Ct value of sample – 28S rRNA Ct value of sample

Step2:
ΔCt is normalised to a reference; in this case, 28S rRNA is set to 1,
ΔΔCt = ΔCt - 1

Step3:
Increase in the amount of target cDNA in comparison to the reference,
$2^{-\Delta\Delta Ct}$

2.2.2.5 Primer validation in tissues

The two sets of primers that were designed for each cDNA were tested in a range of tissues to obtain a primer that satisfied the criteria described in section *2.2.2.4*. The two primers for each cDNA were also tested using serial dilutions of cDNA. A serial dilution of the total cDNA sample from a specific test tissue was prepared in the 96-well plate. Separate wells contained 5 ng, 2.5 ng, 1.25 ng or 0.625 ng of a tissue's total cDNA together with the reaction mixture described in *2.2.2.4*. Primers were tested in duplicates with each serial dilution. Since the dilutions were different by a factor of two, the amplification by a set of primers was expected to be one Ct value apart for each dilution. If the primers could not

correctly detect these changes in total cDNA concentration, they were discarded and replaced with newly designed primers.

2.2.3 Preparation and use of primary rat adipocytes for *in vitro* studies

2.2.3.1 Isolation and preparation of rat adipocytes

6-8 rats were sacrificed by cervical dislocation and their epididymal fat pads were removed and placed in KRBH buffer (maintained at 37°C). 4 fat pads per 5 ml of sterile digestion buffer (131 mM NaCl, 4.7 mM KCl, 1.25 mM $MgSO_4.7H_2O$, 2.5 mM $CaCl_2.2H_2O$, 2.5 mM $NaH_2PO_4.2H_2O$, 10 mM HEPES pH 7.4, 1% BSA (w/v), 0.05% collagenase (type I) (Worthington), 5 mM glucose) were transferred into a 30 ml skirted conical bottom tube (Universal tube) and minced with scissors (approximately 120 chops). The skirted conical bottom tubes were transferred to a water bath at 37°C and shaken at 150 cycles/min for 30-35 min until no lumps were present. The cell suspension was filtered through 2 layers of nylon mesh that had a pore size of 250 µm and the mesh was washed with KRBH buffer into a new 30 ml skirted conical bottom tube. Cells were allowed to float to the top for 1 min in a 37°C water bath. The infranatant was removed using a blunt ended needle; cells suspensions were adjusted to approximately 25 ml with additional KRBH buffer and gently inverted to mix. The KRBH buffer washing process was repeated 3 times and the cell suspension was adjusted to 50% cytocrit. To prepare the cytocrit, adipocyte suspension was roughly adjusted in KRBH buffer to contain 50% (v/v) KRBH buffer to adipocytes in the universal tube. The universal tube was gently inverted to evenly mix the adipocyte suspension and a capillary tube was inserted in this suspension to take a sample. The end of the capillary tube was sealed with plasticine before it was centrifuged at 1000 x *g* for 1 min. The separated adipocyte and buffer volumes were calculated as a fraction of the adipocyte length in the capillary tube. The cytocrit was then adjusted to the required cytocrit with additional KRBH buffer.

2.2.3.2 Electroporation

Dulbeco's Modified Eagles Medium I (DMEM-I) (Dulbeco's Modified Eagles Medium, 0.2 μM adenosine with 2 mM glutamine), DMEM-II (DMEM-I with 100 μg/μl gentamycin) and DMEM-III (DMEM-II with 3.5% (w/v) BSA) were prepared 1-2 h prior to electroporation and placed in an incubator with 5% CO_2 at 37°C. An appropriate concentration of the mammalian expression vector(s) (described in the respective figure legend) was prepared in DMEM-I with 0.5 mg/ml final concentration of herring sperm DNA to yield the DNA mixture. The volume of DNA was diluted to provide sufficient material for 5 cuvettes per reaction condition or 1 ml of DNA mixture per reaction condition. Each electroporation cuvette accommodated 200 μl of the DNA mixture and 200 μl of cell suspension.

Prior to electroporation, the cell suspension that was prepared in *2.2.3.1* was washed once in DMEM-I and allowed to float. The cell suspension was adjusted to 50% cytocrit as described in section *2.2.3.1*. The cytocrit was adjusted to 50% with DMEM-I instead of KRBH buffer. The 50% adipocyte-DMEM-I suspension was placed in a water bath that was maintained at 37°C until electroporation.

Cuvettes containing cell suspension and DNA mixture were electroporated using a Biorad Gene Pulser (Biorad) at 400 V and 500 μF. A time constant of 12-14 ms was achieved under these conditions. Cuvette contents from each condition were pooled into a 15 ml polypropylene centrifuge tube (Fisher Scientific). The 15 ml tube was adjusted to approximately 13 ml with DMEM-II and incubated at 37°C until the next set of cuvettes were electroporated. The infranatant from the 15 ml tube was removed using a sterile blunt ended needle and the remaining cells were re-suspended in 4 ml of DMEM-III. The newly re-suspended cells were transferred to a 5 ml cell culture petri dish and maintained overnight (16 h) in an incubator at 37°C with 5% CO_2, unless otherwise mentioned in a figure legend.

On the next day, adipocytes were transferred to 15 ml flat-bottomed polypropylene tubes (Sarstedt) and washed thrice with KRBH buffer. This was done to remove residual DMEM-III prior to treating the adipocytes with insulin.

2.2.3.3 Insulin stimulation

The adipocyte suspension(s) prepared in section *2.2.3.1* (without electroporated plasmid) or *2.2.3.2* (with electroporated plasmid) were separated into 15 ml flat-bottomed polypropylene tubes that were labelled as basal or insulin samples. The samples from section *2.2.3.1* that were prepared without any electroporation were stimulated with 20 nM insulin for 20 min at 37°C. The samples from section *2.2.3.2* that were electroporated with plasmid(s) were first re-suspended in 10 ml KRBH buffer and allowed to stand at 37°C. The infranatant was then removed with blunt ended needles. This re-suspension step with KRBH buffer was repeated thrice. The samples were then stimulated with 60 nM insulin for 20 min at 37°C.

2.2.3.4 HA-GLUT4 translocation studies

Adipocytes prepared as described in section *2.2.3.2* and *2.2.3.3* were transferred to 4 ml polypropylene tubes prior to insulin stimulation. The polypropylene tubes were labelled as basal or insulin samples. The adipocyte samples were then stimulated with 60 nM insulin. The polypropylene tubes were gently inverted every 5 min to ensure adequate mixing. After 20 min, intracellular GLUT4 trafficking was stopped by addition of KCN to a final concentration of 2 mM. The tubes were gently inverted to mix the KCN. The samples were moved from the 37°C water bath to room temperature. Each adipocyte cell suspension sample was washed twice using blunt ended needles to remove the infranatant after each wash. After each wash, the cells were allowed to float to the top of the tube. Washes were done with 2 ml Krebs-Ringer-HEPES (KRH) buffer (131 mM NaCl, 4.7 mM KCl, 1.25 mM $MgSO_4.7H_2O$, 2.5 mM $CaCl_2.2H_2O$, 2.5 mM $NaH_2PO_4.2H_2O$ with 10 mM HEPES pH 7.4) containing a final concentration of 2 mM KCN. The sample was made up to 1 ml, inverted to mix and 100 μl of the cell suspension was transferred (using cut pipette tips) to a 1.5 ml microfuge tube containing 100 μl SDS sample buffer (2% (w/v) SDS, 62.5 mM Tris-HCl pH 6.8, 0.01% (w/v) bromophenol blue, 10% (w/v) glycerol and 100 mM dithiothreitol (DTT)). The 200

μl cell suspension sample mixed with SDS sample buffer was frozen at -20°C (it was used as a control with the SDS-PAGE gel and western blotted to check the electroporated plasmid expression levels). The remaining adipocyte suspension samples were washed once more with 2 ml KRBH buffer containing 2 mM KCN and incubated with the mouse anti-HA antibody *(see Table 2.2)* for 1 h at room temperature with mixing by inversion every 15 min. The cells were then washed twice with 2 ml KRBH buffer containing 2 mM KCN. The adipocyte suspension was adjusted to 1 ml and incubated with anti-mouse secondary antibody (conjugated with β-galactosidase) (Southern Biotech.) for 1 h at room temperature with mixing by inversion every 15 min. Each of the adipocyte suspensions (treated as basal or insulin) were washed once with 2 ml KRBH buffer containing 2 mM KCN and then thrice with 2 ml KRH buffer only. The adipocyte suspensions were transferred to a Bijou tube and were adjusted to a final 3 ml volume with KRH buffer. A black microtitre plate (Greiner) was set up containing 50 μl of KRH buffer. Simultaneously, the stock fluorescein di-β-D-galactopyranoside (FDG) reagent (Molecular Probes) was prepared at a dilution of 1:200 in KRH buffer. The adipocyte suspension was inverted and mixed well before pipetting 50 μl from each sample as quintuplicates into each well of the microtitre plate that already contained 50 μl KRH buffer. 100 μl of the diluted FDG reagent was added to each well and fluorescence was measured using a PHERAstar FS microplate reader (BMG Labtech.). 50 μl of the adipocyte suspension from the Bijou tube was transferred to a microfuge tube containing 50 μl of 0.2 M NaOH and assayed for protein content using the BCA method *(as described in section 2.2.5.7).*

2.2.3.5 Subcellular fractionation studies

Adipocyte suspensions were electroporated with HA-Noc2 or HA-Noc2 ^{AAA} and maintained overnight *(as described in section 2.2.3.2).* Basal and insulin-treated adipocytes were washed in HEPES-EDTA-sucrose (HES) buffer (20 mM HEPES pH 7.2, 1 mM EDTA and 225 mM sucrose) containing SigmaFAST protease inhibitors (Sigma-Aldrich) and phosphatase inhibitors (10 mM NaF, 200 μM Na_3VO_4, 1 mM Na_2MoO_4, 0.1 μl NIPP1 stock). This washing step was performed

18°C and the adipocytes were allowed to float. The infranatant was removed and 1 ml of HES buffer was added to the adipocytes. The adipocytes were homogenised with 10 strokes of a 55 ml Potter-Elvehjem homogeniser (Thomas Scientific) at a speed of 1600 rpm using a Rexon DP-200 AS bench top drill. The homogenised adipocyte preparation was transferred to 1.5 ml microfuge tubes (Eppendorf) and centrifuged at 1000 x *g* at 4°C for 1 min in a refrigerated centrifuge. 100 μl of this homogenate was saved to run on an SDS-PAGE gel and to analyse protein expression levels. The homogenate was then centrifuged at 17,500 x *g* for 20 min at 5°C. The resulting pellet was used to isolate the plasma membrane and the infranatant was used to isolate the cytosol while the top layer of fat was discarded. The infranatant was removed using a needle (21 G x 1.5") (BD Biosciences) attached to a 2 ml syringe (BD Biosciences) and transferred to a fresh ultra-clear centrifuge tube. All the following centrifugation runs were done in a Beckman TL-100 bench-top ultracentrifuge with a TLA-100.3 fixed angle rotor (Beckman Coulter) maintained at 4°C. The infranatant was centrifuged at 49,000 *x g* for 9 min. The supernatant contained the cytosol and low-density microsomes (LDM) and the pellet contained the high-density microsomes (HDM). The supernatant was centrifuged at 541,000 x *g* for 17 min and the resulting supernatant was transferred to a new 1.5 ml microfuge tube (Eppendorf) and assayed for cytosolic protein content.

To isolate the plasma membrane, the pellet (obtained after the 17,500 x *g* centrifugation for 20 min) was re-suspended in 1 ml of chilled HES buffer, homogenised in a small 5 ml glass homogeniser with 5 strokes and transferred to 2 ml ultra-clear centrifuge tubes (Beckman Coulter). 1 ml of HES buffer was added to the homogeniser and it was homogenised with 2 strokes to mop up any remaining sample. This 1 ml was transferred to the same ultra-clear centrifuge tube containing the pellet homogenate. The pellet homogenate was centrifuged at 17,500 x *g* for 20 min. The pellet was re-suspended in 300 μl of HES buffer and layered onto 600 μl of HES sucrose cushion (20 mM HEPES pH 7.2, 1 mM EDTA and 1.12 M sucrose) and centrifuged at 105,000 x *g* for 20 min in a TLS-55 swing out rotor. The resulting pellet contained mitochondria and nuclei. The interface was used to isolate the plasma membrane. To 700 μl of the plasma membrane, 2

ml of HES buffer was added and it was centrifuged at 74,000 x *g* for 9 min. The plasma membrane pellet was re-suspended in another 2 ml of HES buffer and centrifuged at 74,000 x *g* for 9 min. The plasma membrane was again re-suspended in 100 μl HES buffer and assayed for protein content using the BCA protein assay protocol described in section *2.2.5.7*.

2.2.3.6 Lysis of rat adipocytes

Adipocytes were treated as basal or insulin samples *(as described in section 2.2.3.3),* washed once with 10 ml KRH buffer maintained at 37°C and allowed to float. The infranatant was removed and an equal amount of the lysis buffer containing Halt protease inhibitor cocktail (Fisher Scientific) was added to the adipocyte suspension. HEPES-NaCl lysis buffer (20 mM HEPES pH 7.5, 100 mM NaCl, 2% (v/v) Triton X-100) was used for the Rab3B pull-down studies and Tris-NaCl lysis buffer (20 mM Tris-HCl pH 7.5, 200 mM NaCl, 10% glycerol, 2% (v/v) Triton X-100) was used for the Noc2 pull-down studies. The adipocytes were lysed by vortexing the sample for 15 s and incubating it at 18°C for 20 min. The lysate sample was vortexed once again for 15 s after 20 min and transferred to 1.5 ml microfuge tubes followed by centrifugation at 17500 x *g* for 20 min. The microfuge tubes containing the sample were then kept on ice for 10 min to allow the fat to solidify. A 21 G x 2” needle (BD Biosciences) was used attached to a 2 ml syringe (BD Biosciences) to remove the clear lysate from the solidified fat that formed a white layer at the top of the lysate. The clear lysate was assayed for protein content using the BCA protein assay protocol described in section *2.2.5.7*.

2.2.3.7 Rab3B pull-down studies

Rab3B was loaded with GTPγS or GDP. A GST only protein was also subjected to the following protocol as a control but the buffers for the GST only protein were devoid of any guanine nucleotide. The method in this section is adopted from Christoforidis and Zerial (2000) and involves a number of steps to ensure a stable

Rab3B-(GTPγS/GDP) interaction. Mg^{2+} is required for facilitating the binding and stabilisation of GTP or GDP to the switch region of a Rab GTPase. When EDTA is present in excess, it chelates Mg^{2+} thereby releasing any bound guanine nucleotide from the switch region. The nucleotide loading (NL) buffers that contain excess EDTA in relation to $MgCl_2$ facilitate unloading of any bound guanine nucleotide from the Rab protein and loading of the guanine nucleotide present in the respective buffer. The buffers that contain excess $MgCl_2$ in relation to EDTA facilitate stabilisation of guanine nucleotide present in the respective buffer.

The GST-only construct and GST-Rab3B was expressed as described in *2.2.5.1* and dialysed in HEPES-NaCl buffer (20 mM HEPES pH 7.5, 100 mM NaCl). Glutathione agarose beads (Pierce) were washed once with PBS and twice with HEPES-NaCl buffer to precondition them for GST–Rab3B binding. 20 mg of GST or 40 mg of GST-Rab3B was incubated with 1 ml of glutathione beads in 2 ml Talon disposable gravity column (Clontech Labs Inc.). Incubation was carried out for 1 h at 4°C on a rotator. The following buffers were prepared and the procedure was followed as depicted in Fig. 2.1.

- Nucleotide Loading buffer I (NL-I): 20 mM HEPES-HCl pH 7.5, 100 mM NaCl, 10 mM EDTA, 5 mM $MgCl_2$, 1 mM dithiothreitol (DTT), 10 μM GTPγS (or 10 μM GDP).
- Nucleotide Loading buffer II (NL-II): 20 mM HEPES-HCl pH 7.5, 100 mM NaCl, 10 mM EDTA, 5 mM $MgCl_2$, 1 mM dithiothreitol (DTT), 1 mM GTPγS (or 1 mM GDP).
- Nucleotide Stabilisation buffer I (NS-I): 20 mM HEPES-HCl pH 7.5, 100 mM NaCl, 5 mM $MgCl_2$, 1 mM dithiothreitol (DTT), 10 μM GTPγS (or 10 μM GDP).
- Nucleotide Stabilisation buffer II (NS-II): 20 mM HEPES-HCl pH 7.5, 100 mM NaCl, 5 mM $MgCl_2$, 1 mM dithiothreitol (DTT), 1 mM GTPγS (or 1 mM GDP).

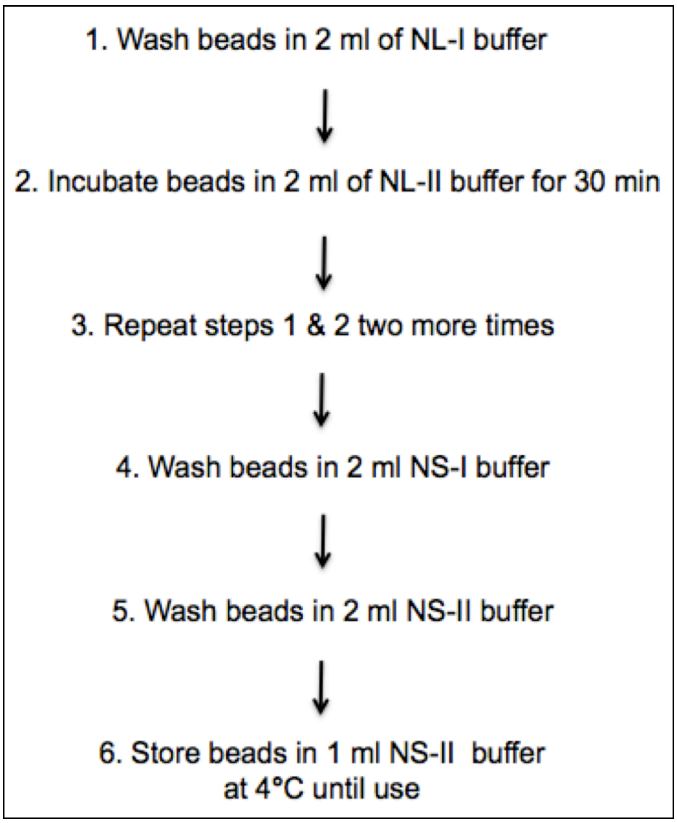

Figure 2.1: Loading of GST-Rab3B with GTPγS or GDP. Nucleotide loading (NL) and nucleotide stabilisation (NS) buffers were prepared separately for Rab3B containing glutathione beads that needed to be loaded with GTPγS or GDP (Sigma-Aldrich). GST-only sample was treated with buffers that were prepared with no nucleotide. The steps in Fig. 2.1 were carried out at 22°C in Talon columns (Clontech Labs Inc.), which contained a preparation of GST-only or GST-Rab3B fusion protein bound to glutathione agarose beads (Pierce). Protocol for Rab3B pull-down was adapted from Christoforidis and Zerial (2000).

The glutathione beads containing Rab3B (loaded with either GTPγS or GDP) and the glutathione beads containing GST-only were washed once with HEPES-NaCl buffer before incubation with adipocyte lysates. The adipocytes were lysed in lysis buffer *(as described in section 2.2.3.6)* and quantified for protein content using the BCA method *(as described in section 2.2.5.7).* An equal concentration of 10 mg adipocyte lysate was added to columns containing GST, GST-Rab3B-GTPγS or GST-Rab3B-GDP immobilised on glutathione beads. The columns were sealed and the lysate and beads were incubated for 2 h at 4°C on a rotator. The lysate was then drained out of each column. The beads in each column were then washed with 10 ml of NS-I buffer followed by 10 ml of Nucleotide Stabilisation buffer III (NS-III) (20 mM HEPES-HCl pH 7.5, 250 mM NaCl, 5 mM $MgCl_2$, 1 mM

dithiothreitol (DTT), 10 μM GTPγS (or 10 μM GDP) and 10 ml of NS-III buffer without any guanine nucleotide. The GST-only column was treated in the same way but the buffers contained no nucleotide. Endogenously bound proteins were eluted from the beads by exchanging the nucleotide on each column using the guanine elution buffer. Proteins from the Rab3B-GTPγS column were eluted with elution buffer containing GDP (20 mM HEPES pH 7.5, 1.5 M NaCl, 20 mM EDTA, 1 mM dithiothreitol (DTT), 5 mM GDP (or GTPγS). Proteins from the Rab3B-GDP column were eluted with elution buffer containing GTPγS while proteins from the GST-only column were eluted with elution buffer containing no nucleotide (the use of GTPγS or GDP in the elution buffers ensured that only the GTPγS or GDP specific proteins that bound to the Rab3B beads were eluted). The beads were incubated with their respective elution buffers at room temperature for 20 min on a rotator. Eluted protein samples were concentrated on a 15 ml Amicon® Ultra spin column (Millipore) (as per manufacturer's instructions) to 100 μl and mixed with SDS sample buffer before being separated on an SDS-PAGE gel.

2.2.3.8 Noc2 pull-down studies

Adipocytes were isolated and electroporated with FLAG-Rab3B and maintained overnight *(as described in sections 2.2.3.1 and 2.2.3.2).* On the next day, the electroporated adipocytes were maintained as basal or treated with insulin *(as described in section 2.2.3.3)* and lysed with Noc2 lysis buffer *(as described in section 2.2.3.6).* The lysates were quantified for protein content using the BCA method *(as described in section 2.2.5.7)* and placed in an ice bucket. The basal lysate volume was split equally into two samples. One sample was maintained as the basal condition and the other sample was segregated so that it could be loaded with GTPγS. GTPγS was added to the segregated basal lysate sample to give a final concentration of 1 mM GTPγS and this sample was incubated for 10 min at 37°C. The basal-GTPγS sample was then transferred to an ice bucket. The GTPγS loading was stabilised by the addition of a final concentration of 10 mM $MgCl_2$ to the basal-GTPγS lysate sample. To maintain consistency, a final

concentration of 10 mM $MgCl_2$ was added to the basal and insulin lysate samples as well.

25 μg of the GST protein or 50 μg of the GST-His-Noc2 fusion protein was added to 100 μl of glutathione agarose beads in a 1.5 ml microfuge tube and maintained for 2 h at 4°C on a rotator. When the MBP-tagged Noc2 construct was used (instead of the GST-His-tagged Noc2 construct), 30 μg of MBP-Noc2 was added to 100 μl of amylose beads and maintained for 2 h at 4°C on a rotator. After the 2 h incubation of beads with GST-His or MBP-tagged Noc2, the beads were washed once with Noc2 lysis buffer. An equal concentration of the lysate from basal, insulin or GTPγS samples (described above) was added to the beads and the incubation was carried out for 1 h at 4°C on a rotator. The beads were washed with 1 ml wash buffer (20 mM Tris pH 7.5, 200 mM NaCl, 5 mM $MgCl_2$, 5% glycerol, 0.2% Triton X-100) five times.

Proteins bound to the GST-tagged Noc2 were eluted with 80 μl SDS sample buffer. Proteins bound to the MBP-tagged Noc2 were eluted with maltose elution buffer (20 mM Tris pH 7.5, 200 mM NaCl, 5 mM $MgCl_2$, 40 mM maltose). Eluted protein samples were separated on an SDS-PAGE gel and western blotted *(as described in sections 2.2.5.3, 2.2.5.5 and 2.2.5.6).*

2.2.4 Confocal microscopy techniques

2.2.4.1 Immunostaining

Basal or insulin stimulated adipocytes were fixed by incubation with 4% (w/v) paraformaldehyde in KRH buffer for 20 min at room temperature, and washed 3 times with PBS using a blunt ended needle and syringe. Cells were then incubated with permeabilisation buffer (1% (w/v) BSA, 3% (v/v) goat serum, 0.1% (w/v) saponin, PBS) for 45 min at 22°C. The permeabilisation buffer was removed and respective primary antibodies *(see Table 2.2)* diluted in permeabilisation buffer were added to the cell samples, which were incubated overnight at 22°C on

a rotary shaker. After 18 h, the cells were washed four times using wash buffer (1% (w/v) BSA, 0.1% (w/v) saponin, PBS). Following the washes, the cell samples were incubated with species-specific fluorophore conjugated secondary antibodies *(see Table 2.5)* for 2 h at 22°C on a rotator.

After the 2 h incubation with the secondary antibody, the cell samples were washed similarly (as done after the primary antibody incubation) with wash buffer five times. The cell samples were roughly adjusted to 50% cells to the wash buffer. 10 μl of a 50% adipocyte cell suspension was added on a microscopy slide containing 10 μl of Vectashield mounting medium (Vector Labs.). Coverslips were sealed onto the cell mount using a transparent lacquer.

Primary antibody	Alexafluor® conjugated secondary antibody
GLUT4 or HA-GLUT4	Anti-rabbit 633
Early Endosomal Antigen 1 (EEA1)	Anti-mouse 568
Transferrin receptor (TfR)	Anti-mouse 546
syntaxin-6 (Stx6)	Anti-mouse 546
Ubiquitin (Ub)	Anti-mouse 568

Table 2.5: Secondary antibodies for immunofluorescence. The table provides a list of the Alexafluor® conjugated secondary antibodies that were directed to the target primary antibody *(see Table 2.2)*.

2.2.4.2 Confocal microscopy

Confocal microscopy was performed using a Zeiss LSM 510 META microscope with 63 x 1.4 NA oil-immersion objective and with dual or triple laser excitation at 458–488, 543 and 633 nm.

2.2.5 Protein biochemistry techniques

2.2.5.1 Expression of fusion proteins in *E.coli*

A glycerol stock of *E.coli* containing the protein expression construct *(listed in Table 2.6)* was gently streaked using sterile pipette tip and inoculated into a 50 ml conical flask containing 10 ml of LB broth and the concerned antibiotic (1 mg per 10 ml of ampicillin for the Amp^R constructs and 0.5 mg per 10 ml of kanamycin for the Kan^R constructs). The culture was grown overnight in a shaking incubator at 37°C at 250 x *g.* This culture was inoculated into a larger 2 l conical flask containing 500 ml LB broth on the next day. The 500 ml culture was incubated on a shaking incubator at 37°C at 250 x *g*. The density of the culture measured from absorption at 600 nm ($A_{600\ nm}$) was checked regularly at 1 h intervals. Once the $A_{600\ nm}$ reached 0.6-0.8, the culture was induced with isopropyl β-D-1 thiogalactopyranoside (IPTG) as described in Table 2.6. The culture was then allowed to express the fusion protein for 3 h at room temperature. In some cases, the expression time and temperature were varied and this is indicated in the respective figure legends. Following expression, the 500 ml culture was centrifuged at 5000 x *g* for 10 min at 4°C. The supernatant was discarded and cell pellet was frozen at -80°C until purification.

Bacterial strain	Genotype	IPTG conc.
E. coli (DE3)	F^- *dcm ompT hsdS* (r_B^- m_B^-) *gal λ*(DE3)	0.1 mM
E.coli Arctic Express (DE3)	F^- ompT hsdS(r_B^- m_B^-) *dcm* Tet^R *gal λ*(DE3) *endA* Hte [*cpn10 cpn60* $Gent^R$]	0.5 mM
E.coli (TB1)	F^- *ara Δ(lac-proAB) [φ80dlac Δ(lacZ)M15] rpsL(Str^R) thi hsdR*	0.3 mM
E.coli Rosetta (DE3) pLysS	F^- *ompT hsdSB* (r_B^- m_B^-) *gal dcm* (DE3) pLysSRARE (Cam^R)	0.5 mM
E.coli Lemo21 (DE3)	*fhuA2 [lon] ompT gal* (λ DE3) *[dcm]* Δ*hsdS/ pLemo*(Cam^R)	0.4 mM

Table 2.6: List of bacterial strains and respective genotypes. The bacterial strains were transformed with the desired bacterial expression vector *(see Supplementary table S1 for list of expression vectors)* and expression was induced with the IPTG concentration listed in this table *(see section 2.2.5.1 for a more detailed explanation on protein expression).*

2.2.5.2 Purification of tagged protein constructs

The frozen pellet obtained from a 500 ml culture *(as described in section 2.2.5.1)* was defrosted on ice and re-suspended with 10 ml of ice cold phosphate buffered saline (PBS) (12.5 mM Na_2HPO_4, 154 mM NaCl pH 7.2) (unless otherwise specified) containing 100 μl Protein Phosphatase Inhibitor Set II (Calbiochem) in a 50 ml conical centrifuge tube (Fisher Scientific). The cell suspension was sonicated on ice using a bench top ultrasonic disintegrator (MSE). Sonication was done at 15 s bursts followed by 45 s of cooling period on ice. This process was repeated 10 times. The sonicated cell suspension was centrifuged at 20,000 x *g* for 45 min at 4°C to clarify the lysate. The clear ~10 ml supernatant was transferred to a new 15 ml conical centrifuge tube and incubated with 500 μl of glutathione agarose beads (Pierce) in the case of GST-tagged fusion proteins. MBP-tagged fusion proteins were purified using an amylose resin (New England Biolabs). Proteins were bound to the beads (or resin) for 1 h at 4°C on a rotator with even mixing. Post binding, the beads were washed 5 times with 10 ml HEPES-NaCl buffer for Rab3B fusion proteins or Tris-NaCl buffer (20 mM Tris-HCl pH 7.4, 200 mM NaCl) for Noc2 fusion proteins. The fusion protein was either left on the beads or eluted using an elution buffer. To elute the fusion proteins, beads were incubated with 500 μl glutathione elution buffer (for GST-tagged fusion proteins) (20 mM HEPES pH 7.5, 100 mM NaCl, 20 mM reduced glutathione, 5 mM β-mercaptoethanol) or maltose elution buffer (for MBP-tagged fusion proteins) (20 mM Tris pH 7.5, 200 mM NaCl, 5 mM $MgCl_2$, 40 mM maltose) and gently mixed for 5 min at room temperature. The 1.5 ml microfuge tube containing beads and eluate was centrifuged for 1 min at 1000 x *g* to sediment the beads. The eluate was transferred to a fresh microfuge tube. This elution process was repeated 5 times and all elutions were pooled together. The pooled eluate was concentrated on a spin column to 0.5-1 ml and dialysed with 5 litres of the respective HEPES-NaCl or Tris-NaCl buffer. The dialysed fusion protein sample was quantified using an SDS-PAGE coomassie gel *(as described in section 2.2.5.4).*

His-tagged fusion proteins were purified on a 1 ml HisTrap FF (GE Healthcare) column using an AKTA FPLC machine (Amersham Biosciences) (Bornhorst and Falke, 2000). The HisTrap FF column was washed with five column volumes of 20% ethanol followed by five column volumes of wash solution (20 mM Tris-HCl pH 7.5, 200 mM NaCl, 20 mM Imidazole). The His-tagged fusion protein sample was injected into the HisTrap FF column. The column was washed with wash solution until the $A_{280\ nm}$ on the FPLC machine dropped to 0, indicating that any unbound proteins had been washed out from the column. The His-tagged fusion protein bound to the column was eluted at a gradient using an elution buffer (20 mM Tris-HCl pH 7.5, 200 mM NaCl, 400 mM imidazole). The eluted fractions were collected, pooled, concentrated on a 15 ml Amicon® Ultra spin column (Millipore) and dialysed in Tris-NaCl buffer (20 mM Tris-HCl pH 7.4, 200 mM NaCl).

2.2.5.3 SDS-PAGE

SDS-PAGE electrophoresis was performed using the Laemmli discontinuous buffer system (Laemmli, 1970). Generally, gel slabs were used that had a thickness of 1.5 mm. For samples that had a small volume, the mini-Protean II gel system (Biorad) was used while for samples of bigger volumes or to achieve better resolution of proteins, the CBS gel system (CBS Scientific) was used. Gels were prepared using ProtoGel (Fisher Scientific) acrylamide/bis-acrylamide (30% w/v acrylamide) in stacking (0.5 M Tris-HCl pH 6.8, 0.4 % (w/v) SDS) or resolving buffers (1.5 M Tris-HCl pH 8.8, 0.4 % (w/v) SDS). The amount of ProtoGel solution used for making the different percentage gels was determined using the following formula: $V_P = (X)\ (V_T) / 30$. Where, V_P is Volume of 30% ProtoGel, X is % of the monomer desired in gel and V_T is the total volume of gel casting solution. The polymerisation of acrylamide and bis-acrylamide was initiated using 10% (w/v) ammonium persulfate (APS) and undiluted N,N,N,N'-tetramethylenediamine (TEMED) as a catalyst. The final concentration of APS was 0.05% in stacking gels and resolving gels while the final concentration of TEMED was 0.1% in the stacking gels and 0.05% in the resolving gels. Protein samples for SDS-PAGE were solubilised by addition of SDS sample buffer and 25 mM DTT followed by

boiling for 5 min on a heat block. Samples were loaded into the wells alongside a Novex® Sharp pre-stained protein maker (Invitrogen). The gels were run using electrophoresis buffer (25 mM Tris-HCl pH 6.3, 0.1% (w/v) SDS, 0.2 M glycine) at a constant voltage of 200 V for 1 h until the dye front had run out of the gel.

2.2.5.4 Coomassie staining

For visualisation of proteins directly on the gel, coomassie staining was carried out. The SDS-PAGE gel was rinsed once in water to get rid of any electrophoresis buffer. The gel was then incubated for 2 h with Fermentas PageBlue™ Staining Solution (Thermo Scientific) and was de-stained overnight in ddH_2O. Images of the gel were taken using a Hamamatsu camera attached to the EPI Chem II darkroom (Ultra-Violet Products).

2.2.5.5 Electrophoretic transfer of proteins for western blotting

Nitrocellulose membrane (Pall Life Sciences) and two pieces of extra thick blot paper (Biorad) were cut to an appropriate size for the gel and soaked in transfer buffer (39 mM glycine, 48 mM Tris pH 8.8, 0.0375% SDS (w/v), 20% methanol (w/v)). For electrophoretic transfer, the TransBlot SD Semi-Dry Transfer Cell apparatus (Biorad) was used. A piece of wet blotting paper was first placed on the anode. The nitrocellulose membrane and then the resolving gel piece were placed on the wet blotting paper. Any air bubbles were gently removed using a handheld roller. Another piece of wet blotting paper was placed over the gel. A roller was rolled across the top of this set-up to remove any air bubbles. The apparatus was sealed with the cathode lid. Electrophoretic transfer was carried out at constant current for 1 h 50 min. The current used was calculated at 0.8 mA per cm^2 of gel area.

2.2.5.6 Western blotting

The nitrocellulose membrane was washed with ddH_2O and stained with Ponceau S solution (0.1% (w/v) Ponceau S, 3% (w/v) trichloroacetic acid). The markers were labelled with a pencil. 5% dried skimmed milk from Marvel was prepared in Tris-buffered saline containing Tween-20 (TBS-T) (10 mM Tris-HCl pH 7.4, 154 mM NaCl, 0.1% (v/v) Tween) to make the 5% blocking solution. The membrane was blocked with 5% blocking solution on a shaker for 1 h. The membrane was washed five times with 5 min each time in TBS-T followed by incubation with the primary antibody on a shaker overnight at 4°C or for 2 h at room temperature. The primary antibody was washed off the membrane five times with 5 min each time in TBS-T followed by incubation with secondary antibody. The secondary antibody was diluted (1:5000 unless otherwise specified) in 5% blocking solution and incubated with the membrane on a shaker at room temperature for 45 min. The secondary antibody was washed off six times with 5 min each time using TBS-T. The membrane was dried on the bench for 1 min and incubated for 3 min with 1:1 ratio of ECL (A and B) or for 5 min with Dura (Thermo Scientific) or ECL advance (Amersham Biosciences). The fluorescent bands were detected on the membrane using a Hamamatsu camera attached to the EPI Chem II darkroom (Ultra-Violet Products).

To re-probe the same blots with another antibody, the nitrocellulose membranes were stripped of the bound antibodies by incubating the membranes with stripping buffer (62.5 mM Tris-HCl pH 6.7, 100 mM β-mercaptoethanol, 2% SDS) for 30 min at 50°C with gentle shaking. The membranes were then washed twice with 10 min each time using TBS-T, blocked with 5% blocking solution and re-probed by following the western blot procedure again.

2.2.5.7 Protein quantification assays

Protein assays were carried out using bicinchoninic acid (BCA) (Pierce) or the ready to use 660 nm Protein Assay reagent (Pierce). The protein standards were prepared from a stock of 1 mg/ml BSA protein solution and diluted to yield 0.2, 0.4, 0.6, 0.8 and 1.0 μg per 10 μl sample. The 10 μl sample was added to each

well of a 96-well microtitre plate (Greiner). Samples were assayed in duplicates. 10 μl of the test protein sample was loaded in duplicates alongside the above standards for quantification. In case of the BCA protocol, Reagent A (Pierce) and Reagent B (4% (w/v) $CuSO_4.5H_2O$) were prepared in a 50:1 dilution. 200 μl of the BCA preparation or 200 μl of the 660 nm Protein Assay reagent was added to each well containing the standards or sample. The 96-well plate was incubated at 37°C for 30 min and then kept at room temperature for 2 min before it was read on a PHERAstar FS microplate reader (BMG Labtech.). Plates prepared with BCA reagent were read at 565 nm while those prepared with the 660 nm Protein Assay reagent were read at 660 nm.

2.2.5.8 Extraction of proteins from SDS-PAGE gels for mass spectrometry

After analysis of the SDS-PAGE coomassie gel, the bands that needed to be excised for analysis were identified. The gel was placed on a clean surface and the bands were cut using a scalpel. The protocol for in-gel trypsin digestion and protein extraction was followed as described by Kinter and Sherman (2000). The gel pieces were transferred into a 1.5 ml microfuge tube containing 200 μl of wash solution (50 % methanol, 5% acetic acid in Milli-Q® H_2O) and put on a rotator overnight. On the second day, the wash solution was removed and the gel sample was washed again with 200 μl of wash solution for 2 h on a rotator. The sample was centrifuged at 1000 x *g* for 1 min and wash solution was discarded. To dehydrate the sample, 200 μl of 50 mM acetonitrile was added and the sample as incubated for 5 min at room temperature. The acetonitrile was removed and the dehydration step was repeated once more. Protein samples were subjected to a reduction step, which was carried out by the addition of 30 μl of 10 mM DTT to the sample and incubating it for 30 min at room temperature. DTT was removed and 30 μl of 50 mM iodoacetamide buffer was added to alkylate the sample. Alkylation was carried out for 30 min at room temperature. Iodoacetamide was removed and 200 μl of 50 mM acetonitrile was added for 5 min at room temperature to dehydrate the sample. Acetonitrile was removed and 30 μl of ice-

cold trypsin solution was added to the sample, which was then placed on ice for 10 min. The sample was centrifuged at 1000 x *g* for 1 min and the excess trypsin solution was removed. 5 μl of ammonium bicarbonate was added to the sample and the protein sample was allowed to trypsin digest overnight at 37°C. On the third day, 50 μl of ammonium bicarbonate was added to the sample and it was incubated for 10 min with gentle vortexing. The supernatant was collected in a new 1.5 ml microfuge tube termed the collection tube. 50 μl of extraction buffer I (50 % acetonitrile, 5 % formic acid in Milli-Q® H_2O) was added to each of the gel pieces. The gel pieces were then incubated for 10 min with occasional and gentle vortexing. The supernatant was transferred to the collection tube prepared in the previous step. 75 μl of extraction buffer II (85 % acetonitrile, 5 % formic acid in Milli-Q® H_2O) was added to the tube containing the gel pieces and this sample was again incubated for 10 min with occasional and gentle vortexing. The supernatant was transferred to the same collection tube. The sample in the collection tube was then dried down in a speed-vac and re-suspended in a re-suspension buffer (98% Milli-Q® H_2O, 2% acetonitrile, 0.1% formic acid). This sample was sent to the liquid chromatography-mass spectrometry facility and analysed on an Agilent Q-TOF instrument in the University of Bath Chemical Characterisation and Analysis facility.

2.2.5.9 Analysis of data

Images (1024 x 942) of individual cells acquired using the confocal microscope were saved as TIFF files that were generated using the Zeiss LSM Image analysis software. The intensity of each wavelength channel was adjusted to a comparable dynamic range using Adobe Photoshop. Each individual channel is then represented in images as black and white signals. The channel intensities were merged into a final image. The merged channels represent the following. Overlap of green and red gives yellow, overlap of blue and red gives magenta, overlap of blue and green gives turquoise and overlap of all the three channels gives white.

Images from the western blots and coomassie gels were analysed using LabWorks (v4) (Ultra-Violet Products).

Statistical analyses (paired two-tailed t-tests) were performed using Microsoft® Excel and graphs were prepared using GraphPad Prism® (v6).

qPCR data were processed using the StepOne™ (v2.3) software (Applied Biosystems) and exported to Microsoft® Excel.

Peptides identified by mass spectrometry were subjected to NCBI's BLAST search to identify the desired protein.

3 GLUT4 traffic through an ESCRT-III-dependent compartment

3.1 Introduction

Membrane proteins and lipids are kept tightly regulated to homeostatic levels by efficient endosomal (or degradative) pathways (Maxfield and McGraw, 2004). Recognisable features of endosomes are the endosomal markers present on the cargo/vesicle membrane. These markers are often proteins, which help endosome protein sorting into the correct compartment and recruitment of the appropriate cellular machinery. GLUT4 undergoes increased endocytosis and is either degraded, stored or recycled back to the plasma membrane, normally in the presence of insulin (Huang et al., 2001; Sargeant and Pâquet, 1993). This chapter delves deeper into the properties of well-established machinery involved in endosomal maturation called Endosomal Sorting Complex Required for Transport (ESCRT) and examines its possible involvement in the GLUT4 endocytic pathway.

3.1.1 ESCRTs

The discovery of *class E* vacuolar protein sorting (Vps) genes in yeast paved the way for identification of ESCRTs in mammals (Table 3.1) (Raymond et al., 1992; Robinson et al., 1988). Fig. 3.1 is representative of the sequential formation of the ESCRT complex. This complex involves recruitment of four ESCRT complexes (ESCRT-0, ESCRT-I, ESCRT-II and ESCRT-III) onto an endosomal membrane (Babst et al., 2002a; Babst et al., 2002b; Bilodeau et al., 2002; Katzmann et al., 2001). The ESCRT-0 protein HRS (hepatocyte growth factor-regulated tyrosine kinase substrate) initiates recruitment of the ESCRT proteins by recruiting clathrin to the endosomal membrane (Raiborg, 2001). Clathrin self-polymerises to form a scaffold and this leads to formation of a clathrin coated vesicle (Edeling et al., 2006). The clathrin coated vesicle also contains ubiquitin and PtdIns(3)P that

facilitate cargo sorting into endosomal compartments. HRS binds to ubiquitin via a UIM (ubiquitin interacting motif) (Raiborg et al., 2002) and a FYVE (Fab1p, YOTB, Vac1p and EEA1) domain that interacts with PtdIns(3)P (Stahelin et al., 2002). A correlation can be drawn here between ESCRT formation and GLUT4 endocytosis. It has been shown that clathrin and PtdIns(3)P is involved with insulin-stimulated GLUT4 trafficking (Huang et al., 2007; Kong et al., 2006). It has also been proposed that ubiquitination of GLUT4 is necessary for sorting GLUT4 to insulin-responsive compartments (Lamb et al., 2010). As ESCRT proteins are implicated in sorting ubiquitinated proteins in the endocytic pathway, it may be hypothesised that ESCRTs may traffic ubiquitinated GLUT4.

3.1.2 ESCRT-III and Vps4

Each ESCRT complex consists of a number of components that converge to form a multi-subunit ESCRT complex (Williams and Urbé, 2007). The ESCRTs aid in compartmentalisation, maturation and subsequent sorting of an endosomal vesicle via formation of a multivesicular compartment (Hanson et al., 2009). The ESCRT-bound multivesicular compartment acts as a hub for intracellular cargo sorting. The ESCRT pathway enters its final stages via the recruitment of the ESCRT-III components following which the ESCRT complex is dissociated (Nickerson et al., 2006). The removal of ubiquitin from the multivesicular ESCRT bound compartment by deubiquitinases (DUBs) (Agromayor and Martin-Serrano, 2006) leads to the delivery of the endosomal cargo to another intracellular storage compartments or to the lysosomes for degradation (Luzio et al., 2009).

ESCRT-III is a hetero-oligomeric protein complex cumulatively 450 kDa in size (Teis et al., 2008). ESCRT-III is anchored to the endosomal membrane via a myristoyl group at the N-terminus of charged multivesicular body protein (CHMP) 6 (Babst et al., 2002a; Yorikawa et al., 2005) and a PtdIns(3,5)P_2 interacting protein CHMP3 (Whitley et al., 2003). CHMP6 and another ESCRT-III member CHMP4 also link ESCRT-III with the ESCRT-II component EAP20 (ELL associated protein of 20 kDa) (Yorikawa et al., 2005). The N-terminal region of CHMP3 interacts with CHMP4 forming a coiled-coil complex. CHMP3 further

associates with CHMP2 and recruits CHMP1. CHMP1 uses its C-terminal MIM (MIT interacting motif) to coordinate binding to the N-terminal MIT (microtubule interacting and trafficking) domain of Vps4 (Nickerson et al., 2006). Perturbation of CHMP3 (Muzioł et al., 2006), CHMP1 (Howard et al., 2001) or the ESCRT-III associating protein Vps4 (Dukes et al., 2008; Fujita et al., 2003) causes accumulation and mis-sorting of cargo. In dendritic cells, ESCRT-III dysfunction causes autophagosome accumulation and leading to age dependent neurodegenerative disorders (Lee et al., 2007).

Complex	*S. cerevisiae* protein	Mammalian protein/isoform
ESCRT-0	Vps27	HRS, Hgs
	Hse1	STAM (1,2)
ESCRT-I	Vps23	Tsg101
	Vps28	Vps28
	Vps37	Vps37 (A,B,C,D)
	Mvb12	Mvb12 (A,B),
		UBAP1, LOC290595
ESCRT-II	Vps22	EAP30
	Vps25	EAP20
	Vps36	EAP45
ESCRT-III	Vps2	CHMP2 (A,B)
	Vps20	CHMP6
	Vps24	CHMP3
	Snf7	CHMP4 (A,B,C)
	Vps60	CHMP5
	Did2	CHMP1 (A,B)
	Ist1	-
Vps4	Vps4	Vps4A and Vps4B (SKD1)
	Vta1	LIP5
Accessory	Bro1	AIP1
Deubiquitinase	Doa4	UBPY
	-	AMSH

Table 3.1: Nomenclature of proteins involved with the ESCRT complex. The table represents the yeast and mammalian homologues for the ESCRT machinery. All ESCRT proteins in this thesis have been referred to with the mammalian ESCRT terminology for consistency.

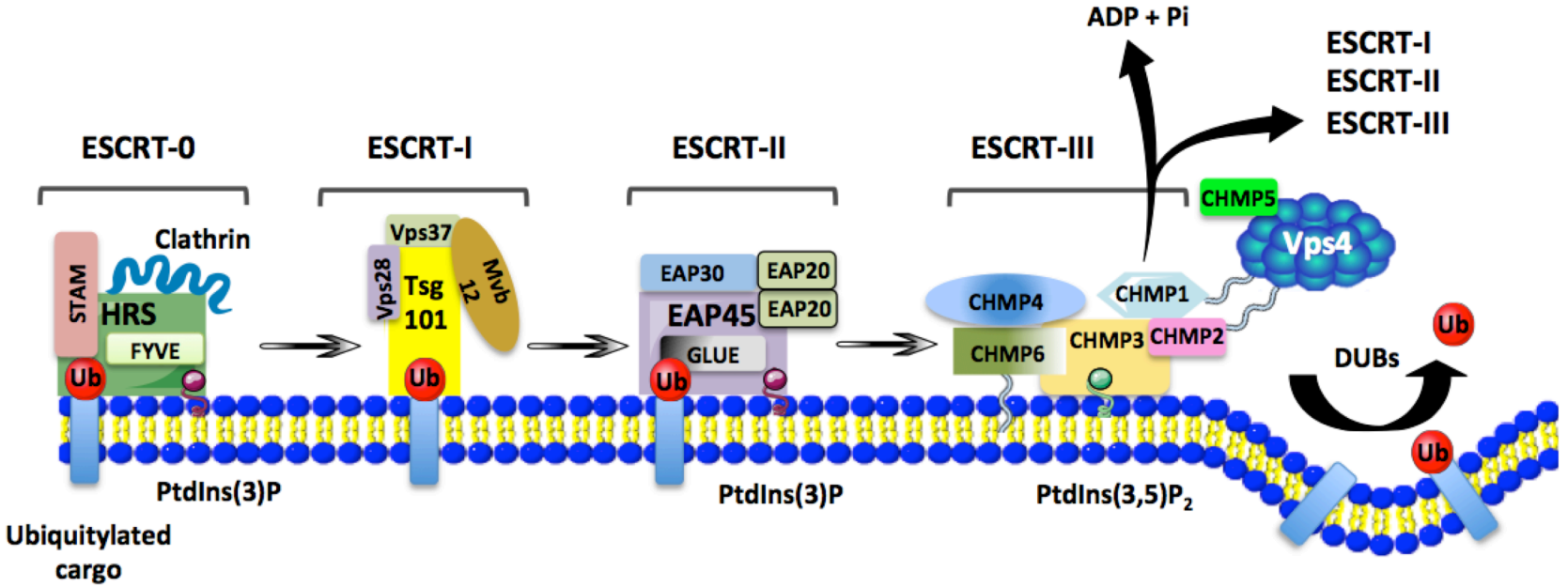

Figure 3.1: Mechanism of ESCRT recruitment to endocytosed cargo. ESCRTs are recruited to the vesicle membrane sequentially. ESCRT recruitment is facilitated by recognition of clathrin and ubiquitin bound cargo by HRS and STAM (signal-transducing adaptor molecule) components of ESCRT-0. HRS also contains a FYVE (Fab1p, YOTB, Vac1p and EEA1) domain that interacts with PtdIns(3)P on the endosomal membrane. Vps37 aids progression in assembly of ESCRT-I. Vps37 is bound to Tsg101 (Tumour susceptibility gene 101). Tsg101 contains an UEV (ubiquitin E2 variant) domain that anchors the other ESCRT-I components to the membrane. ESCRT-I and ESCRT-II are bridged together by the C-terminal of Vps28 and EAP45 (ELL associated protein of 45 kDa). EAP45 is important in ESCRT-II assembly as it is responsible for anchoring the ESCRT-II complex to ubiquitin and PtdIns(3)P via a GLUE (GRAM-like ubiquitin-binding in Eap45) domain. ESCRT-II helps bring together CHMP2, CHMP6, CHMP3, which form the components of the ESCRT-III complex. Additional recruitment of deubiquitinases (DUBs) such as AMSH (associated molecule with the SH3 domain of STAM) and UBPY (ubiquitin-specific protease Y) followed by Vps4 -mediated ATP hydrolysis causes ESCRT-III disassembly leading to formation of an intralumenal vesicle (ILV). The ILV then follows the ESCRT-MVB (multi-vesicular body) pathway described in Fig. 3.2. Figure adapted from Williams and Urbé, 2007, Lobert and Stenmark, 2011.

Vps4 is a 48 kDa protein containing an AAA+ ATPase domain (Babst et al., 1997). This domain folds into two hexameric rings and binds ATP (Iyer et al., 2004); ATP hydrolysis provides the driving force for remodelling and disassembly via unfolding of the ESCRT-III subunit complexes (Snider et al., 2008). The dissociation of ESCRT-III is also accompanied by deubiquiltylation of the endosomal vesicles by DUBs such as AMSH (Hurley, 2011). The dissociation of ESCRT-III via Vps4 is required for the formation of an intralumenal vesicle (ILV) and a multi-vesicular body (MVB). MVBs follow a lysosomal degradative pathway and represent a class of late endosomes destined for degradation (Piper and Katzmann, 2007).

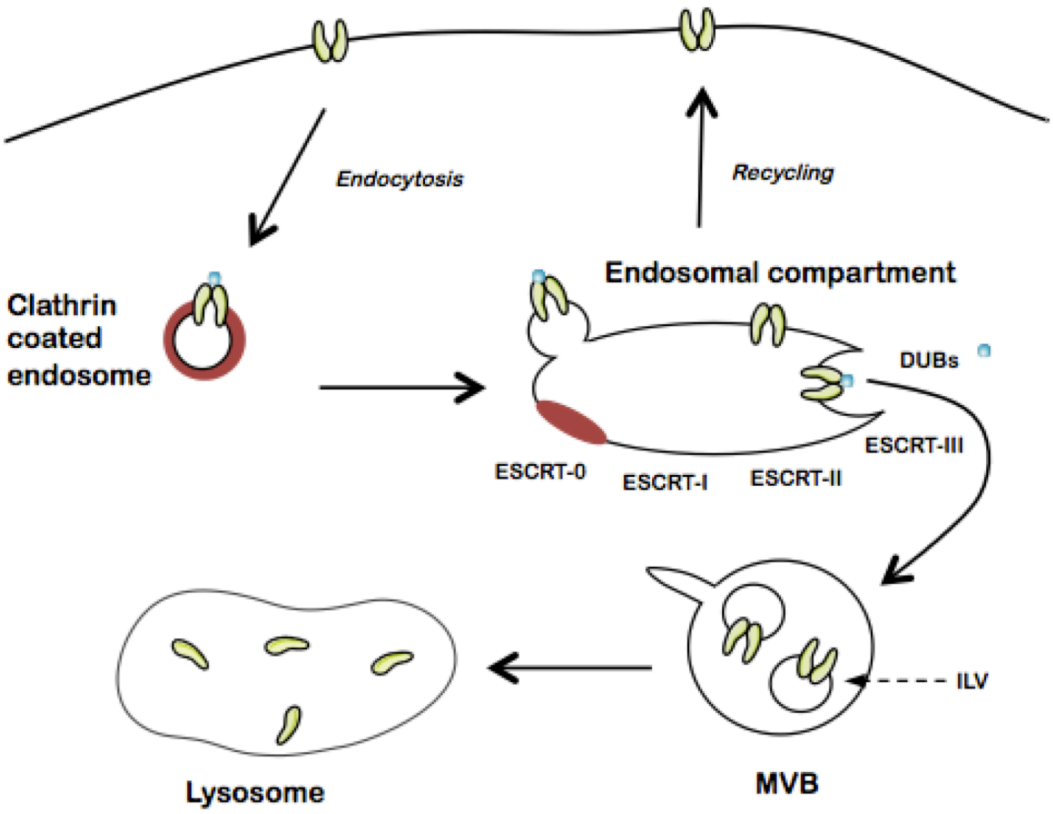

Figure 3.2: ESCRT-MVB pathway. Endocytosed vesicular cargo contains clathrin and ubiquitin. This vesicular cargo is sorted into early endosomes that associate with the ESCRT machinery. ESCRT bound endosomes may be recycled to the plasma membrane or form intralumenal vesicles (ILVs). ILV formation is triggered by ESCRT-III dissociation and removal of ubiquitin by DUBs. ILVs mature into late endosomes and form multi-vesicular bodies (MVBs). MVBs fuse with lysosomes leading to cargo degradation. Figure adapted from Haglund and Dikic, 2012.

3.1.3 Aims and rationale for the study

Phosphoinositides are insulin-regulated secondary messengers that facilitate GLUT4 trafficking (Berwick et al., 2004; Maffucci et al., 2003). Disruption of phosphoinositides may lead to defective GLUT4 trafficking and a reduced insulin signalling response in adipocytes (Ikonomov et al., 2007; Shisheva, 2008). Studies have shown that inhibiting PtdIns(3,5)P_2 production by blocking its synthesising kinase PIKfyve, leads to reduced insulin stimulated GLUT4 translocation and reduced glucose uptake (Ikonomov et al., 2007). PIKfyve is phosphorylated by Akt in response to insulin further implicating it in the insulin signalling pathway (Berwick et al., 2004). PtdIns(3)P was also shown to facilitate GLUT4 fusion with the PM in another study done in mice that contained a knockout for GLUT4 vesicle docking/fusion protein Munc18c (Kanda et al., 2005).

ESCRT proteins are PtdIns(3)P and PtdIns(3,5)P_2 binding proteins. HRS contains a FYVE domain that binds to PtdIns(3)P (Stahelin et al., 2002) while CHMP3 binds to PtdIns(3,5)P_2 (Whitley et al., 2003) via basic residue motifs (Muzioł et al., 2006). Phosphoinositides PtdIns(3)P (Gillooly et al., 2000) and PtdIns(3,5)P_2 (Whitley et al., 2003) are involved in ESCRT biogenesis and are important lipid signalling messengers in GLUT4 trafficking (Shisheva, 2008). Ubiquitin is also involved in ESCRT biogenesis (Shields and Piper, 2011) and has been recently linked to GLUT4 endocytosis (Lamb et al., 2010).

Phosphoinositides PtdIns(3)P and PtdIns(3,5)P_2 and ubiquitin involvement in ESCRT assembly and GLUT4 trafficking provide an interesting link to the possibility of ESCRT involvement in GLUT4 trafficking. The described recent understanding of the role of ubiquitin and phosphoinositides in endocytosis and sorting of cargo has directed the aims of this chapter. It is unknown if GLUT4 traffics though an ESCRT-dependent compartment. I hence aim to investigate if GLUT4 traffics through an ESCRT-dependent pathway in adipocytes.

3.2 Results

3.2.1 ESCRT-III and Vps4 mutants lead to enlarged GLUT4 vesicles

In order to investigate whether GLUT4 traffics thorough an ESCRT-dependent compartment, the localisation of HA-GLUT4 when the ESCRT machinery function is perturbed was studied. The results indicate that HA-GLUT4 was present is enlarged compartments in comparison to the control. There was some overlap in localisation of HA-GLUT4 with the dominant negative ESCRT related constructs.

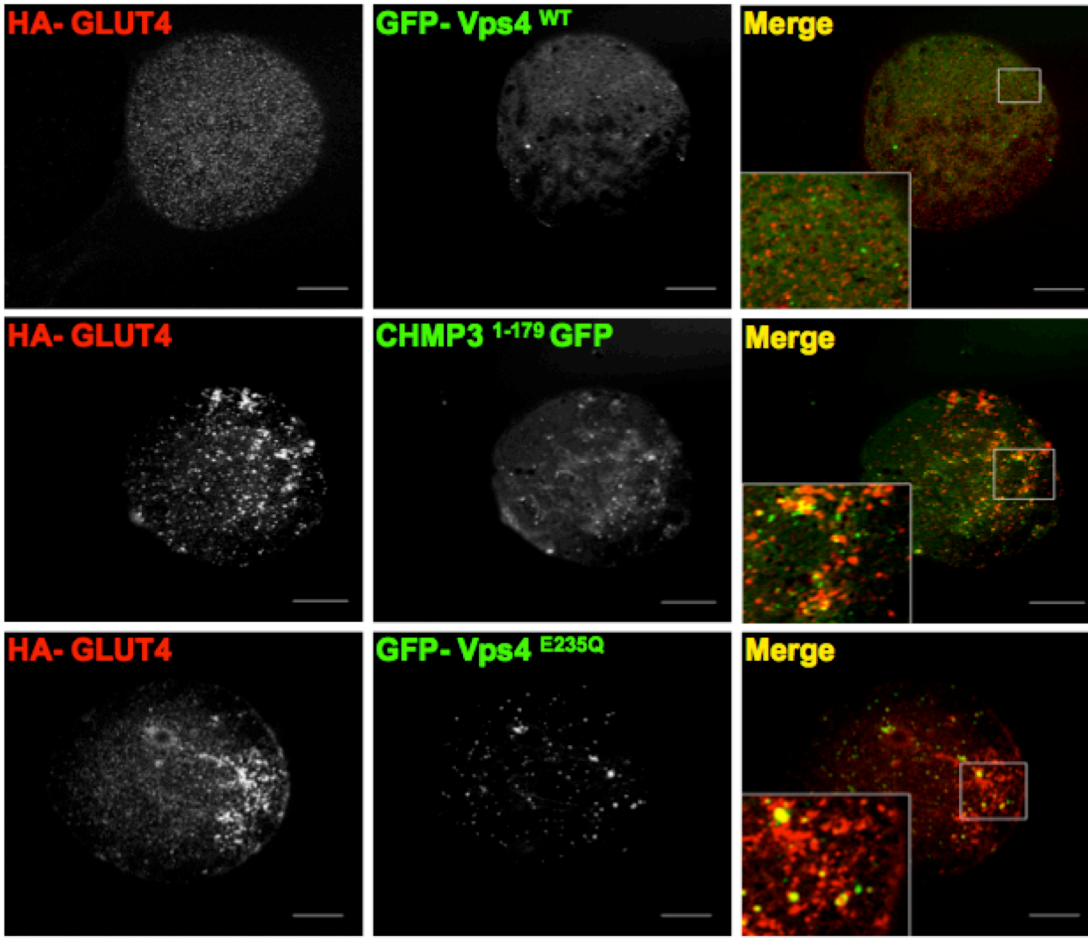

Figure 3.3: Dominant negative CHMP3 and Vps4 constructs lead to formation of enlarged vesicles. Rat adipocytes were co-transfected with HA-GLUT4 (red) and EGFP-tagged Vps4 ^{WT}, Vps4 ^{E235Q} or CHMP $^{31–179}$ (green) and incubated for 5 h at 37°C. After 5 h, cells were stimulated with 60 nM insulin for 20 min. Cells were fixed with 4% paraformaldehyde, permeabilised in 0.1% saponin and immunostained with anti- HA primary antibody and anti-mouse IgG-Alexa 633 secondary antibody. Images represent single adipose cells and were acquired using an LSM510 Meta confocal laser scanning microscope. Results are representative of 3 independent experiments. Bars 20 μm.

Primary rat adipocytes were isolated and transfected with the following pEGFP tagged constructs: Vps4 ^{WT} or N-terminus of CHMP3 $^{1-179}$ or Vps4 ^{E235Q} and HA-tagged GLUT4 using the transfection method described previously (Al-Hasani et al., 1998). The truncated dominant negative mutant CHMP3 $^{1-179}$ was previously characterised as binding to membranes leading to enlarged endosomal compartments (Dukes et al., 2008) but its wild type equivalent could not be used as a control as it was previously shown to mimic this enlarged phenotype (Zamborlini et al., 2006). Vps4 ^{E235Q} is a dominant negative mutant of the AAA ATPase Vps4 (Dukes et al., 2008; Whitley et al., 2003) which is unable to hydrolyse ATP, thereby keeping Vps4 tightly bound to the ESCRT-III complex and preventing its disassembly (Fujita et al., 2003).

Fig. 3.3 shows Vps4 ^{WT} having a dispersed cytosolic appearance, not resulting in any anomaly in these adipocytes. HA-GLUT4 was evenly distributed as spots, which is a common phenomenon (Malide et al., 2000). The EGFP-tagged dominant negative mutants (CHMP3 $^{1-179}$ and Vps4 ^{E235Q}) were detected as forming enlarged and swollen vesicles. These GFP positive ESCRT vesicles showed some colocalisation with HA-GLUT4. The extent of colocalisation between HA-GLUT4 and the dominant negative ESCRT-III constructs however varied on the enlarged structure and at times did not overlap all along this structure.

3.2.2 ESCRT-III disruption leads to an enlarged hybrid compartment

To better characterise the composition of the enlarged compartments, rat adipocytes were stained with endosomal markers. In basal control cells, GLUT4 was cytosolic and sequestered in compartments positive for syntaxin-6 (Stx6) and ubiquitin (Ub); this is consistent with the presence of a TGN-like compartment. GLUT4 did not colocalise with the early endosome antigen 1 (EEA1). GLUT4 however colocalised with the transferrin receptor (TfR) and was observed in compartments distinct from those that stained with Ub and Stx6 (Fig. 3.4*A*).

A

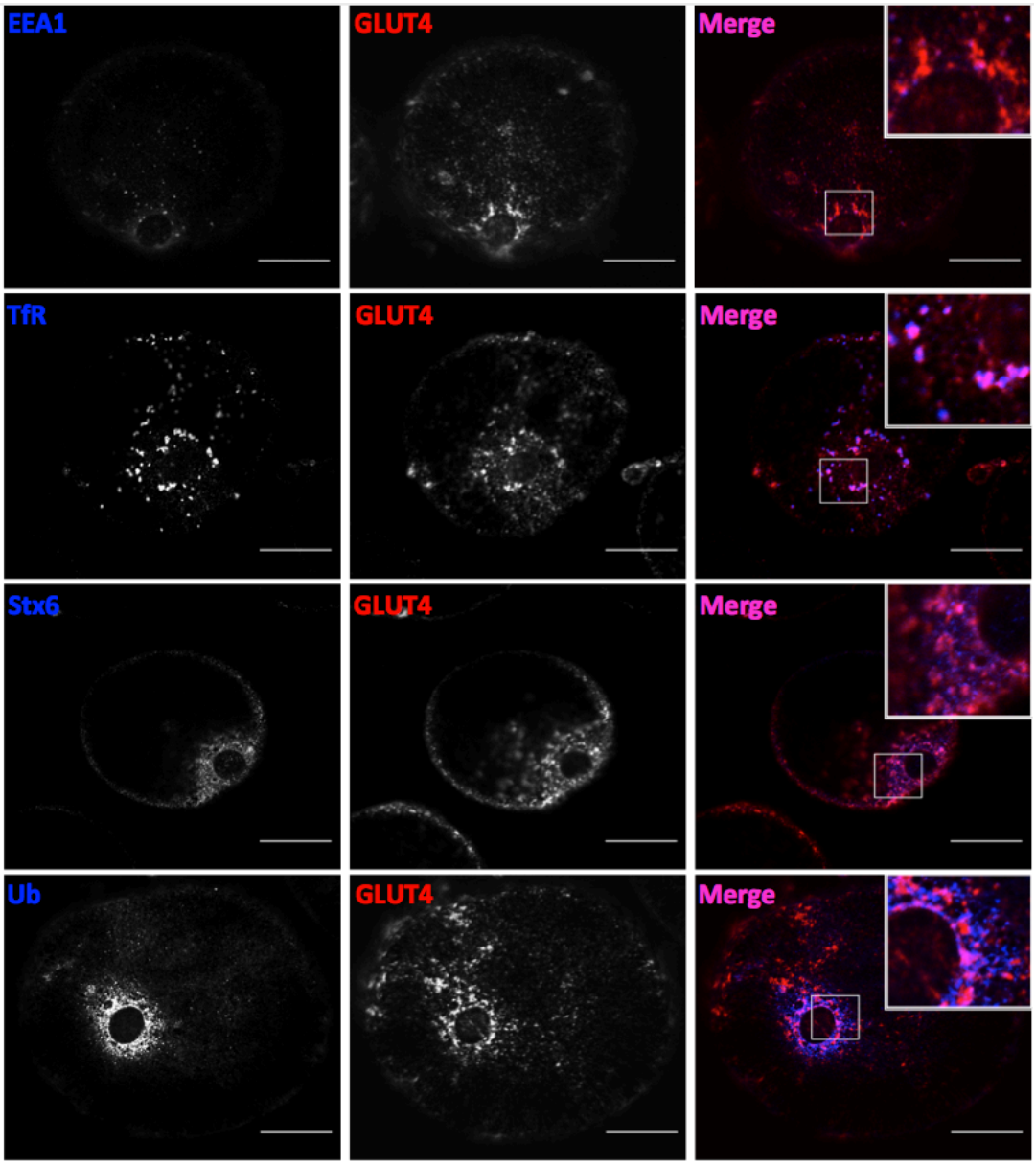
EEA1
GLUT4
Merge
TfR
GLUT4
Merge
Stx6
GLUT4
Merge
Ub
GLUT4
Merge

B

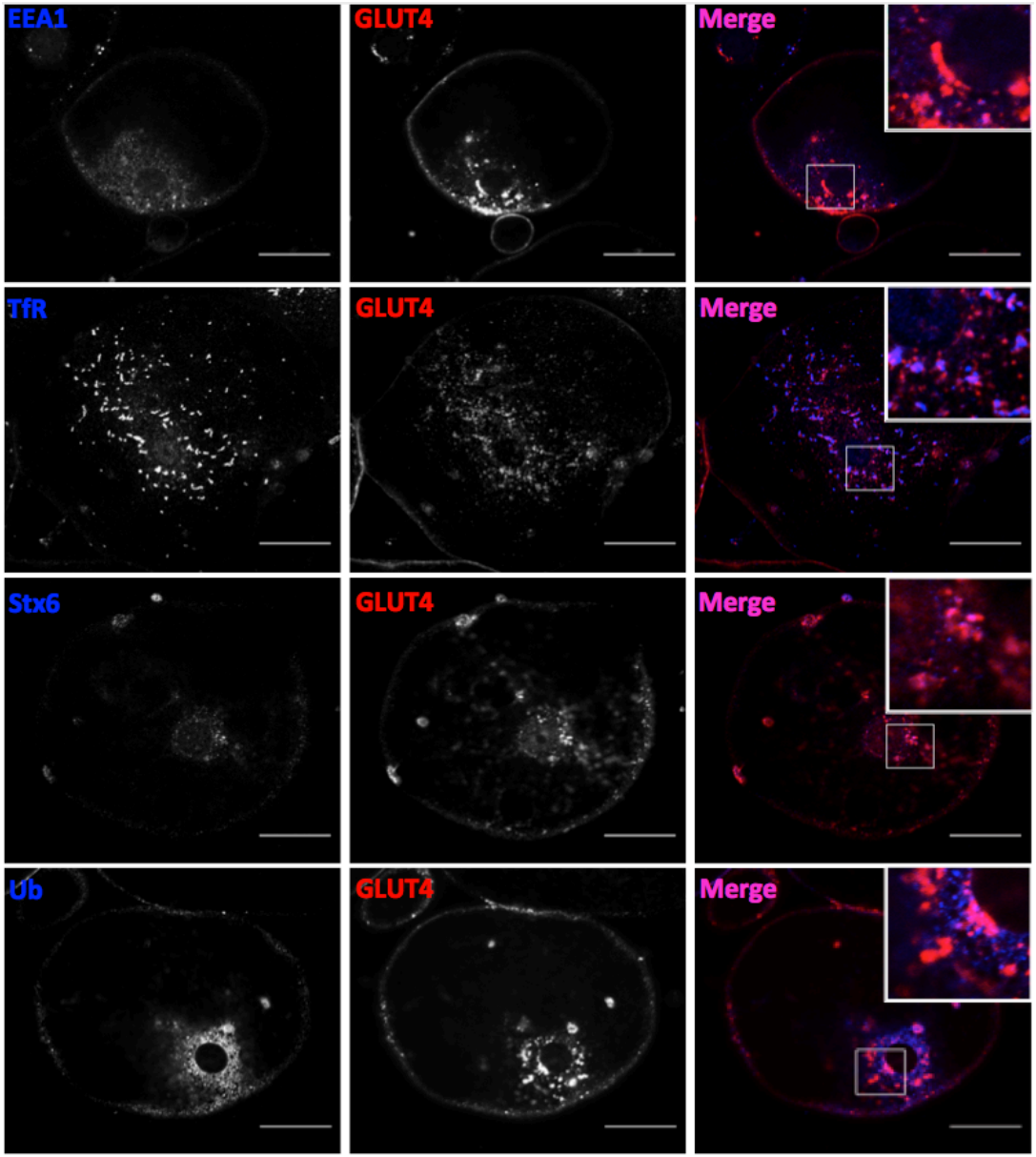
EEA1
GLUT4
Merge
TfR
GLUT4
Merge
Stx6
GLUT4
Merge
Ub
GLUT4
Merge

C

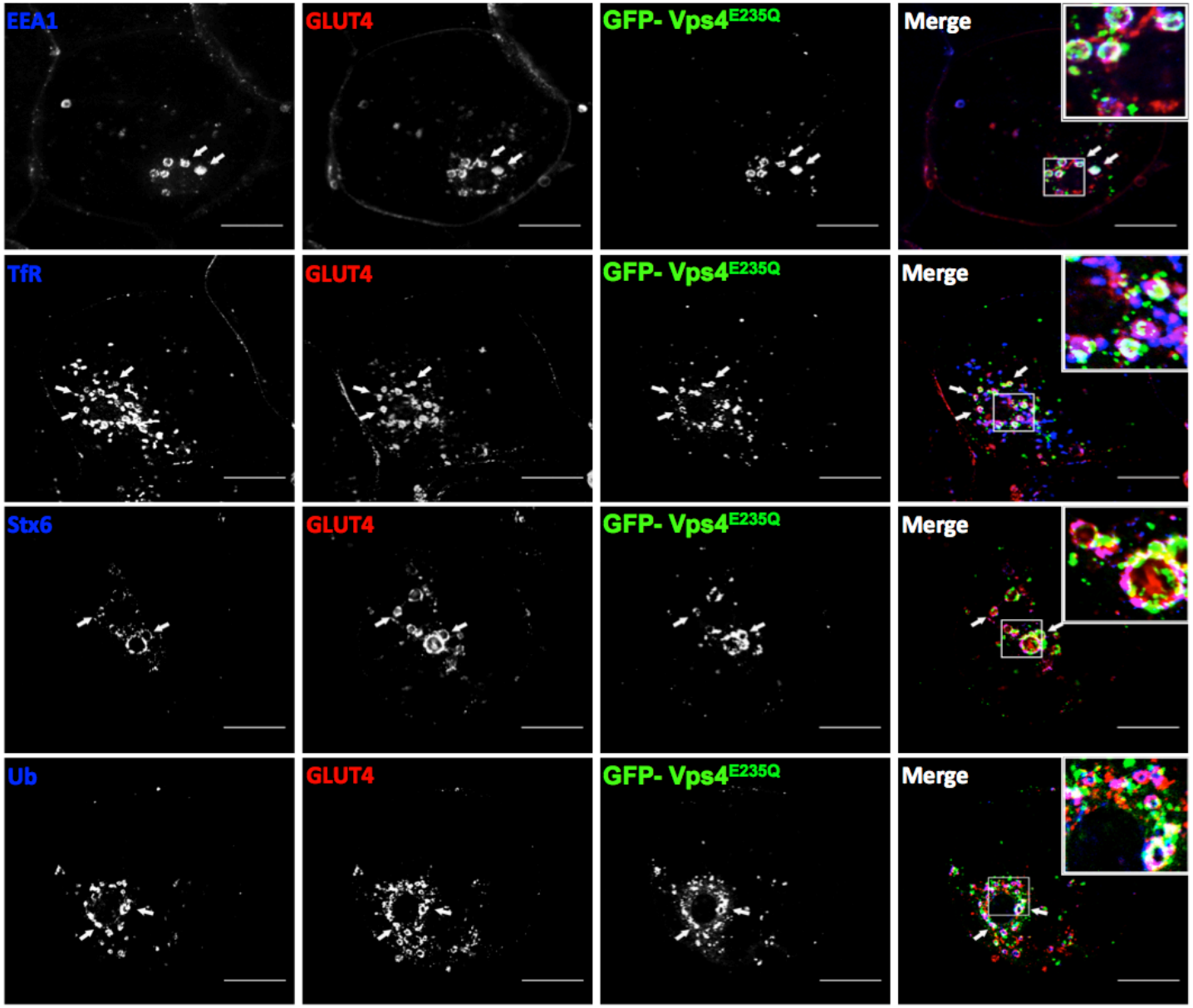
EEA1
GLUT4
GFP- Vps4E235Q
Merge
TfR
GLUT4
GFP- Vps4E235Q
Merge
Stx6
GLUT4
GFP- Vps4E235Q
Merge
Ub
GLUT4
GFP- Vps4E235Q
Merge

D

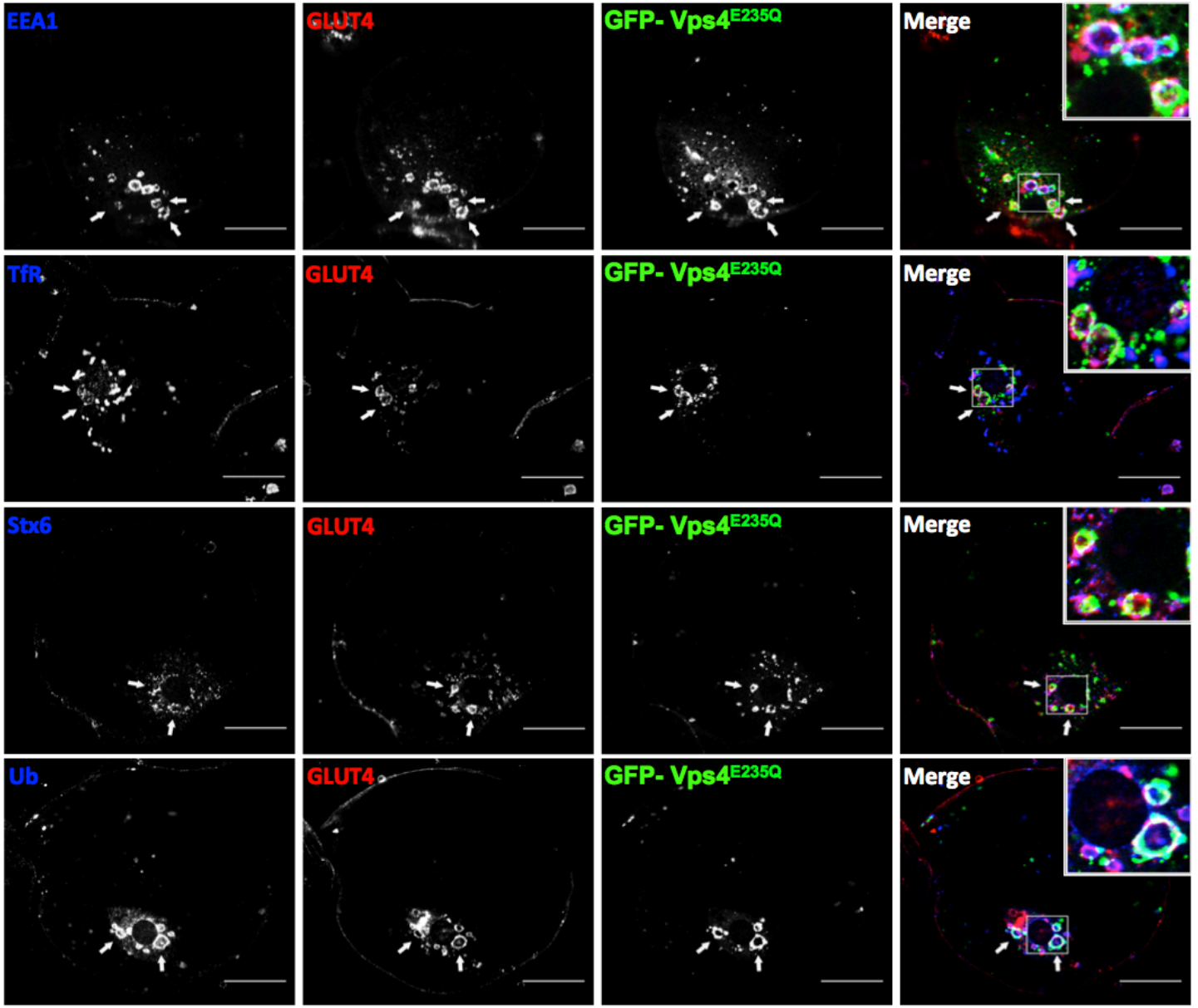
EEA1
GLUT4
GFP- Vps4E235Q
Merge
TfR
GLUT4
GFP- Vps4E235Q
Merge
Stx6
GLUT4
GFP- Vps4E235Q
Merge
Ub
GLUT4
GFP- Vps4E235Q
Merge

Figure 3.4: Vps4 ^{E235Q} overexpression leads to formation of a hybrid compartment. Endogenous GLUT4 was studied in isolated rat adipocytes together with endosomal markers of GLUT4 traffic that included EEA1, ubiquitin (Ub), syntaxin-6 (Stx6) and transferrin receptor (TfR). Localisation of GLUT4 (red in merged images) was compared with EEA1, Ub, Stx6 and TfR (blue in merged images) using the antibodies and dilutions described in *Materials and Methods 2.1.2*. The figures show the subcellular endosomal marker distributions in the presence of non-perturbing pEGFP-Vps4 ^{WT} in the basal state ***(A)*** and the insulin-stimulated state ***(B)***. The overexpressed pEGFP-Vps4 ^{WT} is highly dispersed and is cytosolic under these conditions (not shown for clarity). Overexpression of the mutant pEGFP-Vps4 ^{E235Q} (green in merged images) leads to enlarged tubulo-vesicular GLUT4 compartments. The endosomal markers EEA1, TfR, Stx6 and Ub colocalise with both endogenous GLUT4 and with EGFP-Vps4 ^{E235Q} both in the basal state ***(C)*** and the insulin-stimulated state ***(D)***. Arrows point at enlarged, hybrid compartments. Bars 20 µm.

Stimulating control cells with insulin led to GLUT4 being localised to a larger extent at the adipocyte plasma membrane which can be compared with previous studies (Fig. 3.4*B*) (Malide et al., 2000; Suzuki and Kono, 1980).

Transfection of adipocytes with the dominant negative construct Vps4 ^{E235Q}, led to GLUT4 localising to the enlarged ESCRT-III compartment in an extensive manner (Fig. 3.4, *C* and *D*). The markers EEA1, TfR, Stx6 and Ub all associated with the enlarged compartment and GLUT4, making it a hybrid compartment (Fig. 3.4, *C* and *D*). The colocalisation of these markers with GLUT4 on the hybrid compartment was not significantly different between basal and insulin-treated adipocytes.

Compared to the basal control cells (without Vps4 ^{E235Q}) where the EEA1 signal was low, EEA1 could be detected associating more visibly with GLUT4 and Vps4 ^{E235Q} in cells transfected with Vps4 ^{E235Q} (Fig. 3.4, *C* and *D*). Ub, which also acts as a marker of the ESCRT pathway, associated with GLUT4 in the control cells (without Vps4 ^{E235Q}). However, the colocalisation was prominent in the hybrid compartment of the Vps4 ^{E235Q} transfected cells. The hybrid compartments were larger in size in comparison to the compartments observed in the control cells transfected with the non-perturbing Vps4 ^{WT} *(see Table 3.2)*.

Attempts were made to quantitate the degree of colocalisation between GLUT4, Vps4 ^{E235Q} and endosomal markers using JACoP and Pearson's Scatterplot

plugins in ImageJ but the values did not correspond with the observed colocalisation pattern.

	EGFP-Vps4		EGFP-Vps4^{E235Q}	
	Basal	**Insulin**	**Basal**	**Insulin**
Area (pixels)	85.92 ± 24.11	131.57± 5.37	1411.61 ± 183.32***	1448.52 ± 168.90***
Area (μm^2)	-	-	14.00 ± 1.74	18.04 ± 1.80
Diameter (μm)	-	-	2.40 ± 0.14	2.71 ± 0.18

Table 3.2: Quantification of hybrid compartment sizes in Vps4 ^{E235Q}-transfected cells. The cells transfected with pEGTP-Vps4 ^{WT} (control) or pEGFP-Vps4 ^{E235Q} and positive for EGFP, GLUT4, ubiquitin and endosomal markers were analysed using ImageJ. The area (in pixels) of the visible lumens was determined in μm^2. Results are mean and SEM from 10-14 individual cells. ***p<0.001 (enlarged *vs* control vesicles). Only large pixels from the hybrid compartments were accurately converted to μm^2.

3.2.3 The PIKfyve inhibitor YM201636 does not mimic a Vps4 ^{E235Q} - induced enlarged compartment

The kinase PIKfyve generates PtdIns(3,5)P_2 from PtdIns(3). PtdIns(3,5)P_2 acts as a lipid anchor for ESCRT-III membrane binding via CHMP3 (Whitley et al., 2003). Since PIKfyve is currently the only known kinase generating PtdIns(3,5)P_2, it was considered useful to study the effects of inhibiting PIKfyve using 800 nM of its inhibitor YM201636 (Jefferies et al., 2008). The adipocytes were stained for endogenous GLUT4 and Ub after treatment with YM201636 for 30 min, 2 h and 5 h. The results of the YM201636 study showed that GLUT4 associated with Ub (Fig. 3.5) which has been reported before (Lamb et al., 2010). However, no enlarged compartments were observed when compared to the untreated controls (Fig. 3.5).

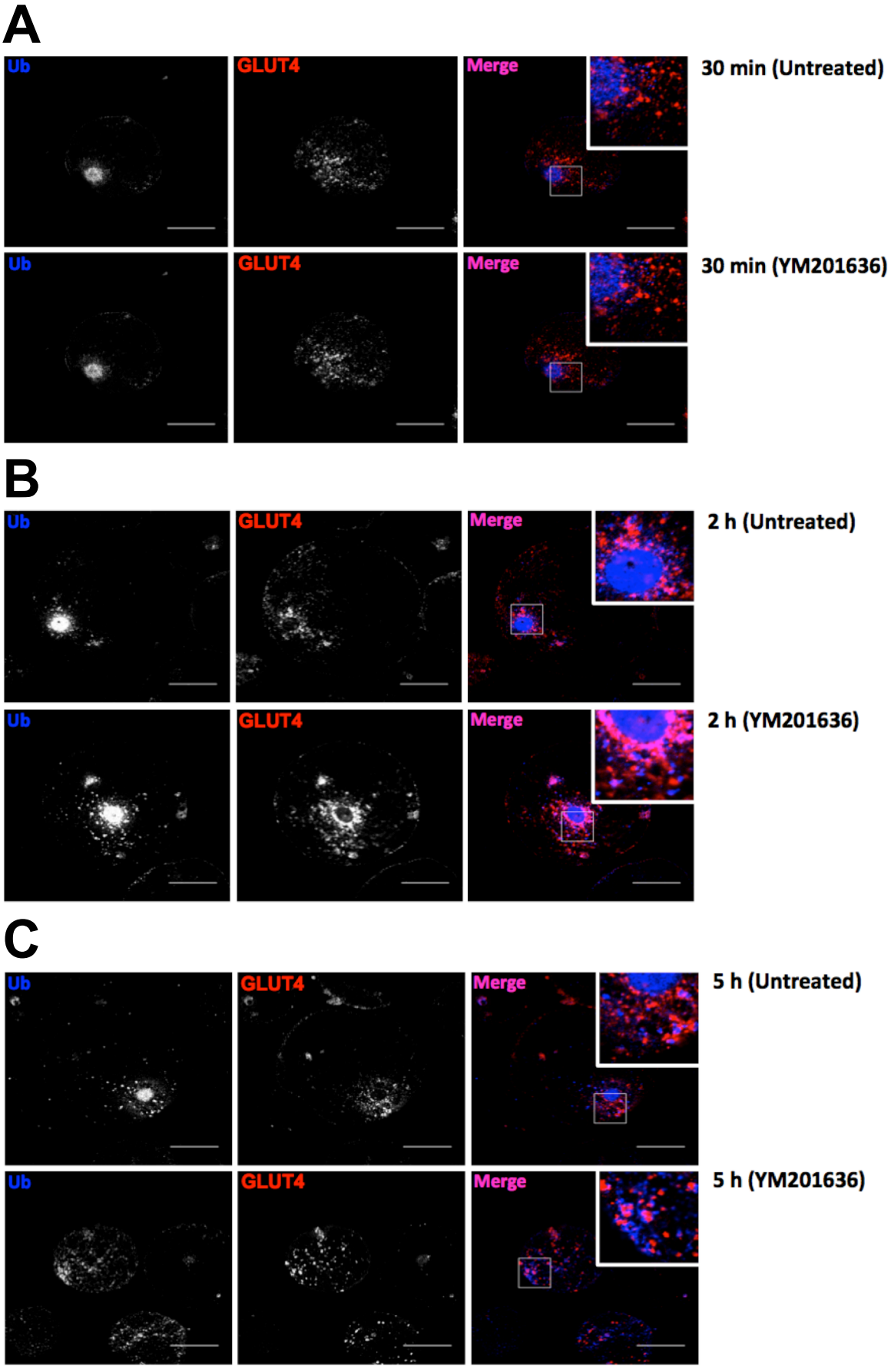
A
Ub
GLUT4
Merge
30 min (Untreated)
Ub
GLUT4
Merge
30 min (YM201636)
B
Ub
GLUT4
Merge
2 h (Untreated)
Ub
GLUT4
Merge
2 h (YM201636)
C
Ub
GLUT4
Merge
5 h (Untreated)
Ub
GLUT4
Merge
5 h (YM201636)

Figure 3.5: The PIKfyve inhibitor YM201636 does not mimic a Vps4 ^{E235Q}-induced swollen compartment. Primary adipocytes were isolated as described previously and either left untreated or treated with 800 nM of the PIKfyve inhibitor YM201636. Cells were then maintained in culture at 37°C for 30 min ***(A)*** 2 h ***(B)*** and 5 h ***(C)***. Confocal microscopy of GLUT4 localisation (red in merged images) was compared with ubiquitin (blue in merged images) using the antibodies described in the *Materials and Methods 2.1.2.* The swollen endosomal phenotype observed with Vps4 ^{E235Q} was not seen in these adipocytes. Images were acquired using the LSM510 Meta confocal laser scanning microscope and represent a population of at least 3 cells. Bars represent 20 μm.

3.2.4 ESCRT-III disruption causes a long-term block of GLUT4 exit from the hybrid compartment

An experiment was performed to determine if the block caused by ESCRT-III on GLUT4 traffic would reduce over time and entrapped GLUT4 would be released. Two time points were compared at 5 h and 24 h. After transfection with GFP-Vps4 ^{WT} and Vps4 ^{E235Q}, it was observed that both the Vps4 (WT and E235Q) constructs increased in expression at 24 h (Fig. 3.6, *A* and *B*). Colocalisation of Ub and GLUT4 with Vps4 ^{E235Q} was consistent (Fig. 3.6*B*) with the other experiments with short-term treatments (Fig. 3.4 *C* and *D*). The colocalisation pattern was similar at 5 h and 24 h indicating that GLUT4 is completely trapped in this hybrid compartment (Fig. 3.6*B*). An incubation beyond 24 h leads to increased lysis of the primary adipocytes and hence these changes were not studied.

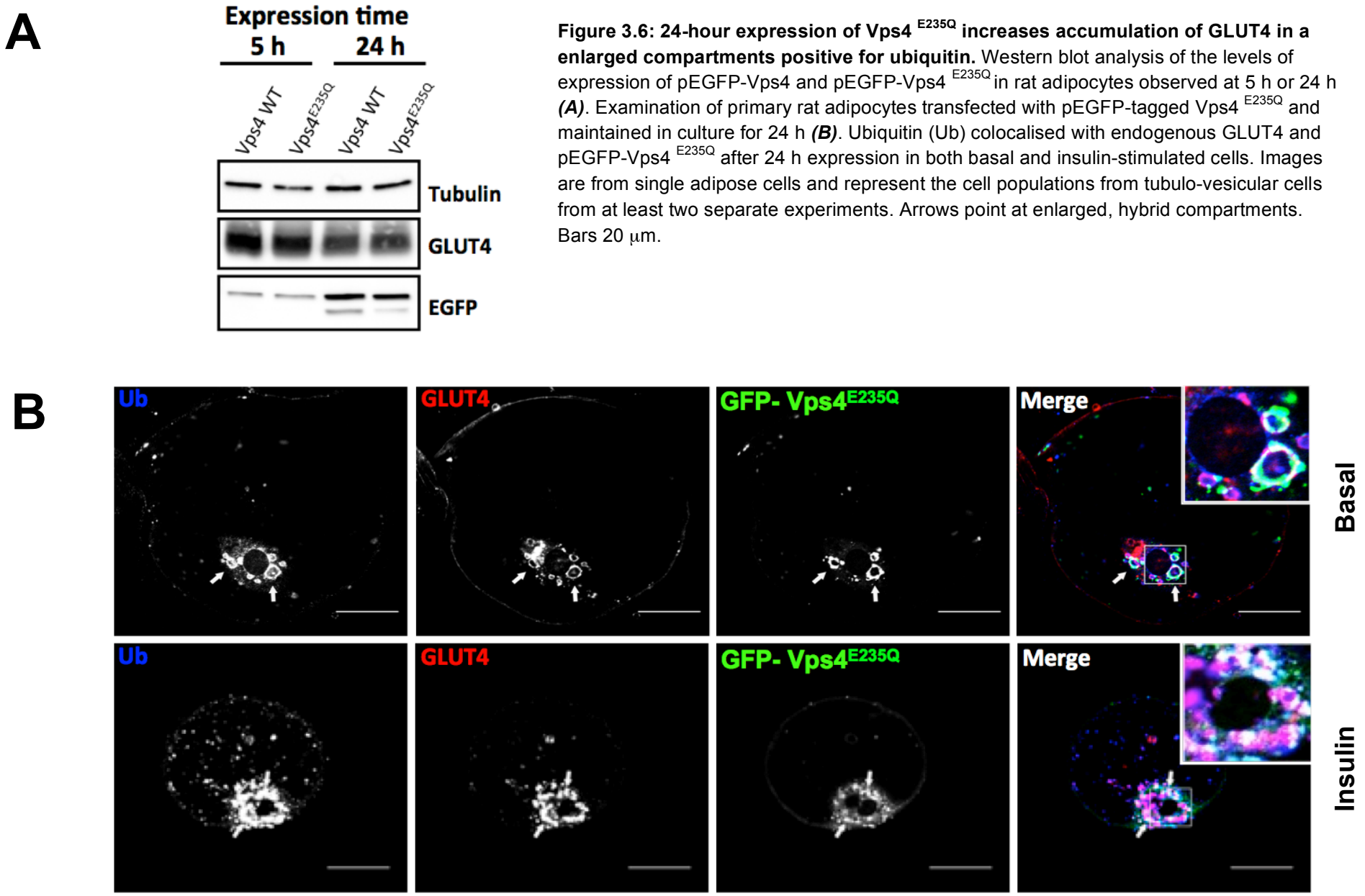

Figure 3.6: 24-hour expression of Vps4 ^{E235Q} increases accumulation of GLUT4 in a enlarged compartments positive for ubiquitin. Western blot analysis of the levels of expression of pEGFP-Vps4 and pEGFP-Vps4 ^{E235Q} in rat adipocytes observed at 5 h or 24 h ***(A)***. Examination of primary rat adipocytes transfected with pEGFP-tagged Vps4 ^{E235Q} and maintained in culture for 24 h ***(B)***. Ubiquitin (Ub) colocalised with endogenous GLUT4 and pEGFP-Vps4 ^{E235Q} after 24 h expression in both basal and insulin-stimulated cells. Images are from single adipose cells and represent the cell populations from tubulo-vesicular cells from at least two separate experiments. Arrows point at enlarged, hybrid compartments. Bars 20 μm.

3.3 Discussion

Insulin stimulation results in a kinetically rapid re-distribution of the GLUT4 transporter causing GLUT4 to be recycled from intracellular compartments to the plasma membrane. Whether GLUT4 is recycled or degraded, endocytosis is an indispensable step in both processes. The study described in this chapter implicates the involvement of the endocytic ESCRT machinery for the first time in GLUT4 traffic. The findings in this chapter and its associated publication (Koumanov et al., 2012), show that GLUT4 upon endocytosis accumulates in perturbed ESCRT-III positive compartments. Locations of various endocytic markers serve as additional evidence to indicate that these compartments are targeted towards the endosomal pathway. Colocalisation of the GLUT4-Vps4 ^{E235Q} compartment with Stx6, EEA1, Ub and TfR all indicate that this compartment is present in fairly late stages of the endosomal pathway. This compartment has been designated as a hybrid compartment due to the presence of EEA1, Stx6, TfR and Ub markers. The results described in this chapter depict a multivesicular compartment. The findings observed suggest that GLUT4 is entrapped in a hybrid multivesicular compartment.

An HA-GLUT4 translocation assay was performed that measured the amount of HA-GLUT4 that translocated to the plasma membrane in rat adipocytes that overexpressed Vps4 ^{E235Q} or CHMP3 $^{1-179}$ (Koumanov et al., 2012). Trapping GLUT4 at an ESCRT or PtdIns(3,5)P_2 dependent trafficking step possibly results in an inability of GLUT4 to traffic to an insulin sensitive compartment. Hence, GLUT4 contained in the hybrid compartment described (in the study in this chapter) cannot recycle or traffic to the plasma membrane in insulin-stimulated adipocytes, thereby causing a drop in plasma membrane GLUT4.

Defects in GLUT4 traffic upon impairment of exocytic (Kanda et al., 2005; Zhao et al., 2009) and endocytic (Al-Hasani et al., 1998) machinery have been shown in adipocytes to affect the levels of GLUT4 translocated to the plasma membrane. Post endocytosis, an efficient sorting system (Maxfield and McGraw, 2004) was proposed as the key in maintaining surface GLUT4, thereby sustaining glucose

uptake during insulin stimulation. Sorting pathways are mainly thought to route insulin-stimulated GLUT4 via recycling endosomes (fast recycling) or via GSVs (slow recycling) to the cell surface or to other intracellular pools (Habtemichael et al., 2011; Leto and Saltiel, 2012). The compartment detected in this study was positive for a number of proteins, one of which was TfR. TfR has a really short half-life which is <2 min. TfR is also present on early endosomes and greater than 95% of TfR recycles back to the plasma membrane (Koval and Pagano, 1989; Mayor et al., 1993; van Dam and Stoorvogel, 2002). Another marker that was detected on the hybrid compartment was EEA1, which is also present on recently endocytosed vesicles (Mu et al., 1995). As recently endocytosed vesicles mature, they are targets of other subcellular markers like those from the TGN. The hybrid compartment showed the presence of Stx6 (in Fig. 3.4, *C* and *D*) which is a predominantly TGN marker. Stx6 is also known to associate with early endosomes via EEA1 (Simonsen et al., 1999) and SHIP164 (Otto et al., 2010). Hence, the presence of the recently described endosomal markers and observation of a tubulo-vesicular phenotype (as seen in Fig 3.4), suggests that the hybrid compartment may be at the 'late' stages of endosomal traffic.

Endocytosis of cargo is thought to occur via clathrin-coated pits. This form of endocytosis is usually accomplished by recruitment of the Clathrin Heavy Chain CHC17 to endocytosing vesicles (Antonescu et al., 2008). However, recent studies by Brodsky's group suggest that GLUT4 traffics via a distinct retrograde endosome-TGN trafficking route (Esk et al., 2010; Vassilopoulos et al., 2009). Retrograde-TGN GLUT4 trafficking utilises the Clathrin Heavy Chain CHC22 protein instead of CHC17. Knockdown of CHC22 produced tubular structures similar to the coalesced and extended structures seen in the results described in this chapter (Vassilopoulos et al., 2009). CHC22 is thought to sort GLUT4 into insulin-responsive compartments or GSVs via the TGN (Esk et al., 2010). The described endosomal markers (EEA1, Stx6 and TfR) used in this study (Figs. 3.4 and 3.6) are indicative of early and TGN-derived compartments leading to the suggestion that the hybrid compartment observed in this study may traffic via recruitment of CHC22. The hybrid compartment may hence be a hub for GLUT4-TGN retrograde trafficking.

Colocalisation of Ub with GLUT4 on the hybrid compartment (Fig. 3.4, *C*, *D* and Fig. 3.6*B*) provided new insights into the possible ubiquitination of the GLUT4 transporter. This study confirmed that GLUT4 is present on the same compartment with ubiquitinated proteins and the ESCRT machinery. Ubiquitination may occur as mono/poly-ubiquitination at the lysine residue of proteins (Sadowski and Sarcevic, 2010), though what governs the production of either the mono/poly form of ubiquitin is still unclear. Ubiquitin-like proteins have previously been linked to GLUT4 vesicles. A ubiquitin-like domain containing protein called TUG (Tether containing an UBX domain, for GLUT4) was shown to tether to the intracellular loop of GLUT4 and sequester it in the basal state (Bogan et al., 2012a). The ubiquitin-like domain of TUG can be cleaved upon insulin stimulation permitting GLUT4 translocation and exocytosis (Bogan et al., 2012b). Also, another small ubiquitin-like modifier (SUMO) conjugating enzyme (Ubc9) and its SUMOlated partner Daxx (death-domain associated protein), both have been shown to bind either GLUT4 or the GLUT4 vesicle (Giorgino et al., 2000; Lalioti et al., 2002; Liu et al., 2007). Overexpression of Ubc9 results in reduced GLUT4 degradation and increased GLUT4 targeting to insulin-responsive storage compartments (Liu et al., 2007). Daxx facilitates GLUT4 vesicle movement along the microtubule by interacting with GLUT4 and the kinesin element KIF5B (Lalioti et al., 2009). In the ESCRT pathway, ubiquitin is eventually removed from the endosomal membrane upon ESCRT-III dissociation. Ubiquitin is removed by deubiquitinases (or DUBs) and can result in a reversal of the ubiquitination process. Deubiquitination may serve as a signal to rescue cargo by recycling it back to the plasma membrane, to intracellular sites, to the TGN or to the lysosome for degradation (Woodman and Futter, 2008). AMSH (associated molecule with SH3 domain of STAM) is a DUB that can be recruited to ESCRT-III and facilitate cargo recycling (Agromayor and Martin-Serrano, 2006; Clague and Urbé, 2006). The precise mechanisms governing where, and to what extent a maturing endosomal compartment is sorted or recycled by DUBs or an alternative process to intracellular sites is still unknown and can be a focus of further investigation.

The term ‘hybrid compartment’ in this study is used in a fairly broad sense and it may include docked GLUT4 vesicles that may or may not be degraded (Futter et

al., 1996; Pavelka et al., 2008). As the hybrid compartment matures, it forms tubulo-vesicular structures with outward budding vesicles on the limiting membrane and it is these vesicle that may be recycled while those that bud inwards (called intralumenal vesicles) are those destined for degradation via the lysosome (Hanson and Cashikar, 2012; Piper and Katzmann, 2007). The described hybrid compartment (Fig. 3.4) does not distinguish between GLUT4 vesicles and may also include newly formed GLUT4 vesicles that bud off from the cisternae of the TGN.

It was described earlier that phosphoinositides are involved during ESCRT maturation. To summarise, PtdIns(3)P helps anchor ESCRT-0 and ESCRT-II while PtdIns(3,5)P_2 assists in anchoring ESCRT-III via CHMP3 to the endosomal membrane (Williams and Urbé, 2007). Studies that used an inhibitor called YM201636 that blocked PIKfyve activity led to reduced cellular PtdIns(3,5)P_2 levels (Jefferies et al., 2008) and also reduced surface GLUT4 (Ikonomov et al., 2009). The study described in this chapter aimed to test whether blocking PIKfyve using YM201636 caused similar hybrid compartments observed following overexpression of the dominant negative Vps4 ^{E235Q} construct in rat adipocytes. Though reduced surface GLUT4 was reported upon treatment with YM201636 (Koumanov et al., 2012), the 800 nM concentration of the YM201636 inhibitor failed to show the degree of enlarged compartments (Fig. 3.5) as seen in Fig. 3.4, *C* and *D*. The reduced surface GLUT4 that that is observed following use of YM201636 (Koumanov et al., 2012) could be due to the fact that YM201636 is not a selective PIKfyve inhibitor as it also prevents >50% of Akt-Ser473 from being phosphorylated (Ikonomov et al., 2009) leading to an inhibition of Akt-mediated GLUT4 translocation. Secondly, an inability to observe enlarged GLUT4 compartments with YM201636 (Fig. 3.5) could be interpreted as an inability of reduction in PtdIns(3,5)P_2 levels to be the sole cause of GLUT4 perturbation in an endosomal trafficking step. Reduced PtdIns(3,5)P_2 could mean that a GLUT4 endosome may not progress to an ESCRT-III- PtdIns(3,5)P_2 dependent stage but may instead be recycled from the ESCRT-I or ESCRT-II stage to another intracellular storage site via DUBs or another cargo retrieval mechanism.

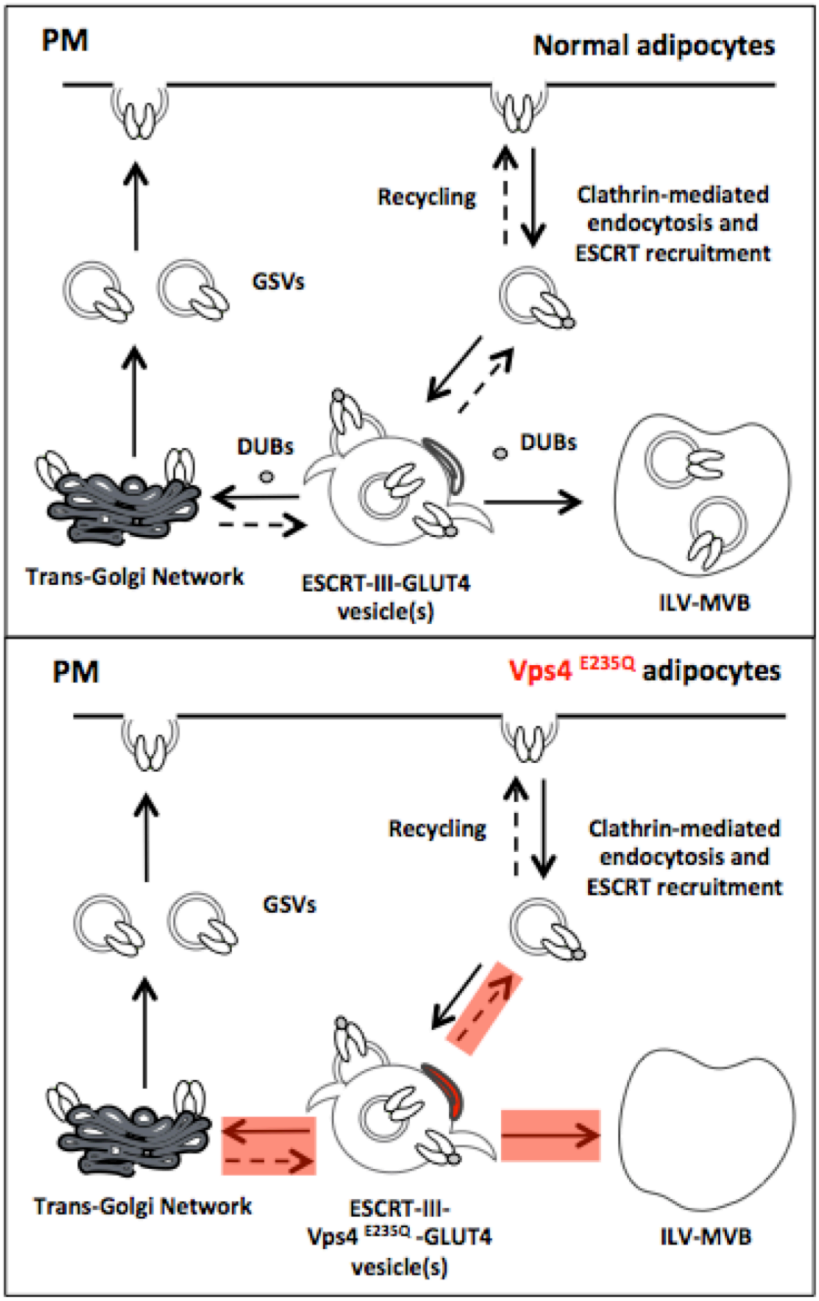

Figure 3.7: Model depicting ESCRT perturbation in rat adipocytes. The findings in this chapter show that perturbation of the ESCRT machinery leads to formation of a hybrid compartment that may contain tubulo-vesicular structures. The hybrid compartment contained early endosomal proteins (EEA1 and TfR) and TGN proteins (Stx6). The compartment may hence act as a sorting station for recently endocytosed GLUT4 vesicles or vesicles undergoing retrograde transport from the TGN. Colocalisation of GLUT4 with ubiquitin was also observed within this compartment. Ubiquitinated GLUT4 may undergo degradation or recycling. Deubiquitination by deubiquitinases (DUBs) may result in GLUT4 vesicles with outward membrane topology being either recycled to the PM or being sorted to GSV pools. Vesicles with inward facing topology of membrane domains in this compartment are likely to form ILVs following ESCRT-III dissociation and deubiquitination. Vesicles forming ILVs move towards an ESCRT-III-MVB lysosomal pathway *(as demonstrated in Fig. 3.2)*.

3.4 Conclusions

The data indicating GLUT4 traffic through the ESCRT pathway is novel. The Vps4 ^{E235Q} mutant generates a 'hybrid' compartment. GLUT4 is sequestered in this hybrid compartment and there is consequently a reduction in GLUT4 recruitment to the cell surface upon insulin stimulation (Koumanov et al., 2012).

There are still some questions that should be addressed in the future. The issue of identification of ubiquitin binding proteins that associate with GLUT4 vesicles need to be addressed together with resolution of the identity of DUBs that are involved in GLUT4-ESCRT traffic. A candidate ubiquitin like protein is TUG, which is known to associate with GLUT4 in the basal state and is cleaved upon insulin stimulation. Could TUG be involved in ESCRT disassembly and in the deubiquitination of GLUT4 prior to recycling? Also, the recent identification of Rab14 (Reed et al., 2013) on endosomal compartments raises the possibility of its involvement in the vesicle processing activity within an ESCRT-related compartment. Since AS160 is a downstream target of Akt and is also a Rab14 GAP, a confirmation of the presence of Rab14 on an ESCRT-related GLUT4 compartments could directly implicate Rab14 as a target of insulin action on the GLUT4-ESCRT pathway.

4 Rab3B, a Rab3 family member regulating GLUT4 exocytosis

4.1 Introduction

In the previous chapter, I discussed how phosphoinositides and ubiquitin played a role in recognition and recruitment of the ESCRT machinery. In this chapter, the focus is on another important class of proteins that give membranes an identity. These proteins are Rab GTPases commonly referred to as Rabs. Rabs were discovered in the yeast secretory pathway and initially classified as 'ras-like' GTPases (Salminen and Novick, 1987). This discovery sparked a special interest in characterising Rabs in mammalian cells, which led to the identification of approximately 60 Rab family members (Bock et al., 2001). This makes Rabs the largest class of proteins in the small GTPase family.

Rabs are small (20-30 kDa) monomeric GTPases and coordinate distinct stages of regulated inter-organellar membrane traffic such as vesicle budding, motility and fusion (Zerial and McBride, 2001). This brings about a need to classify the location and function of Rabs. Rabs work by a simple on/off switch mechanism (Lee et al., 2009). The guanine nucleotide is involved in this switch. For a Rab to be activated, it must be GTP-bound and this leads to the recruitment of other proteins called 'effectors' to the Rab and its associating vesicle (or cargo) (Kawasaki et al., 2005). Rabs are inactivated by the hydrolysis of GTP to GDP. A number of different regulators maintain a Rab in the GTP or GDP-bound state.

Deconstructing Rab-mediated signalling will give us a better idea of how Rabs function. This literature review attempts to provide a structural and functional understanding of Rabs and the domains involved in the recognition of interacting proteins. This outline will aid us in understanding the molecular interactions between Rabs and GLUT4 vesicles or vesicle associating proteins.

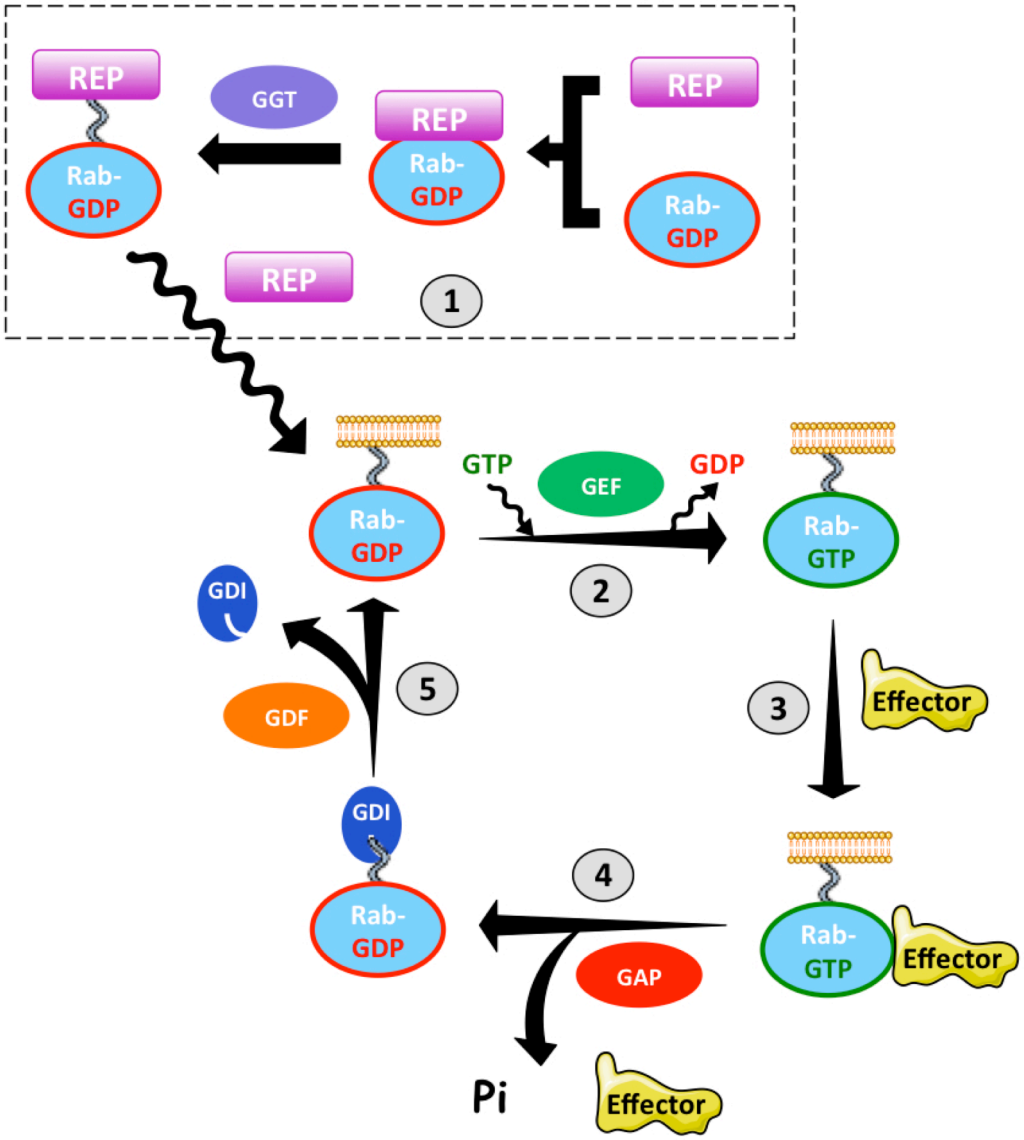

Figure 4.1: Rab activation and regulation. ***(1)*** Nascent cytosolic Rabs are maintained in a stable state by a multifunctional REP (Rab escort protein). A catalytic core region within the Rab acts as the recognition site for a Rab specific GGT (geranylgeranyl transferase). GGTs are activated during a stimulus (Goalstone et al., 1999). A trimeric complex is formed comprising Rab, REP and GGT. GGT prenylates the Rab on its C-terminal cysteine residue(s) and then dissociates. The REP escorts the Rab to an organelle following which REP dissociates. The Rab uses its prenylated moiety to anchor onto the organelle membrane's phospholipid layer. ***(2)*** Once a Rab is anchored to a membrane, GEF (GDP/GTP exchange factor) facilitates exchange of the Rab's GDP for GTP*, making a Rab *'active'*. ***(3)*** An active Rab is recognised by specific effector proteins that are responsible for correctly targeting the organelle. ***(4)*** The Rab is inactivated when a GAP (GTPase activating protein) catalyses the hydrolysis of GTP to GDP. Rabs are extracted from membranes by a GDI (GDP dissociation inhibitor). GDI sequesters the isoprenyl group making the Rab unavailable for membrane interaction. The Rab is now soluble and cytosolic until the next stimulus. ***(5)*** GDF (GDI dissociation factor) frees the sequestered isoprenyl group thereby allowing a Rab to be presented to membranes and continue another round of cycling. Figure adapted from Hutagalung and Novick, 2011.
**Recent studies in Cos-7 cells show that GEFs may also be involved in correctly directing a Rab to the target membrane* (Blümer et al., 2013).

4.1.1 Rabs: From structure to function

A key feature of Rabs is their ability to exchange GDP for GTP. The regulation of GTP-binding is accomplished by the recruitment of GEFs to Rabs. Rab GEFs are thought to cause a structural change in a Rab's nucleotide binding site, thereby facilitating GTP-binding (Delprato and Lambright, 2007). DENN/MADD (differentially expressed in neoplastic versus normal cells domain/MAP-kinase activating death domain) proteins were recently identified as GEFs for a number of Rabs (Yoshimura et al., 2010). Upon binding to GTP, a Rab needs to be stabilised. Rabs contain two conserved switch motifs (*switch 1* and *switch 2*), a *P-loop* motif and an associated Mg^{2+} ion that all play an important role in GTP-binding and stabilisation. Ser/Thr in the *P-loop* motif and Thr in the *switch 1* motif interact with the γ phosphate of GTP. Mg^{2+} coordinates interactions between the GTP's γ phosphate and Ser/Thr in these two motifs. Mg^{2+} is in turn stabilised by an Asp residue in the *switch 2* motif. Structural studies have shown that for Rabs to be in a stable and ordered conformation, they need to be in a GTP-bound state (Dumas et al., 1999; Wittinghofer and Vetter, 2011). Mutation of key residues in the above motifs can mimic a stable Rab-GTP conformation. Mutation of the Ser/Thr in the *P-loop* motif (GxxxxGK(S/T)) to asparagine (creating an SN or TN mutant) abolishes the ability of such a mutant to interact with Mg^{2+}, thereby interfering with GTP-binding while not affecting GDP-binding (Farnsworth and Feig, 1991; Nuoffer et al., 1994; Wittinghofer and Vetter, 2011). SN/TN mutants are hence dominant negative mutants. They mimic the GDP-bound state and are called 'GDP-locked' mutants. Mutation of the DxxGQ region to DxxGL in the *switch 2* motif mimics the GTP conformation (creating a constitutively active QL mutant). In addition to mimicking the GTP-bound state, QL mutants show reduced GAP (GTPase activating protein) catalytic activity i.e. reduced ability to be hydrolysed by a GAP from a GTP to GDP-bound state (Stenmark et al., 1994). Proteins containing the TBC (Tre-2/Bub2/Cdc16) domain form the majority of Rab GAPs known to date (Barr and Lambright, 2010). The only other known Rab GAPs are the Rab3 GAPs (Fukui et al., 1997; Nagano et al., 1998).

A GTP bound Rab is recognised by Rab associating proteins called ‘effectors’. Effectors link Rabs to cytosolic motors, tethers or fusion proteins. Rabs hence serve as a link between a vesicle membrane and cellular scaffolding proteins via effectors (Hammer and Wu, 2002). Rabs are also linked (or attached) to vesicles via their hyper variable carboxy (C) terminal region (Ali et al., 2004). The Rab C-terminus is modified by attachment of a prenyl group to terminal cysteine residue(s) by GGTs (geranylgeranyl transferases) (Joberty et al., 1993; Peter et al., 1992). This prenyl group assists in Rabs’ insertion into membrane phospholipids of vesicles or organelles (Alexandrov et al., 1994). *Switch* motifs and hyper-variable C-termini among with other domains (*interswitch* motifs, $\alpha 3/\beta 5$ loop and complementary determining regions (CDRs)) mutually or exclusively also contribute in distinguishing which effector binds to a Rab (Dumas et al., 1999; Ostermeier and Brunger, 1999). Effector specificity and function will be covered in more detail in Chapter 5.

4.1.2 Rabs and the cellular endomembrane system

Cargo is transported in a cell via vesicles that contain a cytosolic protein coat complex. Rabs can be regarded as either interacting with or forming part of this cytosolic coat complex on a vesicle. As of now, most of the evidence shows that Rabs interact with vesicle/cargo associating proteins, rather than directly with the cargo itself (Fukuda, 2006; Jin et al., 2011; Jordens et al., 2005). In the early stages of vesicle biogenesis, vesicles bud from donor membranes that include the endoplasmic reticulum (ER) or the curved Golgi cisternae or both (Hong, 1998). Rab1b along with other GTPases are responsible for recruiting the COPI/COPII complexes onto newly forming vesicles in the *trans*-Golgi network (TGN) (García et al., 2011). Rab8 and Rab12 facilitates the delivery of the Golgi derived vesicles to the plasma membrane (Huber et al., 1993; Iida et al., 1996). Rab5 and Rab6 facilitates vesicle movement along microtubules towards the cell periphery (Chavrier et al., 1990; Hill et al., 2000). The recruitment of vesicles to microtubules however, may not occur until Rab3 (Schlüter et al., 2002)/Rab10 (Sano et al., 2007)/Rab11 (Takahashi et al., 2012) are activated. These Rabs are important to vesicles as they help in the late stages of vesicle translocation

to the plasma membrane. The late stages of vesicle translocation involve processes that include actin reorganisation and assembly. Rab35 is one of the Rabs thought to facilitate actin assembly (Chua et al., 2010). At the cell periphery, a vesicle is tethered to the PM. Studies in yeast show that Rabs may play a key role in associating with SNARE machinery thereby facilitating tethering and fusion of the vesicle-SNARE complex with the plasma membrane (Cai et al., 2007; Novick et al., 2006). Mis-localisation or mutations in Rabs have been linked to aberrant cellular dynamics (Pal et al., 2006), immune dysfunction (Krzewski and Cullinane, 2013) and neurodegeneration (Baskys et al., 2007).

4.1.3 The exocytic Rab3 GTPase

Preliminary data: In order to obtain more information on Rab proteins activated by insulin and involved in GLUT4 trafficking; a new Bio-ATB-GTP photolabel was employed *(see Supplementary figure S7)*. This GTP analogue contained a biotin tag and a diazirine UV activated group (ATB), which allowed covalent crosslinking of the photolabel to GTP-bound small GTPases (Holman, 2010). A similar photolabelling approach has been described previously (Schwenk and Eckel, 2007; Sun et al., 2010). This Bio-ATB-GTP photolabel bound to GTP-binding proteins from total membrane preparations from rat adipocytes that were left either untreated or insulin-stimulated. The photolabel-bound proteins were isolated, analysed on a 2D gel and identified by mass spectrometry. Along with other known GLUT4 trafficking associated Rabs, Rab3B was identified as an insulin-responsive Rab from two individual experiments using the photolabelling technique. Further studies showed that Rab3B was activated upon insulin stimulation and its GTP loading increased with insulin in a time dependent manner. *(Koumanov et al., manuscript in preparation)*

Since Rab3 has been primarily implicated as an exocytic Rab in a number of studies (Lledo et al., 1993; Ohnishi et al., 1996; van IJzendoorn et al., 2002; Weber et al., 1996), it necessitates the need to better characterise Rab3B's presence in adipocytes and a possible role in GLUT4 trafficking.

Rab3 has four isoforms, which are paralogous to each other. Rab3A, Rab3B, Rab3C and Rab3D all share >75% amino acid identity (Baldini et al., 1992). Rab3A was one of the first in the Rab3 family to be identified and its role in calcium-mediated neurotransmitter exocytosis led to many Rab3 functional studies (Doussau et al., 1998; Geppert and Südhof, 1998; Mahoney et al., 2006; Takai et al., 1996; Tanaka et al., 2001). Rab3A and Rab3D were the identifiable Rab3 isoforms in mouse and rat adipocytes that associated with different intracellular compartments (Baldini et al., 1995; Guerre-Millo et al., 1997).

Rab3 was identified in a number of tissues where it stimulated exocytosis (or secretion). In pancreatic acinar cells, Rab3D overexpression enhanced amylase secretion (Ohnishi et al., 1997). Pancreatic islets were shown to contain Rab3A as the predominant Rab3 isoform that facilitated insulin granule secretion (Regazzi et al., 1996). Rab3A$^{-/-}$ mice showed reduced insulin granule secretion and glucose intolerance in pancreatic beta cells (Yaekura et al., 2003). A study in human pancreatic islets identified Rab3B as the predominant Rab3 isoform that colocalised with insulin granules (Piper et al., 2010). These studies suggest the occurrence of an inter-species difference in localisation of Rab3 isoforms (Piper et al., 2010).

Though most studies have shown Rab3 involvement in vesicle trafficking to increase exocytosis to the plasma membrane, there have been studies that show that Rab3 may not have a positive effect on exocytosis. Overexpression of one or more Rab3 isoforms led to a negative regulation of catecholamine exocytosis (Holz et al., 1994; Johannes et al., 1994; Weber et al., 1996). Rab3A negatively affected exocytosis of dopamine beta hydroxylase in PC12 cells in a calcium-dependent manner (Johannes et al., 1994). In rat adipocytes, overexpression of Rab3D had no discernible effect on GLUT4 subcellular localisation or exocytosis (Cormont et al., 1996).

A Rab3 knockout (KO) study was carried out in mice by Schluter (2004) to identify which of the Rab3 isoforms could be the limiting one in exocytosis. The study employed a single, double, triple and quadruple KO of all the four Rab3 isoforms in mice to identify the limiting Rab3 isoform (Schluter, 2004). The

studies on the KO mice showed that single/double Rab3 isoform knockout mice survived while the triple/quadruple Rab3 isoform knockout mice perished shortly after birth (Schluter, 2004). A tissue-wide analysis of the Rab3 isoforms showed variations in the number and amounts of each isoform across different tissues (Schlüter et al., 2002). These two studies supported the notion that all the four isoforms were likely to act in a functionally redundant manner. Exocytosis via Rab3 may occur in conjunction with other Rabs or in conjunction with effectors. Identifying Rab3 effectors is essential to understanding Rab3's functional role in signalling. It may help us understand why Rab3 shows differences in regulation of exocytosis across tissues/cell types.

4.1.4 Aims and rationale for the study

Rab3 has been characterised as an exocytic Rab in a number of tissues, which include insulin granule exocytosis in the pancreas while preliminary data from the Holman laboratory has suggested that a role in insulin-regulated GLUT4 exocytosis could be explored. The aim of the study described here is to elucidate the role of Rab3 in insulin-regulated GLUT4 traffic in adipocytes. Based on the evidence that Rab3 works with effectors, this study will also aim to identify Rab3 effectors in adipocytes**.**

4.2 Results

4.2.1 Analysis of Rab3 expression in insulin-responsive tissues

To evaluate the level of expression of different Rab3 isoforms in different insulin-sensitive tissues, a real time PCR study was carried out.

A

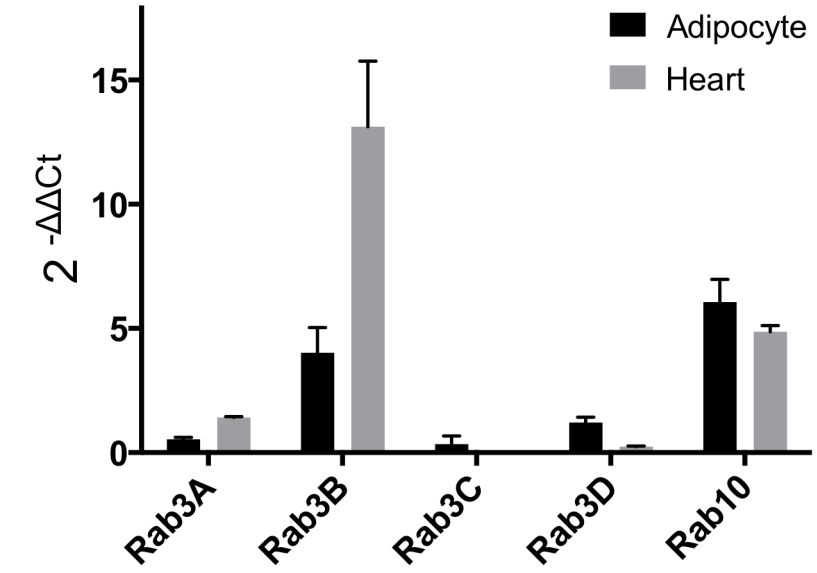

B

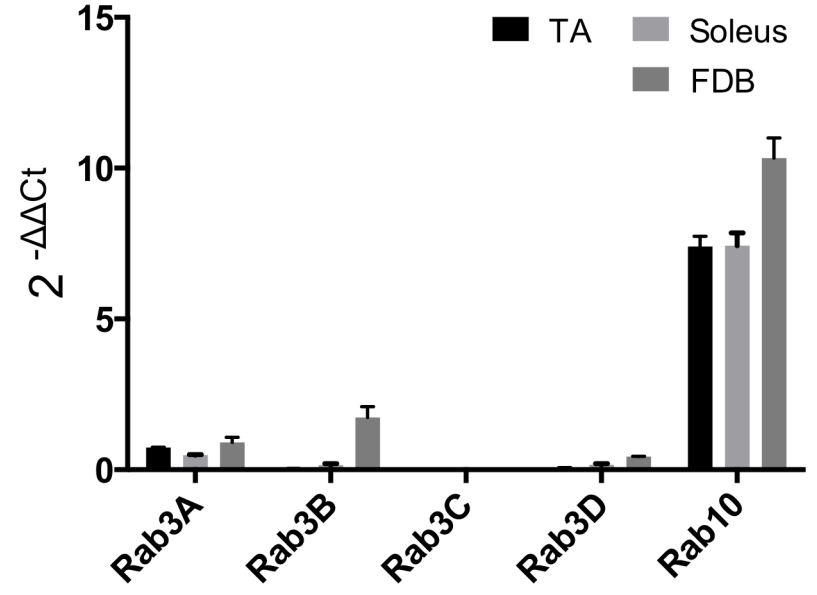

Figure 4.2: Analysis of Rab3 expression in insulin-responsive tissues. *Rattus norvegicus* tissues were isolated and mRNA was extracted using the TRIzol®-chloroform method. cDNA was generated by reverse transcription. The cDNA was used to study level of Rab3 isoforms in various rat tissues using a qPCR approach. Primers used are listed in *Supplementary table S2*. Rab10 was used as a control in the qPCR setup. Data in the bar graph represents an n of 3 from three independent sets of tissues/rats. The raw Ct values were normalised to the 28S rRNA housekeeping gene to yield ΔΔCt values. Error bars represent SEM from 3 sets of rats/tissues.

A qPCR profile of the insulin-responsive tissues revealed that Rab3 isoforms differ in their mRNA expression levels across the different tissues tested (Fig. 4.2). Rab10 was shown to play a critical role in GLUT4 translocation to the plasma membrane in adipocytes (Chen and Lippincott-Schwartz, 2013; Chen et al., 2012; Sadacca et al., 2013; Sano et al., 2007; Sano et al., 2008). Rab10 expression was hence measured as a control to compare it with Rab3 expression in these tissues. In rat adipocytes, Rab3B and Rab10 show similar expression patterns. Rab3B however is the predominantly expressed Rab3 isoform in rat adipocytes followed by Rab3D and Rab3A (Fig. 4.2*A*). The levels of Rab3D in rat adipocytes and heart correspond to a northern blot analysis of Rab3D in 3T3L1 adipocytes (Baldini et al., 1992). In Fig.4.2*A*, Rab3B is the major isoform observed in rat heart followed by Rab3A and Rab3D. Rab3B expression is higher than Rab10 in rat heart. In skeletal muscles, Rab10 shows highest expression while Rab3 isoforms show lower expression levels (Fig. 4.2*B*). In rat flexor digitorum brevis (FDB) Rab3A and Rab3B show similar expression while in tibialis anterior (TA) and soleus, Rab3A is predominantly expressed. Of all the Rab3 isoforms, Rab3C shows marginal or no expression in the insulin-responsive tissues tested. These studies hence confirm the expression of Rab3 in insulin-responsive tissues. Questions hence arise as to Rab3's role in these insulin-responsive tissues and its role in GLUT4 trafficking.

4.2.2 Generation of Rab3B constructs and site-directed mutants

Rab3 mRNA expression studies provided some good evidence that Rab3B is the predominant Rab3 isoform in adipocytes (Fig. 4.2). This section describes attempts to subclone the Rab3B gene to characterise its role in adipocytes.

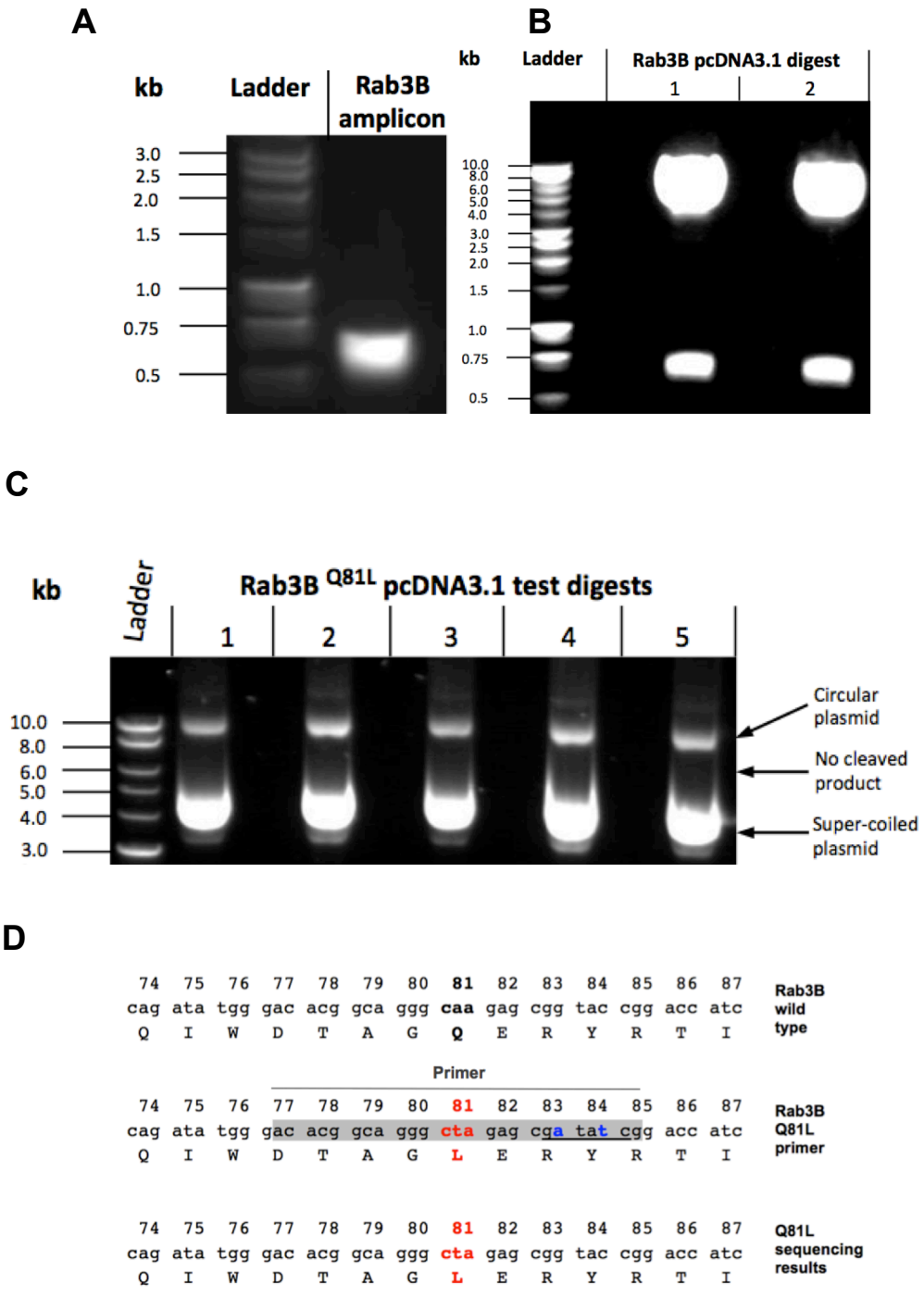

Figure 4.3: Subcloning of the Rab3B cDNA and generation of Rab3B ^{Q81L}. Rab3B was successfully amplified at the correct size (672 bp) from the pET28 vector using primers in *Supplementary table S1* and analysed on a 1% w/v agarose gel ***(A)***. This 672 bp amplicon was inserted into the pcDNA3.1 and a digest using Rab3B flanking restriction enzymes (*BamHI* and *XhoI*) showed a correctly inserted sequence ***(B)***. Site-directed mutagenesis was performed and an internal restriction enzyme (*EcoRV*) site flanking the Rab3B ^{Q81L} mutation was used to test correct mutagenesis ***(C)***. The grey shaded region in ***D*** represents the primer that was designed with the Q81L mutagenesis codon (red) and two silent mutations (blue) such that this site (gat_^atc) could be 'test-digested' by *EcoRV*. Sequencing results confirmed a correctly inserted Q81L mutation but absence of the silent mutations and hence no *EcoRV* cleavage site ***(D)***.

Dr J. D. Richardson (from the Holman lab) had cloned the Rab3B cDNA from an adipocyte library belonging to *Rattus norvegicus* into a pET28 vector. This pET28-Rab3B was used as a template from which Rab3B was amplified (Fig. 4.3*A*) and subcloned into a mammalian expression vector pcDNA3.1 (Fig. 4.3*B*) such that functional studies could be carried out in rat adipocytes. A constitutively active Rab3B ^{Q81L} construct was generated by site-directed mutagenesis (SDM) using the full-length pcDNA3.1-Rab3B as a template. The Rab3B ^{Q81L} construct is useful in understanding how an *'active'* GTP-loaded Rab3B would affect the fate of GLUT4 trafficking in rat adipocytes upon its overexpression.

During the site-directed mutagenesis (SDM) primer design, two silent mutations (shown in blue in Fig. 4.3*D*) were inserted within the framework of the Q81L primer (shaded grey in Fig. 4.3*D*). These silent mutations generated a site for *EcoRV* cleavage (gat_^atc, in Fig. 4.3*D*). A test restriction digest of the SDM samples with *EcoRV* could thus be used to confirm successful amplification from template DNA. This test restriction digest could be done in the laboratory before commercially sequencing the SDM samples. A test restriction digestion using *EcoRV* was attempted on 5 samples generated after the SDM procedure. Digestion with *EcoRV* was expected to yield a single linear 6041 bp fragment. However, upon digesting with *EcoRV* no linear (cleaved) 6041 bp fragment was obtained (Fig. 4.3*C*). The 5 samples were however still sequenced. The sequencing results unexpectedly showed that the Q81L mutation was indeed inserted confirming correct mutagenesis (shown in red in Fig. 4.3*D*). The sequenced constructs however lacked any of the silent mutations that were generated in the primer (shown in blue in Fig. 4.3*D*) to create a restriction site for *EcoRV* (gat_^atc, in Fig. 4.3*D*). This could be an error with the commercially synthesised primer. Since the silent mutations for *EcoRV* were only inserted as a preliminary measure to check for mutagenesis in the laboratory, the construct was still suitable to use as a constitutively active mutant as sequencing results confirmed the necessary Q81L mutation.

The Rab3B ^{T36N} dominant negative construct was prepared in the same way as the Rab3B ^{Q81L} construct, except no silent mutations could be inserted.

However, creating the T36N mutation led to an automatically generated restriction site gaann_^nnttc for which a restriction enzyme (*XmnI*) was available. A restriction map with *XmnI* following the T36N mutation was expected to yield three (3378, 1367 and 1293 bp) DNA products instead of two large (3378 and 2260 bp) DNA products (Fig. 4.4*A*). Test digestion of the SDM samples with *XmnI* was performed. The clones 4 and 10 yielded one large fragment (3378 bp) and two smaller fragments (~1300 bp each) (Fig. 4.4*B*), which indicated successful site-directed mutagenesis. These samples were sent for sequencing and sequencing confirmed correct T36N mutagenesis.

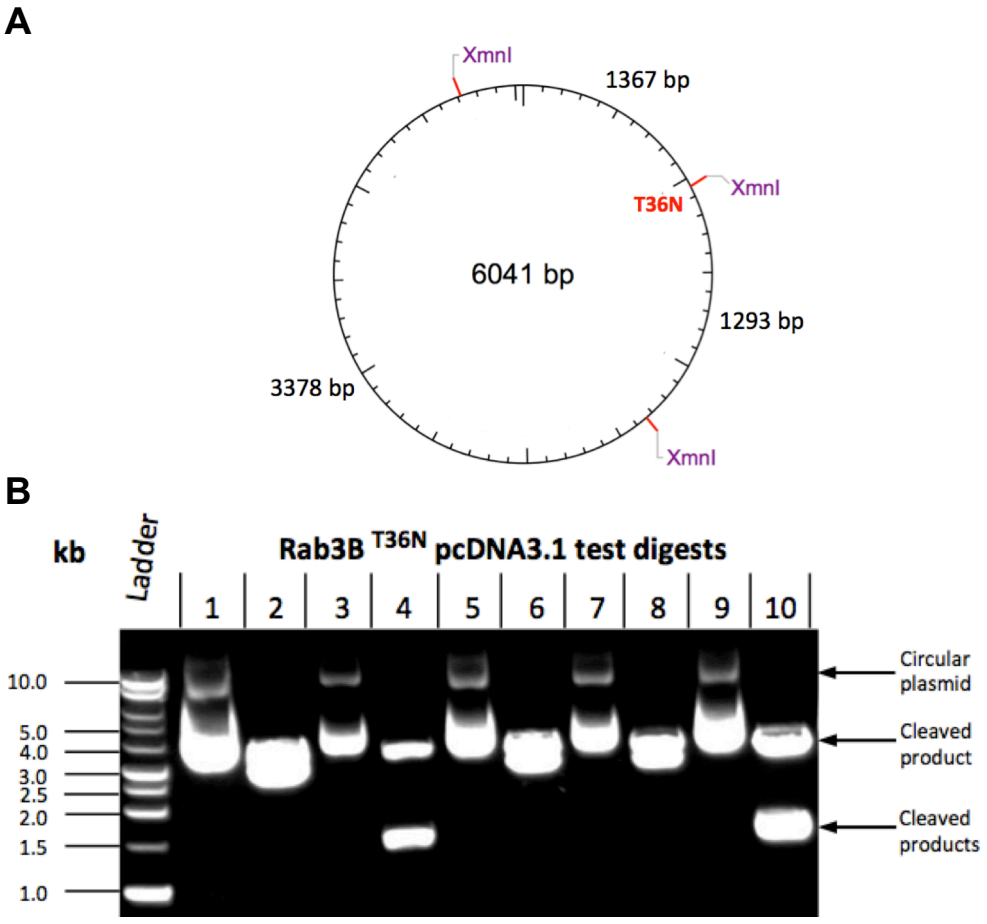

Figure 4.4: Site-directed mutagenesis for generating Rab3B ^{T36N}. (pcDNA3.1) Rab3B was used as a template and site-directed mutagenesis was performed as described in *Methods 2.2.1.2.* An internal restriction site for the restriction enzyme *XmnI* was generated when creating the T36N mutation ***(A)***. 10 colonies from the Rab3B ^{T36N} SDM experiment were isolated and grown overnight. Plasmids from these colonies (clones) were test digested with *XmnI*. Clones 4 and 10 showed one ~3 kb and two ~1.3 kb cleaved products ***(B)***. Clones 4 and 10 were sequenced and confirmed correct insertion of the T36N mutation.

4.2.3 Effect of Rab3B on GLUT4 translocation

The following study was undertaken to study the effect of Rab3B on GLUT4 translocation to the plasma membrane in rat adipocytes treated with or without insulin. The constitutively active Q81L and dominant negative T36N Rab3B constructs were used to understand the effect of GTP-active and GTP-inactive Rab3B on GLUT4 translocation to the plasma membrane. Rab3B constructs were transfected into primary rat adipocytes together with HA-tagged GLUT4, the latter of which was used as a reporter. An empty pcDNA3.1 vector was used as a control. Following insulin stimulation, HA-GLUT4 at the adipocyte cell surface was detected with a mouse anti-HA antibody. The anti-mouse secondary antibody was conjugated to β-galactosidase. A fluorescein di-β-D-galactopyranoside substrate was used in the assay that is hydrolysed by the β-galactosidase conjugated secondary antibody to yield a highly fluorescent fluorescein compound. Fluorescein was released in proportion to the amount of HA on the adipocyte cell surface and was measured at 565 nm.

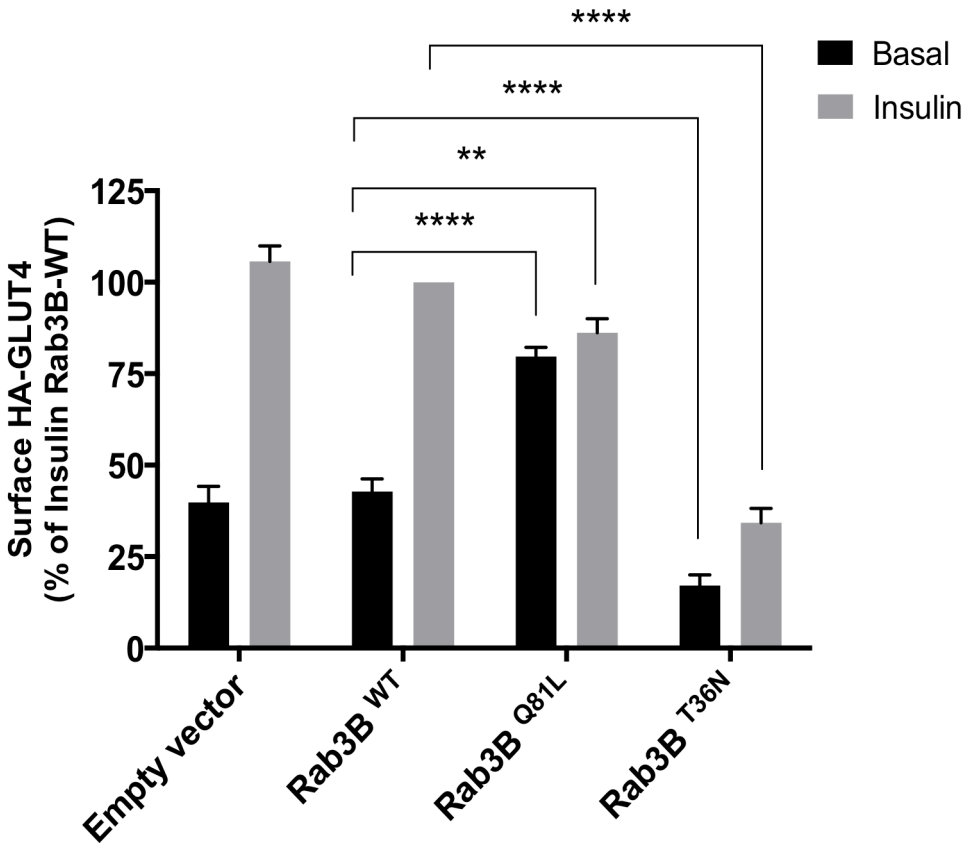

Figure 4.5: Rab3B increases GLUT4 translocation in basal rat adipocytes. Primary rat adipocytes were transfected by electroporation with (pCis) HA-GLUT4 and pcDNA3.1 alone (empty vector), (pcDNA3.1) Rab3B ^{WT}, (pcDNA3.1) Rab3B ^{Q81L} or (pcDNA3.1) Rab3B ^{T36N} and maintained in culture overnight (for 16 h). HA-GLUT4 at the cell surface was detected with an anti-HA primary antibody and b-galactosidase conjugated secondary antibody. The signal from the bound secondary antibody was measured with a fluorescent b-galactosidase substrate. Results are mean and SEM from 3 independent experiments. **** p=<0.0001, **p<0.01 (paired two tailed t-test comparisons vs Rab3B ^{WT}).
Note: I conducted the preliminary experiments for this assay and Dr D.J.Fazakerley repeated the work to obtain an n of 3, which is graphically represented in this figure.

On analysis of the results (Fig. 4.5), the wild type Rab3B-transfected rat adipocytes showed no difference to the empty vector (pcDNA3.1 only) control across basal and insulin-treated samples. The constitutively active Rab3B ^{Q81L}-transfected adipocytes showed a significant 2-fold increase in HA-GLUT4 at the cell surface in basal adipocytes compared to the empty vector control and wild type Rab3B-transfected adipocytes.

The dominant negative Rab3B ^{T36N} construct showed reduced cell surface levels of HA-GLUT4. In Rab3B ^{T36N}-transfected basal cells, surface HA-GLUT4 was significantly reduced by 2.47-fold compared to the basal Rab3B ^{WT} sample. Insulin-treated cells containing Rab3B ^{T36N} showed levels of HA-GLUT4 that were reduced by 2.94-fold compared to the insulin-treated Rab3B ^{WT} sample.

The findings of this HA-GLUT4 translocation assay suggest that the constitutively active form of Rab3B may not be acting alone in GLUT4 exocytosis. Rabs work in concert with effectors and these findings necessitate the need to identify Rab3B effectors in adipocytes.

4.2.4 Rab3B pull-down of effectors from rat adipocytes

Effectors govern the regulatory function of Rabs. Effectors may assist a Rab in vesicle formation, movement, tethering or fusion. With the identification of Rab3B as a regulator of GLUT4 translocation (Fig. 4.5), the identification of a Rab3 effector is likely to yield more information on the interacting partners,

functional characteristics, and the stage of GLUT4 trafficking that Rab3B may be involved with. Different trafficking proteins are recruited at different stages of GLUT4 vesicle movement. Since there has been no study yet, positively linking Rab3B or it's effectors to GLUT4 trafficking in adipocytes, a protein-protein interaction study was employed to uncover novel Rab3B interacting proteins (effectors) from rat adipocytes. GST-Rab3B was bound to either GTPγS or GDP to identify Rab3B-GTPγS specific effectors.

GST-Rab3B was successfully expressed using a 2 l culture and purified via conjugation to glutathione beads (Fig. 4.6) to yield approximately 82.17 mg of GST-Rab3B in a 2 ml protein sample. The GST-Rab3B was bound to either GTPγS or GDP to yield *active* or *inactive* forms of the Rab3B protein. A GST-only control was also employed in this pull-down study. The GST tagged proteins were incubated with glutathione agarose beads. The fusion protein conjugated beads were added to columns *(as described in Materials and Methods* 2.2.3.7*)*. The columns containing GST-only or GST-Rab3B (GTPγS/GDP) conjugated to glutathione beads were incubated with adipocyte lysates.

The pull-down using Rab3B loaded with GTPγS yielded two distinct bands from two individual experiments. Mass spectrometry analysis revealed the two distinct bands (1 and 2 in Fig. 4.7) as members of the heat shock protein 70 (Hsp70) family. Band 1 (71 kDa) was identified as Hsp70-8 and band 2 (74 kDa) was identified as glucose-regulated protein 75/78 (GRP75/GRP78). GRP is also a member of the Hsp70 family. These proteins were not observed in the control GST-only glutathione beads, further confirming Hsp70 specificity to the immobilised Rab3B-GTPγS protein pull-down.

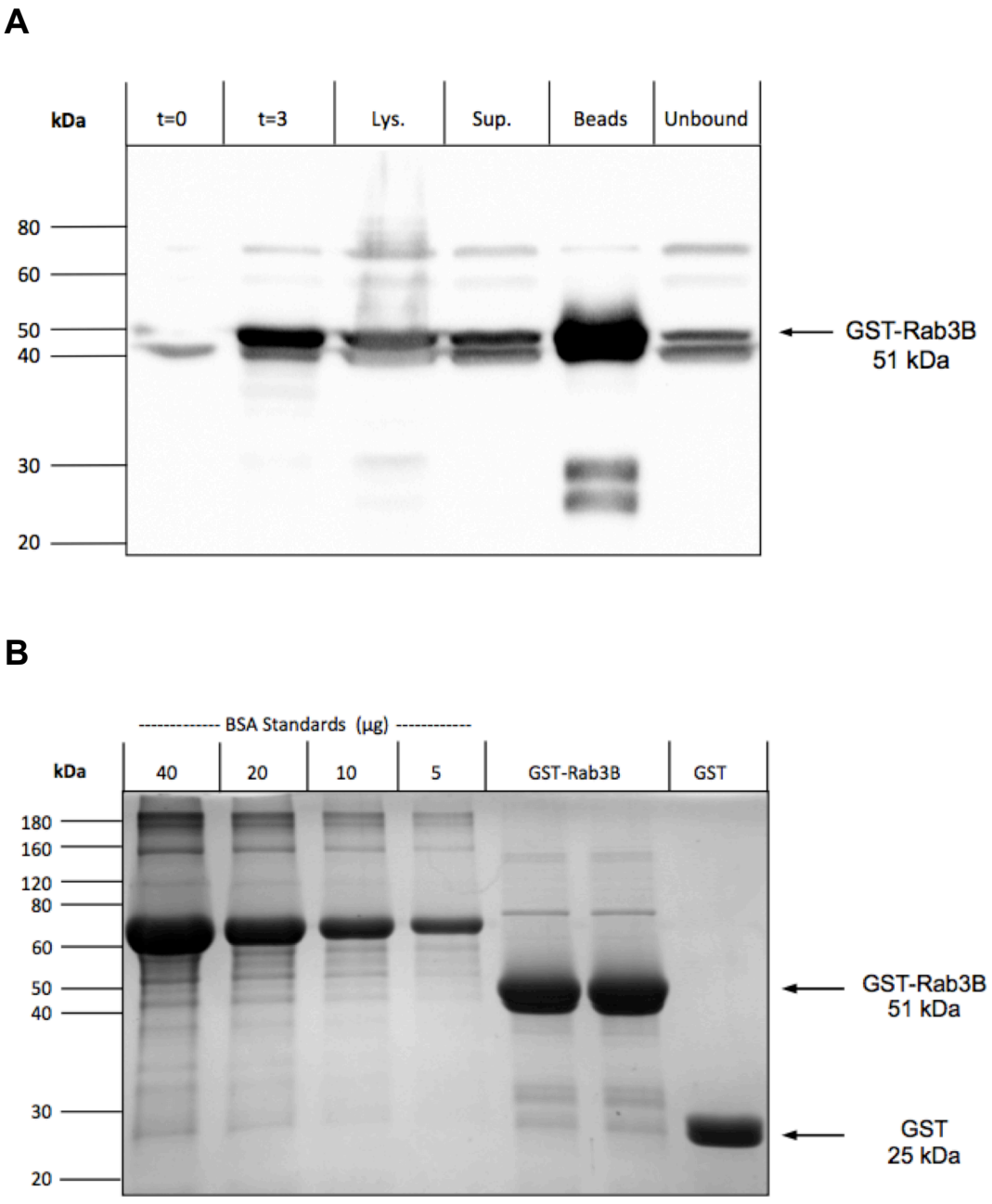

Figure 4.6: Expression of the GST-Rab3B fusion protein. (pGEX4T) GST-Rab3B and (pGEX4T) GST were expressed in BL21 DE3 cells with 0.3 mM IPTG induction at 25°C for 3 h and purified on glutathione beads. The expression and purification profile was analysed on a 12% SDS-PAGE gel followed by western blotting for GST-Rab3B with a goat anti-GST antibody ***(A)***. GST-Rab3B was detected at 51 kDa and GST-only at 25 kDa. Coomassie brilliant blue staining was used for quantification ***(B)***. The purification yielded 82.17 mg (805.6 µM) GST-Rab3B conjugated to 2 ml of beads and 43.5 mg (1740 µM) GST conjugated to 1 ml of beads from a 2 l culture.

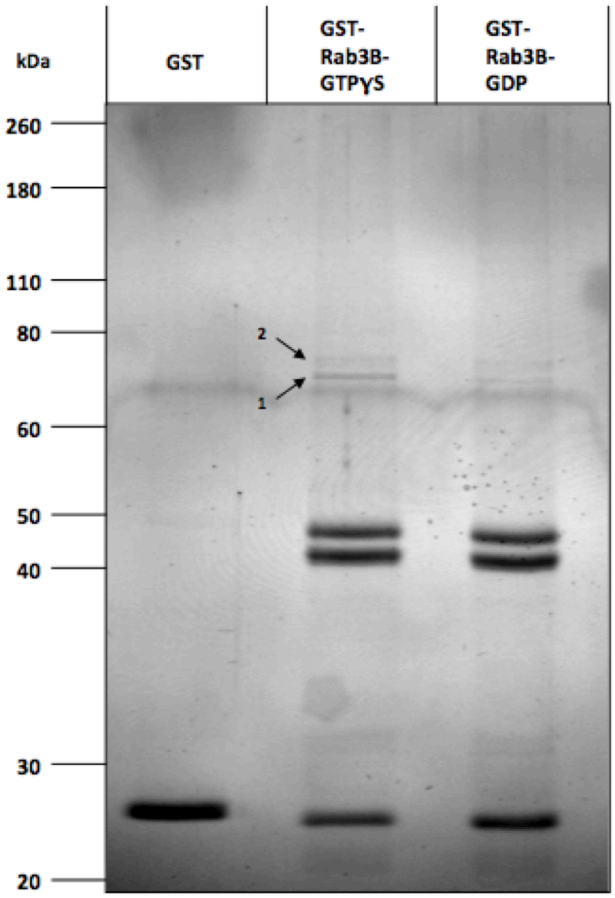

Figure 4.7: Pull-down of Rab3B effectors following GTPγS loading yields an interacting protein. 40 mg (400 μM) of GST-Rab3B or GST alone was conjugated to glutathione beads. GST-Rab3B beads were loaded with nucleotide GTPγS or GDP. The beads were incubated with adipose cell lysates. Bound proteins were eluted with a nucleotide exchange buffer and run on a 10% SDS-PAGE gel. The gel was stained with colloidal coomassie. Numbers 1 (71 kDa) and 2 (74 kDa) on the gel represent the distinct bands that were bound to the Rab3B-GTPγS column. These were extracted and analysed via mass spectrometry. This experiment was repeated again and the same distinct bands were identified between 60-80 kDa. Please refer to 2.2.3.7 in the *Materials and Methods* section for detailed experimental conditions.

4.3 Discussion

This chapter attempts to implicate novel Rabs as regulators in the GLUT4 trafficking pathway. Rab3B was identified using qPCR studies as a Rab3 family member highly expressed in rat adipocyte and heart tissues (Fig. 4.2). This finding adds to a previous study performed in the Holman lab that identified Rab3B as a membrane associated and insulin-responsive Rab, in rat adipocytes *(Koumanov et al., manuscript in preparation)*.

Rabs are involved in a variety of vesicle trafficking steps, one of which is vesicle fusion (Cai et al., 2007). The recent studies identifying Rabs in the GLUT4 exocytic pathway paves the way to make an assumption that a Rab could likely be involved in the final stages of GLUT4 coupling to the plasma membrane. The possibility that this could be the exocytic Rab3B was demonstrated by studying its effect on GLUT4 translocation (Fig. 4.5). The overexpression of the constitutively active Rab3B ^{Q81L} mutant resulted in a significant 2-fold increase in the levels of HA-GLUT4 at the plasma membrane in basal rat adipocytes mimicking an insulin response. The overexpression of a dominant negative Rab3B ^{T36N} mutant resulted in a decrease in the HA-GLUT4 insulin response to basal levels. These results provide new evidence for involvement of Rab3B in GLUT4 trafficking in rat adipocytes. The constitutively active Rab3B acted as a positive regulator of GLUT4 exocytosis. These results however, vary from an earlier study, which demonstrated that blocking Rab3 by microinjection of a Rab3 antibody in 3T3L1 adipocytes had no effect on basal/insulin GLUT4 translocation (Vollenweider et al., 1997). The variation in results can possibly be explained by the fact that an antibody microinjection technique was used by Vollenweider et al. (1997) *vs.* an overexpression of Rab3B in the study in this chapter. Also, an inter-species variation in Rab3 isoform expression/function could exist between 3T3L1 adipocytes and rat adipocytes. The work described in this chapter revealed the potential importance of Rab3B in GLUT4 translocation to the plasma membrane. The effect of Rab3B in this study mirrors other studies where knockdown of Rab3 isoforms reduced exocytosis in neuronal cells (Schluter, 2004). The association between Rab3B and GLUT4

vesicles has been demonstrated to increase in the insulin state with overexpression of Rab3B ^{WT} or Rab3B ^{Q81L} constructs in adipocytes *(Koumanov et al., manuscript in preparation)*. However, earlier studies in rat adipocytes demonstrate that Rab3B is predominantly cytosolic and insulin stimulation did not bring about any change in the localisation of Rab3B (Cormont et al., 1993). The studies by Cormont et al. (1993) did not utilise overexpression of Rab3B or its mutant construct and differences in carrying out experimental procedures could also have contributed to the varied observations (Cormont et al., 1993). Overexpression of Rab3D ^{WT} was carried out but this construct had no effect on GLUT4 translocation in rat adipocytes (Cormont et al., 1996); this observation was similar to overexpression of Rab3B ^{WT} in the studies described in this chapter (Fig. 4.5). Hence, this suggests that an effect on trafficking is likely to be observed preferably with the constitutively active (Q81L) form of Rab3. The studies in this chapter provide the necessary data to investigate Rab3B and its potential effectors in GLUT4 trafficking.

Recruitment of the correct effectors is crucial for Rab function (Grosshans et al., 2006; Stein et al., 2012). An attempt was made using GST-Rab3B to pull-down and uncover potential Rab3B effectors that could assist in GLUT4 trafficking (Fig. 4.7). This effort led to the identification of two proteins from the Hsp70 family, Hsp70-8 (HspA8/Hsc70) and GRP75/GRP78. This is the first finding linking Rab3B to heat shock proteins. Hsp70 is primarily involved in chaperone protein folding (Mayer and Bukau, 2005). Hsp70-chaperone complex may play a role in trafficking Rab3B from the plasma membrane to the cytosol in a similar way that Hsp90 retrieves Rab3A from presynaptic membranes to the cytosol (Sakisaka et al., 2002). Studies in mouse colon also showed that Hsp70 colocalises with Rab4 and Rab5a (Stangl et al., 2011) further implicating Hsp70 in the endocytosis, recycling and the retrieval pathway. The Hsp70-8 protein facilitates recycling by catalysing disassembly of recently endocytosed clathrin coated vesicles (Rothnie et al., 2011). Hsp70 has been detected in adipocytes before (Jiang et al., 2007) and Hsp70-8 was found to be a likely substrate of *O*-linked N-acetylglucosamine (*O*-GlcNAc) in skeletal muscle L6 myotubes (Walgren et al., 2003). Increased modification of proteins by *O*-GlcNAc has been shown to cause insulin resistance and impaired Akt activation in 3T3L1

adipocytes (Vosseller et al., 2002). The association of Rab3B with Hsp70 will be of special interest when studying retrieval of GLUT4 vesicles from the plasma membrane and a further possible link, if any, to insulin resistance. However, there is not enough evidence to implicate Hsp70 as a direct regulator of GLUT4 exocytosis or vesicle fusion.

4.4 Conclusions

This chapter provides results on some novel findings. Firstly, profiling the Rab3 isoforms in insulin-responsive tissues shows that Rab3B is highly expressed in adipocyte and heart tissues. Secondly, the constitutively active form of Rab3B was implicated as a positive regulator of GLUT4 translocation. However, a Rab3B effector that could be involved in GLUT4 translocation could not be positively identified using this pull-down approach. Hsp70 was positively identified as a Rab3B-GTPγS interacting protein which is interesting, but its role and function has been characterised as being primarily involved in chaperone targeting and protein folding (Mayer and Bukau, 2005; Morgan et al., 2013). The search for an effector involved with Rab3B and GLUT4 coupling to the plasma membrane would need another experimental approach.

5 Noc2: A novel Rab3B effector in GLUT4 trafficking

5.1 Introduction

The necessary trafficking proteins must be recruited to vesicles for successful regulated exocytosis. Rabs and their effectors help correctly target a vesicle to its cellular destination by associating with additional intracellular trafficking or cytoskeletal scaffolding proteins (Seabra and Coudrier, 2004). Effectors are also able to tether a vesicle to membrane phospholipids and interact with the PM and vesicle fusion machinery (Tsuboi and Fukuda, 2006). Some effectors multitask the different steps in vesicle exocytosis while others are restricted in the extent of their function. Effectors hence convey specificity and directionality to membrane traffic and are required in concert with Rabs to facilitate proper vesicle targeting.

5.1.1 Rab effectors: Structural aspects and recognition

Effectors usually recognise *'active'* or GTP-bound Rabs. Ostermeier and Brunger (1999) provided the first insights into the interaction between a Rab3 effector called Rabphilin-3A and Rab3A (Ostermeier and Brunger, 1999). The switch region and a specific CDR (complementarity-determining region) of Rab3A conferred specificity to Rabplilin-3A binding (Ostermeier and Brunger, 1999). Structural studies on a Rab5 effector called Rabenosyn-5 led to the identification of small subsets of amino acid residues in the switch and interswitch regions of Rab5 that conferred specificity to Rabenosyn-5 (Eathiraj et al., 2005). An effector called Rabaptin-5 could recognise two Rabs (Rab5 and Rab4), using different sets of amino acid residues located in and around the switch region of Rabs (Eathiraj et al., 2005; Vitale et al., 1998). Like Rabaptin-5, another Rab effector, inositol polyphosphate 5-phosphatase (OCRL-1) also interacts with multiple Rabs (such as Rab1, Rab5, Rab6, Rab8 and Rab14) (Fukuda et al., 2008a). Though Rabs are fairly conserved, minor variations in

amino acids across the switch/interswitch/CDR region(s) lead to structural variations in the Rab protein and consequently functional differences (see Fig. 5.1). Small structural variations can lead to the formation of distinct 'microdomains' which allow further effector specificity to a particular Rab GTPase (Stenmark, 2009).

Effectors are fairly divergent and vary in the composition of their motifs. Effectors also rely on motif diversity and structural folding patterns in order to recognise a cognate Rab (or its microdomain). Hairpins and helical coiled-coil structures formed by distinct amino acid regions on effectors are some of the structural components involved in stabilisation of effector and Rab interactions (Eathiraj et al., 2005). Rab-interacting lysosomal protein (a Rab7 effector) has two coiled-coil domains that self-interact and form a homodimer with two separate Rab7 molecules at a time (Wu et al., 2005). OCRL and Rab8 interaction is facilitated by the ASH domain and C-terminal α-helix region of OCRL (Hagemann et al., 2012; Hou et al., 2011). Rabphilin-3A possesses an N-terminal Rab-binding domain (RBD) and an SGAWFF motif that it uses to stably bind the Rab3 group of GTPases (Ostermeier and Brunger, 1999). To summarise, the affinity between effectors and Rabs is governed by a cumulative effect of interactions between the Rab, its microdomains and unique motifs present on the effector.

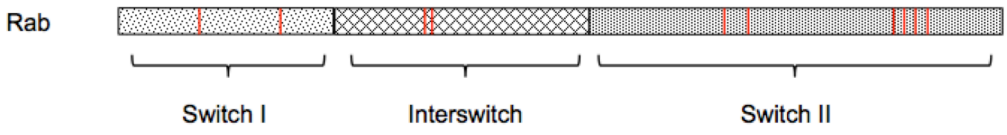

Figure 5.1: Rab domains. Rabs contain two switch domains separted by an interswitch region, These domains are made up of six beta sheets flanked by five alpha helices. Single or groups of amino acids across the domains form the complementarity determining region (CDR). Differences across Rab domains and the CDR contribute to achieving specificity in effector recognition.

5.1.2 Rab effectors: The functional aspects

Effectors are involved with Rabs in various stages of endocytosis and exocytosis. Effector-mediated processes include vesicle recognition, formation, translocation, tethering, docking and fusion. In the early stages of vesicle formation, tail-interacting protein of 47 kDa (TIP47), a Rab9 effector interacts with the mannose 6-phosphate receptor (M6PR) and mediates vesicle trafficking through the TGN (Díaz and Pfeffer, 1998). Trafficking of vesicles in a cell can occur via microtubules and the motor protein kinesin (Goldstein, 1993; Vale et al., 1985). Rab6 is one of the well characterised Rabs that is involved with the microtubule-binding element Rabkinesin-6 (Echard et al., 1998; Hill et al., 2000). Some Rabs associate with microtubules via differentially expressed in normal and neoplastic cells (DENN) domain proteins (Niwa et al., 2008), while others do so via linker proteins, some of which may include receptors (Arimura et al., 2009). DENN domain proteins were incidentally also characterised as Rab GEFs (Yoshimura et al., 2010). The finding that DENN domains have GEF activity leads us to the understanding that once activated, Rabs via GEFs (or DENN domains), chaperone vesicles along a microtubule to its designated organelle. Upon approaching an organelle, the vesicle gets tethered to it and additional Rab effectors are recruited. Tethering proteins (some of which may also act as effectors) then form a link between the organelle's target membrane and the trafficking vesicle. Tethering of endoplasmic reticulum derived vesicles to the Golgi occurs with the Rab1 effectors p115 (Allan et al., 2000) and Golgi reassembly stacking protein of 65 kDa (Moyer et al., 2001). Tethering of an exocytic vesicle to the plasma membrane is thought to be brought about by Rabs and their effectors in a concerted manner with Rho and Ral GTPases (Novick and Guo, 2002). Rho GTPases are involved in actin remodelling at the plasma membrane (Kanzaki and Pessin, 2001) while Ral GTPases facilitate an interaction between the exocytic vesicle and the plasma membrane (Chen et al., 2007). In GLUT4 trafficking, a vesicle associates with an exocyst complex, which is a multimeric complex that interacts with different small GTPases (that include Ral and Rho) and their effectors together with SNARE proteins. Sec1/Munc18 (SM) proteins are part of SNARE-mediated vesicle fusion and are believed to recognise certain Rab effectors. The SM protein, Munc18-1 has been shown to interact with Rab27 effectors during plasma membrane tethering/docking of neuroendocrine vesicles (Tsuboi and Fukuda, 2006).

5.1.3 Rab3 effectors

The Rab3 group of GTPases are primarily involved in exocytosis of secretory vesicles to the cell periphery. A number of Rab3 effectors have concomitantly been shown to interact with another exocytic Rab called Rab27. This group of secretory GTPases (that include Rab3 and Rab27) may have a role in the GLUT4 trafficking pathway as Rab3, Rab27 and their effectors have been implicated in the late stages of vesicle exocytosis in other cell types (Schlüter et al., 2002). Neuronal cells constantly use vesicle exocytosis in signal transmission and hence are some of the best-studied examples of Rab3-mediated exocytosis (Schluter, 2004). Neuronal studies revealed that Rab3 effectors comprise two plasma membrane-interacting C2 domains (Wang et al., 1997). These C2 domains were first identified in protein kinase C as Ca^{2+} and phospholipid-binding domains (Nalefski and Falke, 1996). Incidentally, recent studies have shown the requirement of a Ca^{2+}-dependent mechanism as well as the involvement of plasma membrane-interacting C2 domains in GLUT4 exocytosis (Xie et al., 2011; Yu et al., 2013).

The first Rab3 effector to be identified was the C2 domain containing effector, Rabphilin3A. It was identified in brain tissue (Shirataki et al., 1993) and was shown to interact with Rab3A via an N-terminal zinc finger motif (Ostermeier and Brunger, 1999). Rab3A recruits Rabphilin3A that facilitates vesicle movement along the actin cytoskeleton by binding to the actin component α-actinin (Kato et al., 1996). Upon reaching the cell periphery, Rabphilin-3A is thought to bind soluble NSF attachment protein of 25 kDa (SNAP-25) of the SNARE machinery and prime vesicles for fusion (Deák et al., 2006). Rab3 Interacting Molecule (RIM) is another C2 domain containing effector localised to the plasma membrane and it associates with a number of proteins in the exocytic pathway, such as synaptic Munc13-1 (Dulubova et al., 2005), 14-3-3 (Sun et al., 2003) and SNAP-25 (Coppola et al., 2001). RIM regulates vesicle fusion in a Rab3 dependent manner (Wang et al., 1997) and has also been implicated in insulin exocytosis in the pancreas (Iezzi et al., 2000). Another Rab3 effector called granuphilin (Slp4a) has also been linked to insulin granule exocytosis and fusion in pancreatic cells (Gomi et al., 2005). Like RIM, granuphilin was shown to

interact with Rab3A, Munc-18 and syntaxin-1a of the SNARE fusion machinery (Coppola et al., 2002; Torii et al., 2002).

5.1.4 Noc2: A potential Rab3 effector in adipocytes

A recent study that broadened the understanding of the GLUT4 trafficking pathway was the discovery that double C2-like domain-containing protein (Doc2b) is involved with the SNARE dependent fusion of GLUT4 vesicles to the plasma membrane (Fukuda et al., 2008b). Ca^{2+} was shown to be necessary in this Doc2b dependent fusion process (Yu et al., 2013). Doc2b contains two Ca^{2+}-binding C2 domains and it interacts with the SNARE complex via the Munc18c-syntaxin-4 complex in insulin-responsive tissues (Fukuda et al., 2008b; Ramalingam et al., 2012). These findings suggest the involvement of Ca^{2+}-dependent sensors (that could include Rab3 effectors) in GLUT4 vesicle fusion to the plasma membrane. A Rab3 effector that could be related to Doc2b is Noc2. Noc2 is located next to Doc2b on chromosome 17 in *Homo sapiens* (and chromosome 10 in *Rattus norvegicus*). There could have been an evolutionary gene fission event of a Rab3 effector that resulted in Noc2 and Doc2b evolving as separate genes. The relationship between Noc2 and Doc2b is described in further detail in Figure 5.2.

Noc2 (or No C2) is a Rab3 effector that lacks the C2 domains and was identified to be homologous to another Rab3 effector, Rabphilin3A (Kotake et al., 1997). Noc2 like other effectors binds to the *'active'* form of Rab3 (Shibasaki and Seino, 2005). In neuroendocrine cells, Noc2 was also linked to Ca^{2+}-dependent exocytosis where it was shown to be a negative regulator of exocytosis (Haynes, 2000). In pancreatic acinar cells, it was proposed that Noc2 might be responsible for activating a Ca^{2+}-dependent pathway for exocytosis (Ogata et al., 2012). The role of Noc2 as a positive or negative regulator may indeed vary across cell types. The distinguishing feature of Noc2 is that it lacks the C2 domains that are extensively characterised in exocytic Rab3 effectors. The missing C2 domains, however do not affect Noc2's Rab binding ability. The N-terminal region of Noc2 contains the RBD that is conserved across Rab3

effectors and an SGAWFY motif that assists Noc2 in Rab3 recognition and binding (Fukuda et al., 2004). The interaction between Noc2 and Rab3 has been linked to insulin exocytosis in pancreatic cells as well (Haynes, 2000).

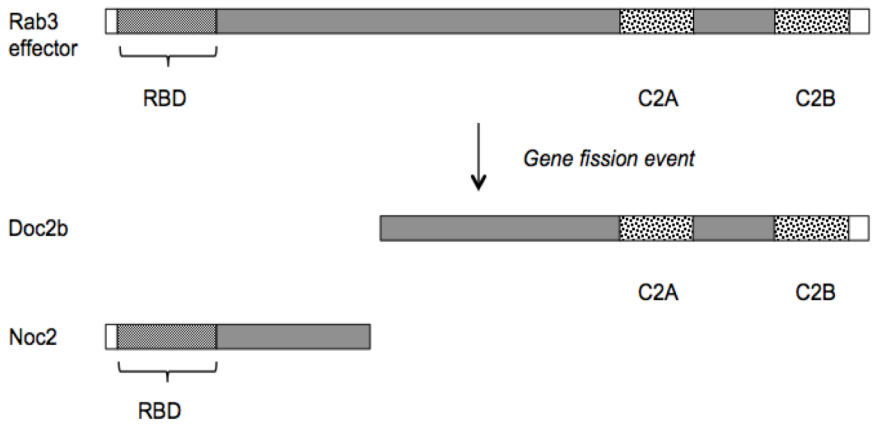

Figure 5.2: Relationship between Doc2b and Noc2. The locus for Doc2b in *Homo sapiens* is 17p13.3. At this very same locus, next to the Doc2b gene, the Rab3 effector Noc2 (Rph3al) is located. Noc2 contains the Rab binding domain (RBD) but it lacks the C2A and C2B domains that is present in most Rab3 effectors (reviewed in Cheviet et al., 2004). Doc2b lacks a RBD but contains the C2A and C2B domains and is well-characterised in GLUT4 traffic. There could have been an evolutionary gene fission event of a Rab3 effector resulting in two seprate genes, Noc2 and Doc2b. Doc2b has been well characterised in SNARE-mediated GLUT4 exocytosis and fusion. The link between Noc2 and Doc2b has not been explored before, nor has Noc2 been implicated in GLUT4 traffikcing.

5.1.5 Aims and rationale for the study

The identification of Rab3 as a candidate Rab in the GLUT4 trafficking pathway also opens the possibility to involvement of Rab3 effectors as regulators of GLUT4 trafficking. Noc2 is a Rab3 effector that shows close chromosomal proximity to a well-characterised GLUT4 vesicle regulating C2 domain protein, Doc2b. Noc2 has been shown to act in concert with Rab3 in regulating vesicle and granule exocytosis in neuronal tissues and pancreas. This makes Noc2 an interesting Rab3 effector to study in relation to GLUT4 exocytosis.

The aim of this chapter would be to investigate if Noc2 is present in adipocytes at the cellular level. The role of Noc2 in GLUT4 trafficking and a relationship with Rab3B will also be explored.

5.2 Results

5.2.1 Analysis of Noc2 expression in insulin-responsive tissues

A quantitative PCR (qPCR) study was designed to check if insulin-responsive tissues contained the putative Rab3 effector, Noc2. The results of the qPCR assay are shown in Fig. 5.3.

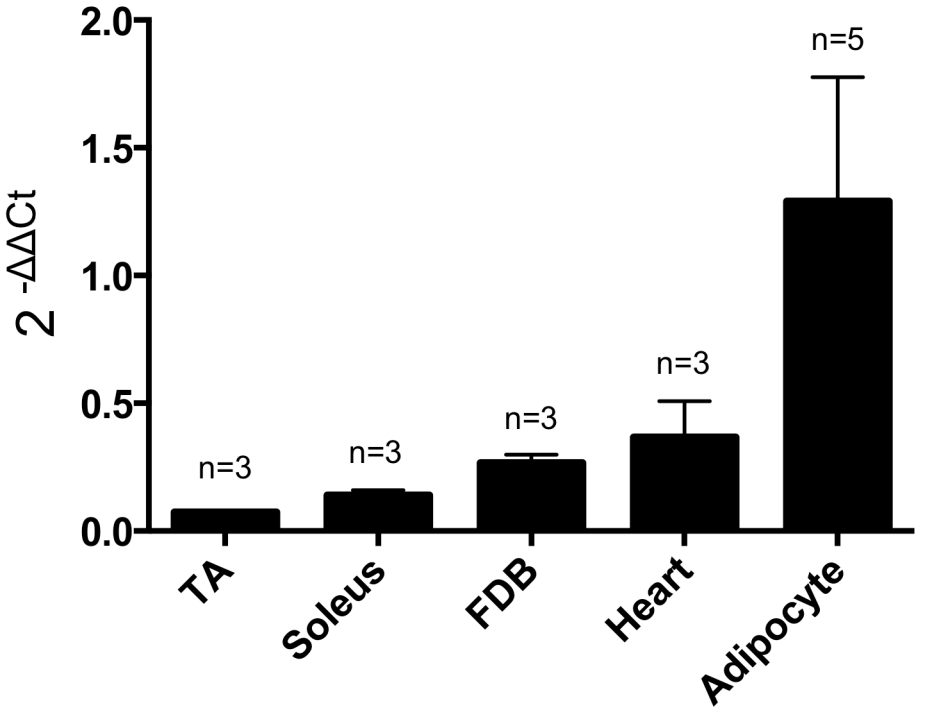

Figure 5.3: Analysis of Noc2 expression in insulin-responsive tissues. mRNA was extracted using the TRIzol®-chloroform method from insulin-responsive tissues belonging to *Rattus norvegicus*. cDNA was generated by reverse transcription. The primers used in this Noc2 study were first validated in rat testes prior to being used *(Supplementary figure S4B)*. The figure shows Noc2 gene expression normalised to the 28S rRNA housekeeping gene. Each bar represents an n of 3 or 5, from independent sets of tissues/rats. Error bars represent mean and SEM from 3 or 5 rats or independently isolated tissues.

The qPCR results demonstrate the variation in the levels of Noc2 across insulin-responsive tissues. Although the insulin-responsive tissues tested here show Noc2 expression, the levels were ~14 times lower in comparison to the cDNA tested for Noc2 expression in rat testes which can be considered as a control

(Supplementary figure S4). However, though the levels were low, it can be concluded that Noc2 is indeed expressed in insulin-responsive tissues and its role will need to be explored to characterise its effect on GLUT4 exocytosis.

Other Rab3 effectors were also screened in insulin-responsive tissues using a qPCR approach, but their levels were found to be well below Noc2 2 $^{-\Delta\Delta Ct}$ values (Supplementary figures S5A and S5B).

5.2.2 Generation of Noc2 constructs and a site-directed mutant

Noc2 contains an SGAWFY motif (conserved across Rab3 effectors) that is proposed to stably bind Rab3/27. Mutations can be made to this conserved motif by substituting amino acids tryptophan (W), phenylalanine (F) and tyrosine (Y) with alanine (A) residues. This generates an SGA**AAA** mutant (or Noc2 ^{AAA}). Noc2 ^{AAA} is incapable of binding to Rab3 or Rab27 (Handley and Burgoyne, 2008; Haynes, 2000).

Noc2 was amplified at 909 bp from adipocyte and heart cDNA *(from the cDNA extracted in Materials and Methods 2.2.2.3 protocol)*. The 909 bp Noc2 amplicon was cloned into the pHM6 mammalian expression vector. The pHM6-Noc2 plasmid was test digested to check for a correctly inserted Noc2 with *HindIII* and *NotI* restriction enzymes. These enzymes correctly recognised the respective restriction sites flanking the Noc2 cDNA (Fig. 5.4*B*). A Noc2 ^{AAA} mutant was generated from the Noc2 ^{WT} construct (Fig. 5.4*C*) using site-directed mutagenesis primers *(Supplementary table S1)*. The Noc2 ^{WT} and Noc2 ^{AAA} genes were subcloned into vectors pGEX-4T (a bacterial expression vector that would yield a GST-Noc2 fusion protein) and p3X-FLAGCMV ^{TM} -10 (Sigma-Aldrich) (a mammalian expression vector that would yield a FLAG-Noc2 fusion protein).

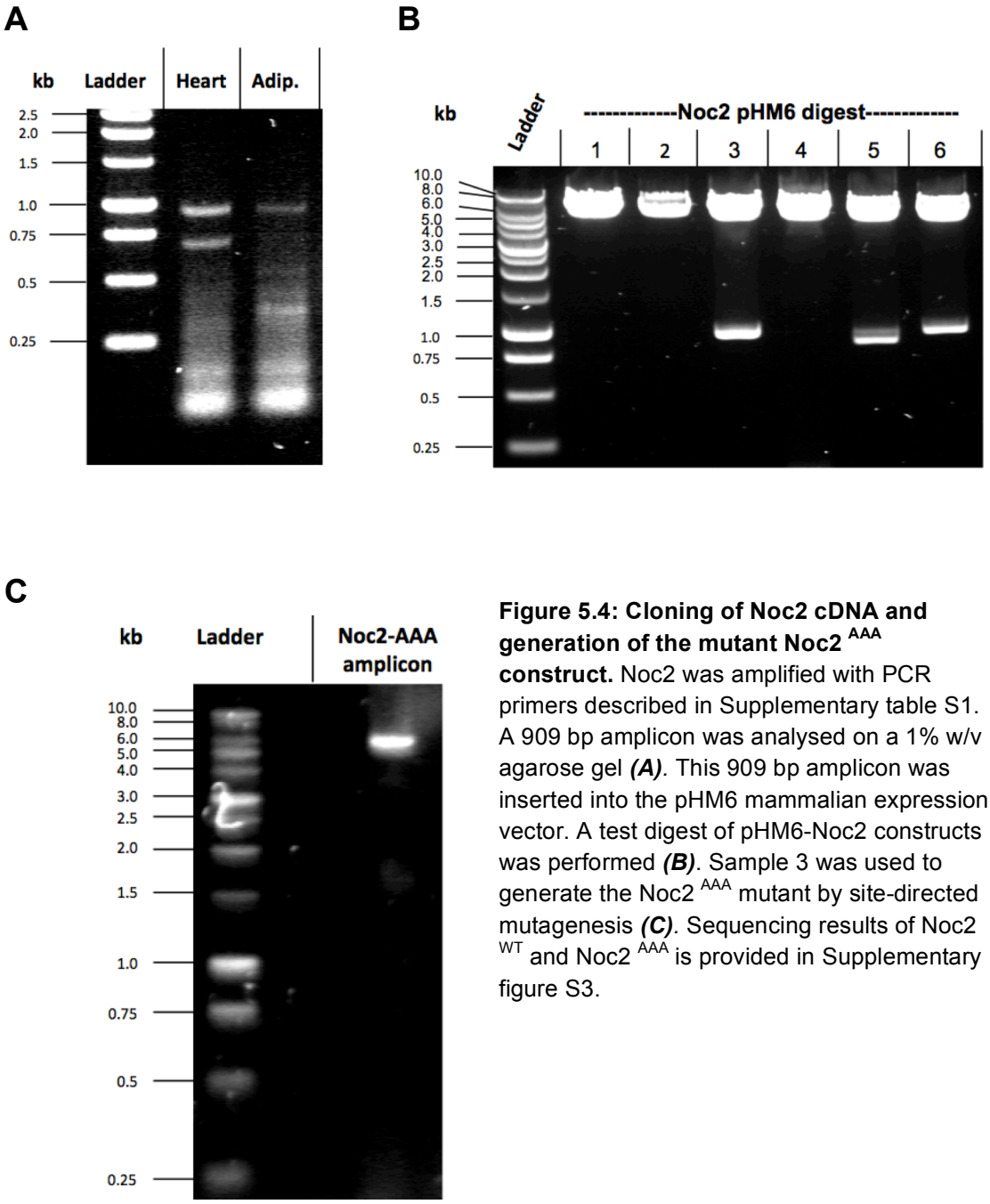

Figure 5.4: Cloning of Noc2 cDNA and generation of the mutant Noc2 ^{AAA} construct. Noc2 was amplified with PCR primers described in Supplementary table S1. A 909 bp amplicon was analysed on a 1% w/v agarose gel ***(A)***. This 909 bp amplicon was inserted into the pHM6 mammalian expression vector. A test digest of pHM6-Noc2 constructs was performed ***(B)***. Sample 3 was used to generate the Noc2 ^{AAA} mutant by site-directed mutagenesis ***(C)***. Sequencing results of Noc2 ^{WT} and Noc2 ^{AAA} is provided in Supplementary figure S3.

5.2.3 Expression and purification of the GST–Noc2 fusion protein

Fusion proteins are efficient tools for studying protein-protein interactions *in vitro*. In order to perform a pull-down of Noc2 to study the interaction of Noc2 with Rab3B, GST-Noc2 and GST-His-Noc2 constructs were prepared.

A

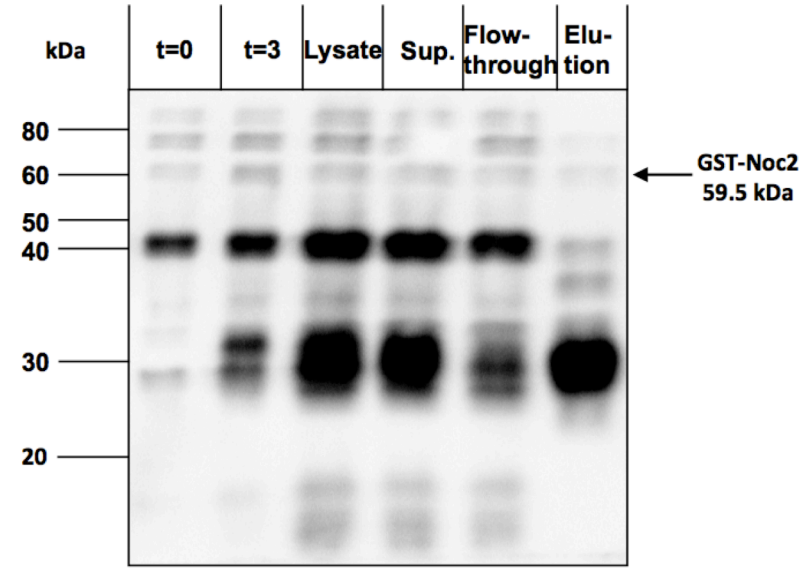
kDa
t=0
t=3
Lysate
Sup.
Flow-through
Elu-tion
80
60
50
40
30
20
GST-Noc2
59.5 kDa

B

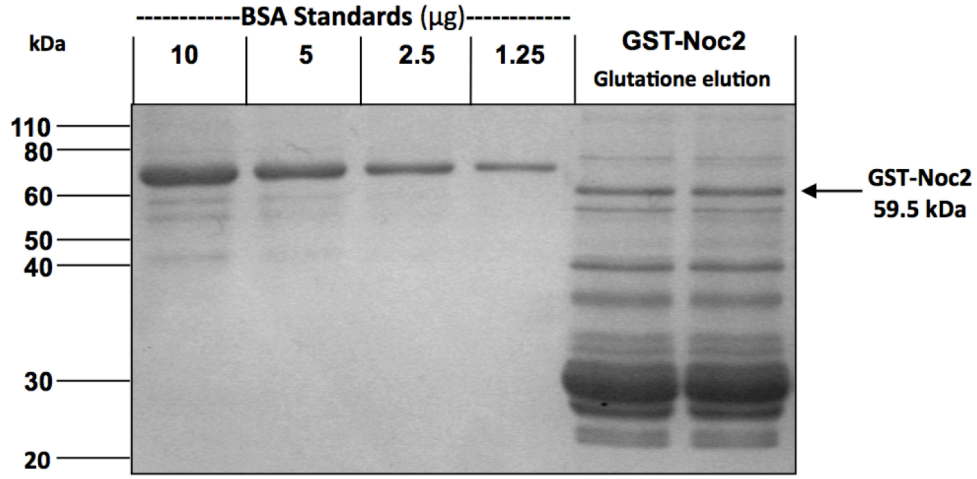
----------BSA Standards (µg)----------
kDa
10
5
2.5
1.25
GST-Noc2
Glutatione elution
110
80
60
50
40
30
20
GST-Noc2
59.5 kDa

C

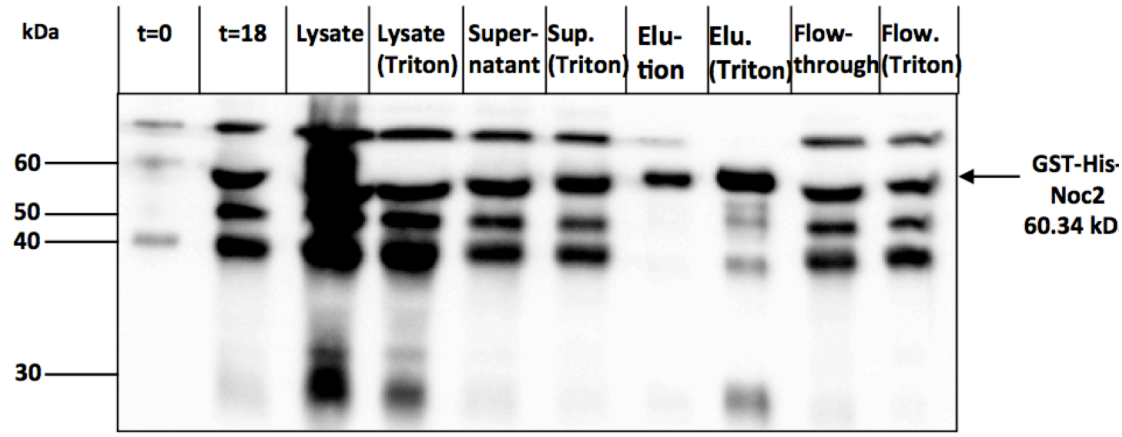
kDa
t=0
t=18
Lysate
Lysate (Triton)
Super-natant
Sup. (Triton)
Elu-tion
Elu. (Triton)
Flow-through
Flow. (Triton)
60
50
40
30
GST-His-Noc2
60.34 kD

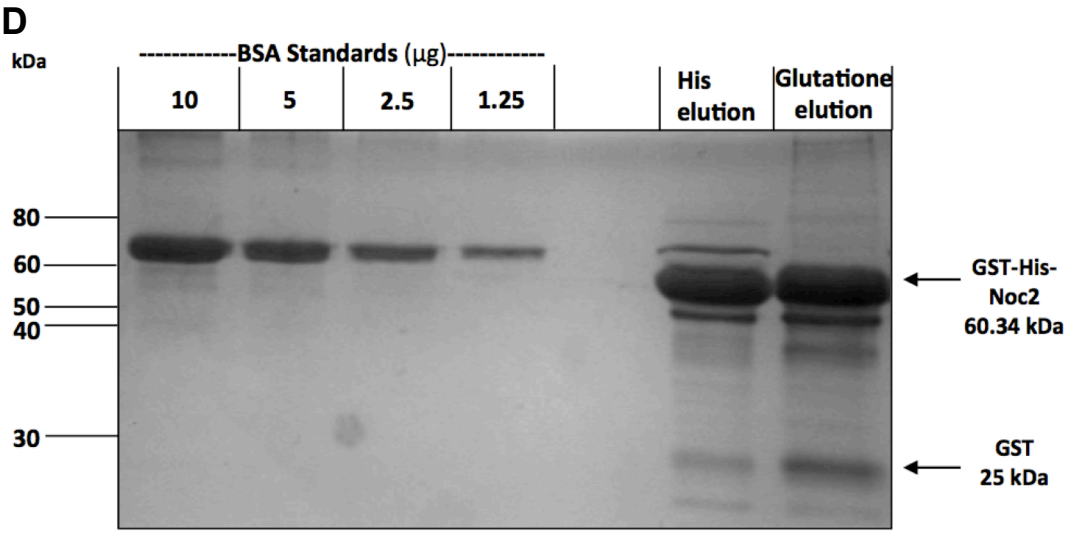

Figure 5.5: Noc2 protein expression. *E.coli* BL21 competent cells were transformed with the GST (or GST-His) tagged Noc2 vector. Induction was carried out with 0.5 mM IPTG and the culture was grown at 14°C overnight. Purification was carried out using glutathione beads. Expression and purification samples were run on a 12% SDS-PAGE gel.
(A) Expression of the (pGEX-4T) GST-Noc2 ^{WT} fusion protein with IPTG stimulation for 5 h at 37°C followed by purification on glutathione beads. Figure shows a western blot with anti-GST antibody.
(B) SDS-PAGE coomassie gel quantification of the purified GST-Noc2 ^{WT} from ***A***.
(C) Expression of the (pAT109) GST-His-Noc2 ^{WT} fusion protein with IPTG stimulation for 16 h at 12°C followed by purification on glutathione beads. Figure shows a western blot with anti-GST antibody.
(D) Coomassie gel quantification of the GST-His-Noc2 ^{WT} protein (from ***C***) following another round of purification on a HisTrap FF column. Figure shows elutions from His and glutathione purifications.

The (pGEX-4T) Noc2 construct was transformed into *E.coli* BL21 cells and expression followed by purification was carried out as described in *Materials and Methods 2.2.5.1*. Fig. 5.5*A* is representative of protein expression carried out at 37°C for 5 h. This expression using *E.coli* BL21 cells yielded 48 μg/ml of GST-Noc2 from 1.5 l of culture and mainly a GST degradation product (Fig. 5.5, *A* and *B*). This yield of protein was insufficient for experimental use. To increase the yield, the (pGEX-4T) Noc2 construct's expression in *E.coli* BL21 was induced with higher concentration of IPTG. 0.5 mM and 1 mM IPTG was used during expression of the GST-Noc2 protein, but the increase in IPTG concentration did not improve the yield of GST-Noc2. The (pGEX-4T) GST-Noc2 construct was then transformed into *E.coli* (Rosetta^{TM}(DE3)pLysS,

Lemo21(DE3) and ArcticExpress(DE3)) strains to obtain a better protein yield. Expression of (pGEX-4T) Noc2 in each strain was tested with different concentrations of IPTG (0.1, 0.3, 0.4 and 0.5 mM) and different expression times (3, 5 and 16 h). The *E.coli* ArcticExpress (DE3) cells gave a good yield of GST-Noc2 though there was still GST degradation at ~25 kDa. To further reduce GST degradation products, Noc2 was subcloned into a pAT109 vector. The pAT109 vector contained an N-terminal GST-tag and a C-terminal His-tag. This vector was used so that the Noc2 fusion protein could be purified using two different approaches. Fig. 5.5*C* shows the expression of the pAT109-Noc2 ^{WT} construct in the *E.coli* ArcticExpress(DE3) cells carried out at 14°C for 18 h. The *E.coli* ArcticExpress(DE3) cell pellet containing GST-His-Noc2 was split into two and each pellet was lysed separately with a different lysis buffer. One pellet was lysed with a lysis buffer containing 1% Triton X-100 while the other pellet was lysed without any Triton X-100. This was done to maximise chances of a pure protein and reduce degradation products. The two differently prepared bacterial lysates were purified using glutathione beads. The cell lysate that did not contain 1% Triton X-100 showed a more pure protein than the cell lysate that contained 1% Triton X-100 (Fig. 5.5*C*). The GST-His-Noc2 obtained from the lysis buffer containing no Triton X-100, was purified again on a HisTrap FF column (GE Healthcare). Fig. 5.5*D* shows a cleaner product with this new (GST-His) purification protocol yielding 530.4 μg/1.5 ml GST-His-Noc2 from 1.5 l of culture compared to 48 μg/ml of GST-Noc2 obtained with the previous protocol (Fig. 5.5*B*).

5.2.3.1 Purification of the GST-His-Noc2 using gel permeation chromatography (GPC)

To remove any residual GST from the preparation, the protein was further purified using gel permeation chromatography (GPC). The GST-His-Noc2 protein product was purified using a Superdex 200 10/300 GL column (GE Healthcare) to get a cleaner GST-His-Noc2 protein. The purified protein fractions were collected from the column (Fig. 5.6*A*) and run on a coomassie gel

(Fig. 5.6, *B* and *C*) to identify the positive GST-His-Noc2 product (or peak) from contaminant products.

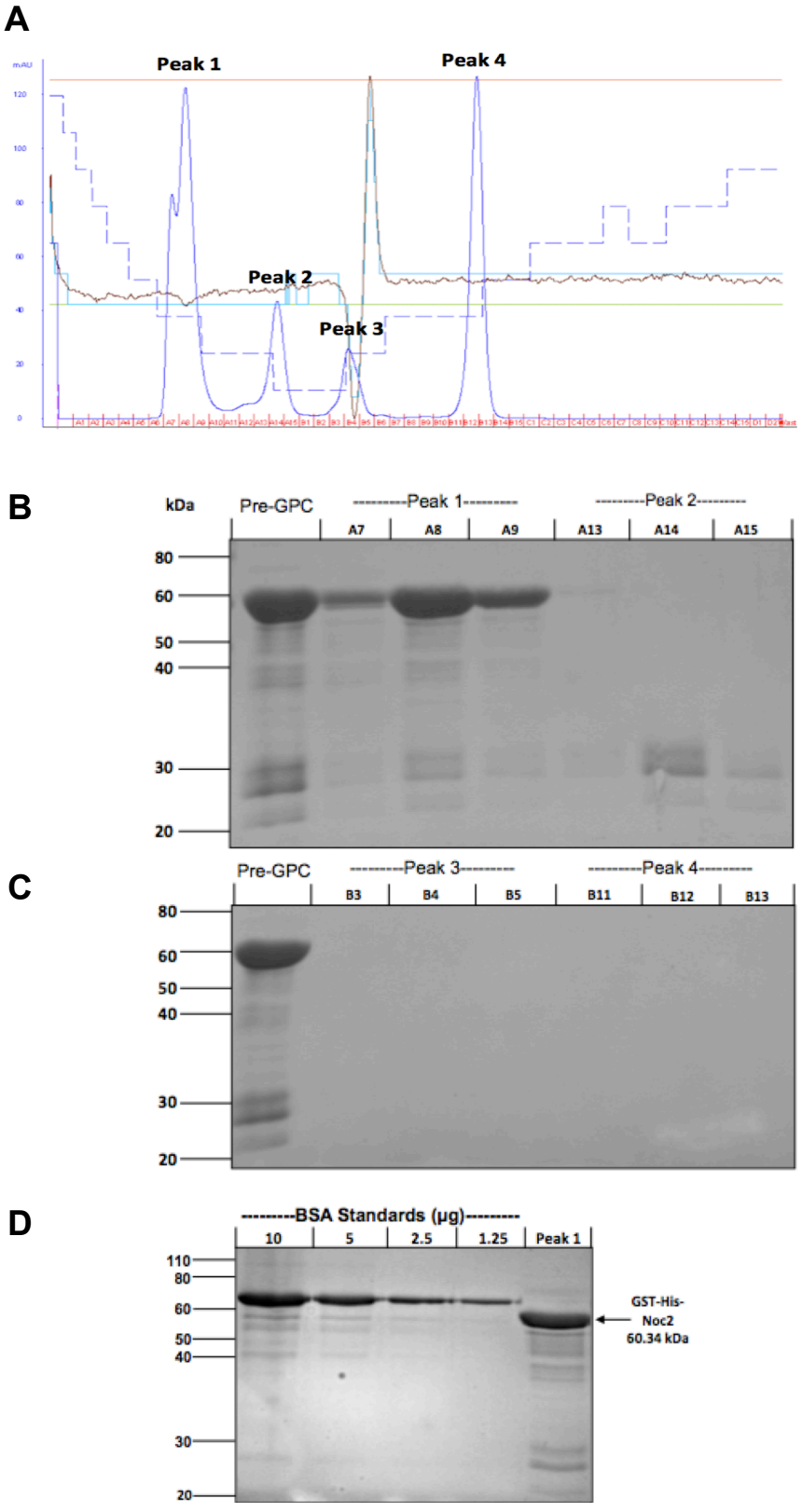

Figure 5.6: Gel permeation purification of GST-His-Noc2. A Superdex 200 10/300 GL column was washed with 20% ethanol and calibrated in a Tris-NaCl buffer. 3 ml of the GST-His-Noc2 protein was loaded onto the column and 1 ml fractions were collected ***(A)***. 20 μl of each of the fractions were run on a 12% SDS PAGE gel ***(B, C)***. The SDS-PAGE gel also contained the GST-His-Noc2 protein sample as a control (labelled as Pre-GPC in figure). Fractions were quantified on a 12% SDS-PAGE coomassie gel containing BSA standards ***(D)***.

The (Pre-GPC) control loaded in these gels (Fig. 5.6) comprised a small amount of the GST-His-Noc2 prior to purifying it on the GPC column. Purified fractions were compared to this Pre-GPC control. Fractions in Peak 1 showed the correct GST-His-Noc2 product. Fractions from Peak 1 were hence pooled together and quantified on a coomassie gel. The GST-His-Noc2 product was quantified to be 350 μg/ml of GST-His-Noc2 obtained from the 1.5 l culture (Fig. 5.6*D*). The yield obtained was of better concentration with less GST degradation products than previous purification attempts (Fig. 5.6*B*).

The GST-His-Noc2 ^{AAA} construct was prepared in exactly the same way as the GST-His-Noc2 ^{WT} (Fig 5.5 and 5.6). The GST-His-Noc2 constructs were used in an antibody-competition study for validating the Noc2 antibody *(see section 5.2.4)* and studying the interaction between Noc2 and Rab3B *(see section 5.2.7)*.

5.2.4 Validation of the Noc2 antibody

A commercial anti-Noc2 antibody was available to test rat adipocyte endogenous Noc2 at the protein level in rat adipocytes. The antibody was tested using western blots of rat adipocyte and heart lysates to check whether the Noc2 antibody could detect the endogenous Noc2 protein. Adipocyte and heart tissues are thought to contain Noc2 based on the qPCR data in Fig. 5.3. The results of the antibody test are shown in Fig. 5.7*A.* The commercial anti-Noc2 antibody detected the presence of a possible Noc2 band at 34.5 kDa. The 34.5 kDa band was 0.5 kDa more than the calculated size of the Noc2 protein, which is 34 kDa. The heart lysate showed 28.85-fold more Noc2 protein compared to the adipocyte lysate (Fig. 5.7*A*). To check if the band at 34.5 kDa was indeed

the Noc2 protein, the anti-Noc2 antibody was validated as follows. The GST-His-Noc2 protein was incubated with the Noc2 antibody overnight on a rotator at 4°C. After incubation of the anti-Noc2 antibody with the His-GST-Noc2 fusion protein, western blotting was performed on adipocyte and heart lysates with this antibody (Fig. 5.7*B*). The 34.5 kDa Noc2 band in the adipocyte lysate was reduced by 92.39% and that in the heart lysate was reduced by 83.96% when compared to their respective controls at 34.5 kDa in Fig. 5.7*A*.

This study demonstrates two crucial findings. First, the commercial anti-Noc2 antibody is able to detect the Noc2 protein in the insulin-responsive tissues tested. Second, the antibody confirms that Noc2 is present at the protein level in adipocyte and heart lysates and we can detect it at an expected size of 34.5 kDa using western blotting.

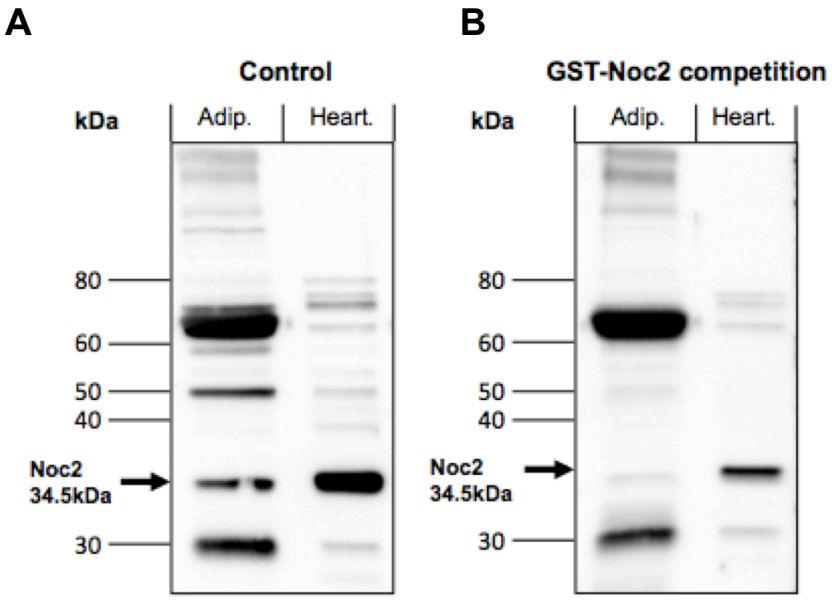

Figure 5.7: Competition assay for validating the Noc2 antibody. Adipose and heart tissues were lysed in lysis buffer (20 mM Tris-HCl pH 7.5, 150 mM NaCl, 1% Triton X-100 and protease inhibitors). 25 μg of the adipose lysate and 5 μg of the heart lysate were run on a 12% SDS-PAGE gel in duplicates and transferred to a nitrocellulose membrane. One nitrocellulose membrane was western-blotted directly with 0.0048 pmoles of the Noc2 antibody ***(A)***. The other membrane was western blotted with 0.0048 pmoles of the Noc2 antibody (which was first preincubated, with 0.24 pmoles (50 times more) of the His-GST-Noc2 fusion protein overnight at 4°C) ***(B)***. The potential Noc2 bands in the two western blots were quantified as a % decrease of the control Noc2 band in ***A***.

5.2.5 Localisation of Noc2 in adipocytes

Studying the cellular localisation of Noc2 may yield more information on its function. Preliminary studies were carried out by Dr F. Koumanov to identify the cellular location of endogenous Noc2 in adipocytes. Subcellular fractions of the plasma membrane and cytosol were western blotted with the Noc2 antibody. The findings (Fig. 5.8*A*) showed that Noc2 was present at the plasma membrane and to a lesser extent in the cytosol. In insulin-treated adipocytes, a significant 63% drop in Noc2 was observed at the plasma membrane when compared to the plasma membrane from basal adipocytes (Fig. 5.8*B*). These findings were further investigated by transfecting adipocytes with the HA-tagged Noc2 constructs to identify differences in subcellular localisation (if any) with the Noc2 ^{AAA} mutant construct.

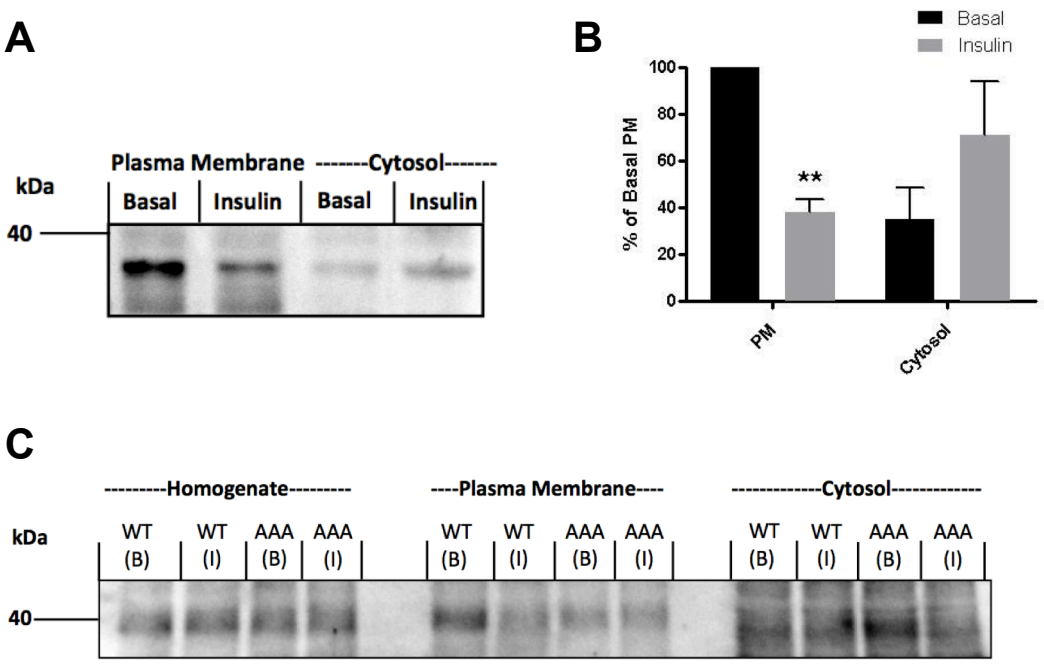

Figure 5.8: Western blots showing Noc2 localisation in adipocytes. Primary rat adipocytes were isolated and treated with insulin. Adipocytes were subfractionated in HES buffer to isolate the plasma membrane and cytosol. The plasma membrane and cytosol were run on a 12% SDS-PAGE gel and blotted with for Noc2 ***(A)***. Amount of Noc2 at the plasma membrane was quantified as a percentage of the basal plasma membrane and represents mean and SEM from 5 independent experiments. *p=<0.001 (paired two tailed t-test vs basal PM)***(B)***. Rat adipocytes with transfected HA-Noc2 ^{WT} or HA-Noc2 ^{AAA} and were maintained overnight at 37°C. On the next day, transfected adipocytes were insulin-treated and subfractionated. Western blot was performed with an anti-HA antibody ***(C)***. Noc2 is detected at ~34.5 kDa.

HA-Noc2 ^{WT} or HA-Noc2 ^{AAA} was transfected into rat adipocytes by electroporation and adipocytes were maintained overnight at 37°C. The next day, adipocytes were left untreated or insulin-stimulated, homogenised and subfractionated. The homogenate, plasma membrane and cytosolic fractions were western blotted. The blots were probed with an anti-HA antibody (Fig. 5.8*C*). Expression of the HA construct was low but fairly even across the Noc2 ^{WT} and Noc2 ^{AAA} samples as seen in the homogenate (Fig. 5.8*C*).

Quantification of Noc2 on western blots was performed using densitometry and LabWorks (UVP products). HA-Noc2 ^{WT} showed a 40.93% decrease at the plasma membrane in the insulin-treated adipocytes (Fig. 5.8*C*) corroborating the earlier study on endogenous Noc2 localisation (Fig 5.8, *A* and *B*). HA-Noc2 ^{AAA} showed no difference across basal and insulin plasma membrane samples and appeared to be at a baseline level (Fig. 5.8*C*). This may suggest that Noc2 ^{WT} could attach to the PM via a Rab, as the Noc2 ^{AAA} is deficient in Rab3/Rab27 binding. The functional relevance of Noc2 ^{WT} and Noc2 ^{AAA} to the GLUT4 trafficking process therefore seemed to warrant further investigation. Also, it was considered that interaction studies between Noc2 and Rab3B would shed more light on potential insulin dependence of the Noc2/Rab3 interaction in adipocytes.

5.2.6 Effect of Noc2 on GLUT4 translocation in adipocytes

Following the confirmation that Noc2 is present in adipocytes, an experimental approach was used to study Noc2's effect on GLUT4 translocation. An HA-GLUT4 translocation assay that was similar to that described in Chapter 4 *(section 4.2.3)* and other literature (Al-Hasani et al., 1998; Koumanov et al., 2012) was employed to study the effect of Noc2 in adipocytes. HA-GLUT4 alone or HA-GLUT4 and FLAG-Noc2 ^{WT} or FLAG-Noc2 ^{AAA} were electroporated into adipocytes and the adipocytes were maintained overnight under culture conditions. The next day, basal and insulin-stimulated adipocytes were assayed for surface HA-GLUT4. As seen in Fig. 5.9, there was an approximately 2.6-fold increase in the surface HA-GLUT4 in insulin-stimulated adipocytes containing only the HA-GLUT4 construct (which was the control). The level of increase in

cell surface HA-GLUT4 was similar in adipocytes transfected with the Noc2 ^{AAA} construct.

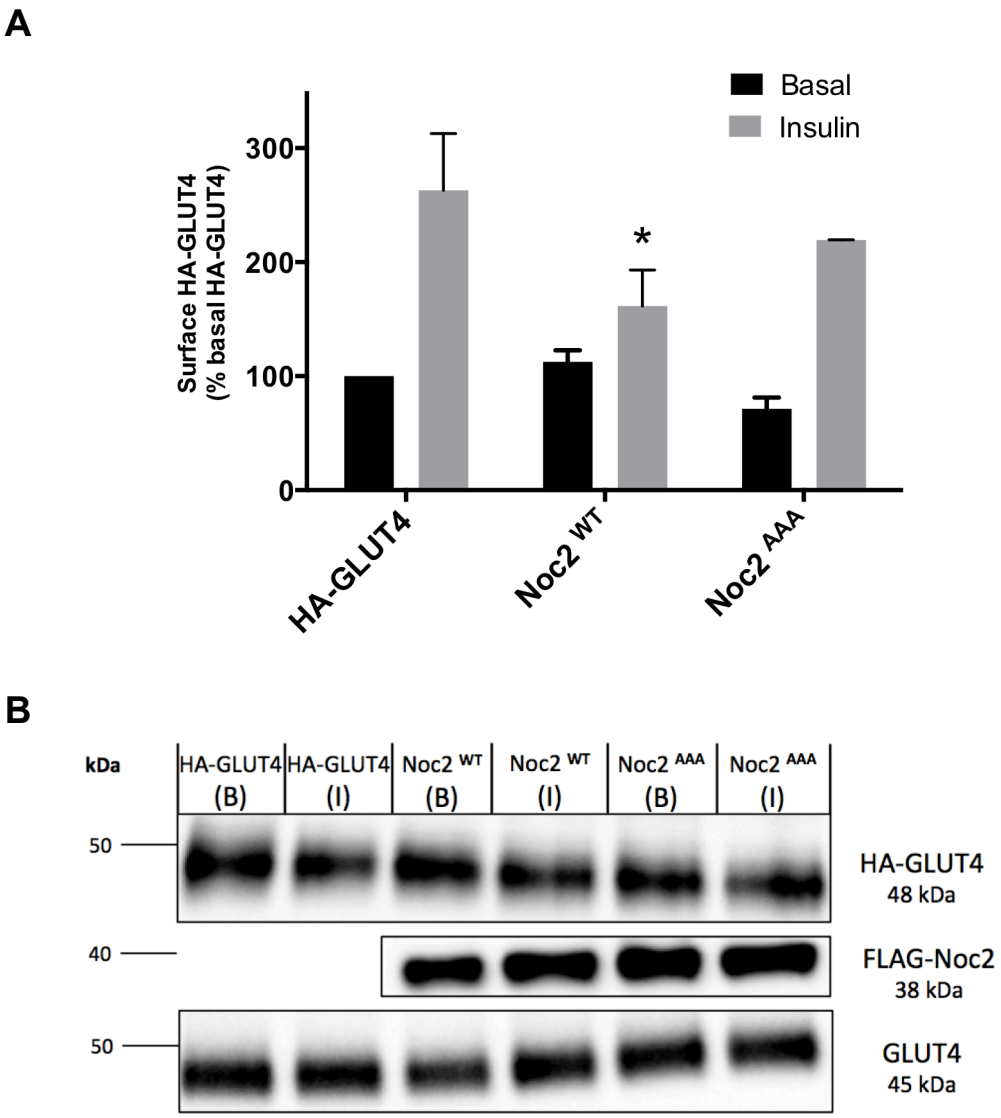

Figure 5.9: Noc2 decreases GLUT4 translocation in insulin-treated adipocytes. Primary rat adipocytes were isolated, transfected by electroporation with HA-GLUT4 or HA-GLUT4 and Noc2 ^{WT} or Noc2 ^{AAA}. The transfected adipocytes were maintained in culture overnight (for 16 h). On day 2, adipocytes were treated as basal or insulin. HA-GLUT4 at the cell surface was detected with an anti-HA antibody and β-galactosidase conjugated secondary antibody. The signal was measured with a fluorescent β-galactosidase substrate. Results are expressed as a percent of HA-GLUT4-Basal and represent mean and SEM from 4 independent experiments. * p=<0.05 (paired two tailed t-test vs HA-GLUT4-Insulin) ***(A)***. Western blots show expression of the transfected HA-GLUT4 and FLAG constructs and endogenous GLUT4 was blotted as a loading control ***(B)***.

However, insulin-stimulated adipocytes containing FLAG-Noc2 ^{WT} showed a significant decrease in the levels of HA-GLUT4 on the cell surface. The translocation assay data suggests that Noc2 ^{WT} overexpression directly or indirectly affects the amount of HA-GLUT4 translocated to the cell surface.

5.2.7 Noc2 pull-down of Rab3B from adipocytes

The results seen in Fig. 5.8 suggest that Noc2 is PM bound in the basal state and cytosolic in the insulin-stimulated state. An inability of the Rab binding deficient mutant (Noc2 ^{AAA}) to be detected at the plasma membrane in either basal/insulin-stimulated states (Fig. 5.8*C*) suggests that a Rab3 isoform might facilitate the Noc2-PM interaction. To study a Noc2-Rab3B interaction, a study was designed to pull-down Rab3B from lysates using GST/MBP-tagged Noc2.

In the study shown in Fig. 5.10*A*, His-GST-Noc2 ^{WT} immobilised on glutathione agarose beads, was used to pull-down FLAG-Rab3B from adipocyte lysates. The lysates were spiked with GTPγS to load Rab3B with guanine and convert it to its *'active'* form. The GST-His-Noc2 ^{AAA} mutant, defective in its Rab3 binding ability, did not pull-down any FLAG-Rab3B, confirming the Noc2 ^{AAA} construct's ineffectiveness in binding a Rab3, in this case Rab3B. The Noc2 ^{WT} protein was able to pull-down Rab3B (Fig. 5.10*A*).

The experiment was repeated using insulin-stimulated adipocytes to understand the effect of insulin on Noc2-Rab3B binding. The GTPγS spiked lysate was used as a positive control for the pull-down. The results obtained from this setup (Fig 5.10*B*) show a difference in amounts of FLAG-Rab3B detected in basal and insulin pull-downs on a western blot. The level of FLAG-Rab3B pulled-down by GST-His-Noc2 in the insulin samples was 65.10% lower than the basal samples (Fig. 5.10*C*). This indicated a lower affinity of Noc2 for Rab3B upon insulin stimulation. The results represent data from two individual experiments. Due to the limitations in expression of the His-GST-Noc2 construct and to obtain a statistically significant result (n=3), a new expression vector (pMAL-C2) was employed that would generate an MBP-tagged Noc2 protein.

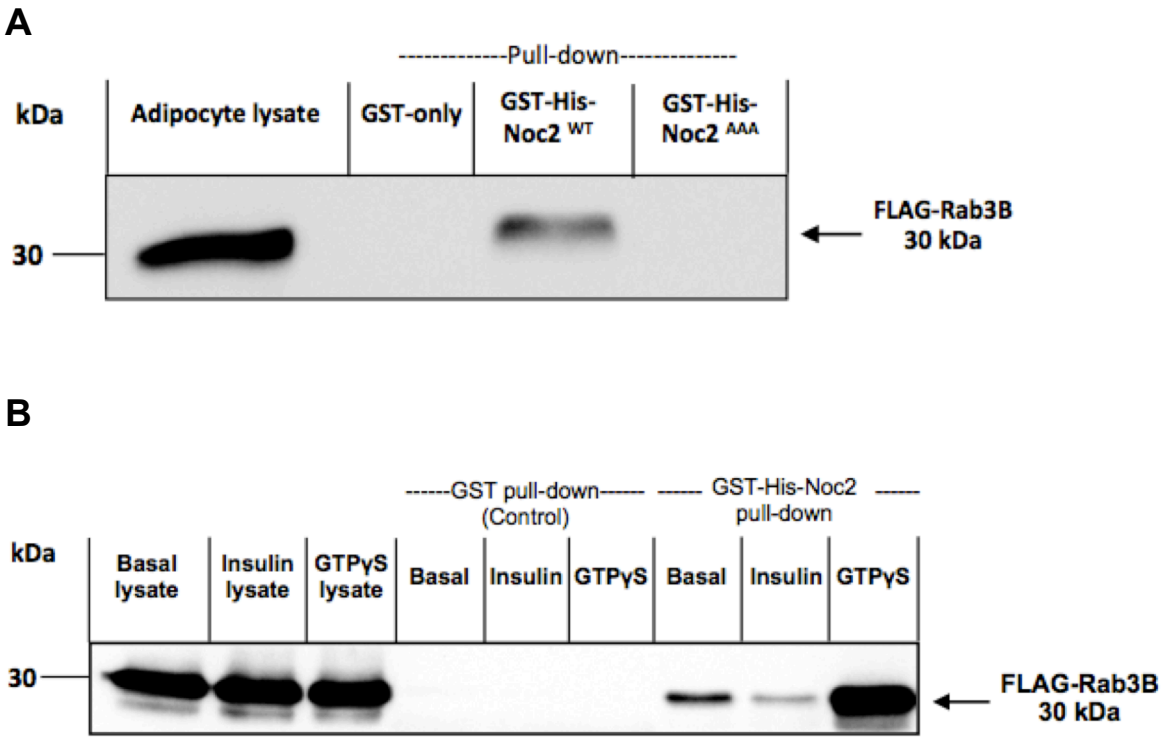

Figure 5.10: Pull-down of Rab3B from adipocytes using GST-His-Noc2. Primary rat adipocytes were transfected with FLAG-Rab3B and maintained overnight at 37°C. On the next day, adipocytes were treated as basal or stimulated with insulin and then lysed. An aliquot of the basal lysate was treated with 1 mM GTPγS. Glutathione conjugated agarose beads were pre-loaded with 25 μg GST or 50 μg His-GST-Noc2 ^{WT} or His-GST-Noc2 ^{AAA}. GST protein pre-loaded beads were incubated with the same concentrations of basal or insulin or GTPγS lysate at 4°C for 1 h. SDS sample buffer was added directly to the beads to elute the bound protein from the beads. Pull-down samples and pre pull-down lysate (controls) were run on a 12% SDS-PAGE gel and western blotted. The blot was probed for FLAG-Rab3B with an anti-FLAG antibody.
(***A)*** This figure shows Noc2 pull-down of FLAG-Rab3B from adipocyte lysates to which GTPγS had been added.
(B) This figure shows Noc2 pull-down of FLAG-Rab3B from adipocyte lysates from basal or insulin-treated or with GTPγS added to the lysate from basal cells.
(C) The graph demonstrates percentage values showing decrease in FLAG-Rab3B pull-down in insulin-treated sample ***(B)*** with respect to the basal. Error bar represents SD from two individual experiments (n=2).

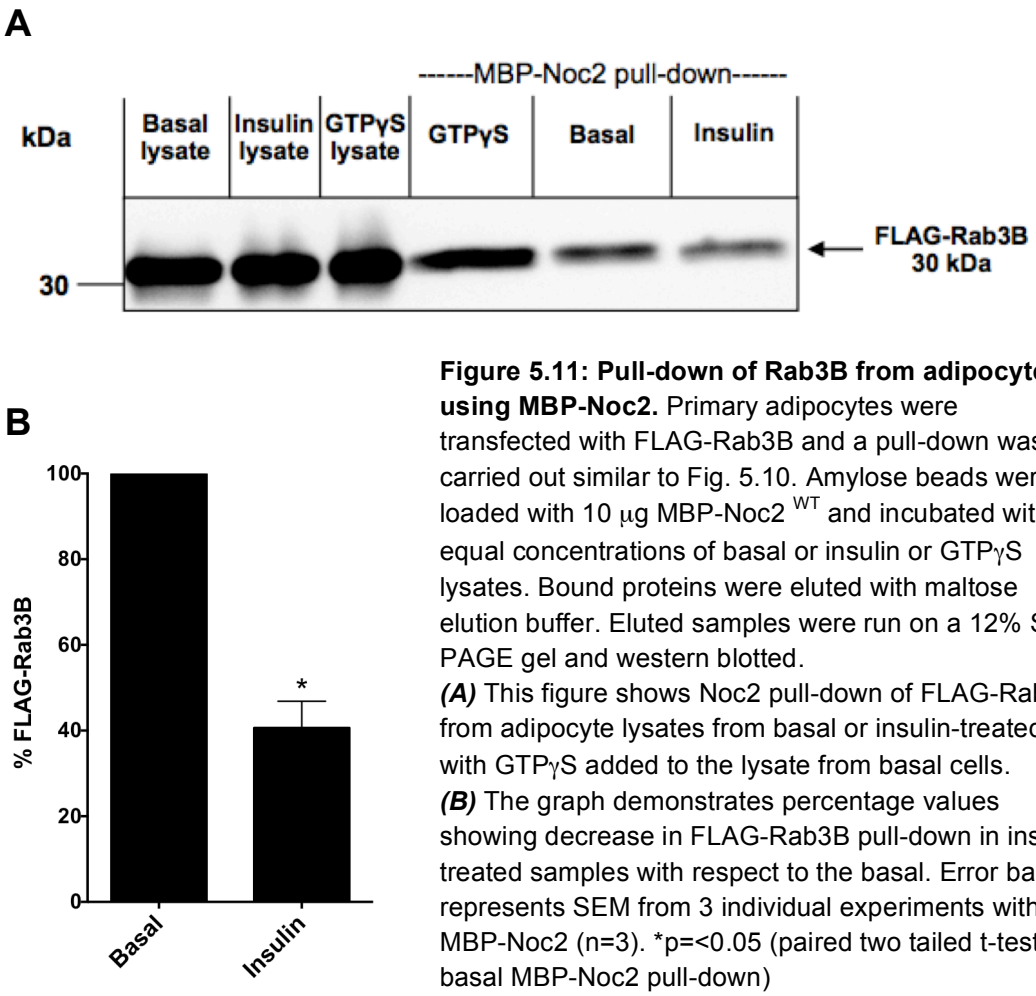

Figure 5.11: Pull-down of Rab3B from adipocytes using MBP-Noc2. Primary adipocytes were transfected with FLAG-Rab3B and a pull-down was carried out similar to Fig. 5.10. Amylose beads were loaded with 10 μg MBP-Noc2 ^{WT} and incubated with equal concentrations of basal or insulin or GTPγS lysates. Bound proteins were eluted with maltose elution buffer. Eluted samples were run on a 12% SDS-PAGE gel and western blotted.
(A) This figure shows Noc2 pull-down of FLAG-Rab3B from adipocyte lysates from basal or insulin-treated or with GTPγS added to the lysate from basal cells.
(B) The graph demonstrates percentage values showing decrease in FLAG-Rab3B pull-down in insulin-treated samples with respect to the basal. Error bar represents SEM from 3 individual experiments with MBP-Noc2 (n=3). *p=<0.05 (paired two tailed t-test *vs.* basal MBP-Noc2 pull-down)

A new vector that incorporated an MBP-tagged Noc2 construct was expressed and purified to yield an MBP-Noc2 fusion protein *(Supplementary figure S6)*. Pull-down of FLAG-Rab3B using the MBP-Noc2 construct (Fig. 5.11) showed similar results to the GST-Noc2 pull-down (Fig. 5.10). There was a basal-insulin difference in the amount of FLAG-Rab3B pulled-down (Fig. 5.11). The insulin samples showed a significant 59.39% decrease in FLAG-Rab3B pulled-down when compared to the basal samples (Fig 5.11*B*).

These pull-downs employed whole cell lysates and did not distinguish between the plasma membrane and cytosol. However, the idea that a Noc2-Rab3B interaction is lost in the insulin-stimulated state may hold true. This is due to the significant decrease in amount of Rab3B pulled-down by Noc2 in the insulin-stimulated state compared to basal state (Fig. 5.11*B*).

5.3 Discussion

The results in this chapter can be summarised with a few key findings. (1) Noc2 is present in adipocytes and is localised mainly to the plasma membrane in the basal state (Figs. 5.3 and 5.8). (2) Upon insulin stimulation, Noc2 levels at the plasma membrane significantly drop (Fig., 5.8 *A* and *B*). (3) Overexpression of Noc2 leads to a significant decrease in the levels of GLUT4 translocated to the plasma membrane (Fig. 5.9). (4) Insulin stimulation of adipocytes leads to less Rab3B binding to exogenous Noc2 as detected using a protein pull-down approach (Figs. 5.10 and 5.11).

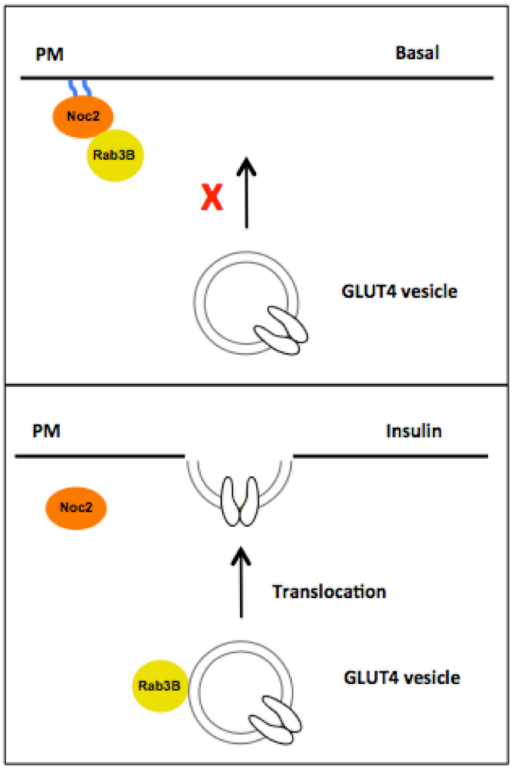

Figure 5.12: Summary of key findings. The findings in Chapter 4 implicated Rab3B ^{Q81L} as a positive regulator of GLUT4 translocation. The findings in this chapter suggest that in the basal state Noc2 is localised to the PM. Noc2 also binds more Rab3B in the basal state. Little to no PM localised Noc2 could be detected in the basal state when the (Rab3/Rab27-binding deficient) Noc2 ^{AAA} construct was overexpressed in adipocytes. Upon insulin-stimulation, Noc2 levels at the PM were reduced. Noc2-Rab3B interaction decreased when adipocytes were treated with insulin. Noc2 was also implicated as a negative regulator of GLUT4 translocation. These findings suggest that Noc2 may sequester Rab3B in the basal state and release it upon insulin-stimulation leading to GLUT4 translocation. It is unclear how Noc2 may be localised to the PM in the basal state and this is an area for further investigation. Additionally, it would be interesting to understand how the Noc2-PM interaction is lost upon insulin-stimulation.

Noc2 has been localised to membranes in pancreatic cells (Cheviet, 2003). Noc2 may also be located at the cell periphery to facilitate the final stages of membrane docking and fusion (Fukuda et al., 2004). However, the inability to detect Noc2^{AAA} at the PM (Fig. 5.8*C*) raises the possibility that Rab3 or Rab27 might be involved via an additional interacting protein (that anchors to the PM) and facilitates the basal Noc2^{WT} or endogenous Noc2 PM localisation (Fig. 5.8, *A* and *C*). Such a tripartite interaction (comprising Noc2-Rab3/27-PM anchoring protein, if it exists) would be devoid of any bound GLUT4 vesicle(s). Firstly, this is because Rab3B for instance associates with GLUT4 vesicles more in the insulin-stimulated state *(Koumanov et al., manuscript in preparation)*. Secondly, evidence that a Rab would likely need to be geranylgeranylated to anchor to a vesicle supports the idea that a 'Rab-bound vesicle' is unlikely to be present in a tripartite complex with Noc2 in the basal state at the PM. This could be the case, as geranylgeranylation of Rab3 at least, is thought to occur primarily upon insulin activation in studies using 3T3L1 adipocytes (Goalstone et al., 1999).

The study described in this chapter implicates Noc2 as a negative regulator of GLUT4 translocation (Fig. 5.9). Overexpression of Noc2 in pancreatic β-cells (Cheviet, 2003), neuroendocrine cells (Haynes, 2000) and epithelial cells (Manabe et al., 2004) leads to an inhibition of regulated exocytosis of vesicles or secretory granules. Granuphilin is another Rab3 effector that negatively affects regulated exocytosis of secretory granules in pancreas and neuroendocrine cells. A study by Handley and Burgoyne (2008) reported that Noc2 closely associates with the C2 domain containing effector granuphilin and this association may affect vesicle tethering/docking at the plasma membrane (Handley and Burgoyne, 2008). Granuphilin was hard to detect at the mRNA level in rat adipocytes using a qPCR approach *(Supplementary figure S5B)* and hence was not investigated at the protein level in the studies described in this thesis. A separate study in the Holman lab was able to detect granuphilin at the protein level in rat adipocyte lysates. Investigating granuphilin in rat adipocytes would hence be interesting as it may associate with Noc2 in regulating GLUT4 exocytosis via an exocytic Rab (such as Rab3).

Noc2 bound ~60% less Rab3B in a pull-down assay from insulin-stimulated adipocyte lysates than basal adipocyte lysates (Figs. 5.10 and 5.11). In ideal conditions, one would expect an insulin stimulus to cause Rab3B activation and lead to Rab3B being in the GTP-bound state, thereby binding more Noc2 presented as an exogenous protein in the pull-down assay (Fig. 5.10 and 5.11). But the data observed in this chapter shows less Rab3B being pulled-down by Noc2 following insulin-stimulation. It must however be noted that the Rab3B that was pulled-down by Noc2 as observed in Figs 5.10 and 5.11, could have been either in the GTP or the GDP-bound state. Noc2 is able to pull-down some of the *'inactive'* GDP form of Rab3B in the presence of the *'active'* GTP form of Rab3B from a lysate (Haynes, 2000; Matsumoto et al., 2004). Hence, in the observed results (Figs. 5.10 and 5.11) the Rab3B detected, as being bound to Noc2 could have been GDP-bound in basal conditions. In the insulin-stimulated state the decrease in Noc2-Rab3B binding can be attributed to the GTP-active Rab3B possibly binding to another Rab3B effector and this would need further investigation.

5.4 Conclusions

With only a limited number of published studies on Noc2, it is difficult to draw a conclusion on the functional aspects of this exocytic Rab effector. Based on the results described in this chapter, it is evident that Noc2 is insulin-responsive and does have an effect on GLUT4 translocation. Its interaction with Rab3B in adipocytes provides an insight into the involvement of exocytic Rabs and their effectors in regulating GLUT4 exocytosis to the plasma membrane.

It was earlier hypothesised that Noc2 and Doc2b might share an evolutionary relationship (Fig. 5.2). However, Doc2b is primarily implicated in translocation to the plasma membrane upon insulin stimulation and facilitates GLUT4 exocytosis, therefore Doc2b acts as a positive regulator (Fukuda et al., 2008b). Noc2 was shown to have the opposite effects to Doc2b in the study described in this chapter. If future studies show that Doc2b associates with Noc2 at the PM or at the subcellular level, it may open consideration of a more complex mechanism in regulation of GLUT4 traffic.

Published data on Noc2 have included competition studies with its cognate Rabs (3, 8A and 27). Some of this published data reports that Noc2 is predominantly a Rab27 effector (Fukuda et al., 2004; Handley and Burgoyne, 2008). Since Rab27 mRNA levels were found to be low (*Supplementary figure S5B)* and the protein was not detected on total membranes using the photolabelling approach *(Chapter 4, 4.1.3)*, Rab27 did not form a part of this study. Probing for Rab27 by western blotting adipocyte protein lysates may yield more information on its presence at the protein level. Rab8A is another Rab involved in GLUT4 translocation and could be a potential Noc2 interacting protein. If Rab27 is not detectable, a competition study in adipocytes between Noc2, Rab8A and Rab3 (A, B, D) could yield some important findings on the preferred Rab for Noc2. Further binding assays between Noc2 and cytoskeletal motors will help map the binding partners for Noc2 in adipocytes. Investigation of Noc2 (and its interacting proteins) will shed more light on the involvement of exocytic Rabs and their effectors in regulating GLUT4 exocytosis to the PM.

6 Final discussion and conclusion

6.1 Final discussion

The overall purpose of the studies described in this thesis was to identify novel proteins that facilitated GLUT4 trafficking in adipocytes. The work in this thesis identifies Rab3B and its effector Noc2 as novel regulators of GLUT4 trafficking. The model in Figure 6.1 illustrates some of the key findings in this thesis and the proposed role of Rab3B and Noc2 in regulating GLUT4 traffic to the plasma membrane. GLUT4 trafficking via the ESCRT pathway was also identified as a new route of GLUT4 trafficking.

A number of Rabs have been extensively characterised in neurotransmitter secreting cells as regulators of cellular development, neurite growth, cell polarisation and vesicle exocytosis (Ng and Tang, 2008). Rab3 has been particularly well characterised in the release of secretory vesicles in a Ca^{2+}-dependent manner and has also been implicated in synaptic vesicle fusion (Schluter, 2004). The involvement of a Rab3 family member in GLUT4 trafficking is suggested from consideration of the data described in this thesis. This involvement provides a mechanism for modulation of the GLUT4 transporter by a class of exocytic GTPases that are known to be involved primarily with secretory vesicles. Overexpression of the Rab3B ^{Q81L} constitutively active construct alone caused a significant increase in GLUT4 at the plasma membrane in basal conditions (Fig. 4.5). Overexpression of the dominant negative Rab3B ^{T36N} constructs showed a decreased basal-insulin response while Rab3B ^{WT} showed a normal basal-insulin response. Rab3 is hence active when it is bound to GTP (or mimicked by the Q81L mutation) (Brondyk et al., 1993). Rab3B's activation to the GTP bound form is triggered in rat adipocytes upon insulin stimulation *(Koumanov et al., manuscript in preparation)*. These results implicate activated Rab3B as a positive regulator of GLUT4 exocytosis.

Insulin signalling is shown to activate a number of Rabs in GLUT4 traffic. Rab10 has been particularly well studied as it is AS160-regulated and knockdown of

Rab10 attenuated GLUT4 translocation (Ng and Tang, 2008; Sano et al., 2007). However, the fact that the AS160-Rab10 system is only partly responsible for GLUT4 translocation (Park et al., 2012; Sadacca et al., 2013), allows consideration for other Rabs as likely candidates in this exocytic pathway. Rab3B is known to facilitate movement of fusion competent vesicles to the plasma membrane (Schonn et al., 2010; Vadlamudi et al., 2000). There is evidence that Rab3B colocalises with SNARE components, SNAP-25 and syntaxin in rat pituitary cells (Matsuno et al., 2003). Rab3 may also be recruited to recycling endosomes upon insulin-stimulation. Rab3B/Rab3C positive recycling compartments have been identified in dendritic cells (Zou et al., 2009). Hence, co-immunostaining of Rab3 with GLUT4 vesicle associating SNAREs, SNAP-23 and/or syntaxin-4 will yield information on Rab3B localisation in rat adipocytes.

The GSV localised Rab10, is regulated by an insulin sensitive GAP (AS160) and not its GEF (DENND4C) (Park et al., 2012; Sadacca et al., 2013; Sano et al., 2011). This finding suggests a possible route for Rab regulation in GLUT4 traffic via Rab GAPs. It would hence be useful to investigate if Rab3B is also regulated by an insulin-dependent GAP. AS160 was identified as an insulin-regulatable GAP for a number of Rabs in GLUT4 traffic (Mîinea et al., 2005; Vadlamudi et al., 2000). AS160 activated Rabs include Rab8A (Sano et al., 2007; Sun et al., 2010), Rab10 (Sadacca et al., 2013; Sano et al., 2007) and Rab14 (Ishikura et al., 2007; Schonn et al., 2010). Studies in muscle cells led to the conclusion that AS160 is not the only insulin-regulatable GAP in insulin-responsive tissues. TBC1D1 (a paralog of AS160) plays a similar role in muscle, in addition to AS160 (Sakamoto and Holman, 2008). Recently, TBC1D13 was identified as a Rab35 GAP in 3T3L1 adipocytes (Davey et al., 2012). Could rat adipocytes harbour a specific GAP for Rab3? A GAP called Rab3-GAP is specific to the Rab3 family, which makes it an ideal study candidate (Fukui et al., 1997). Functional studies on Rab3-GAP suggest that it may be involved in the homeostatic control of Rab3-mediated vesicle release by competing with Rab3 effectors such as Rabphilin-3A or Noc2 (Clabecq et al., 2000; Müller et al., 2011). Studies on synaptic transmission confirm that Rab3 is directly regulated by the Rab3-GAP in synaptic vesicle release (Müller et al., 2011; Sakane et al., 2006). The Rab3-GAP can be identified in rat adipocytes by using quantitative PCR and an antibody can be

used for studying it at the protein level using adipocyte lysates. Alternatively, a TBC domain library can also be screened for a Rab3 GAP using a yeast two-hybrid (Y2H) system (Itoh et al., 2006).

The data described in this thesis showed that Noc2 bound >50% more Rab3B in the basal state than in the insulin-stimulated state. Noc2 hence could be sequestering any free Rab3B until insulin stimulation, following which it releases Rab3B to facilitate GLUT4 translocation to the plasma membrane. It is plausible that Noc2 sequesters Rab3B-GDP in the basal state and this sequestration may encompass a close association with another Rab3 effector, granuphilin. Granuphilin in fact negatively regulates exocytosis (Coppola et al., 2002) and does so by interacting with the GDP-bound form of another exocytic Rab, Rab27 (Fukuda, 2003). Though granuphilin levels were fairly low in the qPCR study *(Supplementary figure S5B)*, it could be detected at the protein level in rat adipocytes (unpublished data). Functional studies on granuphilin could provide more information on its role if any in GLUT4 trafficking.

The dissociation of Noc2 from the plasma membrane in insulin-stimulated rat adipocytes described in this thesis may be explained by an interaction between an SM (Sec1/Munc18-like) protein and Noc2. The SM protein in adipocytes is Munc18c (also known as Munc18-3). Munc18c could be responsible for sequestering Noc2 in the basal state at the plasma membrane and releasing it upon insulin stimulation, at which point Noc2 becomes cytosolic. The role of Munc18c in GLUT4 trafficking is to regulate the SNARE dependent fusion process. Munc18c is known to sequester the SNARE associating protein, syntaxin-4, in an insulin-dependent manner, preventing syntaxin-4 interacting with VAMP2 thereby decreasing GLUT4 vesicle docking/fusion (Thurmond et al., 1998; Thurmond et al., 2000). Noc2 has not been shown to interact with Munc18c or any SM protein as such; an interaction with Munc18c in relation to GLUT4 trafficking will be novel. Interestingly, another SM protein, Munc18-1 has been shown to interact with the Rab3/Rab27 effector granuphilin and Rab27 to mediate exocytosis (Gomi et al., 2005; Tsuboi and Fukuda, 2006). The ability of SM proteins to interact with exocytic Rabs and their effectors make them strong candidates to further explore Rab3-mediated GLUT4 trafficking.

Rabs are known to facilitate vesicle movement via the cell cytoskeleton. Myosin-5A was characterised as a Rab10 partner in GLUT4 vesicle delivery to the plasma membrane in 3T3-L1 adipocytes (Chen et al., 2012). Myosin-5A is a well-known Rab27 associating protein that transports melanosomes along actin filaments (Hume et al., 2001). Movement of myosins along the actin cytoskeleton is facilitated by myosin ATPase activity, or by calcium influx in a calmodulin dependent fashion (Holman and Sakamoto, 2008). The trigger of ATPase activity and calcium influx could well be mediated by insulin (Leto and Saltiel, 2012; Yip et al., 2008). A recent study showed that Rab3 family members too can interact with Myosin-5A (Lindsay et al., 2013) and hence a Rab3-Myosin-5A interaction in GLUT4 traffic is plausible in rat adipocytes.

Vesicle trafficking involves coordination with a number of signalling molecules. Insulin signalling in particular requires a constant supply of lipid secondary messengers called phosphoinositides. Hence, there is bound to be some overlap between Rabs and phosphoinositides along routinely trafficking vesicles. However, the overlap between the two does seem to be more than more than just a mere coexistence of these molecules on the same vesicles. It has been found that some Rabs and phosphoinositides share the same effector molecules as well. This crosstalk or coincidence detection between Rabs and phosphoinositides could be useful in uncovering potential Rab effectors (Jean and Kiger, 2012). A common example is that of Rab5 and PI 3K, which together regulate PtdIns(3)P levels *(described in Introduction 1.5.7)*. Insulin activates Rab5 by recruiting a GEF and this leads to Rab5 being GTP-bound. It is this Rab5, activated in this manner by its GEF, that that was shown to regulate PtdIns(3)P production (Lodhi et al., 2008). PtdIns(3)P, together with Rab5, facilitates endosomal maturation (Lawe et al., 2002). Another Rab3 effector, Rabphilin-3A, binds to PtdIns(4,5)P_2 via its C2 domains and this interaction could help accurate targeting of Rabphilin-3A to membranes/vesicles along the actin cytoskeleton (Montaville et al., 2008). Similarly, the Rab3 effector, granuphilin has C2 domains that show an affinity for PM lipids PtdIns(4,5)P_2 and PtdIns(3,4,5)P_3. These lipids are likely to assist in granuphilin insertion at the PM (Lyakhova and Knight, 2013). Rabs, effectors and phosphoinositides hence

coordinate in membrane recognition and studying them together may add to the larger picture of homeostatic regulation of trafficking at the subcellular level (Jean and Kiger, 2012).

The study in this thesis also demonstrated GLUT4 trafficking through an ESCRT-III-dependent sorting compartment. This finding leads to questions that concern the amount of GLUT4 that may be degraded via the ESCRT endocytic pathway in comparison to the amount that may actually be recycled back to the plasma membrane or to GLUT4 storage/reserve pools. Could ubiquitin-related, GLUT4 associating proteins such as Ubc9 and TUG be recruited to an ESCRT-GLUT4 compartment? Ubc9 is shown to be a regulator of turnover in GLUT4 storage pools (Liu et al., 2007). TUG is a tether that can be cleaved off from GLUT4, facilitating GLUT4 translocation to the plasma membrane (Bogan et al., 2012b). Ubc9/TUG may direct GLUT4 to reserve/storage pools such that the necessary Rabs and/or priming/fusion markers (like VAMP2) can be recruited to recycle GLUT4 back to the plasma membrane.

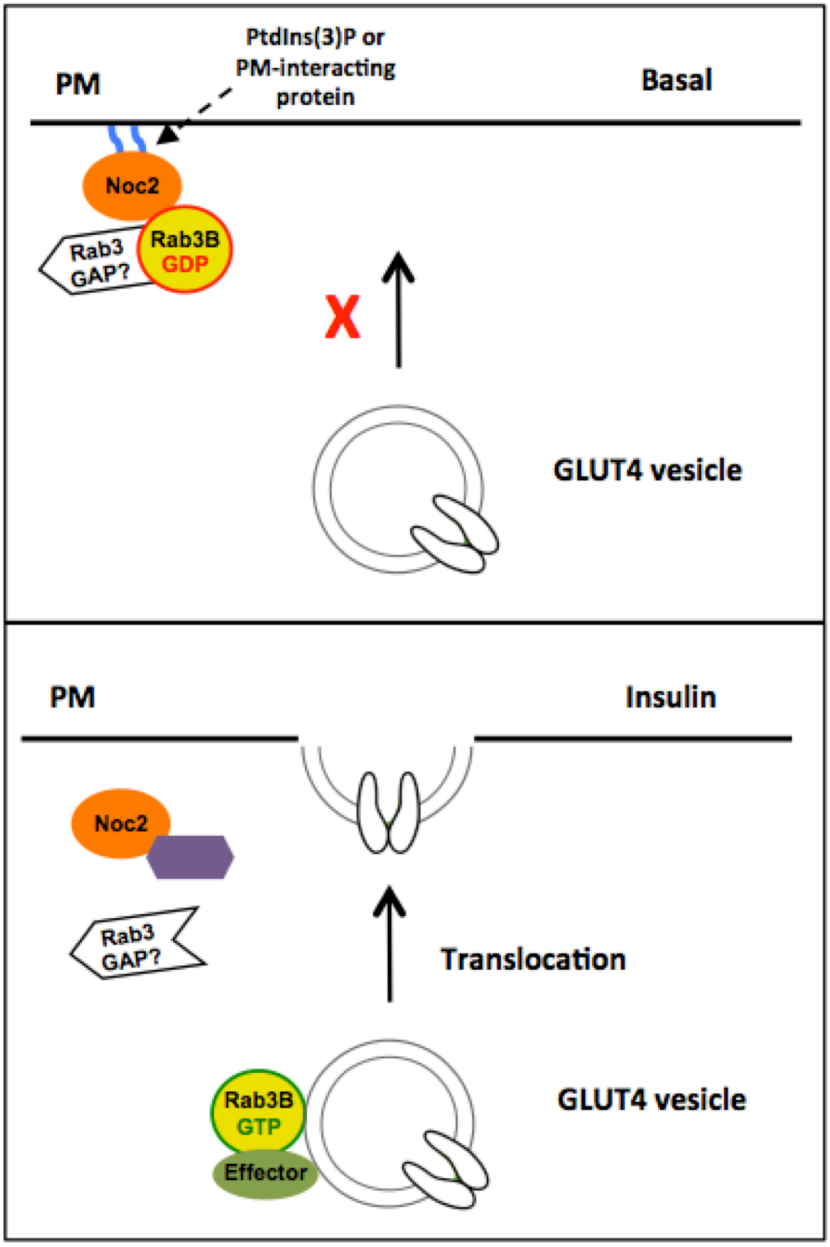

Figure 6.1: Proposed mode of action of Noc2 in regulating GLUT4 trafficking in adipocytes. Noc2 contains a zinc finger FYVE-related domain and this domain is known to interact with PtdIns(3)P (reviewed in Stenmark and Aasland, 1999). In the basal state, Noc2 may be anchored to the PM by a phosphoinositide or another PM-interacting protein. Rab3B is possibly bound to Noc2 at the PM. Rab3-GAP could be a GAP that maintains Rab3B in the inactive GDP-bound state. A Noc2-Rab3B complex may contribute to Noc2 overexpression showing a decrease in GLUT4 translocation *(Fig. 5.9)*. Insulin stimulation causes Noc2 removal from the PM *(Fig. 5.8)* and a cytosolic protein may sequester Noc2. Rab3B is GTP-loaded upon insulin stimulation and binds to GLUT4 vesicles facilitating GLUT4 trafficking *(manuscript in prep. and Fig. 4.5)*. Rabs work in concert with effectors to facilitate vesicle trafficking. A currently yet unidentified Rab3 effector may be involved in GLUT4 vesicle exocytosis upon insulin stimulation.

6.2 Final conclusions

GLUT4 trafficking is a dynamic process. Different interacting proteins are recruited at distinct stages of GLUT4 vesicle transport. The studies on Rabs have gained momentum in recent years. This interest in Rabs is due to their ability to mediate GLUT4 trafficking and ultimately affect the rate of glucose transport into insulin-responsive tissues. Chapters 4 and 5 in this thesis described the examination of the role of Rab3B and its effector Noc2 in regulating GLUT4 exocytosis. To understand whether Rab3 or Noc2 participates in the final stages of GLUT4 translocation, we would need to understand whether vesicle fusion proteins interact with Rab3 or Noc2. This would entail protein-protein interaction studies (such as pull-down assays) between Rab3 or Noc2 and plasma membrane phospholipid-binding proteins (such as C2-domain containing proteins) that facilitate or constitute SNARE-mediated vesicle fusion. Alternatively, to mimic conditions in a cell *in vitro*, a coflotation assay can be used described previously by Yu et al. (2013) that showed an interaction between Doc2b and the SNARE complex. In this assay, SNARE components are reconstituted into liposomes and can be incubated with a Rab or its effector; the incubation is followed by density gradient centrifugation. The protein that interacts with the SNARE liposome, complexes with it and is detected at the top of the gradient (Yu et al., 2013).

The data in Chapter 3 of this thesis showed that the ESCRT pathway is involved in regulating GLUT4 trafficking. A further examination of the fate of endocytosed GLUT4 will be required as an important part of the further understanding of the GLUT4 trafficking process. GLUT4 is known to sort to storage/reserve/recycling pools or undergo retrograde trafficking to the plasma membrane via the TGN. Consideration of how this retrograde trafficking system fits within the ESCRT pathway and which proteins ‘route’ GLUT4 away from a degradative fate will lead to a more detailed endocytic GLUT4 trafficking map. Deubiquitinases (or DUBs) are good candidate proteins that should be considered for further investigation. Studies could investigate how GLUT4 degradation can be prevented such that

more GLUT4 is available for recycling and for replenishing GLUT4 that has become depleted at the plasma membrane.

Future work will hence focus on identifying novel proteins that are activated upon insulin stimulation. In order to identify interacting proteins in the ESCRT system or to identify Rab effectors, the yeast two-hybrid (Y2H) system is a good tool that could be employed. The Y2H system can be explored by utilising a rat adipocyte library to screen for effectors of currently identified Rabs (3B, 4, 5, 8A, 10, 11, 13, 14, 31, 35) involved in GLUT4 traffic or to identify novel binding partners of GLUT4 in the ESCRT pathway. The known Rab or ESCRT component called the 'bait' protein can be inserted in a yeast vector and screened against an adipocyte library of 'prey' proteins to identify which proteins interact with the bait. Clontech's Matchmaker® Gold Y2H system is one of the commercially available tools that uses mating between a haploid yeast bait strain and a haploid yeast library strain to produce a diploid yeast cell yielding a bait-prey interaction. The Matchmaker® system can be used to identify as well as confirm novel protein-protein interactions by using different amino acid selection media. Proteins identified by the Y2H method, or an alternative approach, can be studied to see if they ultimately affect GLUT4 trafficking to the PM. Monitoring of GLUT4 trafficking to the PM can be accomplished using either the HA-GLUT4 translocation assay described in this thesis or alternatively an assay that utilises a fluorescent pH sensitive probe attached to GLUT4 vesicles. The probe called pHluorin (Miesenböck et al., 1998) is attached to IRAP on the GLUT4 vesicle and produces fluorescence when the acidic lumen of the vesicle fuses with the plasma membrane and is exposed to a neutral environment. Such a pH sensitive probe could be used to study GLUT4 vesicle fusion with the plasma membrane as well. Changes in fluorescence at the plasma membrane could be monitored by total internal reflection fluorescence microscopy (Chen et al., 2012; Jiang et al., 2008).

7 References

Agromayor, M. M. and Martin-Serrano, J. J. (2006). Interaction of AMSH with ESCRT-III and deubiquitination of endosomal cargo. *J. Biol. Chem.* **281,** 23083–23091.

Al-Hasani, H., Hinck, C. S. and Cushman, S. W. (1998). Endocytosis of the glucose transporter GLUT4 is mediated by the GTPase dynamin. *J. Biol. Chem.* **273**, 17504–17510.

Alessi, D. R., James, S. R., Downes, C. P., Holmes, A. B., Gaffney, P. R., Reese, C. B., Cohen, P. (1997). Characterization of a 3-phosphoinositide-dependent protein kinase which phosphorylates and activates protein kinase Balpha. *Curr. Biol.* **7,** 261–269.

Alexandrov, K., Horiuchi, H., Steele-Mortimer, O., Seabra, M. C. and Zerial, M. (1994). Rab escort protein-1 is a multifunctional protein that accompanies newly prenylated rab proteins to their target membranes. *EMBO J.* **13,** 5262–5273.

Ali, B. R., Wasmeier, C., Lamoreux, L., Strom, M. and Seabra, M. C. (2004). Multiple regions contribute to membrane targeting of Rab GTPases. *J. Cell Sci.* **117,** 6401–6412.

Allan, B. B., Moyer, B. D. and Balch, W. E. (2000). Rab1 recruitment of p115 into a cis-SNARE complex: programming budding COPII vesicles for fusion. *Science* **289,** 444–448.

Antonescu, C. N., Díaz, M., Femia, G., Planas, J. V. and Klip, A. (2008). Clathrin-dependent and independent endocytosis of glucose transporter 4 (GLUT4) in myoblasts: regulation by mitochondrial uncoupling. *Traffic* **9**, 1173–1190.

Aran, V., Bryant, N. J. and Gould, G. W. (2011). Tyrosine phosphorylation of Munc18c on residue 521 abrogates binding to Syntaxin 4. *BMC Biochem.* **12,** 19.

Arimura, N., Kimura, T., Nakamuta, S., Taya, S., Funahashi, Y., Hattori, A., Shimada, A., Ménager, C., Kawabata, S., Fujii, K., et al. (2009). Anterograde transport of TrkB in axons is mediated by direct interaction with Slp1 and Rab27. *Dev. Cell* **16**, 675–686.

Augustin, R. (2010). The protein family of glucose transport facilitators: It's not only about glucose after all. *IUBMB life* **62**, 315–333.

Babst, M. M., Sato, T. K. T., Banta, L. M. L. and Emr, S. D. S. (1997). Endosomal transport function in yeast requires a novel AAA-type ATPase, Vps4p. *EMBO J.* **16**, 1820–1831.

Babst, M., Katzmann, D. J., Estepa-Sabal, E. J., Meerloo, T. and Emr, S. D.

(2002a). Escrt-III - An endosome-associated heterooligomeric protein complex required for mvb sorting. *Dev. Cell* **3**, 12–12.

Babst, M., Katzmann, D. J., Snyder, W. B., Wendland, B. and Emr, S. D. (2002b). Endosome-associated complex, ESCRT-II, recruits transport machinery for protein sorting at the multivesicular body. *Dev. Cell* **3**, 283–289.

Bakke, J., Bettaieb, A., Nagata, N., Matsuo, K. and Haj, F. G. (2013). Regulation of the SNARE-interacting protein Munc18c tyrosine phosphorylation in adipocytes by protein-tyrosine phosphatase 1B. *Cell Commun. Signal* **11**, 57.

Baldini, G., Hohl, T., Lin, H. Y. and Lodish, H. F. (1992). Cloning of a Rab3 isotype predominantly expressed in adipocytes. *Proc. Natl. Acad. Sci. U.S.A.* **89**, 5049–5052.

Baldini, G., Scherer, P. E. and Lodish, H. F. (1995). Nonneuronal expression of Rab3A: induction during adipogenesis and association with different intracellular membranes than Rab3D. *Proc. Natl. Acad. Sci. U.S.A.* **92**, 4284–4288.

Baltensperger, K., Lewis, R. E., Woon, C. W., Vissavajjhala, P., Ross, A. H. and Czech, M. P. (1992). Catalysis of serine and tyrosine autophosphorylation by the human insulin receptor. *Proc. Natl. Acad. Sci. U.S.A.* **89**, 7885–7889.

Bandyopadhyay, G., Standaert, M. L., Kikkawa, U., Ono, Y., Moscat, J. and Farese, R. V. (1999). Effects of transiently expressed atypical (zeta, lambda), conventional (alpha, beta) and novel (delta, epsilon) protein kinase C isoforms on insulin-stimulated translocation of epitope-tagged GLUT4 glucose transporters in rat adipocytes: specific interchangeable effects of protein kinases C-zeta and C-lambda. *Biochem. J.* **337 (3)**, 461–470.

Barbour, L. A., Shao, J., Qiao, L., Leitner, W., Anderson, M., Friedman, J. E. and Draznin, B. (2004). Human placental growth hormone increases expression of the p85 regulatory unit of phosphatidylinositol 3-kinase and triggers severe insulin resistance in skeletal muscle. *Endocrinology* **145**, 1144–1150.

Barr, F. and Lambright, D. G. (2010). Rab GEFs and GAPs. *Curr. Opin. Cell Biol.* **22**, 461–470.

Baskys, A., Bayazitov, I., Zhu, E., Fang, L. and Wang, R. (2007). Rab-mediated endocytosis: linking neurodegeneration, neuroprotection, and synaptic plasticity? *Ann. N. Y. Acad. Sci.* **1122**, 313–329.

Behnia, R. and Munro, S. (2005). Organelle identity and the signposts for membrane traffic. *Nature* **438**, 597–604.

Bertani, G. (2004). Lysogeny at mid-twentieth century: P1, P2, and other experimental systems. *J. Bacteriol.* **186**, 595–600.

Berwick, D. C. D., Dell, G. C. G., Welsh, G. I. G., Heesom, K. J. K., Hers, I. I., Fletcher, L. M. L., Cooke, F. T. F. and Tavaré, J. M. J. (2004). Protein kinase B phosphorylation of PIKfyve regulates the trafficking of GLUT4 vesicles. *J. Cell Sci.*

117, 5985–5993.

Bilodeau, P. S., Urbanowski, J. L., Winistorfer, S. C. and Piper, R. C. (2002). The Vps27p Hse1p complex binds ubiquitin and mediates endosomal protein sorting. *Nat. Cell Biol.* **4**, 534–539.

Blot, V. and McGraw, T. E. (2006). GLUT4 is internalized by a cholesterol-dependent nystatin-sensitive mechanism inhibited by insulin. *EMBO J.* **25**, 5648–5658.

Blot, V. and McGraw, T. E. (2008). Molecular mechanisms controlling GLUT4 intracellular retention. *Mol. Biol. Cell* **19**, 3477–3487.

Blümer, J., Rey, J., Dehmelt, L., Mazel, T., Wu, Y. W., Bastiaens, P., Goody, R. S. and Itzen, A. (2013). RabGEFs are a major determinant for specific Rab membrane targeting. *J. Cell Biol.* **200**, 287–300.

Bock, J. B., Matern, H. T., Peden, A. A. and Scheller, R. H. (2001). A genomic perspective on membrane compartment organization. *Nature* **409**, 839–841.

Bogan, J. S. (2012a). Regulation of Glucose Transporter Translocation in Health and Diabetes. *Annu. Rev. Biochem.* **81**, 507–532.

Bogan, J. S., Hendon, N., McKee, A. E., Tsao, T.-S. and Lodish, H. F. (2003). Functional cloning of TUG as a regulator of GLUT4 glucose transporter trafficking. *Nature* **425**, 727–733.

Bogan, J. S., Rubin, B. R., Yu, C., Löffler, M. G., Orme, C. M., Belman, J. P., McNally, L. J., Hao, M. and Cresswell, J. A. (2012b). Endoproteolytic cleavage of TUG protein regulates GLUT4 glucose transporter translocation. *J. Biol. Chem.* **287**, 23932–23947.

Boguslavsky, S., Chiu, T., Foley, K. P., Osorio-Fuentealba, C., Antonescu, C. N., Bayer, K. U., Bilan, P. J. and Klip, A. (2012). Myo1c binding to submembrane actin mediates insulin-induced tethering of GLUT4 vesicles. *Mol. Biol. Cell* **23**, 4065–4078.

Bornhorst J. A., Falke J. A., (2000). Purification of Proteins Using Polyhistidine Affinity Tags. *Meth. Enzymol.* **326**, 245.

Bose, A., Robida, S., Furcinitti, P. S., Chawla, A., Fogarty, K., Corvera, S. and Czech, M. P. (2004). Unconventional myosin Myo1c promotes membrane fusion in a regulated exocytic pathway. *Mol. Cell Biol.* **24**, 5447–5458.

Brondyk, W. H., McKiernan, C. J., Burstein, E. S. and Macara, I. G. (1993). Mutants of Rab3A analogous to oncogenic Ras mutants. Sensitivity to Rab3A-GTPase activating protein and Rab3A-guanine nucleotide releasing factor. *J. Biol. Chem.* **268**, 9410–9415.

Brozinick, J. T., McCoid, S. C., Reynolds, T. H., Nardone, N. A., Hargrove, D. M., Stevenson, R. W., Cushman, S. W. and Gibbs, E. M. (2001). GLUT4 Overexpression in db/db Mice Dose-Dependently Ameliorates Diabetes But Is Not

a Lifelong Cure. *Diabetes* **50**, 593–600.

Bruss, M. D., Arias, E. B., Lienhard, G. E. and Cartee, G. D. (2005). Increased Phosphorylation of Akt Substrate of 160 kDa (AS160) in Rat Skeletal Muscle in Response to Insulin or Contractile Activity. *Diabetes* **54**, 41–50.

Buchanan, T. A., Xiang, A. H., Peters, R. K., Kjos, S. L., Marroquin, A., Goico, J., Ochoa, C., Tan, S., Berkowitz, K., Hodis, H. N., et al. (2002). Preservation of pancreatic beta-cell function and prevention of type 2 diabetes by pharmacological treatment of insulin resistance in high-risk hispanic women. *Diabetes* **51**, 2796–2803.

Cai, H., Reinisch, K. and Ferro-Novick, S. (2007). Coats, Tethers, Rabs, and SNAREs Work Together to Mediate the Intracellular Destination of a Transport Vesicle. *Dev. Cell* **12**, 671–682.

Carpenter, C. L., Duckworth, B. C., Auger, K. R., Cohen, B., Schaffhausen, B. S. and Cantley, L. C. (1990). Purification and characterization of phosphoinositide 3-kinase from rat liver. *J. Biol. Chem.* **265**, 19704–19711.

Chavrier, P., Parton, R. G., Hauri, H. P., Simons, K. and Zerial, M. (1990). Localization of low molecular weight GTP binding proteins to exocytic and endocytic compartments. *Cell* **62**, 317–329.

Cheatham, B., Vlahos, C. J., Cheatham, L., Wang, L., Blenis, J. and Kahn, C. R. (1994). Phosphatidylinositol 3-kinase activation is required for insulin stimulation of pp70 S6 kinase, DNA synthesis, and glucose transporter translocation. *Mol. Cell Biol.* **14**, 4902–4911.

Cheatham, B., Volchuk, A., Kahn, C. R., Wang, L., Rhodes, C. J. and Klip, A. (1996). Insulin-stimulated translocation of GLUT4 glucose transporters requires SNARE-complex proteins. *Proc. Natl. Acad. Sci. U.S.A.* **93**, 15169–15173.

Chen, X. W., Leto, D., Chiang, S. H., Wang, Q. and Saltiel, A. R. (2007). Activation of RalA Is Required for Insulin-Stimulated Glut4 Trafficking to the Plasma Membrane via the Exocyst and the Motor Protein Myo1c. *Dev. Cell* **13**, 391–404.

Chen, Y. and Lippincott-Schwartz, J. (2013). Insulin triggers surface-directed trafficking of sequestered GLUT4 storage vesicles marked by Rab10. *smallgtpases* **4**, 193–197.

Chen, Y. and Lippincott-Schwartz, J. (2013). Rab10 delivers GLUT4 storage vesicles to the plasma membrane. *Commun. Integr. Biol.* **6**, e23779.

Chen, Y., Wang, Y., Zhang, J., Deng, Y., Jiang, L., Song, E., Wu, X. S., Hammer, J. A., Xu, T. and Lippincott-Schwartz, J. (2012). Rab10 and myosin-Va mediate insulin-stimulated GLUT4 storage vesicle translocation in adipocytes. *J. Cell Biol.* **198**, 545–560.

Cheviet, S. (2003). The Rab-Binding Protein Noc2 Is Associated with Insulin-

Containing Secretory Granules and Is Essential for Pancreatic -Cell Exocytosis. *Mol. Endocrinol.* **18**, 117–126.

Cheviet, S., Waselle, L. and Regazzi, R. (2004). Noc-king out exocrine and endocrine secretion. *Trends Cell Biol.* **14**, 525–528.

Christoforidis, S., Miaczynska, M., Ashman, K., Wilm, M., Zhao, L., Yip, S. C., Waterfield, M. D., Backer, J. M. and Zerial, M. (1999). Phosphatidylinositol-3-OH kinases are Rab5 effectors. *Nat. Cell Biol.* **1**, 249–252.

Christoforidis, S. and Zerial, M. (2000). Purification and identification of novel Rab effectors using affinity chromatography. *Methods* **20**, 403–410.

Chua, C. E. L., Lim, Y. S. and Tang, B. L. (2010). Rab35 – A vesicular traffic-regulating small GTPase with actin modulating roles. *FEBS LETT.* **584**, 1–6.

Chung, L. T. K., Hosaka, T., Harada, N., Jambaldorj, B., Fukunaga, K., Nishiwaki, Y., Teshigawara, K., Sakai, T., Nakaya, Y. and Funaki, M. (2010). Myosin IIA participates in docking of Glut4 storage vesicles with the plasma membrane in 3T3-L1 adipocytes. *Biochem. Bioph. Res. Co.* **391**, 995–999.

Clabecq, A., Henry, J. P. and Darchen, F. (2000). Biochemical characterization of Rab3-GTPase-activating protein reveals a mechanism similar to that of Ras-GAP. *J. Biol. Chem.* **275**, 31786–31791.

Clague, M. J. and Urbé, S. (2006). Endocytosis: the DUB version. *Trends Cell Biol.* **16**, 551–559.

Clarke, J. F., Young, P. W., Yonezawa, K., Kasuga, M. and Holman, G. D. (1994). Inhibition of the translocation of GLUT1 and GLUT4 in 3T3-L1 cells by the phosphatidylinositol 3-kinase inhibitor, wortmannin. *Biochem. J.* **300 (Pt 3)**, 631–635.

Cooke, F. T. (2002). Phosphatidylinositol 3,5-bisphosphate: metabolism and function. *Arch. Biochem. Biophys.* **407**, 143–151.

Coppola, T., Frantz, C., Perret-Menoud, V., Gattesco, S., Hirling, H. and Regazzi, R. (2002). Pancreatic beta-cell protein granuphilin binds Rab3 and Munc-18 and controls exocytosis. *Mol. Biol. Cell* **13**, 1906–1915.

Coppola, T., Magnin-Luthi, S., Perret-Menoud, V., Gattesco, S., Schiavo, G. and Regazzi, R. (2001). Direct interaction of the Rab3 effector RIM with Ca^{2+} channels, SNAP-25, and synaptotagmin. *J. Biol. Chem.* **276**, 32756–32762.

Cormont, M., Bortoluzzi, M. N., Gautier, N., Mari, M., van Obberghen, E. and Le Marchand-Brustel, Y. (1996). Potential role of Rab4 in the regulation of subcellular localization of Glut4 in adipocytes. *Mol. Cell Biol.* **16**, 6879–6886.

Cormont, M., Tanti, J. F., Zahraoui, A., van Obberghen, E., Tavitian, A. and Le Marchand-Brustel, Y. (1993). Insulin and okadaic acid induce Rab4 redistribution in adipocytes. *J. Biol. Chem.* **268**, 19491–19497.

Coster, A. C. F., Govers, R. and James, D. E. (2004). Insulin stimulates the entry of GLUT4 into the endosomal recycling pathway by a quantal mechanism. *Traffic* **5**, 763–771.

Cozier, G. E., Carlton, J., McGregor, A. H., Gleeson, P. A., Teasdale, B. D., Mellor, H. and Cullen, P. J. (2002). The Phox Homology (PX) domain-dependent, 3-phosphoinositide-mediated association of sorting nexin-1 with an early sorting endosomal compartment is required for its ability to regulate epidermal growth factor receptor degradation. *J. Biol. Chem.* **277**, 48730–48736.

Cushman, S. W. and Wardzala, L. J. (1980). Potential mechanism of insulin action on glucose transport in the isolated rat adipose cell. Apparent translocation of intracellular transport systems to the plasma membrane. *J. Biol. Chem.* **255**, 4758–4762.

Dash, S., Sano, H., Rochford, J. J., Semple, R. K., Yeo, G., Hyden, C. S. S., Soos, M. A., Clark, J., Rodin, A., Langenberg, C., et al. (2009). A truncation mutation in TBC1D4 in a family with acanthosis nigricans and postprandial hyperinsulinemia. *Proc. Natl. Acad. Sci. U.S.A* **106**, 9350–9355.

Davey, J. R. J., Humphrey, S. J. S., Junutula, J. R. J., Mishra, A. K. A., Lambright, D. G. D., James, D. E. D. and Stöckli, J. J. (2012). TBC1D13 is a RAB35 specific GAP that plays an important role in GLUT4 trafficking in adipocytes. *Traffic* **13**, 1429–1441.

Deák, F., Shin, O. H., Tang, J., Hanson, P., Ubach, J., Jahn, R., Rizo, J., Kavalali, E. T. and Südhof, T. C. (2006). Rabphilin regulates SNARE-dependent re-priming of synaptic vesicles for fusion. *EMBO J.* **25**, 2856–2866.

Delicado, E. G., Torres, M. and Miras-Portugal, M. T. (1988). Glucose transporters in chromaffin cells: subcellular distribution and characterization. *FEBS LETT.* **229**, 35–39.

Delprato, A. and Lambright, D. G. (2007). Structural basis for Rab GTPase activation by VPS9 domain exchange factors. *Nat. Struct. Mol. Biol.* **14**, 406–412.

Deng, D., Xu, C., Sun, P., Wu, J., Yan, C., Hu, M. and Yan, N. (2014). Crystal structure of the human glucose transporter GLUT1. *Nature* **510**, 121–125.

Díaz, E. and Pfeffer, S. R. (1998). TIP47: a cargo selection device for mannose 6-phosphate receptor trafficking. *Cell* **93**, 433–443.

Dong, X.-P., Shen, D., Wang, X., Dawson, T., Li, X., Zhang, Q., Cheng, X., Zhang, Y., Weisman, L. S., Delling, M., et al. (2010). PI(3,5)P2 controls membrane trafficking by direct activation of mucolipin Ca^{2+} release channels in the endolysosome. *Nat. Comms.* **1**, 1–11.

Doussau, F., Clabecq, A., Henry, J. P., Darchen, F. and Poulain, B. (1998). Calcium-dependent regulation of rab3 in short-term plasticity. *J. Neurosci.* **18**, 3147–3157.

Draznin, B. (2006). Molecular mechanisms of insulin resistance: serine

phosphorylation of insulin receptor substrate-1 and increased expression of p85alpha: the two sides of a coin. *Diabetes* **55**, 2392–2397.

Dukes, J. D., Fish, L., Richardson, J. D., Blaikley, E., Burns, S., Caunt, C. J., Chalmers, A. D. and Whitley, P. R. (2011). Functional ESCRT machinery is required for constitutive recycling of claudin-1 and maintenance of polarity in vertebrate epithelial cells. *Mol. Biol. Cell* **22**, 3192–3205.

Dukes, J. D., Richardson, J. D., Simmons, R. and Whitley, P. (2008). A dominant-negative ESCRT-III protein perturbs cytokinesis and trafficking to lysosomes. *Biochem. J.* **411**, 233.

Dulubova, I., Lou, X., Lu, J., Huryeva, I., Alam, A., Schneggenburger, R., Südhof, T. C. and Rizo, J. (2005). A Munc13/RIM/Rab3 tripartite complex: from priming to plasticity? *EMBO J.* **24**, 2839–2850.

Dumas, J. J., Zhu, Z., Connolly, J. L. and Lambright, D. G. (1999). Structural basis of activation and GTP hydrolysis in Rab proteins. *Structure* **7**, 413–423.

Eathiraj, S., Pan, X., Ritacco, C. and Lambright, D. G. (2005). Structural basis of family-wide Rab GTPase recognition by rabenosyn-5. *Nature* **436**, 415–419.

Echard, A., Jollivet, F., Martinez, O., Lacapère, J. J., Rousselet, A., Janoueix-Lerosey, I. and Goud, B. (1998). Interaction of a Golgi-associated kinesin-like protein with Rab6. *Science* **279**, 580–585.

Edeling, M. A., Smith, C. and Owen, D. (2006). Life of a clathrin coat: insights from clathrin and AP structures. *Nat. Rev. Mol. Cell Biol.* **7**, 32–44.

Eguez, L., Lee, A., Chavez, J. A., Mîinea, C. P., Kane, S., Lienhard, G. E. and McGraw, T. E. (2005). Full intracellular retention of GLUT4 requires AS160 Rab GTPase activating protein. *Cell Metab.* **2**, 263–272.

Epstein, F. H., Shepherd, P. R. and Kahn, B. B. (1999). Glucose Transporters and Insulin Action — Implications for Insulin Resistance and Diabetes Mellitus. *N. Engl. J. Med.* **341**, 248–257.

Emoto, M., Langille, S. E. and Czech, M. P. (2001). A role for kinesin in insulin-stimulated GLUT4 glucose transporter translocation in 3T3-L1 adipocytes. *J. Biol. Chem.* **276**, 10677–10682.

Esk, C., Chen, C.-Y., Johannes, L. and Brodsky, F. M. (2010). The clathrin heavy chain isoform CHC22 functions in a novel endosomal sorting step. *J. Cell Biol.* **188**, 131–144.

Falasca, M., Hughes, W. E., Dominguez, V., Sala, G., Fostira, F., Fang, M. Q., Cazzolli, R., Shepherd, P. R., James, D. E. and Maffucci, T. (2007). The role of phosphoinositide 3-kinase C2alpha in insulin signaling. *J. Biol. Chem.* **282**, 28226–28236.

Farnsworth, C. L. and Feig, L. A. (1991). Dominant inhibitory mutations in the Mg^{2+}-binding site of RasH prevent its activation by GTP. *Mol. Cell Biol.* **11**, 4822–

4829.

Fili, N., Calleja, V., Woscholski, R., Parker, P. J. and Larijani, B. (2006). Compartmental signal modulation: Endosomal phosphatidylinositol 3-phosphate controls endosome morphology and selective cargo sorting. *Proc. Natl. Acad. Sci. U.S.A.* **103**, 15473–15478.

Foley, K., Boguslavsky, S. and Klip, A. (2011). Endocytosis, Recycling, and Regulated Exocytosis of Glucose Transporter 4. *Biochemistry* **50**, 3048–3061.

Friedman, J. E., Dudek, R. W., Whitehead, D. S., Downes, D. L., Frisell, W. R., Caro, J. F. and Dohm, G. L. (1991). Immunolocalization of glucose transporter GLUT4 within human skeletal muscle. *Diabetes* **40**, 150–154.

Fujita, H., Yamanaka, M., Imamura, K., Tanaka, Y., Nara, A., Yoshimori, T., Yokota, S. and Himeno, M. (2003). A dominant negative form of the AAA ATPase SKD1/VPS4 impairs membrane trafficking out of endosomal/lysosomal compartments: class E vps phenotype in mammalian cells. *J. Cell Sci.* **116**, 401–414.

Fukuda, M. (2003). Slp4-a/Granuphilin-a Inhibits Dense-core Vesicle Exocytosis through Interaction with the GDP-bound Form of Rab27A in PC12 Cells. *J. Biol. Chem.* **278,** 15390–15396.

Fukuda, M. (2006). Rab27 and its effectors in secretory granule exocytosis: a novel docking machinery composed of a Rab27·effector complex. *Biochem. Soc. Trans.* **34**, 691.

Fukuda, M., Kanno, E. and Yamamoto, A. (2004). Rabphilin and Noc2 are recruited to dense-core vesicles through specific interaction with Rab27A in PC12 cells. *J. Biol. Chem.* **279**, 13065–13075.

Fukuda, M., Kanno, E., Ishibashi, K. and Itoh, T. (2008). Large scale screening for novel rab effectors reveals unexpected broad Rab binding specificity. *Mol. Cell Proteomics* **7**, 1031–1042.

Fukuda, N., Emoto, M., Nakamori, Y., Taguchi, A., Miyamoto, S., Uraki, S., Oka, Y. and Tanizawa, Y. (2008). DOC2B: A Novel Syntaxin-4 Binding Protein Mediating Insulin-Regulated GLUT4 Vesicle Fusion in Adipocytes. *Diabetes* **58**, 377–384.

Fukui, K., Sasaki, T., Imazumi, K., Matsuura, Y., Nakanishi, H. and Takai, Y. (1997). Isolation and characterization of a GTPase activating protein specific for the Rab3 subfamily of small G proteins. *J. Biol. Chem.* **272**, 4655–4658.

Fushiki, T., Wells, J. A., Tapscott, E. B. and Dohm, G. L. (1989). Changes in glucose transporters in muscle in response to exercise. *Am. J. Physiol. Endocrinol. Metab.* **256**, E580–E587.

Futter, C. E. C., Pearse, A. A., Hewlett, L. J. L. and Hopkins, C. R. C. (1996). Multivesicular endosomes containing internalized EGF-EGF receptor complexes

mature and then fuse directly with lysosomes. *J. Cell Biol.* **132**, 1011–1023.

García, I. A., Martinez, H. E. and Alvarez, C. (2011). Rab1b regulates COPI and COPII dynamics in mammalian cells. *Cell Logist.* **1**, 159–163.

Gaster, M., Staehr, P., Beck-Nielsen, H., Schrøder, H. D. and Handberg, A. (2001). GLUT4 is reduced in slow muscle fibers of type 2 diabetic patients: is insulin resistance in type 2 diabetes a slow, type 1 fiber disease? *Diabetes* **50**, 1324–1329.

Geppert, M. and Südhof, T. C. (1998). RAB3 and synaptotagmin: the yin and yang of synaptic membrane fusion. *Annu. Rev. Neurosci.* **21**, 75–95.

Gibbs, E. M., Stock, J. L., McCoid, S. C., Stukenbrok, H. A., Pessin, J. E., Stevenson, R. W., Milici, A. J. and McNeish, J. D. (1995). Glycemic improvement in diabetic db/db mice by overexpression of the human insulin-regulatable glucose transporter (GLUT4). *J. Clin. Invest.* **95**, 1512–1518.

Gidon, A., Bardin, S., Cinquin, B., Boulanger, J., Waharte, F., Heliot, L., la Salle, de, H., Hanau, D., Kervrann, C., Goud, B., et al. (2012). A Rab11A/Myosin Vb/Rab11-FIP2 Complex Frames Two Late Recycling Steps of Langerin from the ERC to the Plasma Membrane. *Traffic* **13**, 815–833.

Gillooly, D. J. D., Morrow, I. C. I., Lindsay, M. M., Gould, R. R., Bryant, N. J. N., Gaullier, J. M. J., Parton, R. G. R. and Stenmark, H. H. (2000). Localization of phosphatidylinositol 3-phosphate in yeast and mammalian cells. *EMBO J.* **19**, 4577–4588.

Giorgino, F., de Robertis, O., Laviola, L., Montrone, C., Perrini, S., McCowen, K. C. and Smith, R. J. (2000). The sentrin-conjugating enzyme mUbc9 interacts with GLUT4 and GLUT1 glucose transporters and regulates transporter levels in skeletal muscle cells. *Proc. Natl. Acad. Sci. U.S.A.* **97**, 1125–1130.

Goalstone, M. L., Leitner, J. W., Golovchenko, I., Stjernholm, M. R., Cormont, M., Le Marchand-Brustel, Y. and Draznin, B. (1999). Insulin promotes phosphorylation and activation of geranylgeranyltransferase II. Studies with geranylgeranylation of rab-3 and rab-4. *J. Biol. Chem.* **274**, 2880–2884.

Goldstein, B. J., Bittner-Kowalczyk, A., White, M. F. and Harbeck, M. (2000). Tyrosine dephosphorylation and deactivation of insulin receptor substrate-1 by protein-tyrosine phosphatase 1B. Possible facilitation by the formation of a ternary complex with the Grb2 adaptor protein. *J. Biol. Chem.* **275**, 4283–4289.

Goldstein, L. S. B. (1993). With Apologies to Scheherazade: Tails of 1001 Kinesin Motors. *Annu. Rev. Genet.* **27**, 319–351.

Gomi, H., Mizutani, S., Kasai, K., Itohara, S. and Izumi, T. (2005). Granuphilin molecularly docks insulin granules to the fusion machinery. *J. Cell Biol.* **171**, 99–109.

Grosshans, B. L., Ortiz, D. and Novick, P. (2006). Rabs and their effectors:

achieving specificity in membrane traffic. *Proc. Natl. Acad. Sci. U.S.A.* **103**, 11821–11827.

Guo, H. L., Zhang, C., Liu, Q., Li, Q., Lian, G., Wu, D., Li, X., Zhang, W., Shen, Y., Ye, Z., et al. (2012). The Axin/TNKS complex interacts with KIF3A and is required for insulin-stimulated GLUT4 translocation. *Cell Res.* **22**, 1246–1257.

Guo, W., Roth, D., Walch-Solimena, C. and Novick, P. (1999). The exocyst is an effector for Sec4p, targeting secretory vesicles to sites of exocytosis. *EMBO J.* **18**, 1071–1080.

Guo, Y., Xiao, P., Lei, S., Deng, F., Xiao, G. G., Liu, Y., Chen, X., Li, L., Wu, S., Chen, Y., et al. (2008). How is mRNA expression predictive for protein expression? A correlation study on human circulating monocytes. *Acta Biochim. Biophys. Sin. (Shanghai)* **40**, 426–436.

Habtemichael, E. N., Brewer, P. D., Romenskaia, I. and Mastick, C. C. (2011). Kinetic evidence that Glut4 follows different endocytic pathways than the receptors for transferrin and alpha2-macroglobulin. *J. Biol. Chem.* **286**, 10115–10125.

Hagemann, N., Hou, X., Goody, R. S., Itzen, A. and Erdmann, K. S. (2012). Crystal structure of the Rab binding domain of OCRL1 in complex with Rab8 and functional implications of the OCRL1/Rab8 module for Lowe syndrome. *smallgtpases* **3**, 107–110.

Haglund, K. and Dikic, I. (2012). The role of ubiquitylation in receptor endocytosis and endosomal sorting. *J. Cell Sci.* **125**, 265–275.

Hammer, J. A. and Wu, X. S. (2002). Rabs grab motors: defining the connections between Rab GTPases and motor proteins. *Curr. Opin. Cell Biol.* **14**, 69–75.

Handley, M. T. W. and Burgoyne, R. D. (2008). The Rab27 effector Rabphilin, unlike Granuphilin and Noc2, rapidly exchanges between secretory granules and cytosol in PC12 cells. *Biochem. Bioph. Res. Co.* **373**, 275–281.

Hanson, P. I. and Cashikar, A. (2012). Multivesicular Body Morphogenesis. *Annu. Rev. Cell Dev. Biol.* **28**, 337–362.

Hanson, P. I., Shim, S. and Merrill, S. A. (2009). Cell biology of the ESCRT machinery. *Curr. Opin. Cell Biol.* **21**, 568–574.

Haynes, L. P. (2000). A Direct Inhibitory Role for the Rab3-specific Effector, Noc2, in Ca^{2+}-regulated Exocytosis in Neuroendocrine Cells. *J. Biol. Chem.* **276**, 9726–9732.

Herman, M. A. and Kahn, B. B. (2006). Glucose transport and sensing in the maintenance of glucose homeostasis and metabolic harmony. *J. Clin. Invest.* **116**, 1767–1775.

Hill, E., Clarke, M. and Barr, F. A. (2000). The Rab6-binding kinesin, Rab6-KIFL,

is required for cytokinesis. *EMBO J.* **19**, 5711–5719.

Holman, G. D. (2012). Reagent. C07H19:20 -WO2012049464 (A1), 19 April 2012. *Reagent* 1–30.

Holman, G. D. and Sakamoto, K. (2008). Regulating the motor for GLUT4 vesicle traffic. *Cell Metab.* **8**, 344–346.

Holman, G. D., Kozka, I. J., Clark, A. E., Flower, C. J., Saltis, J., Habberfield, A. D., Simpson, I. A. and Cushman, S. W. (1990). Cell surface labeling of glucose transporter isoform GLUT4 by bis-mannose photolabel. Correlation with stimulation of glucose transport in rat adipose cells by insulin and phorbol ester. *J. Biol. Chem.* **265**, 18172–18179.

Holz, R. W., Brondyk, W. H., Senter, R. A., Kuizon, L. and Macara, I. G. (1994). Evidence for the involvement of Rab3A in Ca(2+)-dependent exocytosis from adrenal chromaffin cells. *J. Biol. Chem.* **269**, 10229–10234.

Hong, W. (1998). Protein transport from the endoplasmic reticulum to the Golgi apparatus. *J. Cell Sci.* **111 (19)**, 2831–2839.

Hosaka, T., Brooks, C. C., Presman, E., Kim, S.-K., Zhang, Z., Breen, M., Gross, D. N., Sztul, E. and Pilch, P. F. (2005). p115 Interacts with the GLUT4 vesicle protein, IRAP, and plays a critical role in insulin-stimulated GLUT4 translocation. *Mol. Biol. Cell* **16**, 2882–2890.

Hou, X., Hagemann, N., Schoebel, S., Blankenfeldt, W., Goody, R. S., Erdmann, K. S. and Itzen, A. (2011). A structural basis for Lowe syndrome caused by mutations in the Rab-binding domain of OCRL1. *EMBO J.* **30**, 1659–1670.

Howard, T. L. T., Stauffer, D. R. D., Degnin, C. R. C. and Hollenberg, S. M. S. (2001). CHMP1 functions as a member of a newly defined family of vesicle trafficking proteins. *J. Cell Sci.* **114**, 2395–2404.

Hruz, P. W. and Mueckler, M. M. (2001). Structural analysis of the GLUT1 facilitative glucose transporter. *Mol. Membr. Biol.* **18**, 183–193.

Huang, C. C., Yang, D. M., Lin, C. C. and Kao, L. S. (2011). Involvement of Rab3A in vesicle priming during exocytosis: interaction with Munc13-1 and Munc18-1. *Traffic* **12**, 1356–1370.

Huang, J. J., Imamura, T. T. and Olefsky, J. M. J. (2001). Insulin can regulate GLUT4 internalization by signaling to Rab5 and the motor protein dynein. *Proc. Natl. Acad. Sci. U.S.A.* **98**, 13084–13089.

Huang, S., Lifshitz, L. M., Jones, C., Bellve, K. D., Standley, C., Fonseca, S., Corvera, S., Fogarty, K. E. and Czech, M. P. (2007). Insulin stimulates membrane fusion and GLUT4 accumulation in clathrin coats on adipocyte plasma membranes. *Mol. Cell Biol.* **27**, 3456–3469.

Huber, L. A., Pimplikar, S., Parton, R. G., Virta, H., Zerial, M. and Simons, K.

(1993). Rab8, a small GTPase involved in vesicular traffic between the TGN and the basolateral plasma membrane. *J. Cell Biol.* **123**, 35–45.

Hume, A. N., Collinson, L. M., Rapak, A., Gomes, A. Q., Hopkins, C. R. and Seabra, M. C. (2001). Rab27a regulates the peripheral distribution of melanosomes in melanocytes. *J. Cell Biol.* **152**, 795–808.

Hume, A. N., Ushakov, D. S., Tarafder, A. K., Ferenczi, M. A. and Seabra, M. C. (2007). Rab27a and MyoVa are the primary Mlph interactors regulating melanosome transport in melanocytes. *J. Cell Sci.* **120**, 3111–3122.

Hurley, J. H. (2010). The ESCRT complexes. *Crit. Rev. Biochem. Mol. Biol.* **45**, 463–487.

Hurley, J. H. (2011). Nipped in the bud: how the AMSH MIT domain helps deubiquitinate lysosome-bound cargo. *Structure* **19**, 1033–1035.

Hutagalung, A. H. and Novick, P. J. (2011). Role of Rab GTPases in membrane traffic and cell physiology. *Physiol. Rev.* **91**, 119–149.

Iezzi, M., Regazzi, R. and Wollheim, C. B. (2000). The Rab3-interacting molecule RIM is expressed in pancreatic beta-cells and is implicated in insulin exocytosis. *FEBS LETT.* **474**, 66–70.

Iida, H., Wang, L., Nishii, K., Ookuma, A. and Shibata, Y. (1996). Identification of rab12 as a secretory granule associated small GTP-binding protein in atrial myocytes. *Circ. Res.* **78**, 343–347.

Ikonomov, O. C., Sbrissa, D. and Shisheva, A. (2009). YM201636, an inhibitor of retroviral budding and PIKfyve-catalyzed PtdIns(3,5)P2 synthesis, halts glucose entry by insulin in adipocytes. *Biochem. Bioph. Res. Co.* **382**, 566–570.

Ikonomov, O. C., Sbrissa, D., Dondapati, R. and Shisheva, A. (2007). ArPIKfyve–PIKfyve interaction and role in insulin-regulated GLUT4 translocation and glucose transport in 3T3-L1 adipocytes. *Exp. Cell Res.* **313**, 2404–2416.

Inoue, M., Chang, L., Hwang, J., Chiang, S. H. and Saltiel, A. R. (2003). The exocyst complex is required for targeting of Glut4 to the plasma membrane by insulin. *Nature* **422**, 629–633.

Ishikura, S. and Klip, A. (2008). Muscle cells engage Rab8A and myosin Vb in insulin-dependent GLUT4 translocation. *Am. J. Physiol.-Cell Ph.* **295**, C1016–25.

Ishikura, S., Bilan, P. J. and Klip, A. (2007). Rabs 8A and 14 are targets of the insulin-regulated Rab-GAP AS160 regulating GLUT4 traffic in muscle cells. *Biochem. Bioph. Res. Co.* **353**, 1074–1079.

Itoh, T., Satoh, M., Kanno, E. and Fukuda, M. (2006). Screening for target Rabs of TBC (Tre-2/Bub2/Cdc16) domain-containing proteins based on their Rab-binding activity. *Genes Cells* **11**, 1023–1037.

Iyer, L. M., Leipe, D. D., Koonin, E. V. and Aravind, L. (2004). Evolutionary

history and higher order classification of AAA+ ATPases. *J. Struct. Biol.* **146**, 21–21.

Jacobs, S., Hazum, E. and Cuatrecasas, P. (1980). The subunit structure of rat liver insulin receptor. Antibodies directed against the insulin-binding subunit. *J. Biol. Chem.* **255**, 6937–6940.

James, D. E., Brown, R., Navarro, J. and Pilch, P. F. (1988). Insulin-regulatable tissues express a unique insulin-sensitive glucose transport protein. *Nature* **333**, 183–185.

James, D. E., Strube, M. and Mueckler, M. (1989). Molecular cloning and characterization of an insulin-regulatable glucose transporter. *Nature* **338**, 83–87.

Jean, S. and Kiger, A. A. (2012). Coordination between RAB GTPase and phosphoinositide regulation and functions. *Nat. Rev. Mol. Cell Biol.* **13**, 463–470.

Jedrychowski, M. P., Gartner, C. A., Gygi, S. P., Zhou, L., Herz, J., Kandror, K. V. and Pilch, P. F. (2010). Proteomic analysis of GLUT4 storage vesicles reveals LRP1 to be an important vesicle component and target of insulin signaling. *J. Biol. Chem.* **285**, 104–114.

Jefferies, H. B. J., Cooke, F. T., Jat, P., Boucheron, C., Koizumi, T., Hayakawa, M., Kaizawa, H., Ohishi, T., Workman, P., Waterfield, M. D., et al. (2008). A selective PIKfyve inhibitor blocks PtdIns(3,5)P2 production and disrupts endomembrane transport and retroviral budding. *EMBO Rep.* **9**, 164–170.

Jewell, J. L., Oh, E., Bennett, S. M., Meroueh, S. O. and Thurmond, D. C. (2008). The tyrosine phosphorylation of Munc18c induces a switch in binding specificity from syntaxin 4 to Doc2beta. *J. Biol. Chem.* **283**, 21734–21746.

Jewell, J. L., Oh, E., Ramalingam, L., Kalwat, M. A., Tagliabracci, V. S., Tackett, L., Elmendorf, J. S. and Thurmond, D. C. (2011). Munc18c phosphorylation by the insulin receptor links cell signaling directly to SNARE exocytosis. *J. Cell Biol.* **193**, 185–199.

Jiang, H., He, J., Pu, S., Tang, C. and Xu, G. (2007). Heat shock protein 70 is translocated to lipid droplets in rat adipocytes upon heat stimulation. *Biochim. Biophys. Acta* **1771**, 66–74.

Jiang, L., Fan, J., Bai, L., Wang, Y., Chen, Y., Yang, L., Chen, L. and Xu, T. (2008). Direct quantification of fusion rate reveals a distal role for AS160 in insulin-stimulated fusion of GLUT4 storage vesicles. *J. Biol. Chem.* **283**, 8508–8516.

Jin, Y., Sultana, A., Gandhi, P., Franklin, E., Hamamoto, S., Khan, A. R., Munson, M., Schekman, R. and Weisman, L. S. (2011). Myosin V transports secretory vesicles via a Rab GTPase cascade and interaction with the exocyst complex. *Dev. Cell* **21**, 1156–1170.

Joberty, G., Tavitian, A. and Zahraoui, A. (1993). Isoprenylation of Rab proteins possessing a C-terminal CaaX motif. *FEBS LETT.* **330**, 323–328.

Johannes, L., Lledo, P. M., Roa, M., Vincent, J. D., Henry, J. P. and Darchen, F. (1994). The GTPase Rab3a negatively controls calcium-dependent exocytosis in neuroendocrine cells. *EMBO J.* **13**, 2029–2037.

Joost, H. G. and Thorens, B. (2001). The extended GLUT-family of sugar/polyol transport facilitators: nomenclature, sequence characteristics, and potential function of its novel members (review). *Mol. Membr. Biol.* **18**, 247–256.

Joost, H. G., Weber, T. M. and Cushman, S. W. (1988). Qualitative and quantitative comparison of glucose transport activity and glucose transporter concentration in plasma membranes from basal and insulin-stimulated rat adipose cells. *Biochem. J.* **249**, 155–161.

Jordens, I., Marsman, M., Kuijl, C. and Neefjes, J. (2005). Rab proteins, connecting transport and vesicle fusion. *Traffic* **6**, 1070–1077.

Jung, C. Y. and Rampal, A. L. (1977). Cytochalasin B binding sites and glucose transport carrier in human erythrocyte ghosts. *J. Biol. Chem.* **252**, 5456–5463.

Kanda, H., Tamori, Y., Shinoda, H., Yoshikawa, M., Sakaue, M., Udagawa, J., Otani, H., Tashiro, F., Miyazaki, J. I. and Kasuga, M. (2005). Adipocytes from Munc18c-null mice show increased sensitivity to insulin-stimulated GLUT4 externalization. *J. Clin. Invest.* **115**, 291–301.

Kane, S., Sano, H., Liu, S. C. H., Asara, J. M., Lane, W. S., Garner, C. C. and Lienhard, G. E. (2002). A method to identify serine kinase substrates. Akt phosphorylates a novel adipocyte protein with a Rab GTPase-activating protein (GAP) domain. *J. Biol. Chem.* **277**, 22115–22118.

Kanzaki, M. and Pessin, J. E. (2001). Insulin-stimulated GLUT4 translocation in adipocytes is dependent upon cortical actin remodeling. *J. Biol. Chem.* **276**, 42436–42444.

Karlsson, H. K. R., Zierath, J. R., Kane, S., Krook, A., Lienhard, G. E. and Wallberg-Henriksson, H. (2005). Insulin-stimulated phosphorylation of the Akt substrate AS160 is impaired in skeletal muscle of type 2 diabetic subjects. *Diabetes* **54**, 1692–1697.

Kato, M., Sasaki, T., Ohya, T., Nakanishi, H., Nishioka, H., Imamura, M. and Takai, Y. (1996). Physical and functional interaction of rabphilin-3A with alpha-actinin. *J. Biol. Chem.* **271**, 31775–31778.

Katzmann, D. J., Babst, M. and Emr, S. D. (2001). Ubiquitin-dependent sorting into the multivesicular body pathway requires the function of a conserved endosomal protein sorting complex, ESCRT-I. *Cell* **106**, 145–155.

Kawanishi, M., Tamori, Y., Okazawa, H., Araki, S., Shinoda, H. and Kasuga, M. (2000). Role of SNAP23 in insulin-induced translocation of GLUT4 in 3T3-L1 adipocytes. Mediation of complex formation between syntaxin4 and VAMP2. *J. Biol. Chem.* **275**, 8240–8247.

Kawasaki, M., Nakayama, K. and Wakatsuki, S. (2005). Membrane recruitment

of effector proteins by Arf and Rab GTPases. *Curr. Opin. Struct. Biol.* **15**, 681–689.

Kent, W. J. (2002). BLAT---The BLAST-Like Alignment Tool. *Genome Res.* **12**, 656–664.

Kessler, A., Tomas, E., Immler, D., Meyer, H. E., Zorzano, A. and Eckel, J. (2000). Rab11 is associated with GLUT4-containing vesicles and redistributes in response to insulin. *Diabetologia* **43**, 1518–1527.

Kibbe, W. A. (2007). OligoCalc: an online oligonucleotide properties calculator. *Nucleic Acids Res.* **35**, W43–6.

Kinter, M., and N. E. Sherman. (2000). Protein sequencing and identification using tandem mass spectrometry. *Wiley & Sons*, N.Y.

Kong, A. M., Horan, K. A., Sriratana, A., Bailey, C. G., Collyer, L. J., Nandurkar, H. H., Shisheva, A., Layton, M. J., Rasko, J. E. J., Rowe, T., et al. (2006). Phosphatidylinositol 3-Phosphate [PtdIns(3)P] Is Generated at the Plasma Membrane by an Inositol Polyphosphate 5-Phosphatase: Endogenous PtdIns(3)P Can Promote GLUT4 Translocation to the Plasma Membrane. *Mol. Cell. Biol.* **26**, 6065–6081.

Kotake, K., Ozaki, N., Mizuta, M., Sekiya, S., Inagaki, N. and Seino, S. (1997). Noc2, a putative zinc finger protein involved in exocytosis in endocrine cells. *J. Biol. Chem.* **272**, 29407–29410.

Kotani, K., Peroni, O. D., Minokoshi, Y., Boss, O. and Kahn, B. B. (2004). GLUT4 glucose transporter deficiency increases hepatic lipid production and peripheral lipid utilization. *J. Clin. Invest.* **114**, 1666–1675.

Koumanov, F., Pereira, V. J., Whitley, P. R. and Holman, G. D. (2012). GLUT4 traffic through an ESCRT-III-dependent sorting compartment in adipocytes. *PLoS ONE* **7**, e44141.

Koumanov, F., Richardson, J. D., Murrow, B. A. and Holman, G. D. (2011). AS160 phosphotyrosine-binding domain constructs inhibit insulin-stimulated GLUT4 vesicle fusion with the plasma membrane. *J. Biol. Chem.* **286**, 16574–16582.

Koval, M. and Pagano, R. E. (1989). Lipid recycling between the plasma membrane and intracellular compartments: transport and metabolism of fluorescent sphingomyelin analogues in cultured fibroblasts. *J. Cell Biol.* **108**, 2169–2181.

Koya, D. and King, G. L. (1998). Protein kinase C activation and the development of diabetic complications. *Diabetes* **47**, 859–866.

Kramer, H. F., Witczak, C. A., Taylor, E. B., Fujii, N., Hirshman, M. F. and Goodyear, L. J. (2006). AS160 Regulates Insulin- and Contraction-stimulated Glucose Uptake in Mouse Skeletal Muscle. *J. Biol. Chem.* **281**, 31478–31485.

Krzewski, K. and Cullinane, A. R. (2013). Evidence for defective Rab GTPase-dependent cargo traffic in immune disorders. *Exp. Cell Res.* **319**, 2360–2367.

Kutateladze, T. and Overduin, M. (2001). Structural mechanism of endosome docking by the FYVE domain. *Science* **291**, 1793–1796.

Kutateladze, T. G. (2010). Translation of the phosphoinositide code by PI effectors. *Nat. Chem. Biol.* **6**, 507–513.

Laemmli, U. K. (1970). Cleavage of structural proteins during the assembly of the head of bacteriophage T4. *Nature* **227**, 680–685.

Lalioti, V. S., Vergarajauregui, S., Pulido, D. and Sandoval, I. V. (2002). The insulin-sensitive glucose transporter, GLUT4, interacts physically with Daxx. Two proteins with capacity to bind Ubc9 and conjugated to SUMO1. *J. Biol. Chem.* **277**, 19783–19791.

Lalioti, V. S., Vergarajauregui, S., Tsuchiya, Y., Hernandez-Tiedra, S. and Sandoval, I. V. (2009). Daxx functions as a scaffold of a protein assembly constituted by GLUT4, JNK1 and KIF5B. *J. Cell. Physiol.* **218**, 416–426.

Lamb, C. A., Mccann, R. K., Stöckli, J., James, D. E. and Bryant, N. J. (2010). Insulin-Regulated Trafficking of GLUT4 Requires Ubiquitination. *Traffic* **11**, 1445–1454.

Larance, M., Ramm, G. and James, D. E. (2007). The GLUT4 Code. *Mol. Endocrinol.* **22**, 226–233.

Larance, M., Ramm, G., Stöckli, J., van Dam, E. M., Winata, S., Wasinger, V., Simpson, F., Graham, M., Junutula, J. R., Guilhaus, M., et al. (2005). Characterization of the role of the Rab GTPase-activating protein AS160 in insulin-regulated GLUT4 trafficking. *J. Biol. Chem.* **280**, 37803–37813.

Latham, C. F., Lopez, J. A., Hu, S. H., Gee, C. L., Westbury, E., Blair, D. H., Armishaw, C. J., Alewood, P. F., Bryant, N. J., James, D. E., et al. (2006). Molecular Dissection of the Munc18c/Syntaxin4 Interaction: Implications for Regulation of Membrane Trafficking. *Traffic* **7**, 1408–1419.

Lawe, D. C., Chawla, A., Merithew, E., Dumas, J., Carrington, W., Fogarty, K., Lifshitz, L., Tuft, R., Lambright, D. and Corvera, S. (2002). Sequential roles for phosphatidylinositol 3-phosphate and Rab5 in tethering and fusion of early endosomes via their interaction with EEA1. *J. Biol. Chem.* **277**, 8611–8617.

Lee, C. H., Li, W., Nishimura, R., Zhou, M., Batzer, A. G., Myers, M. G., White, M. F., Schlessinger, J. and Skolnik, E. Y. (1993). Nck associates with the SH2 domain-docking protein IRS-1 in insulin-stimulated cells. *Proc. Natl. Acad. Sci. U.S.A.* **90**, 11713–11717.

Lee, J., Pilch, P. F., Shoelson, S. E. and Scarlata, S. F. (1997). Conformational changes of the insulin receptor upon insulin binding and activation as monitored by fluorescence spectroscopy. *Biochemistry* **36**, 2701–2708.

Lee, J. A. J., Beigneux, A. A., Ahmad, S. T. S., Young, S. G. S. and Gao, F. B. F. (2007). ESCRT-III Dysfunction Causes Autophagosome Accumulation and Neurodegeneration. *Curr. Biol.* **17**, 7–7.

Lee, M. T. G., Mishra, A. and Lambright, D. G. (2009). Structural mechanisms for regulation of membrane traffic by rab GTPases. *Traffic* **10**, 1377–1389.

Lee, S. A., Eyeson, R., Cheever, M. L., Geng, J., Verkhusha, V. V., Burd, C., Overduin, M. and Kutateladze, T. G. (2005). Targeting of the FYVE domain to endosomal membranes is regulated by a histidine switch. *Proc. Natl. Acad. Sci. U.S.A.* **102**, 13052–13057.

Lemmon, M. A. (2003). Phosphoinositide recognition domains. *Traffic* **4**, 201–213.

Leto, D. and Saltiel, A. R. (2012). Regulation of glucose transport by insulin: traffic control of GLUT4. *Nat. Rev. Mol. Cell Biol.* **13**, 383–396.

Leturque, A., Brot-Laroche, E., Le Gall, M., Stolarczyk, E. and Tobin, V. (2005). The role of GLUT2 in dietary sugar handling. *J. Physiol. Biochem.* **61**, 529–537.

Li, L. V. and Kandror, K. V. (2005). Golgi-localized, gamma-ear-containing, Arf-binding protein adaptors mediate insulin-responsive trafficking of glucose transporter 4 in 3T3-L1 adipocytes. *Mol. Endocrinol.* **19**, 2145–2153.

Lindsay, A. J., Jollivet, F., Horgan, C. P., Khan, A. R., Raposo, G., McCaffrey, M. W. and Goud, B. (2013). Identification and characterization of multiple novel Rab-myosin Va interactions. *Mol. Biol. Cell* **24**, 3420–3434.

Liu, L. B., Omata, W., Kojima, I. and Shibata, H. (2007). The SUMO Conjugating Enzyme Ubc9 is a Regulator of GLUT4 Turnover and Targeting to the Insulin-Responsive Storage Compartment in 3T3-L1 Adipocytes. *Diabetes* **56**, 1977–1985.

Liu, M. L., Gibbs, E. M., McCoid, S. C., Milici, A. J., Stukenbrok, H. A., McPherson, R. K., Treadway, J. L. and Pessin, J. E. (1993). Transgenic mice expressing the human GLUT4/muscle-fat facilitative glucose transporter protein exhibit efficient glycemic control. *Proc. Natl. Acad. Sci. U.S.A.* **90**, 11346–11350.

Lizunov, V. A., Matsumoto, H., Zimmerberg, J., Cushman, S. W. and Frolov, V. A. (2005). Insulin stimulates the halting, tethering, and fusion of mobile GLUT4 vesicles in rat adipose cells. *J. Cell Biol.* **169**, 481–489.

Lledo, P. M., Vernier, P., Vincent, J. D., Mason, W. T. and Zorec, R. (1993). Inhibition of Rab3B expression attenuates Ca(2+)-dependent exocytosis in rat anterior pituitary cells. *Nature* **364**, 540–544.

Lodhi, I. J., Bridges, D., Chiang, S. H., Zhang, Y., Cheng, A., Geletka, L. M., Weisman, L. S. and Saltiel, A. R. (2008). Insulin stimulates phosphatidylinositol 3-phosphate production via the activation of Rab5. *Mol. Biol. Cell* **19**, 2718–2728.

Lodhi, I. J. I., Chiang, S. H. S., Chang, L. L., Vollenweider, D. D., Watson, R. T. R., Inoue, M. M., Pessin, J. E. J. and Saltiel, A. R. A. (2007). Gapex-5, a Rab31 Guanine Nucleotide Exchange Factor that Regulates Glut4 Trafficking in Adipocytes. *Cell Metab.* **5**, 14–14.

Longo, N., Wang, Y., Smith, S. A., Langley, S. D., DiMeglio, L. A. and Giannella-Neto, D. (2002). Genotype-phenotype correlation in inherited severe insulin resistance. *Hum. Mol. Genet.* **11**, 1465–1475.

Luo, J., Field, S. J., Lee, J. Y., Engelman, J. A. and Cantley, L. C. (2005). The p85 regulatory subunit of phosphoinositide 3-kinase down-regulates IRS-1 signaling via the formation of a sequestration complex. *J. Cell Biol.* **170**, 455–464.

Luzio, J. P., Piper, S. C., Bowers, K., Parkinson, M. D., Lehner, P. J. and Bright, N. A. (2009). ESCRT proteins and the regulation of endocytic delivery to lysosomes. *Biochem. Soc. Trans* **37**, 178–178.

Lyakhova, T. A. and Knight, J. D. (2013). The C2 domains of granuphilin are high-affinity sensors for plasma membrane lipids. *Chem. Phys. Lipids* **182**, 29–37.

Maddux, B. A. and Goldfine, I. D. (2000). Membrane glycoprotein PC-1 inhibition of insulin receptor function occurs via direct interaction with the receptor alpha-subunit. *Diabetes* **49**, 13–19.

Maffucci, T., Brancaccio, A., Piccolo, E., Stein, R. C. and Falasca, M. (2003). Insulin induces phosphatidylinositol-3-phosphate formation through TC10 activation. *EMBO J.* **22**, 4178–4189.

Mahoney, T. R., Liu, Q., Itoh, T., Luo, S., Hadwiger, G., Vincent, R., Wang, Z. W., Fukuda, M. and Nonet, M. L. (2006). Regulation of synaptic transmission by RAB-3 and RAB-27 in Caenorhabditis elegans. *Mol. Biol. Cell* **17**, 2617–2625.

Malide, D., Ramm, G., Cushman, S. W. and Slot, J. W. (2000). Immunoelectron microscopic evidence that GLUT4 translocation explains the stimulation of glucose transport in isolated rat white adipose cells. *J. Cell Sci.* **113 (23)**, 4203–4210.

Manabe, S., Nishimura, N., Yamamoto, Y., Kitamura, H., Morimoto, S., Imai, M., Nagahiro, S., Seino, S. and Sasaki, T. (2004). Identification and characterization of Noc2 as a potential Rab3B effector protein in epithelial cells. *Biochem. Bioph. Res. Co.* **316**, 218–225.

Marette, A., Burdett, E., Douen, A., Vranic, M. and Klip, A. (1992). Insulin Induces the Translocation of GLUT4 From a Unique Intracellular Organelle to Transverse Tubules in Rat Skeletal Muscle. *Diabetes* **41**, 1562–1569.

Mari, M., Monzo, P., Kaddai, V., Keslair, F., Gonzalez, T., Le Marchand-Brustel, Y. and Cormont, M. (2006). The Rab4 effector Rabip4 plays a role in the endocytotic trafficking of Glut 4 in 3T3-L1 adipocytes. *J. Cell Sci.* **119**, 1297–1306.

Martelli, A. M., Baldini, G., Tabellini, G., Koticha, D., Bareggi, R. and

Baldini, G. (2000). Rab3A and Rab3D control the total granule number and the fraction of granules docked at the plasma membrane in PC12 cells. *Traffic* **1**, 976–986.

Martin, L. B., Shewan, A., Millar, C. A., Gould, G. W. and James, D. E. (1998). Vesicle-associated membrane protein 2 plays a specific role in the insulin-dependent trafficking of the facilitative glucose transporter GLUT4 in 3T3-L1 adipocytes. *J. Biol. Chem.* **273**, 1444–1452.

Martin, O. J., Lee, A. and McGraw, T. E. (2006). GLUT4 distribution between the plasma membrane and the intracellular compartments is maintained by an insulin-modulated bipartite dynamic mechanism. *J. Biol. Chem.* **281**, 484–490.

Martin, S., Ramm, G., Lyttle, C. T., Meerloo, T., Stoorvogel, W. and James, D. E. (2000). Biogenesis of insulin-responsive GLUT4 vesicles is independent of brefeldin A-sensitive trafficking. *Traffic* **1**, 652–660.

Martin, L. B., Shewan, A., Millar, C. A., Gould, G. W. and James, D. E. (1998). Vesicle-associated membrane protein 2 plays a specific role in the insulin-dependent trafficking of the facilitative glucose transporter GLUT4 in 3T3-L1 adipocytes. *J. Biol. Chem.* **273**, 1444–1452.

Matsumoto, M., Miki, T., Shibasaki, T., Kawaguchi, M., Shinozaki, H., Nio, J., Saraya, A., Koseki, H., Miyazaki, M., Iwanaga, T., et al. (2004). Noc2 is essential in normal regulation of exocytosis in endocrine and exocrine cells. *Proc. Natl. Acad. Sci. U.S.A.* **101**, 8313–8318.

Matsuno, A., Itoh, J., Takekoshi, S., Itoh, Y., Ohsugi, Y., Katayama, H., Nagashima, T. and Osamura, R. Y. (2003). Dynamics of subcellular organelles, growth hormone, Rab3B, SNAP-25, and syntaxin in rat pituitary cells caused by growth hormone releasing hormone and somatostatin. *Microsc. Res. Tech.* **62**, 232–239.

Mauvais-Jarvis, F., Ueki, K., Fruman, D. A., Hirshman, M. F., Sakamoto, K., Goodyear, L. J., Iannacone, M., Accili, D., Cantley, L. C. and Kahn, C. R. (2002). Reduced expression of the murine p85alpha subunit of phosphoinositide 3-kinase improves insulin signaling and ameliorates diabetes. *J. Clin. Invest.* **109**, 141–149.

Maxfield, F. R. and McGraw, T. E. (2004). Endocytic recycling. *Nat. Rev. Mol. Cell Biol.* **5**, 121–132.

Mayer, M. P. and Bukau, B. (2005). Hsp70 chaperones: cellular functions and molecular mechanism. *Cell. Mol. Life Sci.* **62**, 670–684.

Mayor, S., Presley, J. F. and Maxfield, F. R. (1993). Sorting of membrane components from endosomes and subsequent recycling to the cell surface occurs by a bulk flow process. *J. Cell Biol.* **121**, 1257–1269.

Miesenböck, G., De Angelis, D. A. and Rothman, J. E. (1998). Visualizing secretion and synaptic transmission with pH-sensitive green fluorescent proteins. *Nature* **394**, 192–195.

Mîinea, C. P., Sano, H., Kane, S., Sano, E., Fukuda, M., Peränen, J., Lane, W. S. and Lienhard, G. E. (2005). AS160, the Akt substrate regulating GLUT4 translocation, has a functional Rab GTPase-activating protein domain. *Biochem. J.* **391**, 87.

Mokdad, A. H., Bowman, B. A., Ford, E. S., Vinicor, F., Marks, J. S. and Koplan, J. P. (2001). The continuing epidemics of obesity and diabetes in the United States. *JAMA* **286**, 1195–1200.

Mokdad, A. H., Ford, E. S., Bowman, B. A., Dietz, W. H., Vinicor, F., Bales, V. S. and Marks, J. S. (2003). Prevalence of obesity, diabetes, and obesity-related health risk factors, 2001. *JAMA* **289**, 76–79.

Montaville, P., Coudevylle, N., Radhakrishnan, A., Leonov, A., Zweckstetter, M. and Becker, S. (2008). The PIP2 binding mode of the C2 domains of rabphilin-3A. *Protein Sci.* **17**, 1025–1034.

Morgan, J. R., Jiang, J., Oliphint, P. A., Jin, S., Gimenez, L. E., Busch, D. J., Foldes, A. E., Zhuo, Y., Sousa, R. and Lafer, E. M. (2013). A role for an Hsp70 nucleotide exchange factor in the regulation of synaptic vesicle endocytosis. *J. Neurosci.* **33**, 8009–8021.

Moyer, B. D., Allan, B. B. and Balch, W. E. (2001). Rab1 interaction with a GM130 effector complex regulates COPII vesicle cis--Golgi tethering. *Traffic* **2**, 268–276.

Mu, F. T., Callaghan, J. M., Steele-Mortimer, O., Stenmark, H., Parton, R. G., Campbell, P. L., McCluskey, J., Yeo, J. P., Tock, E. P. and Toh, B. H. (1995). EEA1, an early endosome-associated protein. EEA1 is a conserved alpha-helical peripheral membrane protein flanked by cysteine “fingers” and contains a calmodulin-binding IQ motif. *J. Biol. Chem.* **270**, 13503–13511.

Müller, M., Pym, E. C. G., Tong, A. and Davis, G. W. (2011). Rab3-GAP Controls the Progression of Synaptic Homeostasis at a Late Stage of Vesicle Release. *Neuron* **69**, 749–762.

Muretta, J. M. and Mastick, C. C. (2009). How insulin regulates glucose transport in adipocytes. *Vitam. Horm.* **80**, 245–286.

Muzioł, T., Pineda-Molina, E., Ravelli, R. B., Zamborlini, A., Usami, Y., Göttlinger, H. and Weissenhorn, W. (2006). Structural Basis for Budding by the ESCRT-III Factor CHMP3. *Dev. Cell* **10**, 10–10.

Myers, M. G., Wang, L. M., Sun, X. J., Zhang, Y., Yenush, L., Schlessinger, J., Pierce, J. H. and White, M. F. (1994). Role of IRS-1-GRB-2 complexes in insulin signaling. *Mol. Cell Biol.* **14**, 3577–3587.

Nagano, F., Sasaki, T., Fukui, K., Asakura, T., Imazumi, K. and Takai, Y. (1998). Molecular cloning and characterization of the noncatalytic subunit of the Rab3 subfamily-specific GTPase-activating protein. *J. Biol. Chem.* **273**, 24781–24785.

Nalefski, E. A. and Falke, J. J. (1996). The C2 domain calcium-binding motif: Structural and functional diversity. *Protein Sci.* **5**, 2375–2390.

Ng, E. L. and Tang, B. L. (2008). Rab GTPases and their roles in brain neurons and glia. *Brain Res. Rev.* **58**, 236–246.

Nickerson, D. P. D., West, M. M. and Odorizzi, G. G. (2006). Did2 coordinates Vps4-mediated dissociation of ESCRT-III from endosomes. *J. Cell Biol.* **175**, 715–720.

Nishimura, N., Araki, K., Shinahara, W., Nakano, Y., Nishimura, K., Higashio, H. and Sasaki, T. (2008). Interaction of Rab3B with microtubule-binding protein Gas8 in NIH 3T3 cells. *Arch. Biochem. Biophy.* **474**, 136–142.

Niwa, S., Tanaka, Y. and Hirokawa, N. (2008). KIF1Bβ- and KIF1A-mediated axonal transport of presynaptic regulator Rab3 occurs in a GTP-dependent manner through DENN/MADD. *Nat. Cell Biol.* **10**, 1269–1279.

Novick, P. and Guo, W. (2002). Ras family therapy: Rab, Rho and Ral talk to the exocyst. *Trends Cell Biol.* **12**, 247–249.

Novick, P., Medkova, M., Dong, G., Hutagalung, A., Reinisch, K. and Grosshans, B. (2006). Interactions between Rabs, tethers, SNAREs and their regulators in exocytosis. *Biochem. Soc. Trans* **34**, 683–686.

Nuoffer, C., Davidson, H. W., Matteson, J., Meinkoth, J. and Balch, W. E. (1994). A GDP-bound of rab1 inhibits protein export from the endoplasmic reticulum and transport between Golgi compartments. *J. Cell Biol.* **125**, 225–237.

Ogata, S., Miki, T., Seino, S., Tamai, S., Kasai, H. and Nemoto, T. (2012). A novel function of Noc2 in agonist-induced intracellular Ca^{2+} increase during zymogen-granule exocytosis in pancreatic acinar cells. *PLoS ONE* **7**, e37048.

Ohnishi, H., Ernst, S. A., Wys, N., McNiven, M. and Williams, J. A. (1996). Rab3D localizes to zymogen granules in rat pancreatic acini and other exocrine glands. *Am. J. Physiol.* **271**, G531–G538.

Ohnishi, H., Samuelson, L. C., Yule, D. I., Ernst, S. A. and Williams, J. A. (1997). Overexpression of Rab3D enhances regulated amylase secretion from pancreatic acini of transgenic mice. *J. Clin. Invest.* **100**, 3044–3052.

Olson, A. L., Knight, J. B. and Pessin, J. E. (1997). Syntaxin 4, VAMP2, and/or VAMP3/cellubrevin are functional target membrane and vesicle SNAP receptors for insulin-stimulated GLUT4 translocation in adipocytes. *Mol. Cell Biol.* **17**, 2425–2435.

Ostermeier, C. and Brunger, A. T. (1999). Structural basis of Rab effector specificity: crystal structure of the small G protein Rab3A complexed with the effector domain of rabphilin-3A. *Cell* **96**, 363–374.

Otto, G. P., Razi, M., Morvan, J., Stenner, F. and Tooze, S. A. (2010). A novel syntaxin 6-interacting protein, SHIP164, regulates syntaxin 6-dependent sorting

from early endosomes. *Traffic* **11**, 688–705.

Pal, A., Severin, F., Lommer, B., Shevchenko, A. and Zerial, M. (2006). Huntingtin-HAP40 complex is a novel Rab5 effector that regulates early endosome motility and is up-regulated in Huntington's disease. *J. Cell Biol.* **172**, 605–618.

Park, J. H., Kim, S. J., Park, S. H., Son, D. G., Bae, J. H., Kim, H. K., Han, J. and Song, D. K. (2012). Glucagon-Like Peptide-1 Enhances Glucokinase Activity in Pancreatic β-Cells through the Association of Epac2 with Rim2 and Rab3A. *Endocrinology* **153**, 574–582.

Pavelka, M., Neumüller, J. and Ellinger, A. (2008). Retrograde traffic in the biosynthetic-secretory route. *Histochem. Cell Biol.* **129**, 277–288.

Peter, M., Chavrier, P., Nigg, E. A. and Zerial, M. (1992). Isoprenylation of rab proteins on structurally distinct cysteine motifs. *J. Cell Sci.* **102 (Pt 4)**, 857–865.

Piper Hanley, K., Hearn, T., Berry, A., Carvell, M. J., Patch, A.-M., Williams, L. J., Sugden, S. A., Wilson, D. I., Ellard, S. and Hanley, N. A. (2010). In vitro expression of NGN3 identifies RAB3B as the predominant Ras-associated GTP-binding protein 3 family member in human islets. *J. Endocrinol.* **207**, 151–161.

Piper, R. C. and Katzmann, D. J. (2007). Biogenesis and Function of Multivesicular Bodies. *Annu. Rev. Cell Dev. Biol.* **23**, 519–547.

Raiborg, C. (2001). Hrs recruits clathrin to early endosomes. *EMBO J.* **20**, 5008–5021.

Raiborg, C., Bache, K. G., Gillooly, D. J., Madshus, I. H., Stang, E. and Stenmark, H. (2002). Hrs sorts ubiquitinated proteins into clathrin-coated microdomains of early endosomes. *Nat. Cell Biol.* **4**, 394–398.

Ralston, E. and Ploug, T. (1996). GLUT4 in cultured skeletal myotubes is segregated from the transferrin receptor and stored in vesicles associated with TGN. *J. Cell Sci.* **109 (13)**, 2967–2978.

Ramalingam, L., Oh, E., Yoder, S. M., Brozinick, J. T., Kalwat, M. A., Groffen, A. J., Verhage, M. and Thurmond, D. C. (2012). Doc2b is a key effector of insulin secretion and skeletal muscle insulin sensitivity. *Diabetes* **61**, 2424–2432.

Ramm, G., Slot, J. W., James, D. E. and Stoorvogel, W. (2000). Insulin Recruits GLUT4 from Specialized VAMP2-carrying Vesicles as well as from the Dynamic Endosomal/Trans-Golgi Network in Rat Adipocytes. *Mol. Biol. Cell* **11**, 4079–4091.

Randhawa, V. K., Ishikura, S., Talior-Volodarsky, I., Cheng, A. W. P., Patel, N., Hartwig, J. H. and Klip, A. (2008). GLUT4 vesicle recruitment and fusion are differentially regulated by Rac, AS160, and Rab8A in muscle cells. *J. Biol. Chem.* **283**, 27208–27219.

Raymond, C. K., Howald-Stevenson, I., Vater, C. A. and Stevens, T. H. (1992).

Morphological classification of the yeast vacuolar protein sorting mutants: evidence for a prevacuolar compartment in class E vps mutants. *Mol. Biol. Cell* **3**, 1389–1402.

Rea, S. and James, D. E. (1997). Moving GLUT4: the biogenesis and trafficking of GLUT4 storage vesicles. *Diabetes* **46**, 1667–1677.

Rea, S., Martin, L. B., McIntosh, S., Macaulay, S. L., Ramsdale, T., Baldini, G. and James, D. E. (1998). Syndet, an adipocyte target SNARE involved in the insulin-induced translocation of GLUT4 to the cell surface. *J. Biol. Chem.* **273**, 18784–18792.

Reaven, G. M. (1988). Role of Insulin Resistance in Human Disease. *Diabetes* **37**, 1595–1607.

Redzic, Z. (2011). Molecular biology of the blood-brain and the blood-cerebrospinal fluid barriers: similarities and differences. *Fluids Barriers CNS* **8**, 3.

Reed, S. E., Hodgson, L. R., Song, S., May, M. T., Kelly, E. E., McCaffrey, M. W., Mastick, C. C., Verkade, P. and Tavaré, J. M. (2013). A role for Rab14 in the endocytic trafficking of GLUT4 in 3T3-L1 adipocytes. *J. Cell Sci.* **126**, 1931–1941.

Regazzi, R., Ravazzola, M., Iezzi, M., Lang, J., Zahraoui, A., Andereggen, E., Morel, P., Takai, Y. and Wollheim, C. B. (1996). Expression, localization and functional role of small GTPases of the Rab3 family in insulin-secreting cells. *J. Cell Sci.* **109(9)**, 2265–2273.

Robinson, J. S., Klionsky, D. J., Banta, L. M. and Emr, S. D. (1988). Protein sorting in Saccharomyces cerevisiae: isolation of mutants defective in the delivery and processing of multiple vacuolar hydrolases. *Mol. Cell Biol.* **8**, 4936–4948.

Ros-Baro, A., Lopez-Iglesias, C., Peiro, S., Bellido, D., Palacin, M., Zorzano, A. and Camps, M. (2001). Lipid rafts are required for GLUT4 internalization in adipose cells. *Proc. Natl. Acad. Sci. U.S.A* **98**, 12050–12055.

Rothnie, A., Clarke, A. R., Kuzmic, P., Cameron, A. and Smith, C. J. (2011). A sequential mechanism for clathrin cage disassembly by 70-kDa heat-shock cognate protein (Hsc70) and auxilin. *Proc. Natl. Acad. Sci. U.S.A* **108**, 6927–6932.

Sadowski, M. M. and Sarcevic, B. B. (2010). Mechanisms of mono- and poly-ubiquitination: Ubiquitination specificity depends on compatibility between the E2 catalytic core and amino acid residues proximal to the lysine. *Cell Div.* **5**, 19–19.

Sadacca, L. A., Bruno, J., Wen, J., Xiong, W. and McGraw, T. E. (2013). Specialized sorting of GLUT4 and its recruitment to the cell surface are independently regulated by distinct Rabs. *Mol. Biol. Cell* **24,** 2544–2557

Sakamoto, K. and Holman, G. D. (2008). Emerging role for AS160/TBC1D4 and TBC1D1 in the regulation of GLUT4 traffic. *Am. J. Physiol-Endoc. M.* **295**, E29–E37.

Sakane, A., Manabe, S., Ishizaki, H., Tanaka-Okamoto, M., Kiyokage, E., Toida, K., Yoshida, T., Miyoshi, J., Kamiya, H., Takai, Y., et al. (2006). Rab3 GTPase-activating protein regulates synaptic transmission and plasticity through the inactivation of Rab3. *Proc. Natl. Acad. Sci. U.S.A.* **103**, 10029–10034.

Sakisaka, T., Meerlo, T., Matteson, J., Plutner, H. and Balch, W. E. (2002). Rab-alphaGDI activity is regulated by a Hsp90 chaperone complex. *EMBO J.* **21**, 6125–6135.

Salminen, A. and Novick, P. J. (1987). A ras-like protein is required for a post-Golgi event in yeast secretion. *Cell* **49**, 527–538.

Saltiel, A. R. and Kahn, C. R. (2001). Insulin signalling and the regulation of glucose and lipid metabolism. *Nature* **414**, 799–806.

Sano, H. (2003). Insulin-stimulated Phosphorylation of a Rab GTPase-activating Protein Regulates GLUT4 Translocation. *J. Biol. Chem.* **278**, 14599–14602.

Sano, H., Eguez, L., Teruel, M. N., Fukuda, M., Chuang, T. D., Chavez, J. A., Lienhard, G. E. and McGraw, T. E. (2007). Rab10, a Target of the AS160 Rab GAP, Is Required for Insulin-Stimulated Translocation of GLUT4 to the Adipocyte Plasma Membrane. *Cell Metab.* **5**, 293–303.

Sano, H., Peck, G. R., Kettenbach, A. N., Gerber, S. A. and Lienhard, G. E. (2011). Insulin-stimulated GLUT4 Protein Translocation in Adipocytes Requires the Rab10 Guanine Nucleotide Exchange Factor Dennd4C. *J. Biol. Chem.* **286**, 16541–16545.

Sano, H., Roach, W. G., Peck, G. R., Fukuda, M. and Lienhard, G. E. (2008). Rab10 in insulin-stimulated GLUT4 translocation. *Biochem. J.* **411**, 89.

Sargeant, R. J. and Pâquet, M. R. (1993). Effect of insulin on the rates of synthesis and degradation of GLUT1 and GLUT4 glucose transporters in 3T3-L1 adipocytes. *Biochem. J.* **290 (Pt 3)**, 913–919.

Schmelzle, K., Kane, S., Gridley, S., Lienhard, G. E. and White, F. M. (2006). Temporal dynamics of tyrosine phosphorylation in insulin signaling. *Diabetes* **55**, 2171–2179.

Schlüter, O. M. (2004). A Complete Genetic Analysis of Neuronal Rab3 Function. *J. Neurosci.* **24**, 6629–6637.

Schlüter, O. M., Khvotchev, M., Jahn, R. and Südhof, T. C. (2002). Localization versus function of Rab3 proteins. Evidence for a common regulatory role in controlling fusion. *J. Biol. Chem.* **277**, 40919–40929.

Schonn, J. S., van Weering, J. R. T., Mohrmann, R., Schlüter, O. M., Südhof, T. C., de Wit, H., Verhage, M. and Sørensen, J. B. (2010). Rab3 proteins involved in vesicle biogenesis and priming in embryonic mouse chromaffin cells. *Traffic* **11**, 1415–1428.

Schwenk, R. W. and Eckel, J. (2007). A novel method to monitor insulin-

stimulated GTP-loading of Rab11a in cardiomyocytes. *Cell. Signal.* **19**, 825–830.

Scott, L. J., Mohlke, K. L., Bonnycastle, L. L., Willer, C. J., Li, Y., Duren, W. L., Erdos, M. R., Stringham, H. M., Chines, P. S., Jackson, A. U., et al. (2007). A genome-wide association study of type 2 diabetes in Finns detects multiple susceptibility variants. *Science* **316**, 1341–1345.

Seabra, M. C. and Coudrier, E. (2004). Rab GTPases and myosin motors in organelle motility. *Traffic* **5**, 393–399.

Semiz, S., Park, J. G., Nicoloro, S. M. C., Furcinitti, P., Zhang, C., Chawla, A., Leszyk, J. and Czech, M. P. (2003). Conventional kinesin KIF5B mediates insulin-stimulated GLUT4 movements on microtubules. *EMBO J.* **22**, 2387–2399.

Shields, S. B. and Piper, R. C. (2011). How Ubiquitin Functions with ESCRTs. *Traffic* **12**, 1306–1317.

Shepherd, P. R., Gnudi, L., Tozzo, E., Yang, H., Leach, F. and Kahn, B. B. (1993). Adipose cell hyperplasia and enhanced glucose disposal in transgenic mice overexpressing GLUT4 selectively in adipose tissue. *J. Biol. Chem.* **268**, 22243–22246.

Shewan, A. M., Mccann, R. K., Lamb, C. A., Stirrat, L., Kioumourtzoglou, D., Adamson, I. S., Verma, S., James, D. E. and Bryant, N. J. (2013). Endosomal sorting of GLUT4 and Gap1 is conserved between yeast and insulin-sensitive cells. *J. Cell Sci.* **126**, 1576–1582.

Shewan, A. M. A., van Dam, E. M. E., Martin, S. S., Luen, T. B. T., Hong, W. W., Bryant, N. J. N. and James, D. E. D. (2003). GLUT4 recycles via a trans-Golgi network (TGN) subdomain enriched in Syntaxins 6 and 16 but not TGN38: involvement of an acidic targeting motif. *Mol. Biol. Cell* **14**, 973–986.

Shi, J. and Kandror, K. V. (2005). Sortilin is essential and sufficient for the formation of Glut4 storage vesicles in 3T3-L1 adipocytes. *Dev. Cell* **9**, 99–108.

Shibasaki, T. & Seino, S. (2005) Physical and Functional interaction of Noc2/Rab3 in Exocytosis. *Methods Enzymol.* **403,** 408–419

Shin, H. W., Hayashi, M., Christoforidis, S., Lacas-Gervais, S., Hoepfner, S., Wenk, M. R., Modregger, J., Uttenweiler-Joseph, S., Wilm, M., Nystuen, A., et al. (2005). An enzymatic cascade of Rab5 effectors regulates phosphoinositide turnover in the endocytic pathway. *J. Cell Biol.* **170**, 607–618.

Shirataki, H., Kaibuchi, K., Sakoda, T., Kishida, S., Yamaguchi, T., Wada, K., Miyazaki, M. and Takai, Y. (1993). Rabphilin-3A, a putative target protein for smg p25A/rab3A p25 small GTP-binding protein related to synaptotagmin. *Mol. Cell Biol.* **13**, 2061–2068.

Shisheva, A. (2008). Phosphoinositides in insulin action on GLUT4 dynamics: not just PtdIns (3, 4, 5) P3. *Am. J. Physiol. Endocrinol. Metab.* **295**, E536–E544.

Shisheva, A., Sbrissa, D. and Ikonomov, O. (1999). Cloning, characterization, and expression of a novel Zn2+-binding FYVE finger-containing phospboinositide kinase in insulin-sensitive cells. *Mol. Cell Biol.* **19**, 623–634.

Simonsen, A., Gaullier, J. M., D'Arrigo, A. and Stenmark, H. (1999). The Rab5 effector EEA1 interacts directly with syntaxin-6. *J. Biol. Chem.* **274**, 28857–28860.

Slagsvold, T., Aasland, R., Hirano, S., Bache, K. G., Raiborg, C., Trambaiolo, D., Wakatsuki, S. and Stenmark, H. (2005). Eap45 in mammalian ESCRT-II binds ubiquitin via a phosphoinositide-interacting GLUE domain. *J. Biol. Chem.* **280**, 19600–19606.

Slot, J. W., Geuze, H. J., Gigengack, S., James, D. E. and Lienhard, G. E. (1991). Translocation of the glucose transporter GLUT4 in cardiac myocytes of the rat. *Proc. Natl. Acad. Sci. U.S.A.* **88**, 7815–7819.

Snider, J., Thibault, G. and Houry, W. A. (2008). The AAA+ superfamily of functionally diverse proteins. *Genome Biol.* **9**, 216.

Stahelin, R. V., Long, F., Diraviyam, K., Bruzik, K. S., Murray, D. and Cho, W. (2002). Phosphatidylinositol 3-phosphate induces the membrane penetration of the FYVE domains of Vps27p and Hrs. *J. Biol. Chem.* **277**, 26379–26388.

Stangl, S., Gehrmann, M., Dressel, R., Alves, F., Dullin, C., Themelis, G., Ntziachristos, V., Staeblein, E., Walch, A., Winkelmann, I., et al. (2011). In vivo imaging of CT26 mouse tumours by using cmHsp70.1 monoclonal antibody. *J. Cell. Mol. Med.* **15**, 874–887.

Stein, M., Pilli, M., Bernauer, S., Habermann, B. H., Zerial, M. and Wade, R. C. (2012). The interaction properties of the human Rab GTPase family--comparative analysis reveals determinants of molecular binding selectivity. *PLoS ONE* **7**, e34870.

Stenbit, A. E., Tsao, T. S., Li, J., Burcelin, R., Geenen, D. L., Factor, S. M., Houseknecht, K., Katz, E. B. and Charron, M. J. (1997). GLUT4 heterozygous knockout mice develop muscle insulin resistance and diabetes. *Nat. Med.* **3**, 1096–1101.

Stenmark, H. (2009). Rab GTPases as coordinators of vesicle traffic. *Nat Rev Mol. Cell Biol.* **10**, 513–525.

Stenmark, H. and Aasland, R. (1999). FYVE-finger proteins--effectors of an inositol lipid. *J. Cell Sci.* **112(23)**, 4175–4183.

Stenmark, H., Aasland, R., Toh, B. H. and D'Arrigo, A. (1996). Endosomal localization of the autoantigen EEA1 is mediated by a zinc-binding FYVE finger. *J. Biol. Chem.* **271**, 24048–24054.

Stenmark, H., Parton, R. G., Steele-Mortimer, O., Lütcke, A., Gruenberg, J. and Zerial, M. (1994). Inhibition of rab5 GTPase activity stimulates membrane fusion in endocytosis. *EMBO J.* **13**, 1287–1296.

Stöckli, J., Davey, J. R., Hohnen-Behrens, C., Xu, A., James, D. E. and Ramm, G. (2008). Regulation of Glucose Transporter 4 Translocation by the Rab Guanosine Triphosphatase-Activating Protein AS160/TBC1D4: Role of Phosphorylation and Membrane Association. *Mol. Endocrinol.* **22**, 2703–2715.

Stöckli, J., Fazakerley, D. J. and James, D. E. (2012). GLUT4 exocytosis. *J. Cell Sci.* **124**, 4147–4159.

Sun, L., Bittner, M. A. and Holz, R. W. (2003). Rim, a component of the presynaptic active zone and modulator of exocytosis, binds 14-3-3 through its N terminus. *J. Biol. Chem.* **278**, 38301–38309.

Sun, Y., Bilan, P. J., Liu, Z. and Klip, A. (2010). Rab8A and Rab13 are activated by insulin and regulate GLUT4 translocation in muscle cells. *Proc. Natl. Acad. Sci. U.S.A* **107**, 19909–19914.

Sun, Y., Chiu, T. T., Foley, K. P., Bilan, P. J. and Klip, A. (2014). Myosin Va mediates Rab8A-regulated GLUT4 vesicle exocytosis in insulin-stimulated muscle cells. *Mol. Biol. Cell*. **25**, 1159–1170.

Suzuki, K. and Kono, T. (1980). Evidence that insulin causes translocation of glucose transport activity to the plasma membrane from an intracellular storage site. *Proc. Natl. Acad. Sci. U.S.A.* **77**, 2542–2545.

Takahashi, S., Kubo, K., WAGURI, S., Yabashi, A., Shin, H. W., Katoh, Y. and Nakayama, K. (2012). Rab11 regulates exocytosis of recycling vesicles at the plasma membrane. *J. Cell Sci.* **125**, 4049–4057.

Takai, Y., Sasaki, T., Shirataki, H. and Nakanishi, H. (1996). Rab3A small GTP-binding protein in Ca^{2+}-dependent exocytosis. *Genes Cells* **1**, 615–632.

Tanaka, M., Miyoshi, J., Ishizaki, H., Togawa, A., Ohnishi, K., Endo, K., Matsubara, K., Mizoguchi, A., Nagano, T., Sato, M., et al. (2001). Role of Rab3 GDP/GTP exchange protein in synaptic vesicle trafficking at the mouse neuromuscular junction. *Mol. Biol. Cell* **12**, 1421–1430.

Teis, D. D., Saksena, S. S. and Emr, S. D. S. (2008). Ordered assembly of the ESCRT-III complex on endosomes is required to sequester cargo during MVB formation. *Dev. Cell* **15**, 578–589.

Tellam, J. T., Macaulay, S. L., McIntosh, S., Hewish, D. R., Ward, C. W. and James, D. E. (1997). Characterization of Munc-18c and syntaxin-4 in 3T3-L1 adipocytes. Putative role in insulin-dependent movement of GLUT-4. *J. Biol. Chem.* **272**, 6179–6186.

Terauchi, Y., Tsuji, Y., Satoh, S., Minoura, H., Murakami, K., Okuno, A., Inukai, K., Asano, T., Kaburagi, Y., Ueki, K., et al. (1999). Increased insulin sensitivity and hypoglycaemia in mice lacking the p85 alpha subunit of phosphoinositide 3-kinase. *Nat. Genet.* **21**, 230–235.

Thurmond, D. C., Ceresa, B. P., Okada, S., Elmendorf, J. S., Coker, K. and Pessin, J. E. (1998). Regulation of insulin-stimulated GLUT4 translocation by

Munc18c in 3T3L1 adipocytes. *J. Biol. Chem.* **273**, 33876–33883.

Thurmond, D. C., Kanzaki, M., Khan, A. H. and Pessin, J. E. (2000). Munc18c Function Is Required for Insulin-Stimulated Plasma Membrane Fusion of GLUT4 and Insulin-Responsive Amino Peptidase Storage Vesicles. *Mol. Cell Biol.* **20**, 379–388.

Torii, S., Zhao, S., Yi, Z., Takeuchi, T. and Izumi, T. (2002). Granuphilin modulates the exocytosis of secretory granules through interaction with syntaxin 1a. *Mol. Cell Biol.* **22**, 5518–5526.

Tsuboi, T. and Fukuda, M. (2006). The Slp4-a linker domain controls exocytosis through interaction with Munc18-1.syntaxin-1a complex. *Mol. Biol. Cell* **17**, 2101–2112.

Tuomilehto, J., Lindström, J., Eriksson, J. G., Valle, T. T., Hämäläinen, H., Ilanne-Parikka, P., Keinänen-Kiukaanniemi, S., Laakso, M., Louheranta, A. and Rastas, M. (2001). Prevention of type 2 diabetes mellitus by changes in lifestyle among subjects with impaired glucose tolerance. *New Eng. J. Med.* **344**, 1343–1350.

Ueki, K., Algenstaedt, P., Mauvais-Jarvis, F. and Kahn, C. R. (2000). Positive and negative regulation of phosphoinositide 3-kinase-dependent signaling pathways by three different gene products of the p85alpha regulatory subunit. *Mol. Cell Biol.* **20**, 8035–8046.

Ueki, K., Kondo, T. and Kahn, C. R. (2004). Suppressor of cytokine signaling 1 (SOCS-1) and SOCS-3 cause insulin resistance through inhibition of tyrosine phosphorylation of insulin receptor substrate proteins by discrete mechanisms. *Mol. Cell Biol.* **24**, 5434–5446.

Uhlig, M., Passlack, W. and Eckel, J. (2005). Functional role of Rab11 in GLUT4 trafficking in cardiomyocytes. *Mol. Cell Endocrinol.* **235**, 1–9.

Uldry, M., Ibberson, M., Horisberger, J. D., Chatton, J. Y., Riederer, B. M. and Thorens, B. (2001). Identification of a mammalian H(+)-myo-inositol symporter expressed predominantly in the brain. *EMBO J.* **20**, 4467–4477.

Untergasser, A., Nijveen, H., Rao, X., Bisseling, T., Geurts, R. and Leunissen, J. A. M. (2007). Primer3Plus, an enhanced web interface to Primer3. *Nucleic Acids Res.* **35**, W71–W74.

Vadlamudi, R. K., Wang, R. A., Talukder, A. H., Adam, L., Johnson, R. and Kumar, R. (2000). Evidence of Rab3A expression, regulation of vesicle trafficking, and cellular secretion in response to heregulin in mammary epithelial cells. *Mol. Cell Biol.* **20**, 9092–9101.

van Dam, E. M. E. and Stoorvogel, W. W. (2002). Dynamin-dependent transferrin receptor recycling by endosome-derived clathrin-coated vesicles. *Mol. Biol. Cell* **13**, 169–182.

van IJzendoorn, S. C. D., Tuvim, M. J., Weimbs, T., Dickey, B. F. and Mostov,

K. E. (2002). Direct interaction between Rab3b and the polymeric immunoglobulin receptor controls ligand-stimulated transcytosis in epithelial cells. *Dev. Cell* **2**, 219–228.

van Weering, J. R. T., Toonen, R. F. and Verhage, M. (2007). The Role of Rab3a in Secretory Vesicle Docking Requires Association/Dissociation of Guanidine Phosphates and Munc18-1. *PLoS ONE* **2**, e616.

Vale, R. D., Reese, T. S. and Sheetz, M. P. (1985). Identification of a novel force-generating protein, kinesin, involved in microtubule-based motility. *Cell* **42**, 39–50.

Vander Haar, E., Lee, S. I., Bandhakavi, S., Griffin, T. J. and Kim, D. H. (2007). Insulin signalling to mTOR mediated by the Akt/PKB substrate PRAS40. *Nat. Cell Biol.* **9**, 316–323.

Vannucci, S. J., Maher, F. and Simpson, I. A. (1997). Glucose transporter proteins in brain: Delivery of glucose to neurons and glia. *Glia* **21**, 2–21.

Vassilopoulos, S., Esk, C., Hoshino, S., Funke, B. H., Chen, C.-Y., Plocik, A. M., Wright, W. E., Kucherlapati, R. and Brodsky, F. M. (2009). A role for the CHC22 clathrin heavy-chain isoform in human glucose metabolism. *Science* **324**, 1192–1196.

Vincze, T., Posfai, J. and Roberts, R. J. (2003). NEBcutter: A program to cleave DNA with restriction enzymes. *Nucleic Acids Res.* **31**, 3688–3691.

Vitale, G., Rybin, V., Christoforidis, S., Thornqvist, P., McCaffrey, M., Stenmark, H. and Zerial, M. (1998). Distinct Rab-binding domains mediate the interaction of Rabaptin-5 with GTP-bound Rab4 and Rab5. *EMBO J.* **17**, 1941–1951.

Vollenweider, P., Martin, S. S., Haruta, T., Morris, A. J., Nelson, J. G., Cormont, M., Le Marchand-Brustel, Y., Rose, D. W. and Olefsky, J. M. (1997). The small guanosine triphosphate-binding protein Rab4 is involved in insulin-induced GLUT4 translocation and actin filament rearrangement in 3T3-L1 cells. *Endocrinology* **138**, 4941–4949.

Vosseller, K., Wells, L., Lane, M. D. and Hart, G. W. (2002). Elevated nucleocytoplasmic glycosylation by O-GlcNAc results in insulin resistance associated with defects in Akt activation in 3T3-L1 adipocytes. *Proc. Natl. Acad. Sci. U.S.A.* **99**, 5313–5318.

Walgren, J. L. E., Vincent, T. S., Schey, K. L. and Buse, M. G. (2003). High glucose and insulin promote O-GlcNAc modification of proteins, including alpha-tubulin. *Am. J. Physiol. Endocrinol. Metab.* **284**, E424–E434.

Wallberg-Henriksson, H. and Zierath, J. R. (2001). GLUT4: a key player regulating glucose homeostasis? Insights from transgenic and knockout mice. *Mol. Membr. Biol.* **18**, 205–211.

Wang, Y., Okamoto, M., Schmitz, F., Hofmann, K. and Südhof, T. C. (1997). Rim is a putative Rab3 effector in regulating synaptic-vesicle fusion. *Nature* **388**, 593–598.

Weber, E., Jilling, T. and Kirk, K. L. (1996). Distinct functional properties of Rab3A and Rab3B in PC12 neuroendocrine cells. *J. Biol. Chem.* **271**, 6963–6971.

White, M. F. (1998). The IRS-signalling system: a network of docking proteins that mediate insulin action. *Mol. Cell. Biochem.* **182**, 3–11.

Whitley, P. R., Reaves, B. J., Hashimoto, M., Riley, A. M., Potter, B. V. L. and Holman, G. D. (2003). Identification of mammalian Vps24p as an effector of phosphatidylinositol 3,5-bisphosphate-dependent endosome compartmentalization. *J. Biol. Chem.* **278**, 38786–38795.

Whitman, M., Downes, C. P., Keeler, M., Keller, T. and Cantley, L. (1988). Type I phosphatidylinositol kinase makes a novel inositol phospholipid, phosphatidylinositol-3-phosphate. *Nature* **332**, 644–646.

Wick, K. R., Werner, E. D., Langlais, P., Ramos, F. J., Dong, L. Q., Shoelson, S. E. and Liu, F. (2003). Grb10 inhibits insulin-stimulated insulin receptor substrate (IRS)-phosphatidylinositol 3-kinase/Akt signaling pathway by disrupting the association of IRS-1/IRS-2 with the insulin receptor. *J. Biol. Chem.* **278**, 8460–8467.

Williams, D., Hicks, S. W., Machamer, C. E. and Pessin, J. E. (2006). Golgin-160 is required for the Golgi membrane sorting of the insulin-responsive glucose transporter GLUT4 in adipocytes. *Mol. Biol. Cell* **17**, 5346–5355.

Williams, R. L. and Urbé, S. (2007). The emerging shape of the ESCRT machinery. *Nat. Rev. Mol. Cell Biol.* **8**, 355–368.

Wittinghofer, A. and Vetter, I. R. (2011). Structure-function relationships of the G domain, a canonical switch motif. *Annu. Rev. Biochem.* **80**, 943–971.

Wu, M., Wang, T., Loh, E., Hong, W. and Song, H. (2005). Structural basis for recruitment of RILP by small GTPase Rab7. *EMBO J.* **24**, 1491–1501.

Xie, X., Gong, Z., Mansuy-Aubert, V., Zhou, Q. L., Tatulian, S. A., Sehrt, D., Gnad, F., Brill, L. M., Motamedchaboki, K., Chen, Y., et al. (2011). C2 domain-containing phosphoprotein CDP138 regulates GLUT4 insertion into the plasma membrane. *Cell Metab.* **14**, 378–389.

Xu, Y., Rubin, B. R., Orme, C. M., Karpikov, A., Yu, C., Bogan, J. S. and Toomre, D. K. (2011). Dual-mode of insulin action controls GLUT4 vesicle exocytosis. *J. Cell Biol.* **193**, 643–653.

Yaekura, K., Julyan, R., Wicksteed, B. L., Hays, L. B., Alarcon, C., Sommers, S., Poitout, V., Baskin, D. G., Wang, Y., Philipson, L. H., et al. (2003). Insulin secretory deficiency and glucose intolerance in Rab3A null mice. *J. Biol. Chem.* **278**, 9715–9721.

Ye, J., Coulouris, G., Zaretskaya, I., Cutcutache, I., Rozen, S. and Madden, T. L. (2012). Primer-BLAST: a tool to design target-specific primers for polymerase chain reaction. *BMC Bioinformatics* **13**, 134.

Yeh, T. Y. J., Sbodio, J. I., Tsun, Z. Y., Luo, B. and Chi, N. W. (2007). Insulin-stimulated exocytosis of GLUT4 is enhanced by IRAP and its partner tankyrase. *Biochem. J.* **402**, 279–290.

Yip, M. F., Ramm, G., Larance, M., Hoehn, K. L., Wagner, M. C., Guilhaus, M. and James, D. E. (2008). CaMKII-mediated phosphorylation of the myosin motor Myo1c is required for insulin-stimulated GLUT4 translocation in adipocytes. *Cell Metab.* **8**, 384–398.

Yoshimura, R., Araki, E., Ura, S., Todaka, M., Tsuruzoe, K., Noboru, F., Motoshima, H., Yoshizato, K., Kaneko, K. and Matsuda, K. (1997). Impact of natural IRS-1 mutations on insulin signals: mutations of IRS-1 in the PTB domain and near SH2 protein binding sites result in impaired function at different steps of IRS-1 signaling. *Diabetes* **46**, 929–936.

Yoshimura, S. I., Gerondopoulos, A., Linford, A., Rigden, D. J. and Barr, F. A. (2010). Family-wide characterization of the DENN domain Rab GDP-GTP exchange factors. *J. Cell Biol.* **191**, 367–381.

Yu, H., Rathore, S. S., Davis, E. M., Ouyang, Y. and Shen, J. (2013). Doc2b promotes GLUT4 exocytosis by activating the SNARE-mediated fusion reaction in a calcium- and membrane bending-dependent manner. *Mol. Biol. Cell* **24**, 1176–1184.

Zamborlini, A., Usami, Y., Radoshitzky, S. R., Popova, E., Palu, G. and Göttlinger, H. (2006). Release of autoinhibition converts ESCRT-III components into potent inhibitors of HIV-1 budding. *Proc. Natl. Acad. Sci. U.S.A.* **103**, 19140–19145.

Zeigerer, A., Lampson, M. A., Karylowski, O., Sabatini, D. D., Adesnik, M., Ren, M. and McGraw, T. E. (2002). GLUT4 retention in adipocytes requires two intracellular insulin-regulated transport steps. *Mol. Biol. Cell* **13**, 2421–2435.

Zerial, M. and McBride, H. (2001). Rab proteins as membrane organizers. *Nat. Rev. Mol. Cell Biol.* **2**, 107–117.

Zhao, F. Q. and Keating, A. F. (2007). Functional properties and genomics of glucose transporters. *Curr. Genomics* **8**, 113–128.

Zhao, P., Yang, L., Lopez, J. A., Fan, J., Burchfield, J. G., Bai, L., Hong, W., Xu, T. and James, D. E. (2009). Variations in the requirement for v-SNAREs in GLUT4 trafficking in adipocytes. *J. Cell Sci.* **122**, 3472–3480.

Ziel, F. H., Venkatesan, N. and Davidson, M. B. (1988). Glucose transport is rate limiting for skeletal muscle glucose metabolism in normal and STZ-induced diabetic rats. *Diabetes* **37**, 885–890.

Zolov, S. N., Bridges, D., Zhang, Y., Lee, W.-W., Riehle, E., Verma, R., Lenk,

G. M., Converso-Baran, K., Weide, T., Albin, R. L., et al. (2012). In vivo, Pikfyve generates PI(3,5)P2, which serves as both a signaling lipid and the major precursor for PI5P. *Proc. Natl. Acad. Sci. U.S.A.* **109**, 17472–17477.

Zou, L., Zhou, J., Zhang, J., Li, J., Liu, N., Chai, L., Li, N., Liu, T., Li, L., Xie, Z., et al. (2009). The GTPase Rab3b/3c-positive recycling vesicles are involved in cross-presentation in dendritic cells. *Proc. Natl. Acad. Sci. U.S.A* **106**, 15801–15806.

Zuker, M. (2003). Mfold web server for nucleic acid folding and hybridization prediction. *Nucleic Acids Res.* **31**, 3406–3415.

Supplementary section

Gene/Target	Vector	Cloning primers 5' – 3'
Rab3B	pcDNA3.1	CAAGGATCCGAGATGGCCTCAGTAAC (sense); CAGCTCGAGCTAGCAAGAGCAGTT C (antisense)
Rab3B ^{Q8L}	pcDNA3.1	ACACGGCAGGGCTAGAGCGATATCG (sense); CGATATCGCTCTAGCCCTGCCGTGT (antisense)
Rab3B ^{T36N}	pcDNA3.1	GCAGCGTCGGGAAGAACTCCTTCCTTTTCCG (sense); CGGAAAAGGAAGGAGTTCTTCCCGACGCTGC (antisense)
Noc2	pHM6	CGCACGAAGCTTTATGGCTGACACCATCT (sense); TGAATGCGGCCGCTCAGTAATGGGTAG (antisense)
Noc2 ^{AAA}	pHM6	GGTCTGGAAGAGGTCAGGGGCCGCGGCCGCCAAAGG GCTCCCCAAGTACATC (sense); GATGTACTTGGGGAGCCCTTTGGCGGCCGCGGCCCCT GACCTCTTCCAGACC (antisense)
Noc2	pGEX4T-1	CGCATCGAATCCATGGCTGACACCATC (sense); GCAGCCCTCGAGTCAGTAATGGGTAG (antisense)
Noc2	p3XFLAG	GCCGCGAAGCTTATGGCTGACACCATCTT (sense); GTGCCGGATCCTCAGTAATGGGTAGTTGCC (antisense)
Noc2	pAT109	CGGCGGGATCCATGGCTGACACCATCTT (sense); GCCGGGGTACCGTAATGGGTAGTTGCC (antisense)
Noc2	pMAL-c2	CGGCGGGATCCATGGCTGACACCATCTT (sense); GCAGCCCTCGAGTCAGTAATGGGTAG (antisense)

S1: Primers designed for cloning. The table shows the list of primers designed for cloning the Rab3B and Noc2 genes in the different vectors. *Rattus norvegicus* gene sequences were obtained from NCBI. Primers were designed using Northwestern University's OigoCalc software to calculate the Tm and identify any undesired self-complementarity. Primers were ordered from Invitrogen or MWG Biotech.

Gene	Sequence ID	qPCR primers 5' – 3'
Rab3A	NM_013018.2	GCCAGCGTTGTCTCAGTTTA (sense); AATGAGGTTTTGCCCACACT (antisense)
Rab3B	NM_031091.2	CAGGTTACTGTGTGGGTGAAGA (sense); TGGGAGTTGTATCTTGGTAAATGA (antisense)
Rab3C	NM_133536.1	AAGGAAGTCTTTGATGTCAGTGG (sense); TGCAAGTAGCAGGTGTTTATAGATG (antisense)
Rab3D	NM_080580.2	ACCTGTCCTTCTTGCCTCTTC (sense); GAGAGAAAGGGAGCTGAACTTG (antisense)
Rab10	NM_017359.2	TGTGACATGGACGACAAGAGA (sense); TACCATGCTCCCTTGCAATCT (antisense)
Rab27A	NM_017317.2	GAGTGGGGAAGACCAGTGT (sense); ACACCACTCTCTTTTCCCTGAA (antisense)
Rab27B	NM_053459.1	GGACACTGCTGGACAAGAG (sense); TTGACTCATCCAGTTTCTGACATT (antisense)
Noc2	NM_133591.2	CCCCTGTGGCTGTGTAAGAT (sense); CTTGGGGAGCCCTTTGTAGA (antisense)
RIM1	NM_052829.1	CTTACCAGGGCAACTCTCAGT (sense); CTGGGACGGCCATCTACTC (antisense)
RIM2	AF199322	CCACAGGGATGGAAGGGATT (sense); TCTAGGAGAGGCCGTTGTTC (antisense)
Granuphilin	NM_080410.1	GAGAATGCCGAGTTCTGGAG (sense); CCAGTTGCTTTCTTCAGCTCTAT (antisense)
Rabphilin3A	NM_133518.1	GCTCTCTATGAGGAGGAGCA (sense); CATGAGGGACACCAGGATCT (antisense)
28S rRNA	NM_001047909.1	TTCACATCGTGGAGGATGATCT (sense); TACACAGTGAAACTTGCCACC (antisense)

S2: Primers selected for qPCR study. The table shows the list of primers selected for quantitating the amount of cDNA of the desired genes. Primer gene IDs correspond to NCBI's reference sequence ID or Genbank ID, both of which are searchable in NCBI. Two sets of primers were designed and validated in tissues that expressed the desired gene *(Materials and Methods 2.2.2.5)*. The selected primers were checked for primer efficiency, self-complementarity and the ability to yield a better Ct value than the other set of primers.

S3: Sequencing results of the Noc2^{AAA} construct. Following site directed mutagenesis, the Noc2 ^{AAA} construct was sequenced to confirm correct insertion of the triple alanine residues. The figure shows the (shaded) primer for generating the mutant using the wild type Noc2 sequence as a template. The sequencing results shown for the Noc ^{AAA} construct confirm correct site directed mutagenesis.

A

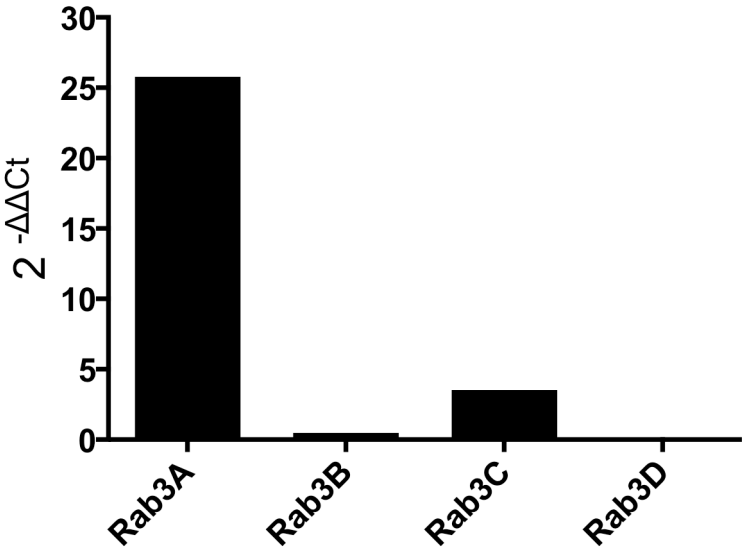

B

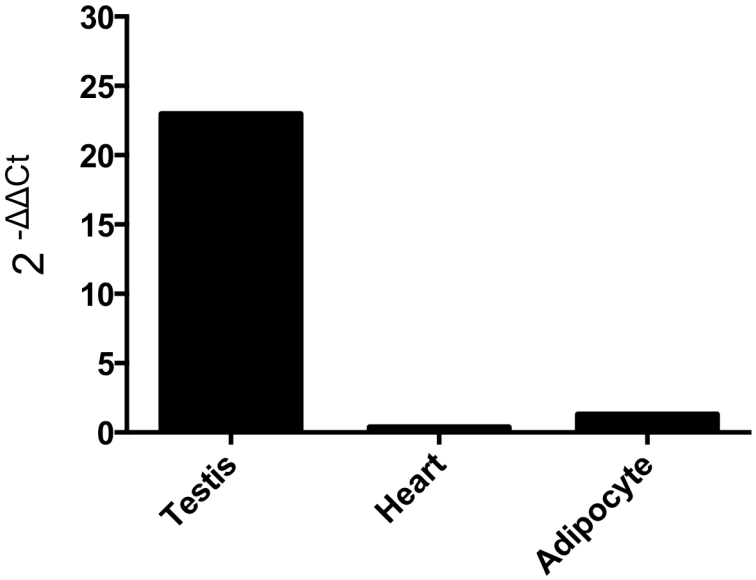

S4: Validation of Rab3 and Noc2 primers in rat tissues. mRNA from rat tissues was isolated using the TRIzol®-chloroform method. cDNA was generated by reverse transcription and 5 ng of cDNA was tested using a qPCR approach to quantify gene expression levels. cDNA was prepared as described in *Materials and Methods 2.2.2.3*. Primers for quantitating the cDNA levels of Rab3 were validated in rat brain ***(A)*** while for Noc2, primers were validated in rat testes and compared with heart and adipocyte levels ***(B)***.

A

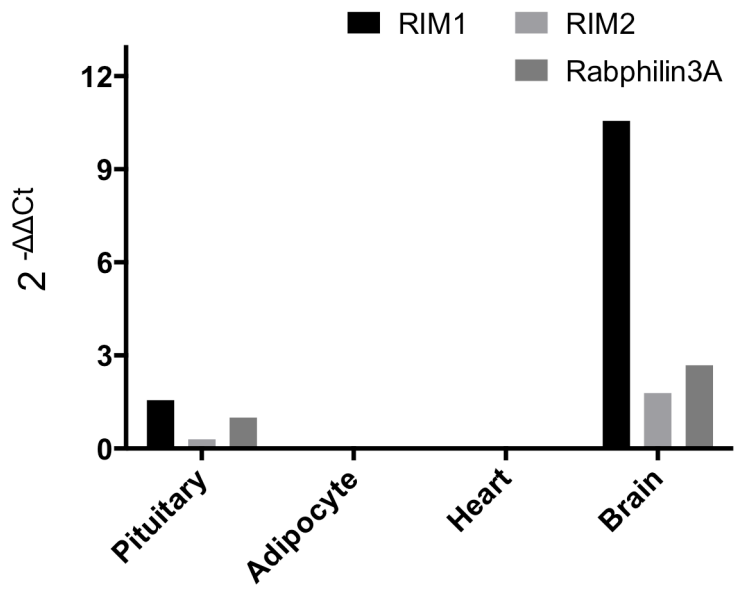

B

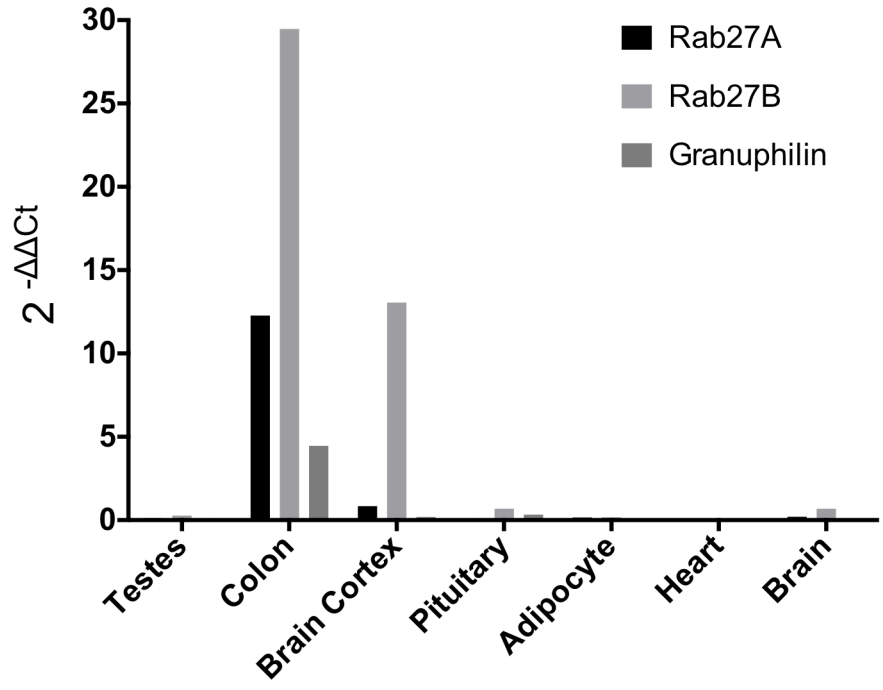

S5: Tissue qPCR profile of Rab3 effectors. mRNA from rat tissues was isolated using the TRIzol®-chloroform method. cDNA was generated by reverse transcription and 5 ng of cDNA was tested using a qPCR approach to quantify gene expression levels. cDNA was prepared as described in *Materials and Methods 2.2.2.3*. A qPCR profile was generated using a number of rat tissues. Potential Rab3 effectors were analysed with primers listed in *Supplementary table S2*. Rab27, which was previously been shown by others to co-exist with Rab3 in a number of tissues, was also profiled in this study.

A

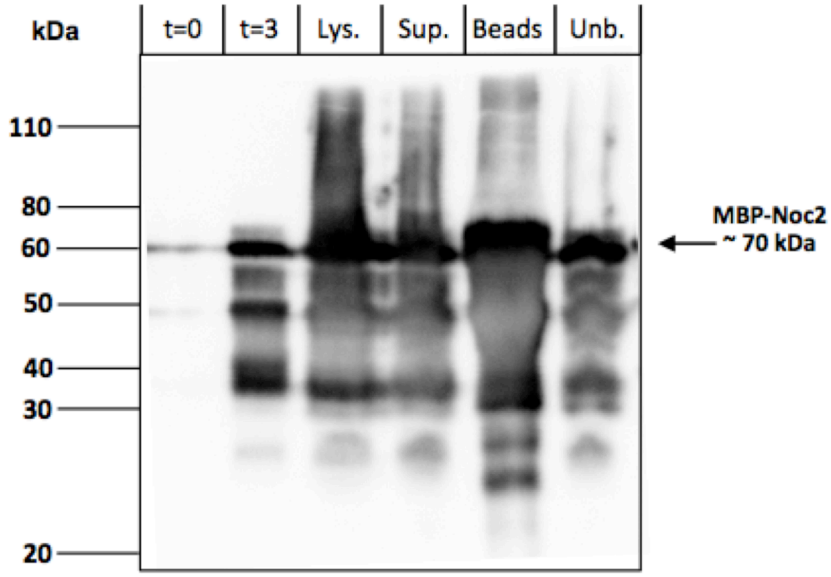

B

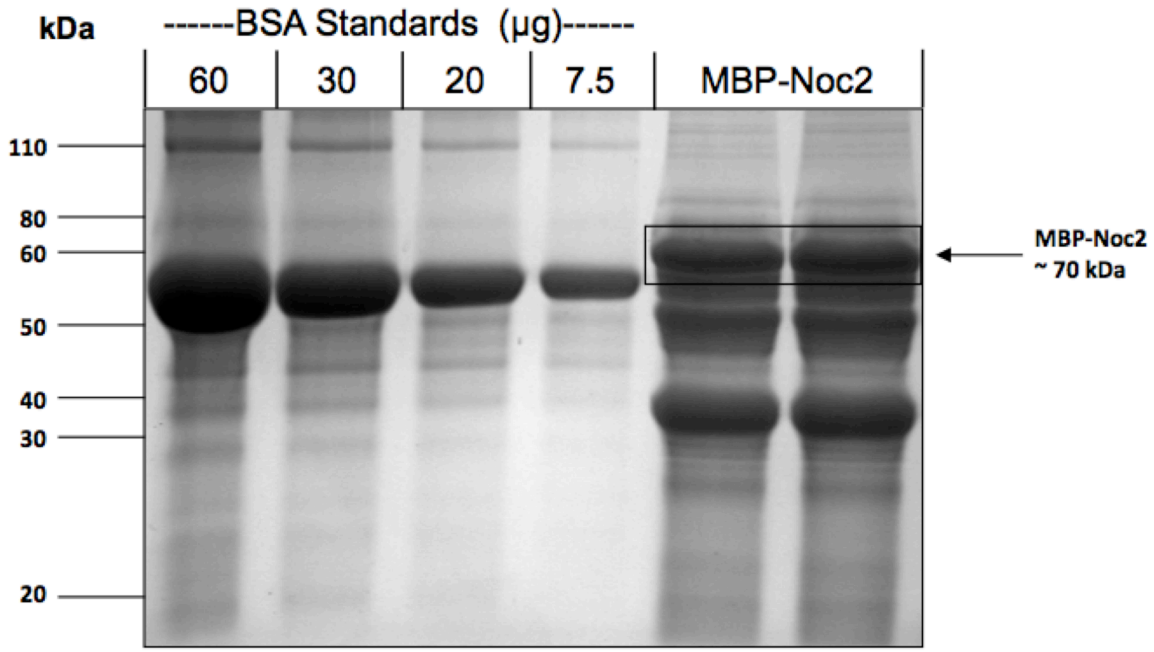

S6: Expression and purification of MBP-Noc2. MBP-Noc2 was cloned into the pMAL-c2 bacterial gene expression system. The cloned construct was verified by sequencing. For expression of the MBP-Noc2, the construct was transformed into *E.coli* TB1 cells. Expression of the fusion protein was induced with 0.3 mM IPTG (final) and carried out at room temperature for 3 h. Purification was done using an amylose resin (beads). The figure ***A*** shows a western blot with the different stages of expression and purification. The western blot was probed with an anti-MBP antibody which identified MBP-Noc2 at ~70 kDa ***(A)***. MBP-Noc2 was quantified on a 10% SDS-PAGE coomassie gel using BSA standards ***(B)*** to yield 10 µg of MBP-Noc2 per 50 µl of resin slurry per 2 l culture. The total amount of slurry was 1.5 ml.

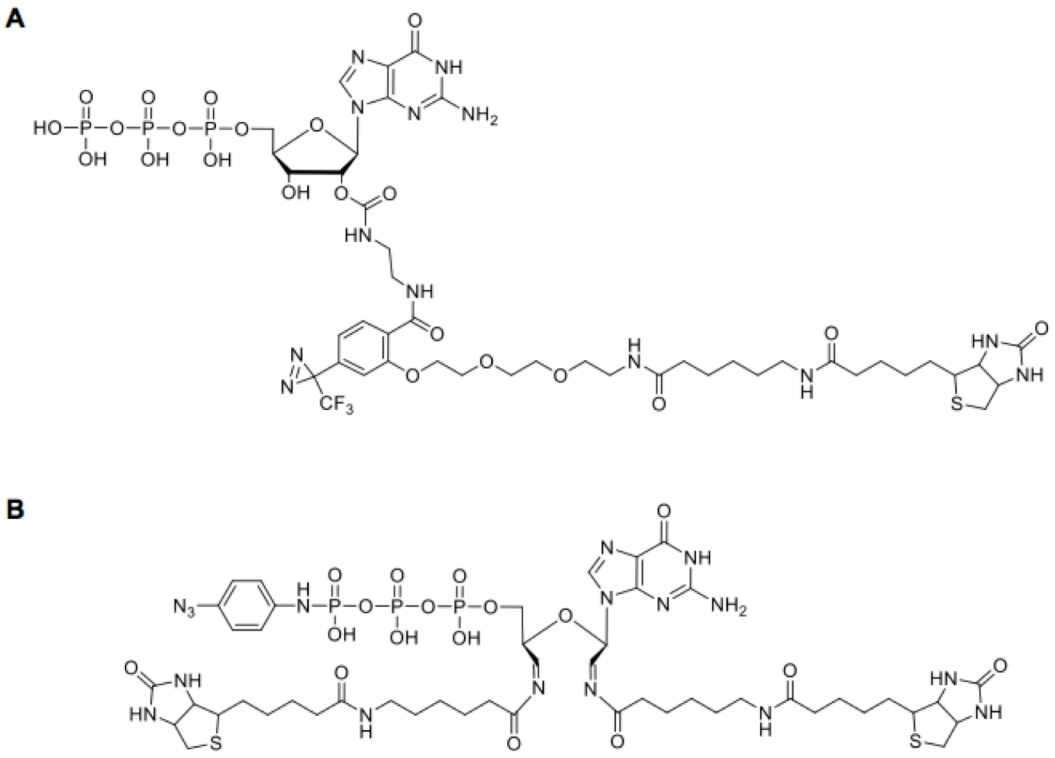

S7: Structure of GTP photolabels. Bio-ATB-GTP is substituted on the ribose hydroxyls 2/3-OH with both the photolabelling diazirine group and a biotin moiety ***(A)*****.** Azidoanilide-GTP biotin-hydrozone is substituted in the terminal phosphate of oxidized GTP with a photolabelling azide group while the biotin moiety is substituted onto the ribose aldehydes from oxidation to form biotin hydrazones ***(B)*** (the structure is re-drawn from reference Schwenk et al 2007).

OPEN ACCESS Freely available online

PLOS ONE

GLUT4 Traffic through an ESCRT-III-Dependent Sorting Compartment in Adipocytes

Françoise Koumanov*, Vinit J. Pereira, Paul R. Whitley, Geoffrey D. Holman

Department of Biology and Biochemistry, University of Bath, Bath, United Kingdom

Abstract

In insulin target tissues, GLUT4 is known to traffic through multiple compartments that may involve ubiquitin- and/or SUMO-dependent targeting. During these trafficking steps, GLUT4 is sorted into a storage reservoir compartment that is acutely released by insulin signalling processes that are downstream of PI 3-kinase associated changes in inositol phospholipids. As ESCRT components have recently been found to influence cellular sorting processes that are related to changes in both ubiquitination and inositol phospholipids, we have examined whether GLUT4 traffic is routed through ESCRT dependent sorting steps. Introduction of the dominant negative inhibitory constructs of the ESCRT-III components CHMP3 (CHMP3(1–179)) and Vps4 (GFP-Vps4^{E235Q}) into rat adipocytes leads to the accumulation of GLUT4 in large, coalesced and extended vesicles structures that co-localise with the inhibitory constructs over large parts of the extended structure. A new swollen hybrid and extensively ubiquitinated compartment is produced in which GLUT4 co-localises more extensively with the endosomal markers including EEA1 and transferrin receptors but also with the TGN marker syntaxin6. These perturbations are associated with failure of insulin action on GLUT4 traffic to the cell surface and suggest impairment in an ESCRT-dependent sorting step used for GLUT4 traffic to its specialised reservoir compartment.

Citation: Koumanov F, Pereira VJ, Whitley PR, Holman GD (2012) GLUT4 Traffic through an ESCRT-III-Dependent Sorting Compartment in Adipocytes. PLoS ONE 7(9): e44141. doi:10.1371/journal.pone.0044141

Editor: Jean Gruenberg, University of Geneva, Switzerland

Received March 13, 2012; **Accepted** July 30, 2012; **Published** September 25, 2012

Funding: This study was supported by Wellcome Trust (081168/Z/06/Z) and Diabetes UK (08/0003788). The funders had no role in study design, data collection and analysis, decision to publish, or preparation of the manuscript.

Competing Interests: The authors have declared that no competing interests exist.

* E-mail: f.koumanov@bath.ac.uk

Introduction

The Endosomal Sorting Complex Required for Transport (ESCRT) is essential for membrane compartment and membrane protein organisation [1]. ESCRT proteins are conserved in organisms ranging from archaea to eukaryotes where they fulfil a range of diverse roles [1,2]. The ESCRT system has been implicated in processes that include lysosome biogenesis via multivesicular body (MVB) formation [3], cytokinesis [4,5], enveloped virus budding [6] and autophagy [7]. A common functional role for the protein components of the system is the deformation of membrane lipids and the generation of invaginated membrane structures including membrane tubes, buds and multivesicular endosomes (MVE) [1]. The complexes are also involved in membrane protein sorting and with selection of cargo membrane proteins for degradation, recycling to the plasma membrane or the trans-Golgi network (TGN).

The four ESCRT complexes include ESCRT-0, ESCRT-I, ESCRT-II and ESCRT-III which are recruited sequentially to membranes, particularly membranes of the endosome system that are rich in phosphatidylinositol 3-phosphate (PI(3)P). Components of ESCRT-0 have ubiquitin interacting motifs (UIM) and ubiquitin binding domains (VHS) and these are thought to facilitate the gathering of ubiquitinated cargo proteins into membrane patches [8]. ESCRT-I and ESCRT-II continue the process of concentrating membrane proteins while Charged Multivesicular Body Protein (CHMP) components of ESCRT-III allow membrane sorting and membrane deformation. The CHMP proteins of ESCRT-III include CHMP4, CHMP3 and CHMP2. These proteins can be autoinhibited through interactions between their N- and C-terminal domains [9,10]. Removal of this autoinhibition allows the separate roles of the N- and C-termini to be manifest [11]. C-terminal regions of both CHMP3 and CHMP4 bind the ESCRT-III regulator Vps4 [12] and the de-ubiquitinating hydrolases (DUBs) including AMSH [9,13]. The CHMP protein positively charged N-terminal regions interact with negatively charged phosphoinositides including phosphatidylinositol 3,5-bisphosphate (PI(3,5)P_2) and this association may allow a number of specific lipid targeting processes [11,14].

ESCRT dependent selection of cargo appears to be associated with ubiquitination cycles involving ubiquitin ligases and DUBs [15,16] (including AMSH and USP8 in mammals [13]). Similar considerations probably apply to the handling of SUMOylated cargos, including Top1, by ESCRT proteins [17], but this has not been widely studied. The sorting role for ubiquitin-like domains in GLUT4 traffic is beginning to emerge from recent studies [18–22] but the possibility of ESCRT-dependent sorting of the tagged GLUT4 has not been previously addressed. Here we provide evidence that GLUT4 is routed through an ESCRT compartment in insulin-target cells and that perturbation of this traffic leads to a failure of GLUT4 to reach its normal intracellular storage vesicle compartment (GSVs) and by an inability of GLUT4 to be recruited to the cell surface upon insulin stimulation.

Materials and Methods

DNA constructs

pCis2 HA-GLUT4 was a gift from Dr. Samuel Cushman and has been described previously [23]. pEGFP-C1-VPS4, pEGFP-C1-VPS4^{E235Q} and pEGFP-N1-CHMP3$^{1–179}$ constructs have been described previously [5,11].

Antibodies

Rabbit polyclonal GLUT4 antibody was raised against a GLUT4 C-terminal peptide [24]. Mouse anti HA antibody (Clone 16B12) was purchased from Covance, mouse anti-EEA1 antibody from BD Biosciences, mouse anti-Ubiquitin antibody (Clone FK2) from BIOMOL, mouse anti-Syntaxin 6 antibody from BD Biosciences and mouse anti-Transferrin receptor (TfR) antibody from Zymed. AlexaFluor 546 conjugated goat anti-mouse IgG and Alexa Fluor 633 conjugated goat anti-rabbit IgG were from Molecular Probes. Mouse IgG secondary antibody β-galactosidase conjugate was from SouthernBiotech.

Isolation of primary rat adipocytes

Adipose cells from epididymal fat pads of male Wistar rats, weighing 180–200 g, were prepared by collagenase digestion as described previously [25]. Cells were maintained at 37°C in Krebs-Ringer-HEPES (KRH) buffer (140 mM NaCl, 4.7 mM KCl, 2.5 mM $CaCl_2$, 1.25 mM $MgSO_4$, 2.5 mM NaH_2PO_4, 10 mM HEPES, (pH 7.4)) with 1% (w/v) bovine serum albumin (BSA) and 200 nM adenosine. Before transfection the cells were washed twice with DMEM supplemented with 200 nM adenosine and brought to a 50% cytocrit.

Adipocyte transfection

Rat adipocytes were electroporated with pCis2 HA-GLUT4 alone or together with pEGFP-VPS4, pEGFP-VPS4^{E235Q} or pEGFP-CHMP3$^{1–179}$ according to the method described by Al-Hasani et al. [23]. Briefly, 200 µl of 50 % cytocrit rat adipocytes were added to 200 µl of DMEM containing 100 µg of carrier DNA (hearing sperm DNA, Promega) and 0.1 µg of pCis2 HA-GLUT4 alone or together with 0.8 µg of pEGFP-VPS4, pEGFP-VPS4^{E235Q} or pEGFP-CHMP3$^{1–179}$. The amounts of HA-GLUT4 and inhibitory construct cDNA were optimised as described [23]. Electroporation was carried out using the BioRad Gene pulser with a capacitance extender attached in 0.4-cm gap-width cuvettes (Bio-Rad). Each cuvette was electroporated once at 400 V, 500 µF. Cells from 4 to 5 cuvettes were pooled together, washed once with DMEM supplemented with 200 nM adenosine and then resuspended in DMEM supplemented with 3.5 % BSA and 200 nM adenosine. The transfected adipocytes were incubated for 5 h at 37°C. After washing in KRH buffer supplemented with 1% BSA and 200 nM adenosine cells were left un-stimulated or stimulated with 60 nM insulin for 20 min at 37°C. Using the above described electroporation conditions we obtained 20 to 25 % transfection efficiency as estimated by examining the cells by fluorescent microscopy and recording GFP positive cells.

Determination of HA-GLUT4 antibody binding

Transfected rat adipocytes, left un-stimulated or stimulated with 60 nM insulin, were incubated in presence of 2 mM KCN for 3 min to stop GLUT4 recycling. Cells were then incubated with 1 µg/ml anti-HA antibody in Krebs-Ringer-HEPES buffer supplemented with 5% BSA and 200 nM adenosine for 1 h at room temperature with occasional mixing. After three washes in Krebs-Ringer-HEPES buffer supplemented with 5% BSA and 200 nM adenosine, adipocytes were incubated with 1 µg/ml anti-mouse IgG secondary antibody β-galactosidase conjugate. Cells were then washed in Krebs-Ringer-HEPES buffer supplemented with 200 nM adenosine 4 times and 10 µl of cell suspension were added in quadruplicated in black 96 well plates (Fluotrac 200, Greiner). Fluorescein digalactosidase (FDG) at a final concentration of 0.1 mM in Krebs-Ringer-HEPES buffer was added to each well. The rates of fluorescence generated per mg protein were then determined from measurements (for an hour at 15 sec intervals) in a Pherastar (FS) fluorescent plate reader (BMG) at 520 nm. An aliquot of cells from each condition was analyzed by immunoblotting to assess and normalize for the level of expression of HA-GLUT4 cDNA.

Indirect immunofluorescence microscopy

Stimulated adipocytes were fixed by incubation with 4% (w/v) paraformaldehyde in KRH buffer for 20 min at room temperature, and washed 3 times with PBS. Cells were then treated with permeabilisation buffer (0.1% saponin, 1% (w/v) BSA, 3% (v/v) goat serum in PBS) for 45 min. The co-localisation of the EGFP tagged constructs with GLUT4 and cell organelle markers was determined in adipocytes that were incubated with primary antibodies diluted in permeabilisation buffer overnight at 22°C. The primary antibodies were used at the following dilutions: rabbit anti GLUT4 antibody (1:1000), mouse anti HA antibody (1:500), mouse anti-EEA1 antibody (1:250), mouse anti-Ubiquitin antibody (1:400), mouse anti-Syntaxin 6 antibody (1:200) and mouse anti-Transferrin receptor antibody (1:100). 18 hours later, the cells were washed in permeabilisation buffer, incubated with species-specific fluorophore conjugated secondary antibodies (1:300 dilution) for 2 h at room temperature with a final wash step in permeabilisation buffer. Cells were mounted onto a glass coverslip with Vectashield mounting medium (Vector Laboratories).

Confocal microscopy was performed on a Zeiss LSM 510 META microscope with 63×1.4 NA oil-immersion objective and with dual or triple laser excitation at 458–488, 543 and 633 nm. Images (1024×942) of individual cells were saved as TIFF files using the Zeiss LSM Image analysis software and intensity levels of the individual channels were adjusted to comparable dynamic range [26] in Adobe Photoshop.

To measure the extent of enlargement of vesicles in which the fluorescent signals from EGFP-VPS4^{E235Q}, endogenous GLUT4 and endosomal markers co-localised, individual cells were analysed with the Measure tool in the ImageJ National Institute of Health software (http://imagej.nih.gov/ij/). Individual enlarged vesicles with a visible lumen were selected using the circular tool to define the regions of interest and the areas (in pixels) of these structures were then determined. As a control, the areas of vesicles positive for GLUT4 or for ubiquitin or for the endosomal markers in cells transfected with pEGFP-Vps4 were measured. On average 5 to 10 enlarged structures and 15 to 20 control structures were measured per cell. Data were presented as average values from 10 to 14 individual cells. Statistical significance was calculated using two-tailed unpaired t-test. P values of less than 0.05 were considered significant.

Results

ESCRT-III constructs inhibit insulin-stimulated HA-GLUT4 translocation in rat adipocytes

We have used two ESCRT constructs to investigate the dependence of GLUT4 translocation on movement through the ESCRT pathway in insulin-stimulated adipocytes. The first construct encodes the N-terminal portion of CHMP3, amino acids 1 to 179. We have previously developed this N-terminal

construct as a dominant negative inhibitor of ESCRT-III function [5]. The construct has an open conformation and is not autoinhibited by the C-terminal domain. This construct has been shown to bind to membranes and to induce an enlarged endosomal compartment. The second construct, GFP-Vps4^{E235Q}, encodes the dominant-negative mutant of the AAA ATPase Vps4 which is deficient in ATPase activity, and consequently stops the disassembly of the ESCRT-III components. The usual cellular change induced by this construct includes the generation of enlarged endosomal vesicles.

EGFP versions of these constructs were co-transfected into primary rat adipocytes together with HA-tagged GLUT4 [23] used as a reporter. The effects of GFP-Vps4^{E235Q} and CHMP3$^{1–179}$GFP on insulin-stimulated GLUT4 translocation were followed by measuring the amount of HA-tag present at the surface of intact cells. Both constructs decreased insulin-stimulated GLUT4 translocation by 70–80% without significantly affecting the basal levels of GLUT4 present at the cell surface (Figure 1A). Expression of the wild-type GFP-Vps4 construct had no effect on insulin-stimulated HA-GLUT4 translocation to the cell surface. Wild-type CHMP3-GFP could not be used as a control in this experiments as over-expression of the wild-type protein has been reported to induce an enlarged phenotype [27]. Immunoblotting analysis indicated that the HA-GLUT4 was expressed to a similar level in all conditions and that co-expression of the GFP-tagged ESCRT constructs did not affect the level of expression of the HA tagged GLUT4 (Figure 1B).

Localisation studies (Figure 2) revealed that the dominant negative, but not the wild-type, GFP-Vps constructs generate a distinct GFP-positive punctate staining of enlarged and swollen structures throughout the cell. In the absence of the dominant negative constructs GLUT4 is distributed widely and most of the GLUT4 is present in small punctuate spots. This is typical of mature rat fat cell GLUT4 [28], but typically GLUT4 distribution in the adipose cell line 3T3-L1 is a mixture of dispersed vesicular structures and a larger perinuclear compartment. Following the perturbation of ESCRT-III, much of the HA-GLUT4 became localised to enlarged coalesced-vesicular structures which partially co-localised with the ESCRT proteins. The extent of co-localisation of GLUT4 and the GFP-Vps4^{E235Q} in the enlarged vesicular structures was variable and in many cases these two proteins appeared to be localised to the same swollen structures but to non-overlapping and distinct sub-regions of these structures (Figure 2).

As CHMP3 (and possibly other ESCRT components) interact with PI(3,5)P_2 [11] we have examined whether inhibition of PI(3,5)P_2 production with the PIKfyve inhibitor YM201636 also reduces the insulin-stimulated translocation of HA-GLUT4 to the cell surface of adipocytes. YM201636 at concentrations previously reported to inhibit PIKyve [29] significantly inhibit translocation of GLUT4 (Figure 1 C, D). However, we did not observe (data not shown) the formation of an enlarged compartment comparable with that observed following introduction of Vps4^{E235Q} and CHMP3$^{1–179}$.

ESCRT-III perturbation induces the formation of a hybrid compartment

In the absence of ESCRT-III perturbation and in basal cells, endosome marker experiments indicate that GLUT4 is sequestered in a cellular compartment in which there is extensive co-localisation with Syntaxin6. Syntaxin6 localisation defines a TGN-like compartment but is distinct from compartments in which TfR and EEA1 are highly localised (Figure 3A). Following insulin stimulation of these cells GLUT4 becomes more localised at the cell surface and just below it (Figure 3B). These observations are consistent with previous studies on rat fat cells [28,30–32].

Following the expression of the GFP-Vps4^{E235Q} construct GLUT4 becomes more extensively localised with the syntaxin6, EEA1 and transferrin receptor in the swollen ESCRT-III compartment (Figure 3 C,D). This suggests the formation of a hybrid compartments in which there is merging, or lack of sorting, of distinct endosome and TGN protein components. Under these conditions, there are no significant differences between basal and insulin-stimulated cells in the distributions of syntaxin6, EEA1 or transferrin receptors.

In the absence of ESCRT-III perturbation the levels of co-localisation of GLUT4 and ubiquitin are low (Figure 3 A,B). This is partly a consequence of low and indistinct signal from the cytosol and small membrane particles. The extent to which ubiquitinated proteins cluster on enlarged membrane structures is increased in the presence of the GFP-Vps4^{E235Q} and there is also increased co-localisation with GLUT4 and the co-associated markers that reveal a hybrid endosome-TGN compartment (Figure 3 C,D). Analysis of individual cells positive for the GFP-Vps4^{E235Q} signal revealed that on average 7.69±0.60 enlarged vesicles with a visible lumen and positive for GFP-Vps4^{E235Q}, GLUT4, ubiquitin or the endosomal/TGN markers were detected in the perinuclear region of non-stimulated cells. Similarly, in insulin-stimulated cells positive for GFP-Vps^{E235Q} 7.37±0.56 enlarged vesicles were observed per cell. The relative areas of these enlarged structures were determined with the Measure tool in the ImageJ software. This analysis revealed a 10-fold increase in the pixel areas of the enlarged structures compared to the control structures (Table 1). No differences were observed in the sizes of the enlarged structures in comparing un-stimulated with insulin-stimulated cells. Using the area measurement tool in the LSM imaging software the areas of the enlarged compartments in basal or insulin-stimulated cells were estimated to be 14.00±1.74 μm^2 and 18.04±1.79 μm^2 respectively (Table 1). The areas of control vesicles could not be accurately calculated because of the limits of light microscopy resolution. The average diameter of the hybrid structures was 2.40±0.14 μm for unstimulated and 2.71±0.18 μm for insulin-stimulated cells.

In order to determine if extended expression of the ESCRT-III construct would further affect GLUT4 distribution we compared rat adipocytes expressing GFP-Vps4 or GFP-Vps4^{E235Q} for 5 h or 24 h. Immunoblot analysis revealed an increase expression of GFP-Vps4 and GFP-Vps4^{E235Q} after 24 h expression (Figure 4A). Immunofluorescent analysis revealed that after 24 h expression, GLUT4 and ubiquitin colocalise extensively with the increased GFP-Vps4^{E235Q} (Figure 4B). The distribution of GLUT4 is very similar to that observed after 5 h expression. We conclude that GLUT4 is completely trapped in the enlarged endosomal compartment by the 5 h treatment. As the onset of the trapping is relatively rapid we cannot make an inference as to whether GLUT4 is first moved to the PM before transit to a sorting hub for generation of GSV.

Discussion

GLUT4 proteins are sorted to insulin-responsive GLUT4 storage vesicles from which they are released to the cell surface upon insulin stimulation. The signals involved in sorting GLUT4 to GSV's are complex and various intracellular trafficking itineraries have been proposed [33]. However, the involvement of an ESCRT-dependent step in this traffic has not been previously considered. We report here that perturbations of the ESCRT machinery result in reduced levels of GLUT4 transloca-

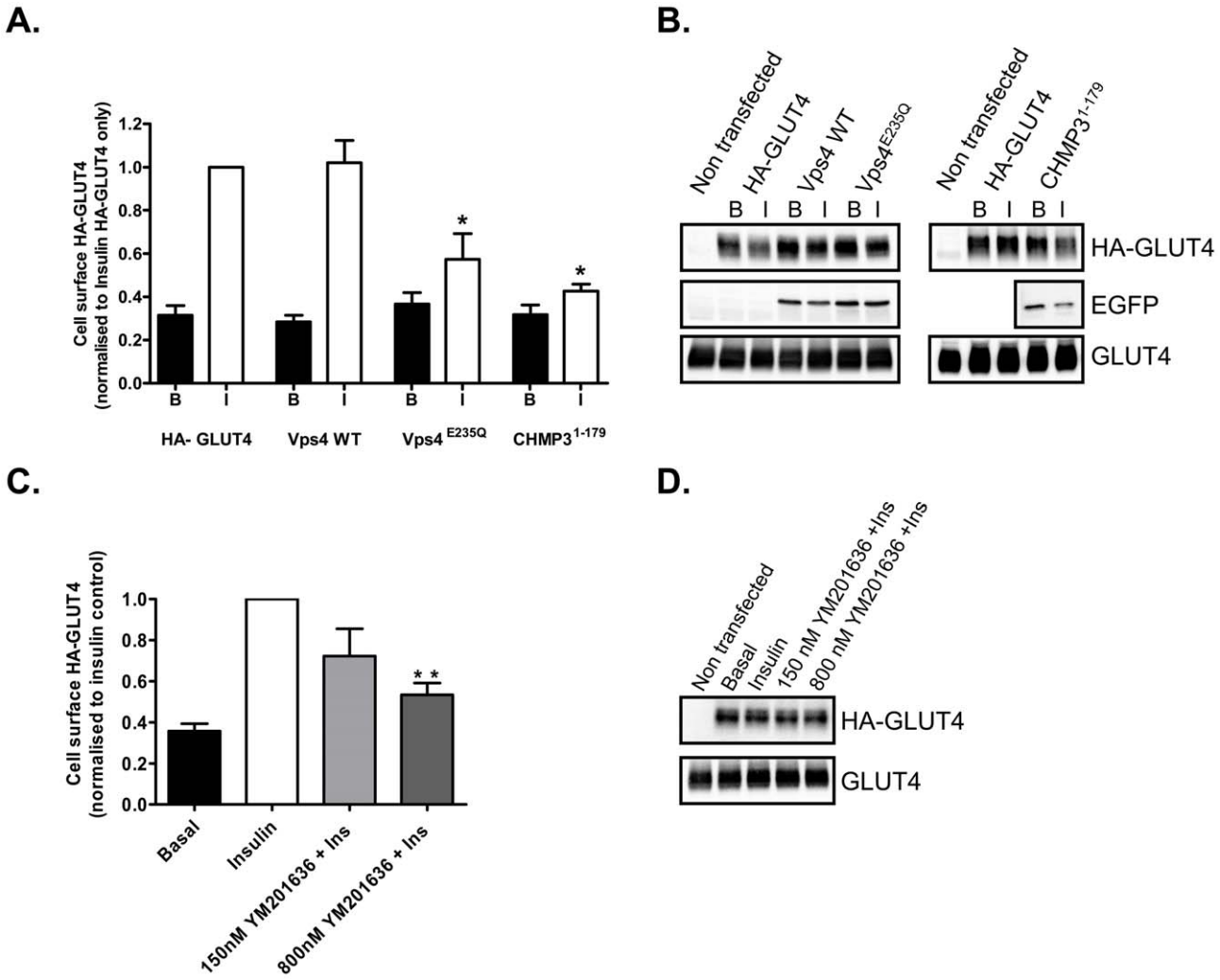

Figure 1. ESCRT-III constructs lead to inhibition of GLUT4 translocation to the cell surface of rat adipose cells. (A) Primary rat adipocytes were transfected by electroporation with pCis HA-GLUT4 and pEGFP VPS4, pEGFP VPS4^{E235Q} or pEGFP CHMP3$^{1-179}$ and then maintained in culture for 5 h. HA-GLUT4 at the cell surface was detected with anti-HA antibody and β-galactosidase conjugated secondary antibody. The signal was measured with a fluorescent β-galactosidase substrate. Results are mean and SEM from 3 independent experiments. * $p<0.05$ (comparison of pCis HA-GLUT4 only control *vs*. pCis HA-GLUT4 co-transfected with ESCRT-III pEGFP constructs). (B) Representative immunoblots for the levels of expression of HA-GLUT4, EGFP-Vps4, EGFP-Vps4^{E235Q}, CHMP3$^{1-179}$-EGFP and total GLUT4 in the transfected rat adipocytes. (C) The PIKfyve inhibitor YM201636 decreases GLUT4 translocation to the cell surface in a dose dependent manner. Primary rat adipocytes were transfected by electroporation with pCis HA-GLUT4 and then maintained in culture for 5 h. Cells were left untreated or incubated with 150 nM or 800 nM YM201636 for 30 min prior to insulin stimulation. HA-GLUT4 at the cell surface was detected with anti-HA antibody and β-galactosidase conjugated secondary antibody. The signal was measured with a fluorescent β-galactosidase substrate. Results are mean and SEM from 3 independent experiments. ** $p<0.01$ (comparison of Insulin stimulated control cells *vs*. YM201636 treated cells prior to insulin stimulation). (D) Representative immunoblots for the levels of expression of HA-GLUT4 and total GLUT4 in the transfected rat adipocytes treated with YM201636.
doi:10.1371/journal.pone.0044141.g001

tion to the plasma membrane in response to insulin. Furthermore, we show that disrupting the function of the ESCRT machinery leads to extensive accumulation of GLUT4 on intracellular membranes containing endosomal markers and the TGN marker syntaxin6 suggesting an accumulation in a hybrid enlarged tubulo- and multivesicular compartment. This suggests that a large proportion of GLUT4 is trapped by ESCRT perturbation and is unable to gain access to an insulin-responsive compartment. In comparison with unperturbed GLUT4 intracellular vesicle compartments, the enlarged GLUT4 compartment produced by ESCRT perturbation is highly enriched in ubiquitinated proteins. This suggests that, like other cargos that are routed through multivesicular endosomes, GLUT4 may undergo changes in tagging with ubiquitin-like domains or associate with chaperone proteins that are ubiquitin tagged [8].

Insulin action in adipocytes is highly dependent on inositol lipid signalling and perturbations in the levels of the phosphatidylinositides, mainly phosphatidylinositol 3,4,5-trisphosphate (PIP3), have been shown to be associated with formation of extended, enlarged and vacuolated GLUT4 compartments [34]. Studies on insulin-regulated GLUT4 traffic have led to the well-supported proposal that signalling is mediated through activation of Class1A PI 3-kinases and increases in PIP3. However, levels of PI(3,5)P_2 are also increased by insulin signalling via activation of Class2 and Class3 PI 3-kinases to produce PI(3)P and by activation of PIKfyve [35–37]. It is therefore of note that ESCRT traffic is highly

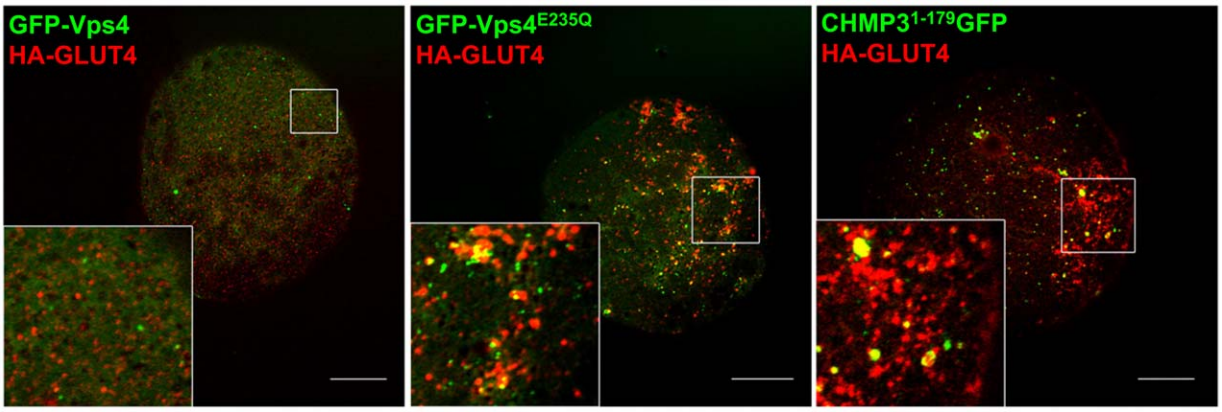

Figure 2. ESCRT-III constructs lead to swollen and extended GLUT4 compartments in rat adipose cells. Confocal microscopy examination of primary rat adipocytes co-transfected with HA-GLUT4 (red) and EGFP-tagged Vps4 WT, $Vps4^{E235Q}$ or $CHMP3^{1-179}$ (green) and stimulated with 60 nM insulin for 20 min**.** Cells were fixed with 4% paraformaldehyde, permeabilised in 0.1% saponin and immuno-stained with anti-HA antibody and anti-mouse IgG-Alexa 633 secondary antibody. Images were acquired with LSM510 Meta confocal laser scanning microscope and are from single adipose cells representative of the cell populations from at least three separate experiments. Bars 20 μm.
doi:10.1371/journal.pone.0044141.g002

dependent on CHMP3 which has been shown to bind inositol lipids, particularly $PI(3,5)P_2$. We observed inhibition of GLUT4 traffic following treatment with a PIKfyve inhibitor but we did not observe a marked enlargement of endosomes. We cannot therefore directly correlate the binding of CHMP3 to $PI(3,5)P_2$ or to the function of PIKfyve. An enlarged endosome phenotype does occur in several other cell types following treatment with the PIKfyve inhibitor [29,38]. By contrast, the morphological changes associated with inhibition of PIKfyve are generally not evident in adipocytes [39]. Furthermore, the kinase dead PIKfyve mutant does not induce an enlarged endosome phenotype in 3T3-L1 adipocytes [40]. This may mean that in adipocytes reduction in $PI(3,5)P_2$ alone is insufficient to fully perturb ESCRT function. It will be of interest in future to determine the extent to which the traffic of GLUT4 through the ESCRT compartment is dependent on, or influenced by, insulin dependent changes in both PIP3 and $PI(3,5)P_2$. Similarly, silencing of CHMP3 with siRNA treatment HeLa cells does not produce enlargement of endosomes and the endosome enlargement effect is confined to the dominant negative CHMP3 [41,42].

It has recently been reported that GLUT4 is ubiquitinated and that this modification is necessary for its sorting into an insulin responsive compartment [22]. However, only a very low percentage (0.1%) of GLUT4 is reported to be ubiquitinated at steady-state. In our studies, we were unable to detect this low level of GLUT4 ubiquitination using immunoprecipitation of HA-tagged GLUT4 followed by ubiquitin detection by western blot. However, GLUT4 may associate with other proteins that may be tagged with ubiquitin-like domains. The genesis of this compartment is dependent on GGA adapters that bind to sortilin on the GSVs. Additional proteins associated with this compartment include TUG (Tether containing UBX domain for GLUT4). UBX (ubiquitin associated) domains of TUG (which are similar in structure to ubiquitin) are thought to retain the GSV and a construct of the UBX domain can lead to release of the GSVs from an intracellular storage location to the cell surface [43,44]. However, the mechanism by which insulin action leads to a change in the GSV-TUG interaction is currently unknown. Direct SUMOylation of GLUT4 has been reported to occur at quite high levels [18,19,45]. In addition GLUT4 can associate with the Ubc9, a SUMO conjugating enzyme [18] and with another SUMOylated protein Daxx [19]. All these studies point towards a complex array of processing of GLUT4 in conjunction with ubiquitin-containing or ubiquitin-like protein domains and it will be of interest in future to determine how much of this processing is dependent on the ESCRT complexes.

Parallels have been drawn between the traffic of GLUT4 and the yeast amino acid transporter Gap1p [22,46]. This protein traffics between three main compartments, the TGN, the plasma membrane and the vacuole. The Gap1p storage compartment is associated with the TGN and residence in this compartment is dependent on GGA and on ubiquitination. Under nitrogen deficient conditions Gap1p is deubiquitinated and moves towards the plasma membrane. Under nitrogen rich conditions the ubiquitinated Gap1p is directed towards multivesicular endosomes (MVEs) and to the vacuole for degradation as it is no longer needed. In the case of GLUT4 it is proposed here that sequential ubiquitination and deubiquitination of GLUT4 (or a GLUT4 vesicle associated protein) are required for directing GLUT4 to the GSV compartment [22] rather than the plasma membrane (as in the Gap1 case). This distinction probably occurs because insulin action is required for movement from the GSV compartment to the plasma membrane (Figure 5). The comparisons with the Gap1p system [22,47,48] are relevant here as it has been determined that amongst the yeast mutants that have defective Gap1p traffic are ESCRT components including Vps24 (CHMP3) and Vps4. In this case ESCRT mutants lead to reduced vacuole targeting of Gap1p and increased traffic to the plasma membrane [47,48]. Distinct roles of mono- and poly-ubiquitination have been demonstrated in studies on ESCRT dependent traffic between MVEs and the plasma membrane and between the TGN and the MVEs, respectively [47].

GLUT4 that accumulates in the MVE upon ESCRT perturbation may have previously entered from the plasma membrane or trafficked to the MVE from the TGN. The latter route is more consistent with the ubiquitin and GGA dependent sorting of GLUT4 [22], but this route may require polyubiquitination [47]. GLUT4 is relatively stable protein with a half life of 48 hours in 3T3L1 adipocytes [49,50] and each GLUT4 molecule possibly gains access to the plasma membrane and endosomes multiple times before being eventually degraded, even in unstimulated cells [51]. GLUT4 is now known to follow an unusual retrograde trafficking route from endosomes to the TGN that involves the Clathrin Heavy Chain CHC22 rather than CHC17 [26,52]. This

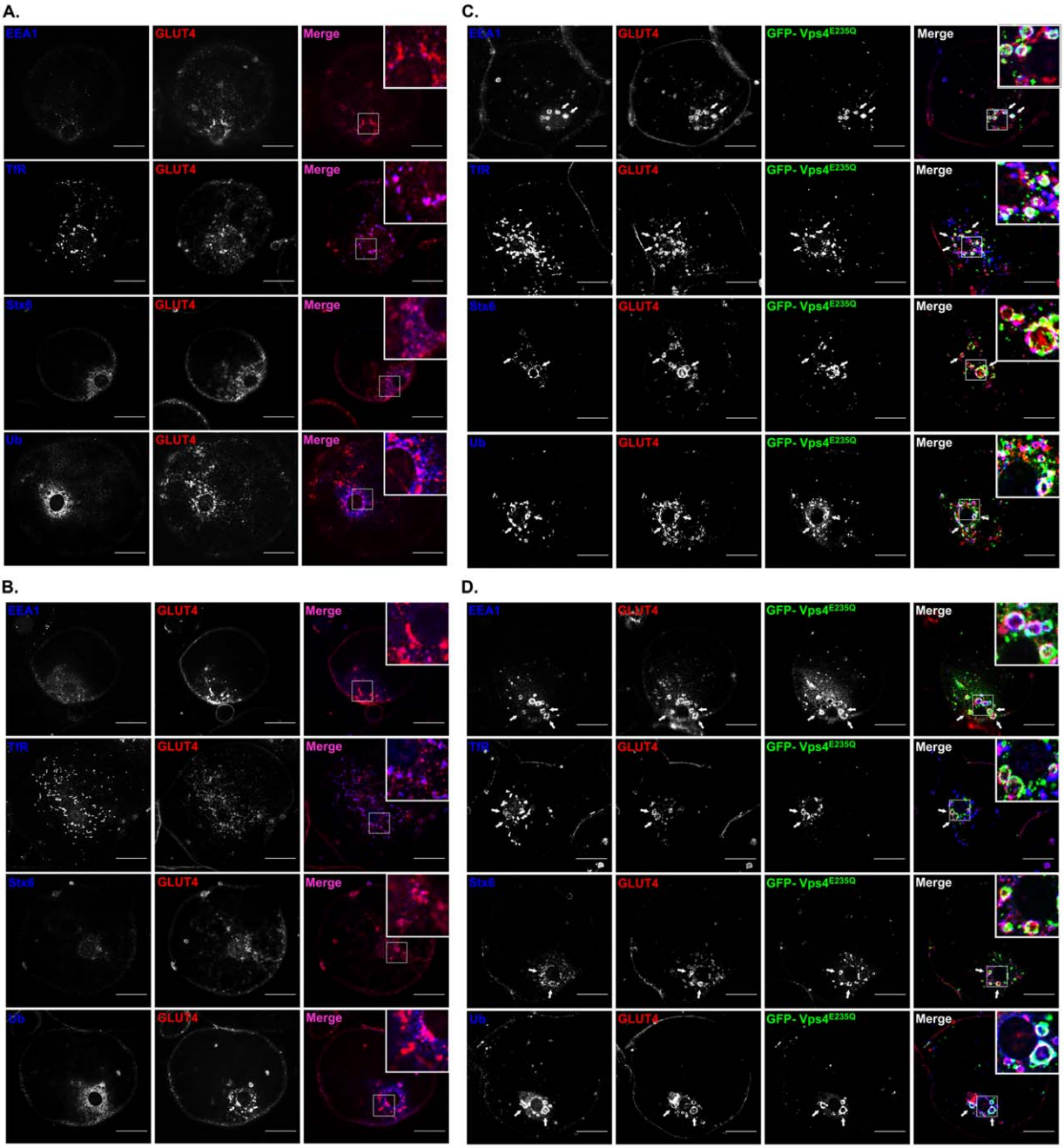

Figure 3. ESCRT-III constructs lead to formation of a hybrid compartment in which endosomal markers co-localise with GLUT4. The distribution of endogenous GLUT4 was detected with a rabbit polyclonal anti GLUT4 C-terminal peptide antibody. GLUT4 localization (red in merged images) was compared with EEA1, ubiquitin, syntaxin6 and transferrin receptors (blue in merged images) using the antibodies described in the Materials and Methods section. Endosomal marker distributions in the presence of non-perturbing wild-type GFP-Vps4 in the basal state (**A**) and the insulin stimulated state (**B**). The EGFP-Vps4 is highly dispersed and is cytosolic under these conditions (not shown for clarity). Expression of the EGFP-Vps4^{E235Q} (green in merged images) leads GLUT4 vesicle coalescence to form swollen compartments. The endosomal markers EEA1, transferrin receptors (TfR), syntaxin6 (Stx6) and ubiquitin (Ub) colocalise with both endogenous GLUT4 and with EGFP-Vps4^{E235Q} both in the basal state (**C**) and the insulin stimulated state (**D**). Images were acquired with LSM510 Meta confocal laser scanning microscope and are from single adipose cells representative of the cell populations from at least three separate experiments. Bars 20 μm. Arrows point at hybrid enlarged tubulo- vesicular structures.
doi:10.1371/journal.pone.0044141.g003

route is distinct from the early endosome to TGN pathway. The CHC22 dependent step is downstream of the CHC17-dependent early endosome sorting step suggesting that some cargos, such as GLUT4, enter a "non-early" endosome compartment before retrograde traffic to the TGN. CHC22 deletion interferes with this step and causes GLUT4 loss, possibly due to GLUT4 degradation [26]. Furthermore, knockdown of CHC22 causes some increased tubulation of the GLUT4 [26] which is similar to the extended and coalesced GLUT4 compartment reported here and illustrated in a model form in Figure 5. GLUT4 may access this

Table 1. Enlargement of a coalesced tubulo-vesicular structure in adipocytes treated with ESCRT-III constructs.

	EGFP-Vps4		EGFP-Vps4^{E235Q}	
	Basal	**Insulin**	**Basal**	**Insulin**
Area (pixels)	85.92±24.11	131.57±5.37	1411.61±183.32***	1448.52±168.90***
Area (μm^2)	-	-	14.00±1.74	18.04±1.80
Diameter (μm)	-	-	2.40±0.14	2.71±0.18

The areas of enlarged vesicular structures, with visible lumens and positive for EGFP, GLUT4 and ubiquitin or the endosomal markers, were measured in pEGFP VPS4^{E235Q} and in wild-type pEGFP-Vps4 transfected adipocytes (as described in the Materials and Methods section). Results are mean and SEM from 10 to 14 individual cells. *** $p<0.001$ (enlarged *vs* control vesicles). Only the large pixel areas from the enlarged structures could be accurately converted to μm^2.

doi:10.1371/journal.pone.0044141.t001

compartment so that it can either be conserved by retrograde traffic to the TGN-associated GSV compartment or alternatively degraded by following an MVE to lysosome route. Consistent with this possibility is the observation that residues close to the C-terminal LL targeting signals on GLUT4 and Gap1p are similar, but not identical, to those in the lysosome resident protein LIMPII [53]. Mutation of GLUT4 in the vicinity of the LL motif can lead to its traffic to the lysosome [53]. We envisage that the tubular-vesicular MVE structures are an immature MVB (as described [3]) which acts as a hub or sorting station. This hub structure would likely facilitate docking and fusion of incoming GLUT4 vesicles with outward-facing topology and allow budding of vesicles with cargos (such as GLUT4) not destined for degradation. Changes in lipid domains within the same MVE could then be a platform for ESCRT protein activity with production of an inward-facing topology of membrane domains that leads to the degradation route. Testing of the model described will require a dynamic and kinetic analysis of movement between the proposed MVE compartment and the GSV and plasma membrane compartments.

Membrane proteins such as EGFR and CXCR4 require deubiquitination by DUBs prior to sorting into MVEs [54,55] and the accumulation of ubiquitinated proteins suggests a failure in the functional recruitment of DUBs to this compartment. Two DUBs, AMSH and USP8 have both been shown to associate with the ESCRT machinery via ESCRT-0 and ESCRT-III proteins [56–59]. In the case of the interactions with ESCRT-III, both DUBs contain MIT domains that interact with C-terminal MIT interacting motifs (MIMs) of a number of ESCRT-III proteins [60]. There is mounting evidence that spatial and temporal

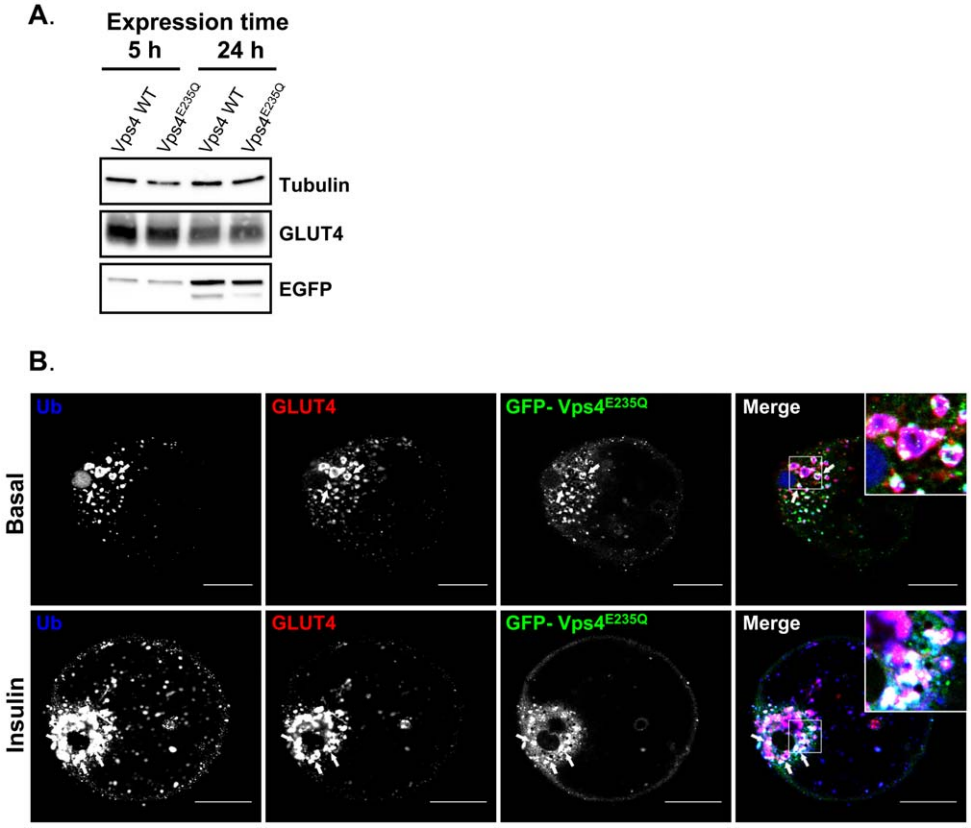

Figure 4. 24-hour expression of ESCRT-III constructs increases the intracellular accumulation of GLUT4 in a coalesced enlarged compartment positive for ubiquitin. (A) Immunoblot analysis of the levels of expression of EGFP-Vps4 and EGFP-Vps4^{E235Q} in rat adipocytes transfected and maintained in culture for 5 h or 24 h. (B) Confocal microscopy examination of primary rat adipocytes transfected with EGFP-tagged Vps4 WT or Vps4^{E235Q} and maintained in culture for 24 h. Ubiquitin (Ub) colocalises with endogenous GLUT4 and with EGFP-Vps4^{E235Q} after 24 h expression in both basal and insulin-stimulated cells. Images were acquired with LSM510 Meta confocal laser scanning microscope and are from single adipose cells representative of the cell populations from at tubulo- vesicular least two separate experiments. Bars 20 μm. Arrows point at hybrid enlarged structures.

doi:10.1371/journal.pone.0044141.g004

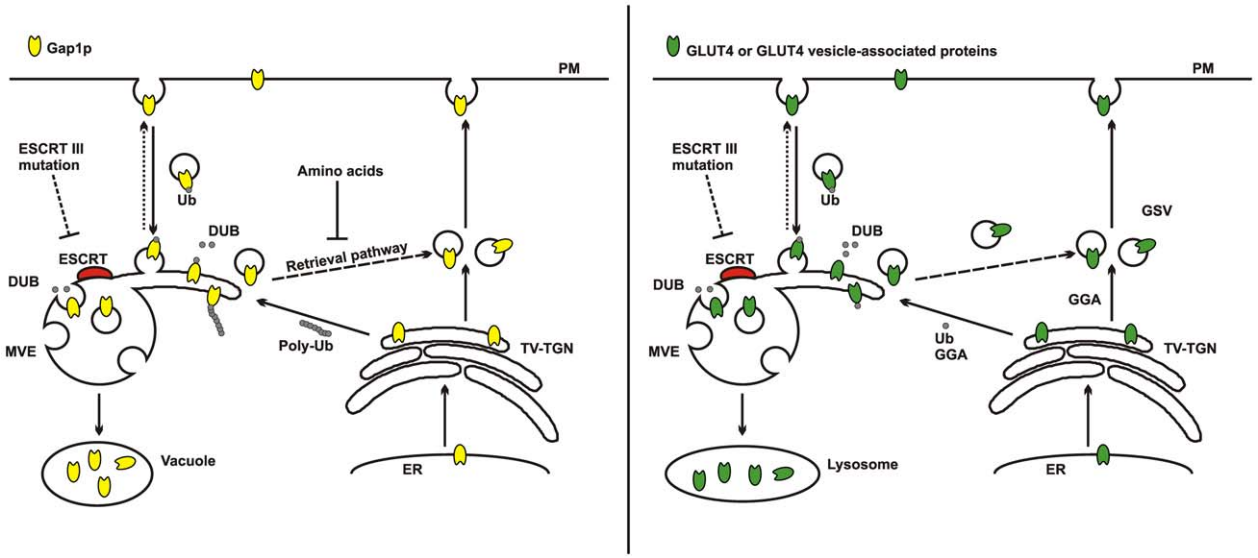

Figure 5. A model depicting the parallel between Gap1p trafficking in yeast and insulin-sensitive GLUT4 trafficking in mammalian cells. Left panel: Amino acid regulated Gap1p trafficking in yeast. In response to fluctuations in amino acid levels Gap1p traffics to the vacuole for degradation or to the plasma membrane (PM). This trafficking is regulated by Gap1p ubiquitination (Ub) and is dependent on ubiquitin ligases and deubiquitinating hydrolases (DUB). Before it reaches the vacuole Gap1p is sorted to the multivesicular endosomes (MVE), where, depending on the amino acid environment, it will either be degraded or redirected to the PM directly or via the tubulo-vesicular TGN (TV-TGN). The ESCRT-III mutants have been reported to block Gap1p trafficking to the vacuole and instead Gap1p is redirected to the plasma membrane. Model adapted from that described by the Kaiser's group [47,48] **Right panel: Insulin stimulated GLUT4 trafficking.** In response to insulin stimulation GLUT4 traffics from a storage compartment (GSV) to the plasma membrane (PM). The traffic of GLUT4 back to the GSVs is complex and requires ubiquitin (Ub) and is dependent on GGA proteins. It is currently unclear whether ubiquitinylation of GLUT4 or a GLUT4 vesicle resident protein is responsible for the extensive localization with Ub and GLUT4. In our study we report that ESCRT-III mutants block GLUT4 trafficking and trap it an enlarged hybrid compartment together with endosomal and TGN markers. We propose that ESCRT compartment is an extended tubulo-vesicular structure that may act as a hub that sorts GLUT4 that is destined either for degradation or for insulin-regulated traffic. ESCRT dependent membrane curvature machinery and associated DUB activity may facilitate the targeting of GLUT4 (see Discussion text for details). Such a model is consistent with a previously proposed model of endosomal maturation and formation of tubulo-vesicular MVE structures [3].
doi:10.1371/journal.pone.0044141.g005

regulation of deubiquitination, rather than ubiquitination *per se*, may be crucial in determining the fate of ubiquitinated proteins at endosome, TGN and MVE sorting steps. For example AMSH and USP8 can have very different effect on the sorting of ubiquitinated membrane proteins. While AMSH is required for sorting of EGFR into MVEs and degradation in lysosomes [61], deubiquitination of EGFR by USP8 protects it from lysosomal degradation [54]. How the ESCRT machinery is involved in regulating ESCRT related DUB activity and alters the fate of cargo proteins needs to be explored in further detail. We hypothesise that by functionally disrupting the ESCRT machinery, and by interference with deubiquitination of GLUT4 (or GLUT4 associated proteins), a failure to sort GLUT4 to GSVs occurs (Figure 5 right panel). Both of the dominant negative constructs used in this study could interfere with the recruitment of MIT containing DUBs. The truncated CHMP3$^{1-179}$GFP lacks its C-terminus which would normally contain its MIT interacting motif (MIM) [61]. GFP-Vps4^{E235Q} contains an MIT domain that binds to MIMs on ESCRT-III components [62]. This may prevent binding of MIT containing DUBs as this mutated form of Vps4 cannot be released from ESCRT-III due to defective ATPase activity. However, the DUB family is very large and unidentified DUBs may influence GLUT4 traffic during ESCRT-III sorting. It will be interesting to determine whether knock down of levels of specific DUBs will result in a failure of GLUT4 to sort to GSVs and thereby lead to decreased levels of GLUT4 at the plasma membrane in response to insulin. In addition, the possibility of ESCRT involvement in the perturbation of GLUT4 traffic that occurs in insulin-resistant cells remains to be explored.

Acknowledgments

We thank Samuel Cushman for the gift of the HA-tagged GLUT4 construct and Peter Shepherd for the gift of the PIKfyve inhibitor YM201636.

Author Contributions

Conceived and designed the experiments: FK PRW GDH. Performed the experiments: FK VJP. Analyzed the data: FK VJP. Contributed reagents/materials/analysis tools: FK PRW GDH. Wrote the paper: FK PRW GDH.

References

1. Peel S, Macheboeuf P, Martinelli N, Weissenhorn W (2011) Divergent pathways lead to ESCRT-III-catalyzed membrane fission. Trends Biochem Sci 36: 199–210.
2. Samson RY, Obita T, Freund SM, Williams RL, Bell SD (2008) A role for the ESCRT system in cell division in archaea. Science 322: 1710–1713.
3. Woodman PG, Futter CE (2008) Multivesicular bodies: co-ordinated progression to maturity. Curr Opin Cell Biol 20: 408–414.
4. Carlton JG, Martin-Serrano J (2007) Parallels between cytokinesis and retroviral budding: a role for the ESCRT machinery. Science 316: 1908–1912.
5. Dukes JD, Richardson JD, Simmons R, Whitley P (2008) A dominant-negative ESCRT-III protein perturbs cytokinesis and trafficking to lysosomes. Biochem J 411: 233–239.

6. Carlton JG, Agromayor M, Martin-Serrano J (2008) Differential requirements for Alix and ESCRT-III in cytokinesis and HIV-1 release. Proc Natl Acad Sci U S A 105: 10541–10546.
7. Lee JA, Liu L, Gao FB (2009) Autophagy defects contribute to neurodegeneration induced by dysfunctional ESCRT-III. Autophagy 5: 1070–1072.
8. Shields SB, Piper RC (2011) How Ubiquitin Functions with ESCRTs. Traffic 12: 1306–1317.
9. Lata S, Roessle M, Solomons J, Jamin M, Gottlinger HG, et al. (2008) Structural basis for autoinhibition of ESCRT-III CHMP3. J Mol Biol 378: 818–827.
10. Lata S, Schoehn G, Jain A, Pires R, Piehler J, et al. (2008) Helical structures of ESCRT-III are disassembled by VPS4. Science 321: 1354–1357.
11. Whitley P, Reaves BJ, Hashimoto M, Riley AM, Potter BV, et al. (2003) Identification of mammalian Vps24p as an effector of phosphatidylinositol 3,5 bisphosphate dependent endosome compartmentalization. J Biol Chem 278: 38786–38795.
12. Obita T, Saksena S, Ghazi-Tabatabai S, Gill DJ, Perisic O, et al. (2007) Structural basis for selective recognition of ESCRT-III by the AAA ATPase Vps4. Nature 449: 735–739.
13. Komander D, Clague MJ, Urbe S (2009) Breaking the chains: structure and function of the deubiquitinases. Nat Rev Mol Cell Biol 10: 550–563.
14. Lin Y, Kimpler LA, Naismith TV, Lauer JM, Hanson PI (2005) Interaction of the mammalian endosomal sorting complex required for transport (ESCRT) III protein hSnf7-1 with itself, membranes, and the AAA+ ATPase SKD1. J Biol Chem 280: 12799–12809.
15. Stringer DK, Piper RC (2011) A single ubiquitin is sufficient for cargo protein entry into MVBs in the absence of ESCRT ubiquitination. J Cell Biol 192: 229–242.
16. Shields SB, Oestreich AJ, Winistorfer S, Nguyen D, Payne JA, et al. (2009) ESCRT ubiquitin-binding domains function cooperatively during MVB cargo sorting. J Cell Biol 185: 213–224.
17. Reid RJ, Gonzalez-Barrera S, Sunjevaric I, Alvaro D, Ciccone S, et al. (2011) Selective ploidy ablation, a high-throughput plasmid transfer protocol, identifies new genes affecting topoisomerase I-induced DNA damage. Genome Res 21: 477–486.
18. Giorgino F, de Robertis O, Laviola L, Montrone C, Perrini S, et al. (2000) The sentrin-conjugating enzyme mUbc9 interacts with GLUT4 and GLUT1 glucose transporters and regulates transporter levels in skeletal muscle cells. Proc Natl Acad Sci U S A 97: 1125–1130.
19. Lalioti VS, Vergarajauregui S, Pulido D, Sandoval IV (2002) The insulin-sensitive glucose transporter, GLUT4, interacts physically with Daxx. Two proteins with capacity to bind Ubc9 and conjugated to SUMO1. J Biol Chem 277: 19783–19791.
20. Bogan JS, Hendon N, McKee AE, Tsao TS, Lodish HF (2003) Functional cloning of TUG as a regulator of GLUT4 glucose transporter trafficking. Nature 425: 727–733.
21. Yu CF, Cresswell J, Loffler MG, Bogan JS (2007) The glucose transporter 4-regulating protein TUG is essential for highly insulin-responsive glucose uptake in 3T3-L1 adipocytes. J Biol Chem 282: 7710–7722.
22. Lamb CA, McCann RK, Stockli J, James DE, Bryant NJ (2010) Insulin-regulated trafficking of GLUT4 requires ubiquitination. Traffic 11: 1445–1454.
23. AlHasani H, Kinck CS, Cushman SW (1998) Endocytosis of the glucose transporter GLUT4 is mediated by the GTPase dynamin. J Biol Chem 273: 17504–17510.
24. Satoh S, Nishimura H, Clark AE, Kozka IJ, Vannucci SJ, et al. (1993) Use of bis-Mannose photolabel to elucidate insulin-regulated GLUT4 subcellular trafficking kinetics in rat adipose cells: Evidence that exocytosis is a critical site of hormone action. J Biol Chem 268: 17820–17829.
25. Taylor LP, Holman GD (1981) Symmetrical kinetic parameters for 3-*O*-methyl-D-glucose transport in adipocytes in the presence and absence of insulin. Biochim Biophys Acta 642: 325–335.
26. Esk C, Chen CY, Johannes L, Brodsky FM (2010) The clathrin heavy chain isoform CHC22 functions in a novel endosomal sorting step. J Cell Biol 188: 131–144.
27. Zamborlini A, Usami Y, Radoshitzky SR, Popova E, Palu G, et al. (2006) Release of autoinhibition converts ESCRT-III components into potent inhibitors of HIV-1 budding. Proc Natl Acad Sci U S A 103: 19140–19145.
28. Malide D, Ramm G, Cushman SW, Slot JW (2000) Immunoelectron microscopic evidence that GLUT4 translocation explains the stimulation of glucose transport in isolated rat white adipose cells. J Cell Sci 113: 4203–4210.
29. Jefferies HB, Cooke FT, Jat P, Boucheron C, Koizumi T, et al. (2008) A selective PIKfyve inhibitor blocks PtdIns(3,5)P(2) production and disrupts endomembrane transport and retroviral budding. EMBO Rep 9: 164–170.
30. Malide D, Dwyer NK, BlanchetteMackie EJ, Cushman SW (1997) Immunocytochemical evidence that GLUT4 resides in a specialized translocation post-endosomal VAMP2-positive compartment in rat adipose cells in the absence of insulin. Journal Of Histochemistry & Cytochemistry 45: 1083–1096.
31. Martin S, Tellam J, Livingstone C, Slot JW, Gould GW, et al. (1996) The glucose transporter (GLUT4) and Vesicle-Associated Membrane Protein-2 (VAMP-2) are segregated from recycling endosomes in insulin-sensitive cells. J Cell Biol 134: 625–635.
32. Slot JW, Geuze HJ, Gigengack S, Lienhard GE, James DE (1991) Immunolocalization of the insulin regulatable glucose transporter in brown adipose-tissue of the rat. J Cell Biol 113: 123–135.
33. Foley K, Boguslavsky S, Klip A (2011) Endocytosis, recycling, and regulated exocytosis of glucose transporter 4. Biochemistry 50: 3048–3061.
34. Shpetner H, Joly M, Hartley D, Corvera S (1996) Potential sites of PI-3 kinase function in the endocytic pathway revealed by the PI-3 kinase inhibitor, wortmannin. J Cell Biol 132: 595–605.
35. Shisheva A (2008) PIKfyve: Partners, significance, debates and paradoxes. Cell Biol Int 32: 591–604.
36. Ikonomov OC, Sbrissa D, Dondapati R, Shisheva A (2007) ArPIKfyve-PIKfyve interaction and role in insulin-regulated GLUT4 translocation and glucose transport in 3T3-L1 adipocytes. Exp Cell Res 313: 2404–2416.
37. Berwick DC, Dell GC, Welsh GI, Heesom KJ, Hers I, et al. (2004) Protein kinase B phosphorylation of PIKfyve regulates the trafficking of GLUT4 vesicles. J Cell Sci 117: 5985–5993.
38. Dukes JD, Whitley P, Chalmers AD (2012) The PIKfyve Inhibitor YM201636 Blocks the Continuous Recycling of the Tight Junction Proteins Claudin-1 and Claudin-2 in MDCK cells. Plos One 7: e28659.
39. Sbrissa D, Ikonomov OC, Filios C, Delvecchio K, Shisheva A (2012) Functional dissociation between PIKfyve-synthesized PtdIns5P and PtdIns(3,5)P2 by means of the PIKfyve inhibitor YM201636. Am J Physiol Cell Physiol [Epub ahead of print].
40. Ikonomov OC, Sbrissa D, Mlak K, Shisheva A (2002) Requirement for PIKfyve Enzymatic Activity in Acute and Long-Term Insulin Cellular Effects. Endocrinology 143: 4742–4754.
41. Bache KG, Stuffers S, Malerod L, Slagsvold T, Raiborg C, et al. (2006) The ESCRT-III subunit hVps24 is required for degradation but not silencing of the epidermal growth factor receptor. Mol Biol Cell 17: 2513–2523.
42. Baldys A, Raymond JR (2009) Critical Role of ESCRT Machinery in EGFR Recycling. Biochemistry 48: 9321–9323.
43. Bogan JS, Kandror KV (2010) Biogenesis and regulation of insulin-responsive vesicles containing GLUT4. Curr Opin Cell Biol 22: 506–512.
44. Xu Y, Rubin BR, Orme CM, Karpikov A, Yu C, et al. (2011) Dual-mode of insulin action controls GLUT4 vesicle exocytosis. J Cell Biol 193: 643–653.
45. Lalioti VS, Vergarajauregui S, Tsuchiya Y, Hernandez-Tiedra S, Sandoval IV (2009) Daxx functions as a scaffold of a protein assembly constituted by GLUT4, JNK1 and KIF5B. J Cell Physiol 218: 416–426.
46. Bryant NJ, Govers R, James DE (2002) Regulated transport of the glucose transporter GLUT4. Nat Rev Mol Cell Biol 3: 267–277.
47. Risinger AL, Kaiser CA (2008) Different ubiquitin signals act at the Golgi and plasma membrane to direct GAP1 trafficking. Mol Biol Cell 19: 2962–2972.
48. Rubio-Texeira M, Kaiser CA (2006) Amino acids regulate retrieval of the yeast general amino acid permease from the vacuolar targeting pathway. Mol Biol Cell 17: 3031–3050.
49. Pryor PR, Liu SC, Clark AE, Yang J, Holman GD, et al. (2000) Chronic insulin effects on insulin signalling and GLUT4 endocytosis are reversed by metformin. Biochem J 348: 83–91.
50. Sargeant RJ, Paquet MR (1993) Effect of insulin on the rates of synthesis and degradation of GLUT1 and GLUT4 glucose transporters in 3T3-L1 adipocytes. Biochem J 290 (Pt 3): 913–919.
51. Karylowski O, Zeigerer A, Cohen A, McGraw TE (2004) GLUT4 is retained by an intracellular cycle of vesicle formation and fusion with endosomes. Mol Biol Cell 15: 870–882.
52. Vassilopoulos S, Esk C, Hoshino S, Funke BH, Chen CY, et al. (2009) A role for the CHC22 clathrin heavy-chain isoform in human glucose metabolism. Science 324: 1192–1196.
53. Sandoval IV, Martinez-Arca S, Valdueza J, Palacios S, Holman GD (2000) Distinct reading of different structural determinants modulates the dileucine-mediated transport steps of the lysosomal membrane protein LIMPII and the insulin-sensitive glucose transporter GLUT4. J Biol Chem 275: 39874–39885.
54. Berlin I, Higginbotham KM, Dise RS, Sierra MI, Nash PD (2010) The deubiquitinating enzyme USP8 promotes trafficking and degradation of the chemokine receptor 4 at the sorting endosome. J Biol Chem 285: 37895–37908.
55. Sierra MI, Wright MH, Nash PD (2010) AMSH interacts with ESCRT-0 to regulate the stability and trafficking of CXCR4. J Biol Chem 285: 13990–14004.
56. McCullough J, Row PE, Lorenzo O, Doherty M, Beynon R, et al. (2006) Activation of the endosome-associated ubiquitin isopeptidase AMSH by STAM, a component of the multivesicular body-sorting machinery. Curr Biol 16: 160–165.
57. Agromayor M, Martin-Serrano J (2006) Interaction of AMSH with ESCRT-III and deubiquitination of endosomal cargo. J Biol Chem 281: 23083–23091.
58. Kato M, Miyazawa K, Kitamura N (2000) A deubiquitinating enzyme UBPY interacts with the Src homology 3 domain of Hrs-binding protein via a novel binding motif PX(V/I)(D/N)RXXKP. J Biol Chem 275: 37481–37487.
59. Wright MH, Berlin I, Nash PD (2011) Regulation of endocytic sorting by ESCRT-DUB-mediated deubiquitination. Cell Biochem Biophys 60: 39–46.
60. Row PE, Liu H, Hayes S, Welchman R, Charalabous P, et al. (2007) The MIT domain of UBPY constitutes a CHMP binding and endosomal localization signal required for efficient epidermal growth factor receptor degradation. J Biol Chem 282: 30929–30937.
61. Ma YM, Boucrot E, Villen J, Affar eB, Gygi SP, et al. (2007) Targeting of AMSH to endosomes is required for epidermal growth factor receptor degradation. J Biol Chem 282: 9805–9812.
62. Stuchell-Brereton MD, Skalicky JJ, Kieffer C, Karren MA, Ghaffarian S, et al. (2007) ESCRT-III recognition by VPS4 ATPases. Nature 449: 740–744.